National Library of Canada
Bibliothèque nationale du Canada

Canadian Theses Service
Service des thèses canadiennes

Ottawa, Canada
K1A 0N4

NOTICE

The quality of this microform is heavily dependent upon the quality of the original thesis submitted for microfilming. Every effort has been made to ensure the highest quality of reproduction possible.

If pages are missing, contact the university which granted the degree.

Some pages may have indistinct print especially if the original pages were typed with a poor typewriter ribbon or if the university sent us an inferior photocopy.

Previously copyrighted materials (journal articles, published tests, etc.) are not filmed.

Reproduction in full or in part of this microform is governed by the Canadian Copyright Act, R.S.C. 1970, c. C-30.

AVIS

La qualité de cette microforme dépend grandement de la qualité de la thèse soumise au microfilmage. Nous avons tout fait pour assurer une qualité supérieure de reproduction.

S'il manque des pages, veuillez communiquer avec l'université qui a conféré le grade.

La qualité d'impression de certaines pages peut laisser à désirer, surtout si les pages originales ont été dactylographiées à l'aide d'un ruban usé ou si l'université nous a fait parvenir une photocopie de qualité inférieure.

Les documents qui font déjà l'objet d'un droit d'auteur (articles de revue, tests publiés, etc.) ne sont pas microfilmés.

La reproduction, même partielle, de cette microforme est soumise à la Loi canadienne sur le droit d'auteur, SRC 1970, c. C-30.

NL-339 (r. 88/04)

Canada

THE UNIVERSITY OF ALBERTA

GEOGRID PULL-OUT TESTS IN CLAY

by

(C) MARIA ALICE DOS REIS COSTALONGA

A THESIS

SUBMITTED TO THE FACULTY OF GRADUATE STUDIES AND RESEARCH

IN PARTIAL FULFILMENT OF THE REQUIREMENTS FOR THE DEGREE

OF MASTER OF SCIENCE

DEPARTMENT OF CIVIL ENGINEERING

EDMONTON, ALBERTA

Fall of 1988

Permission has been granted to the National Library of Canada to microfilm this thesis and to lend or sell copies of the film.

The author (copyright owner) has reserved other publication rights, and neither the thesis nor extensive extracts from it may be printed or otherwise reproduced without his/her written permission.

L'autorisation a été accordée à la Bibliothèque nationale du Canada de microfilmer cette thèse et de prêter ou de vendre des exemplaires du film.

L'auteur (titulaire du droit d'auteur) se réserve les autres droits de publication; ni la thèse ni de longs extraits de celle-ci ne doivent être imprimés ou autrement reproduits sans son autorisation écrite.

ISBN 0-315-45610-8

THE UNIVERSITY OF ALBERTA

RELEASE FORM

NAME OF AUTHOR MARIA ALICE DOS REIS COSTALONGA

TITLE OF THESIS GEOGRID PULL-OUT TESTS IN CLAY

DEGREE FOR WHICH THESIS WAS PRESENTED MASTER OF SCIENCE

YEAR THIS DEGREE GRANTED Fall of 1988

Permission is hereby granted to THE UNIVERSITY OF ALBERTA LIBRARY to reproduce single copies of this thesis and to lend or sell such copies for private, scholarly or scientific research purposes only.

The author reserves other publication rights, and neither the thesis nor extensive extracts from it may be printed or otherwise reproduced without the author's written permission.

(SIGNED) Maria Alice R. Costalonga

PERMANENT ADDRESS:

SQN 203 - Bl J - ap 305

70833 - Brasilia - DF

Brazil

DATED Edm., July 12, 1988

THE UNIVERSITY OF ALBERTA

FACULTY OF GRADUATE STUDIES AND RESEARCH

The undersigned certify that they have read, and recommend to the Faculty of Graduate Studies and Research, for acceptance, a thesis entitled *Geogrid Pull-Out Tests in Clay* submitted by Maria Alice Dos Reis Costalonga in partial fulfilment of the requirements for the degree of Master of Science.

.....

Supervisor

.....

.....

.....

Date..July 12, 1988.....

ABSTRACT

This work analyses and discusses the results and mechanisms of a laboratory testing program on the interaction between soil and geogrids during pull-out. This research contributes to the limited knowledge of resistance of geogrids anchored in cohesive soil.

Reinforcement in an earth structure must be adequately safe against tensile and pull-out failures. Pull-out failure appears to be the more critical in the design procedure due to uncertainties in the soil-reinforcement interaction and pull-out characteristics. Assumptions about the magnitude of the maximum tensile force imposed in the reinforcement and the distribution of the tensile forces along the reinforcement are required in design procedures.

The load transfer method, as applied to axially loaded piles, was used to calculate the magnitude and distribution of the tension in the geogrids. The input required for the computation included the pull-out force-displacement curves, soil shear stress-displacement curves, the load-extension curves of the geogrids and the geometric characteristics of the geogrids, all of which were experimentally determined. Good agreement was found between predictions of the load transfer method and the experimental results.

To my parents, Avelino and Zoraide,

Stela, Isabela, Claudia

and

Flu

ACKNOWLEDGEMENTS

I wish to thank my parents for their continuing love and support. I am also grateful for the support and understanding of my sisters.

I would also like to express my appreciation to Dr. J.D. Scott for his supervision throughout this study.

Suggestions made during the experimental work by A. Negro and J. Brandt are appreciated.

Financial support for this research was provided by CNPq - Conselho Nacional de Desenvolvimento Cientifico e Tecnologico, Brazil, and through research funds provided by NSERC (National Science and Engineering Research Council) Operating Grant No. OGP 0872.

Mirafi Inc., Signode Corp. and Tensar Corp. are acknowledged for the material provided.

I would like to express my gratitude to Christine Hereygers and Steve Gamble whose assistance during the pull-out tests was really appreciated.

Special thanks to Tanya Schulz for typing this thesis.

Finally, I wish to thank Flavio Kuwajima. I am grateful for his invaluable suggestions throughout this work and help in writing the program to analyse the results.

LIST OF SYMBOLS

P_r	shear force component of bond
A_r	geogrid surface area = $W_r.L_r$
a_s	fraction of geogrid surface area that is solid
δ	friction angle beweensoil and reinforcement surface
γ	unit weight of soil
z	depth
σ'_b	effective bearing stress between soil and reinforcement
σ'_n	normal effective stress between soil and reinforcement
ϕ	angle of friction of soil
S_x	space between two consecutive anchor members
S	S_x
L_e	effective length of reinforcement in resistance
b	width of reinforcement = W_s
σ'_n	σ'_v
f^*	coefficient of bond
B	thickness of anchor member
S_i	initial degree of saturation
a_b	fraction of geogrid width over which bearing surface extends
a_B	a_b
N_c	bearing capacity factor
c_u	undrained shear strength of the soil
Σa_b	sum of the areas of the geogrid anchor members normal to the direction of pull-out

β	interfacial stress factor
Σa_s	sum of surface areas parallel to the direction of pull-out
ψ =	δ
DI	degree of interference for a grid and soil
P_p	maximum pull-out force for a grid with "n" anchor members
P_o	maximum pull-out force for an isolated anchor member of the same grid
ϕ_{RS}	angle of friction between sand and reinforcement
a	adhesion factor
w_i	initial moisture content
w_f	final moisture content
F_i	force at element i
F_{i+1}	force at element i+1
σ_i	axial stress in element i
A_i	cross section area of element i
ϵ_i	elongation or strain of element i
a,b	geogrid tensile parameter
A,B	soil shear strength parameters
e_o	initial void ratio
τ_u	peak undrained shear strength of the soil
τ_{tp}	total interfacial shear strength
τ_p =	τ_u
E	efficiency
E_c	cohesion efficiency
E_ϕ	friction efficiency

c	cohesion of soil
x_i	displacement of element i
A_{pi}	plane area of element i
A_{bi}	bearing area of element i
P_{bond}	maximum pull-out force
P_a	component of pull-out force due to adhesion
P_b	component of pull-out force due to bearing
c_v	coefficient of consolidation
D_{50}	grain diameter for 50% finer by weight
G	specific gravity

Table of Contents

Chapter — Page

1. INTRODUCTION 1

1.1 Statement of Problem 1

1.2 Objective of the Thesis 2

1.3 Organization of the Thesis 3

2. LITERATURE REVIEW 4

2.1 Introduction 4

2.2 Purpose of a Pull-Out Test 4

2.3 The Mechanisms of Interaction Between Soil and Geogrids in a Pull-Out Test 6

2.3.1 Mechanisms of Interaction between Soil and Reinforcement in a Pull-Out Test in Drained Conditions 8

2.3.1.1 Shear between Soil and Plane Surfaces 10

2.3.1.2 Soil Bearing on Surface Area Perpendicular to the Direction of the Pull-Out Force 11

2.3.2 Interaction between Soil and Reinforcement in Undrained Conditions 16

2.4 Factors Affecting the Pull-Out Test Results 17

2.5 Pull-Out Test Results 23

3. PROPERTIES OF THE SOIL AND REINFORCEMENTS 40

3.1 Introduction 40

3.2 Properties of the Cohesive Soil 40

3.2.1 Index, Particle Size and Specific Gravity Tests 40

3.2.2 Compaction Curve 42

3.2.3 Consolidation Test 42

3.2.4 Consolidated Undrained Shear Strength 42

3.3 Properties of the Reinforcements 49

4. PULL-OUT TEST 59
4.1 Introduction 59
4.2 Large Pull-out Apparatus 59
4.2.1 Pull-out Box 59
4.2.2 Horizontal Loading System 61
4.2.3 Vertical Loading System 64
4.3 Instrumentation 68
4.3.1 Pull-out Box Instrumentation 68
4.3.2 Geogrid Instrumentation 68
4.4 Sample Preparation 70
4.4.1 Soil Sample Preparation 70
4.4.1.1 Thickness of the Soil Sample 73
4.4.2 Geogrid Sample Preparation 74
4.5 Test Procedure and Tests Performed 75
4.5.1 Tests Performed 75
4.5.1.1 Calibration Tests 75
4.5.1.2 Other Tests 75
4.5.2 Test Procedure 77
5. PULL-OUT TEST RESULTS 81
5.1 Introduction 81
5.2 Pull-Out Test Results 81
5.2.1 Pull-Out Force 83
5.2.2 Progressive Horizontal Displacement 83
5.2.3 Passive Force at the Front Face of the Soil Sample 94
5.2.4 Vertical Displacement During Tests 95
6. LOAD TRANSFER APPROACH TO PREDICT THE TENSILE FORCES ALONG THE GEOGRIDS 114

6.1 Introduction 114

6.2 An Analytical Approach Based on the Load Transfer Method 114

6.3 Soil and Reinforcement Parameters 115

6.4 Interaction Between the Soil and Reinforcements in a Pull-Out Test 117

6.4.1 The Interfacial Stress Factor, β 117

6.4.2 The Bearing Capacity Factor, N_c 129

6.5 Analytical Determination of the Tensile Forces Along the Reinforcements 132

6.6 Effect of the Reinforcement Tensile Moduli on the Pull-Out Resistance 164

6.7 Contribution of each Mechanism of Interaction between Soil and Geogrid in the Total Pull-Out Force 179

6.8 Design Procedure to Predict the Required Anchoring Length of a Geogrid 181

7. CONCLUSIONS AND RECOMMENDATIONS FOR FUTURE RESEARCH 184

7.1 Summary 184

7.2 Conclusions 184

7.2.1 Analyses and Results 184

7.2.2 Test Apparatus and Procedure 185

7.3 Recommendations for Future Research 186

REFERENCES 187

A. PULL-OUT TEST RESULTS ON SILTY CLAY SOIL REINFORCED WITH PARAGRID 50S 191

B. CALIBRATION AND COMPLIANCE OF PULL-OUT APPARATUS ...198

C. Listing of the Basic Program which Calculates the Axial Force and Displacements along the Geogrids SR2 and TNX5001 203

List of Tables

Table		Page
2.1	Interface Frictional Angle (after Rowe et.al. 1985)	28
2.2	Summary of Pull-Out Test Results	39
3.1	Consolidated Undrained Direct Shear Test Results on Silty Clay	44
3.2	Properties of the Reinforcements	50
4.1	Average Distances Related to the Front End of the Pull-Out Box (cm)	76
5.1	Pull-Out Test Results	82
5.2	Force on Front End of the Soil Sample	105
6.1	Values of the Interfacial Stress Factor from Consolidated Undrained Direct Shear Tests	130
6.2	Values of the Interfacial Stress Factor from Consolidated Drained Direct Shear Tests	131
6.3	Soil Undrained Shear Strength Parameters and Geogrid Tensile Parameters	138
6.4	Contribution of Each Mechanism in the Maximum Pull-Out Force	180
A.1	Pull-Out Test Results on Silty Clay Reinforced with ParaGrid 50S	192
A.2	Force on Front End of the Soil Sample	193
B.1	Calibration Factors and Correlation Coefficients for Linear Variable Differential Transformers	199

List of Figures

Figure		Page
2.1	Pull-Out Failure along Length AB	5
2.2	Typical Configurations and Boundary Conditions which have been Adopted in Pull-Out Tests (modified from Jewell, 1980)	7
2.3	Bond Between Soil and Geogrid (modified from Jewell et.al., 1984)	9
2.4	Bearing Stresses on a Geogrid Anchor Member During Punching Failure, ϕ=35°, (modified from Jewell et.al., 1984	13
2.5	Factors Affecting the Value of the Coefficient of Bond f* (modified from Mitchell, J.K. and Schlosser, R.)	19
2.6	Effect of Wall Roughness on Pull-Out Test Results (modified from Palmeira, E.M. and Milligan, G.W.E., 1987)	22
2.7	Pattern of Displacement in Sand Parallel to a Grid Reinforcement (after Jewell, 1980) a) in a direct shear test and b) in a pull-out test	26
2.8	The Adhesion Factors Measured in a Pull-Out Test a) Netlon 1168 b) Terran Rf/12	29
2.9	The Required Length of Reinforcement to Prevent Sliding (after Salomone, 1978)	35
2.10	Tensile Force Along Reinforcement (after Holtz, 1978)	37
3.1	Grain Size Distribution, Devon Silty Clay	41
3.2	Compaction Curve	45
3.3	Consolidation Curve	46
3.4	Consolidated Undrained Direct Shear Test on Silty Clay	47
3.5	Consolidated Undrained Direct Shear Test on Silty Clay (Results from Graduate Laboratory)	48
3.6	Force Strain Curves of the SR2	51

Figure Page

3.7 Force Strain Curves of the TNX5001 52

3.8 Force Strain Curves of the ParaGrid 50S 53

3.9 Typical Force Strain Curves - SR2 and TNX5001 (modified from Beech, 1987) 57

4.1 Vertical Head Loading 66

4.2 Instrumentation of the Geogrid Samples with Piano Wire 71

5.1 Pull-Out Force and Displacement Curves for Silty Clay Reinforced with SR2 84

5.2 Pull-Out Force and Displacement Curves for Silty Clay Reinforced with TNX5001 85

5.3 Progressive Displacements, SR2, 20 kPa 86

5.4 Progressive Displacements, SR2, 50 kPa 87

5.5 Progressive Displacements, SR2, 51 kPa 88

5.6 Progressive Displacements, SR2, 102.5 kPa 89

5.7 Progressive Displacements, TNX5001, 20 kPa 90

5.8 Progressive Displacements, TNX5001, 50 kPa 91

5.9 Progressive Displacements, TNX5001, 51.7 kPa 92

5.10 Progressive Displacements, TNX5001, 100.7 kPa 93

5.11 Pull-Out Force - Horizontal Force at Front End of the Box, SR2, 20 kPa 96

5.12 Pull-Out Force - Horizontal Force at Front End of the Box, SR2, 50 kPa 97

5.13 Pull-Out Force - Horizontal Force at Front End of the Box, SR2, 51 kPa 98

5.14 Pull-Out Force - Horizontal Force at Front End of the Box, SR2, 102.5 kPa 99

5.15 Pull-Out Force - Horizontal Force at Front End of the Box, TNX5001, 20 kPa 100

Figure Page

5.16 Pull-Out Force - Horizontal Force at Front End of the Box, TNX5001, 50 kPa 101

5.17 Pull-Out Force - Horizontal Force at Front End of the Box, TNX5001, 51.7 kPa 102

5.18 Pull-Out Force - Horizontal Force at Front End of the Box, TNX5001, 100.7 kPa 103

5.19 Soil Sample Behaviour During Pull-Out Test, SR2, 20 kPa 106

5.20 Soil Sample Behaviour During Pull-Out Test, SR2, 50 kPa 107

5.21 Soil Sample Behaviour During Pull-Out Test, SR2, 51 kPa 108

5.22 Soil Sample Behaviour During Pull-Out Test, SR2, 102.5 kPa 109

5.23 Soil Sample Behaviour During Pull-Out Test, TNX5001, 20 kPa 110

5.24 Soil Sample Behaviour During Pull-Out Test, TNX5001, 50 kPa 111

5.25 Soil Sample Behaviour During Pull-Out Test, TNX5001, 51.7 kPa 112

5.26 Soil Sample Behaviour During Pull-Out Test, TNX5001, 100.7 kPa 113

6.1 Model of Interaction Between Cohesive Soil and Geogrid in a Pull-Out Test 118

6.2 Stress-Strain Fitting and Measured Curves of Tensile Test on a Constant Cross Section of SR2, 20 kPa 119

6.3 Force-Strain Fitting and Measured Curves during Pull-Out Test, SR2, 20 kPa 120

6.4 Stress-Strain Fitting and Measured Curves of Tensile Test on a Constant Cross Section of SR2, 50 kPa 121

6.5 Force-Strain Fitting and Measured Curves during Pull-Out Test, SR2, 50 kPa 122

6.6 Stress-Strain Fitting and Measured Curves of Tensile Test on a Constant Cross Section of SR2, 51 kPa 123

Figure Page

6.7 Force-Strain Fitting and Measured Curves during Pull-Out Test, SR2, 51 kPa 124

6.8 Stress-Strain Fitting and Measured Curves of Tensile Test on a Constant Cross Section of SR2, 102.5 kPa 125

6.9 Force-Strain Fitting and Measured Curves during Pull-Out Test, SR2, 102.5 kPa 126

6.10 Plan and Cross Section Views of a SR2 Tension Member 134

6.11 Plan and Cross Section Views of a TNX5001 Tension Member 135

6.12 Fitting Curve of the Soil Undrained Shear Strength. Parameters Used in the SR2 20 kPa Analysis 139

6.13 Fitting Curve of the Soil Undrained Shear Strength. Parameters Used in the SR2 50 kPa Analysis 140

6.14 Fitting Curve of the Soil Undrained Shear Strength. Parameters Used in the SR2 51 kPa Analysis 141

6.15 Fitting Curve of the Soil Undrained Shear Strength. Parameters Used in the SR2 102.5 kPa Analysis 142

6.16 Fitting Curve of the Soil Undrained Shear Strength. Parameters Used in the TNX5001 20 kPa Analysis 143

6.17 Fitting Curve of the Soil Undrained Shear Strength. Parameters Used in the TNX5001 50 kPa Analysis 144

6.18 Fitting Curve of the Soil Undrained Shear Strength. Parameters Used in the TNX5001 51.7 kPa Analysis 145

6.19 Fitting Curve of the Soil Undrained Shear Strength. Parameters Used in the TNX5001 100.7 kPa Analysis 146

6.20 Progressive Displacements along the Geogrid SR2, 20 kPa 148

6.21 Progressive Displacements along the Geogrid SR2, 50 kPa 149

Figure Page

6.22 Progressive Displacements along the Geogrid SR2, 51 kPa 150

6.23 Progressive Displacements along the Geogrid SR2, 102.5 kPa 151

6.24 Progressive Displacements along the Geogrid TNX5001, 20 kPa 152

6.25 Progressive Displacements along the Geogrid TNX5001, 50 kPa 153

6.26 Progressive Displacements along the Geogrid TNX5001, 51.7 kPa 154

6.27 Progressive Displacements along the Geogrid TNX5001, 100.7 kPa 155

6.28 Tensile Force along Geogrid SR2, 20 kPa 156

6.29 Tensile Force along Geogrid SR2, 50 kPa 157

6.30 Tensile Force along Geogrid SR2, 51 kPa 158

6.31 Tensile Force along Geogrid SR2, 102.5 kPa 159

6.32 Tensile Force along Geogrid TNX5001, 20 kPa 160

6.33 Tensile Force along Geogrid TNX5001, 50 kPa 161

6.34 Tensile Force along Geogrid TNX5001, 51.7 kPa 162

6.35 Tensile Force along Geogrid TNX5001, 100.7 kPa 163

6.36 Measured and Calculated Values of Pull-Out Force, SR2, 20 kPa 165

6.37 Measured and Calculated Values of Pull-Out Force, SR2, 50 kPa 166

6.38 Measured and Calculated Values of Pull-Out Force, SR2, 51 kPa 167

6.39 Measured and Calculated Values of Pull-Out Force, SR2, 102.5 kPa 168

6.40 Measured and Calculated Values of Pull-Out Force, TNX5001, 20 kPa 169

Figure Page

6.41 Measured and Calculated Values of Pull-Out Force, TNX5001, 50 kPa 170

6.42 Measured and Calculated Values of Pull-Out Force, TNX5001, 51.7 kPa 171

6.43 Measured and Calculated Values of Pull-Out Force, TNX5001, 100.7 kPa 172

6.44 Progressive Displacement Along the Geogrid TNX5001, 20 kPa, β=0.7 173

6.45 Tensile Force Along Geogrid TNX5001, 20 kPa, β=0.7 174

6.46 Predicted Tensile Forces along Geogrids SR2 (51 kPa) and TNX5001 (51.7 kPa) at Pull-Out Displacement of 4 mm 175

6.47 Predicted Tensile Forces along Geogrids SR2 (51 kPa) and TNX5001 (51.7 kPa) at Pull-Out Displacement of 8 mm 176

6.48 Predicted Tensile Forces along Geogrids SR2 (102.5 kPa) and TNX5001 (100.7 kPa) at Pull-Out Displacement of 4 mm 177

6.49 Predicted Tensile Forces along Geogrids SR2 (102.5 kPa) and TNX5001 (100.7 kPa) at Pull-Out Displacement of 22 mm 178

6.50 Contribution of Each Mechanism of Interaction between Soil and Geogrid in the Maximum Pull-Out Force 183

A.1 Pull-Out Force and Displacement Curve, ParaGrid, 50 kPa 194

A.2 Pull-Out Force and Displacement Curve, ParaGrid, 20 kPa 195

A.3 Progressive Horizontal Displacement, ParaGrid 50 kPa 196

A.4 Progressive Horizontal Displacement, ParaGrid 20 kPa 197

B.1 Calibration Curve for Load Cell 20790 200

B.2 Calibration Curve for Load Cell 1 200

B.3 Calibration Curve for Load Cell 2 201

Figure Page

B.4 Calibration Curve for Load Cell 3 201

B.5 Calibration Curve for Load Cell 4 202

C.1 Flow Chart 204

List of Plates

Plate		Page
3.1	Tensar SR2	54
3.2	Signode /ITW TNX5001	54
3.3	ParaGrid 50S	55
4.1	Large Pull-Out Box	63
4.2	Horizontal Loading System	63
4.3	Vertical Head Loading	67
4.4	Detail of the Geogrid Instrumentation Outside the Pull-Out Box	72

1. INTRODUCTION

1.1 Statement of Problem

Few areas of geotechnical engineering have developed so quickly as has soil reinforcement. In the past twenty years geosynthetics have come to play a major role in geotechnical engineering. Synthetic nets, developed by Netlon Ltd., U.K., were used for the first time in 1967 in a civil engineering project. This field trial, the reinforcement of a soft ground in Japan, was successful and inspired the development of geogrids (Giroud, 1986). Reinforced soil walls of many types have been used extensively worldwide replacing traditional concrete and timber retaining structures. The geosynthetic reinforcement improves the stability of these structures against shear failure.

The modes of failure of a reinforcing layer include sliding failure of the soil mass along the geosynthetic surface and pull-out failure of the geosynthetic. In the second mode of failure, the geosynthetic has the function of bonding together the active and passive zones. The reinforcement must be capable of resisting pull-out from the restraint zone (Ingold, 1980). The pull-out test seems to be the most adequate test to model this type of interaction between soil and reinforcement. The mechanism of interaction between soil and reinforcement in a pull-out test is similar to the bond between concrete and reinforcement in reinforced conrete structures. The bond under undrained or drained

shear conditions comprises shear along the planar surface of the reinforcement and bearing against the anchor members of the reinforcement. Both mechanisms are functions of the physical properties of the soil, the normal stress acting on the reinforcement plane and the geometry of the reinforcement. The interaction mechanisms between soil and reinforcement is of major concern in design methods for reinforced structures.

Many studies have been made on the behaviour mechanisms in a pull-out test. Most of the studies used granular soils and the reinforcing materials included both smooth and rough sheets, strips of metal and geotextiles of various widths and lengths. Interaction data for other reinforcements and soil types are needed. At the present time, neither a standard test apparatus nor a standard procedure exists for the pull-out test.

1.2 Objective of the Thesis

The main objective of this study is to determine the mechanism of load transfer between soil and reinforcement for a cohesive soil in a pull-out test. To achieve this objective, a large pull-out box apparatus was designed and constructed and the test procedure necessary to obtain the required information was developed.

1.3 Organization of the Thesis

Published information concerning pull-out test methods, mechanisms of interaction between soil and reinforcement and published results of these studies are reviewed in Chapter 2. Chapter 3 contains index and strength properties of the cohesive soil used in this research. In addition, the geometric and tensile properties of the geogrids are presented.

A description of the laboratory apparatus and the test procedure and the instrumentation employed in the experimental program are presented in Chapter 4. The experimental results and discussion of the tests on the reinforced silty clay soil are presented in Chapter 5. The analysis and discussion of the pull-out test results are included in Chapter 6.

Chapter 7 presents the summary of the main conclusions drawn from this research, as well as recommendations for future research.

2. LITERATURE REVIEW

2.1 Introduction

This chapter presents a summary of the literature review on pull-out tests. The mechanism of interaction between soil and reinforcement during a pull-out test is presented. The scale and factors affecting the pull-out test results are described. Pull-out test conclusions drawn from research mainly in granular soil reinforced with either metal or geosynthetic materials are summarized.

2.2 Purpose of a Pull-Out Test

The mechanism of reinforcement in the context of a reinforced earth structure is not a trivial phenomenon and depends on the stress field in operation (Ingold, 1980). This mechanism is manifested in many structures including reinforced earth walls where an important function of the reinforcement is to bond the "active zone" and the "restrained zone" in the soil mass (Schollsser, 1978). Figure 2.1 illustrates the pull-out mechanisms of failure in a reinforced soil structure. The reinforcement must be capable of resisting pull-out from the restrained zone. A similar mechanism occurs in reinforced earth embankments. Since phenomena such as the development of friction between soil and reinforcement, the transfer of shear stress in the soil mass to the reinforcement and the thickness of the zone of influence of the reinforcement in the soil mass are to be

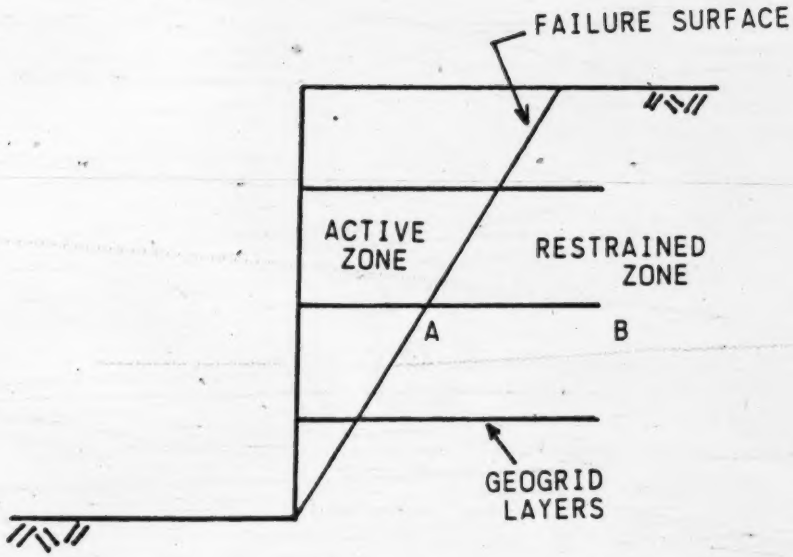

Figure 2.1 Pull-Out Failure along Length AB

analysed, a suitable model test is best described by the pull-out test (Holtz, 1977). Lee (1978) in a state-of-the-art paper, drew attention to the research work and papers developed in soil reinforcement dealing with shear resistance. Different interpretations and some apparent contradictions seemed to exist in the data from pull-out tests and direct shear tests on granular soils reinforced with either smooth or rough sheets and strips. Some of the results appeared difficult to explain in terms of the usual concepts of shear strength properties of granular soils and sliding friction between materials. The main conclusion drawn from these various studies was that much work was still required in order to develop generally accepted answers.

Figure 2.2 illustrates typical configurations and boundary conditions that have been adopted for pull-out tests.

2.3 The Mechanisms of Interaction Between Soil and Geogrids in a Pull-Out Test

Jewell et.al. (1984) presented the mechansims of interaction between soil and grid reinforcements. The interaction is similar to the bond between concrete and reinforcment in reinforced concrete and therefore is referred to as bond.

The rate of change of axial force along reinforcement embedded in soil is limited by bond strength. The

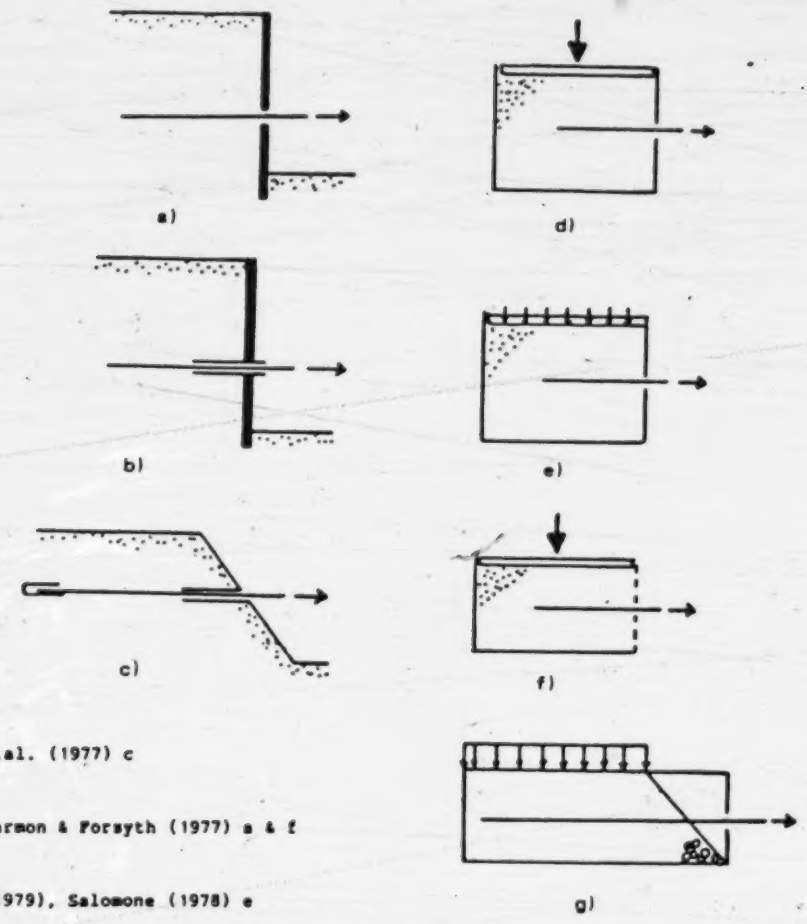

Alimi et.al. (1977) c

Chang, Harmon & Forsyth (1977) a & f

Ingold (1979), Salomone (1978) e

Murray, Carder & Krawczyk (1979)a

Schlosser & Elias (1978), Collios (1981) d

Schlosser & Guilloux (1979) b

Shen et.al. (1979) a & e

Mowafy (1986) g

Figure 2.2 Typical Configurations and Boundary Conditions which have been Adopted in Pull-Out Tests (modified from Jewell, 1980)

distribution and changes in axial force close to the free end of the reinforcement embedded in the soil in an embankment or retaining wall are important to evaluate the length of reinforcement required to enable the axial force to be generated. The axial reinforcement force is caused by the development of linear soil strains in the direction of the reinforcement. A stiff reinforcement will resist such strains which, in the case of tensile strains in the reinforced soil, results in axial tensile force in the reinforcement.

Only two mechanisms of interaction are applied in the case of pull-out failure since there is no soil to soil resistance developed as there is no relative movement of the soil on either side of the reinforcement. The two mechanisms are:

1. soil shearing on plane surface areas of the reinforcement, and
2. soil bearing or passive soil resistance developed against bearing surfaces normal to the direction of the force to be resisted.

The two mechanisms are illustrated in Figure 2.3.

2.3.1 Mechanisms of Interaction between Soil and Reinforcement in a Pull-Out Test in Drained Conditions

The transfer of stress between soil and reinforcement in a pull-out test is by two components: friction and passive soil resistance or lateral bearing capacity. Both

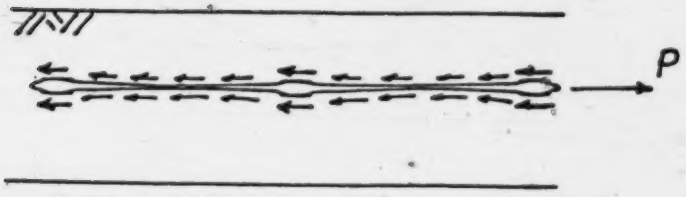

a) Shear on Plane Surface

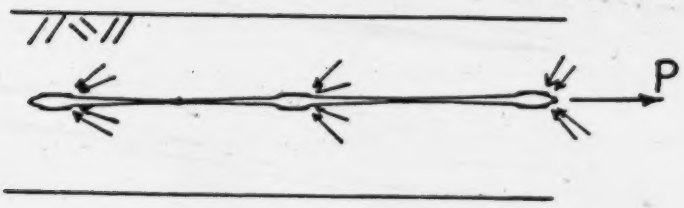

b) Bearing Against Anchor Members

Figure 2.3 Bond Between Soil and Geogrid (modified from Jewell et.al., 1984)

mechanisms are present in many reinforcement systems.

Mitchell (1987) discussed both mechanisms of interaction. Pull-out tests, model tests and measurements on full scale structures are used to determine the effective coefficient of friction between soil and reinforcement as well as the passive soil resistance developed against bearing surfaces normal to the direction of force being resisted. For example, the values of coefficient of friction for strip reinforcements range from 0.5 for smooth reinforcement and large burial depths to more than 1.0 for rough or ribbed reinforcements and small overburden depths.

2.3.1.1 Shear between Soil and Plane Surfaces

The shear force component of bond for a reinforcement grid of length L_r and width W_r placed horizontally in granular soil under self weight loading provides the following maximum force (Jewell et.al., 1984).

$$P_r = 2A_r a_s \gamma z \tan\delta \qquad [2.1]$$

where

A_r = geogrid surface area = $W_r L_r$

a_s = fraction of geogrid surface area that is solid

γ = unit weight of soil

z = depth

δ = friction angle between soil and reinforcement surface

2.3.1.2 Soil Bearing on Surface Area Perpendicular to the Direction of the Pull-Out Force

The passive soil resistance to reinforcement pull-out develops against bearing surfaces normal to the direction of the force to be resisted. This is similar to the pressure on the base of deep foundations in soil. Parameters such as soil density, foundation depth and size of bearing area have an important influence on bearing pressures. They are not a function of the soil friction angle.

Jewell et.al. (1984) discussed a theoretical estimation of bearing stress for geogrids embedded in sand. The relationship among bearing effective stress σ'_b, vertical stress σ'_n, and soil friction angle is presented in the form of a chart. The lower bound curve is associated with a punching failure mode in soil (Figure 2.4). In this case, $\sigma'_n=\gamma z$ and the relationship is:

$$\frac{\sigma'_b}{\sigma'_n} = e^{(\frac{\pi}{2}+\phi)\tan\phi}.\tan(\frac{\pi}{4}+\frac{\phi}{2}) \qquad [2.2]$$

The upper bound relationship is found by taking the conventional stress characteristic field for a footing foundation (Prandtl, 1921; Reissner, 1923) rotated to the horizontal position. The horizontal stress in the soil is assumed to be $\sigma'_h=\sigma'_v=\sigma'_n$. The relationship is as follows:

$$\frac{\sigma'_b}{\sigma'_n} = e^{\pi\tan\phi}.\tan^2(\frac{\pi}{4}+\frac{\phi}{2}) \qquad [2.3]$$

Jewell et.al. (1984) reported that pull-out test results from experimental data on grids and anchors embedded in sand agreed well with the theoretical prediction despite the large spread and variability of the test results. All the data were bounded by the lower and upper predictions given by the previous equations.

Theoretical expressions for estimating the reinforcement pull-out capacity are presented by Mitchell, (1987). For the particular case of Tensar geogrid the expression is as follows:

$$P = L_e b \gamma z [2\alpha_s \tan\delta + \frac{\sigma'_b}{\sigma'_n} \frac{t}{S_x} \alpha_b] \qquad [2.4]>$$

$$\text{for } 5 < \frac{\sigma'_b}{\sigma'_v} < 100$$

where

S_x = space between two consecutive anchor members

L_e = effective length of reinforcement in the resisting zone

b = width of reinforcement

γ = unit weight of soil

z = depth

α_s = fraction of geogrid surface area that is solid

δ = friction angle between soil and reinforcement surface

σ'_b = bearing effective stress on anchor members

$\sigma'_n = \sigma'_v$ = vertical effective stress

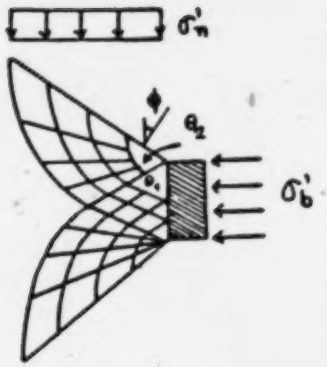

$$\theta_1 = \theta_2 = 45 + \frac{\phi}{2}$$

$$\frac{\sigma'_b}{\sigma'_n} = e^{(90+\phi)\tan\phi} \cdot \tan\left(45+\frac{\phi}{2}\right)$$

Figure 2.4 Bearing Stresses on a Geogrid Anchor Member During Punching Failure, ϕ=35°, (modified from Jewell et.al., 1984

a_b = fraction of geogrid width over which bearing surface extends

t = thickness of anchor member

Two general assumptions are used for the prediction of the Tensar geogrid pull-out capacity: these are the frictional and the bearing resistances between reinforcement and soil. The limit $5<\frac{\sigma'_b}{\sigma'_v}<100$ stands for the average curve between lower and upper bound curves of predictions of $\frac{S_x}{t}$ to have a fully rough bond.

The derivation of equation 2.4 can be performed by following the derivation of the theoretical expression for bond strength proposed by Jewell et.al., 1984.

$$f^* = a_s\frac{\tan\delta}{\tan\phi} + \frac{\sigma'_b}{\sigma'_n}\cdot\frac{B}{S}\cdot\frac{a_B}{2\tan\phi} \qquad [2.5]$$

where

f^* = coefficient of bond

B = thickness of anchor members

S = space between two consecutive anchor members

a_B = a_b (equation 2.4)

In Jewell et.al. (1984), it is suggested that values of σ'_b/σ'_n be measured directly in pull-out tests. The length of the geogrid reinforcement should be relatively short and the reinforcement should be embedded in soil remote from rigid boundaries. The anchor members should be widely spaced to ensure that full bearing stress develops on each member. However, if this ratio cannot be determined, the pull-out

test result can be used directly to estimate the total bond coefficient for the grid.

Milligan and Palmeira (1987) also discussed the prediction of bond between soil and reinforcement. They reported that equations 2.3 and 2.3 assumed that the soil may be treated as a continuum. This assumption is not valid in the case of coarse-grained soils and grids where the dimensions of the anchor members may be relatively small in comparison with the average particle size of the soil. They showed that the value of σ'_b/σ'_n increases significantly when B/D_{50} is less than about 15. However, equation 2.2 may provide safe design values when B/D_{50} exceeds 15.

The degree of interference between anchor members also influences the values of bond between soil and reinforcement. When S/B is smaller than 50, the value of bond will be markedly affected by interference.

The average particle size cannot be very large compared with the aperture of the grids otherwise, interlock of the soil into the grid may not occur. This will reduce the bond. When the grid aperture size is about the same as the soil D_{50} size, there is likely to develop sufficient interlock for the grid. Mowafy (1986) suggested that the soil particle size be equal to one quarter to one third of the smallest mesh dimension for meshes immersed in sandy soil. These dimensions will provide good confinement resistance components.

2.3.2 Interaction between Soil and Reinforcement in Undrained Conditions

Ingold (1984) showed that similar theory can be applied to the undrained analysis of interaction between soil and reinforcement in a pull-out mechanism. The equation proposed by Ingold combines two simple mechanisms: adhesion (instead of friction) and bearing forces. The expression is as follows:

$$T = N_c c_u \Sigma a_b + \beta c_u \Sigma a_s \qquad [2.6]$$

where the first member is the product of a bearing capacity factor, N_c, the undrained shear strength of the clay, c_u, and the sum of the areas of the geogrid anchor members, Σa_b, normal to the direction of pull-out. The second term relates the surface adhesion, βc_u, generated on the sum of the surface area, Σa_s, parallel to the direction of pull-out. The equation is a general expression which can be developed for a planar punched grid or a welded rod grid.

In his thesis, Ingold (1980) used values of 7.5 and 0.5 for N_c and β respectively, which resulted in good agreement between measured and calculated adhesion factors. The mean measured value was 0.39 and the calculated value was 0.38. The soil was a kaolin clay and Weldmesh 5119 was used for reinforcement. He concluded that since the factors of bearing capacity and adhesion are reasonable, it indicates that the general equation 2.6 was of correct form. Koerner,

Martin and Koerner (1986) worked on geomembranes and defined efficiency values which are explained in more detail in Chapter 6.

Ingold (1984) also showed the influence of grid geometry in the value of the adhesion factor. Taking a unit grid cell and calling $n_x D$ the space between two consecutive anchor members and $n_y D$, the space between two tension members, where D is the equivalent member diameter and rearranging equation 2.6, a plot of dimensionless spacing n_y versus adhesion factor α is presented for various values of dimensionless n_x. From the theoretical analysis, it was concluded that a grid with $n_x=4$ and $n_y>6$ was the most efficient in terms of adhesion factor ($\alpha=0.9$); however, larger transverse rod spacing might be very economic.

Milligan and Palmeira (1987) also supported the value of N_c equal to 7.5, a value based on cavity expansion in stiff compacted clay. They also reported that the interference between anchor members is not a significant factor for grids of typical geometry with S/B>5.

2.4 Factors Affecting the Pull-Out Test Results

The factors affecting the values of the apparent friction coefficient were reviewed and summarized by Schlosser and Elias (1978) and by McKittrick (1978). It is clear that both peak and residual values of f^* are functions of the soil type, density, effective normal stress, geometric factors and surface roughness. Figure 2.5

illustrates significant factors affecting the values of f^*. Increasing soil density results in increased f^* because the soil friction angle increases when density increases and the denser the soil, the more dilatant it is.

Reinforcement with roughened surface gives greater values of f^* than smooth strips. The bearing force contribution for a rough strip might contribute significantly to the value of f^*.

As the overburden suppresses dilation there is a decrease in f^* with an increase in overburden. In Figure 2.5, $\psi=\delta$ (friction angle between soil and reinforcement surface).

Palmeira and Milligan (1987) reported on scale and other factors affecting the results of pull-out tests of grids buried in sand. Differences in boundary conditions and scale lead to limitations in the modelling of the problem.

Two boxes were used in the research. A small one (25.3 cm long, 15.0 cm wide, 20 cm deep) and a large one (100 cm long, 100 cm wide, 100 cm deep). The normal stress was applied by rubber bags filled with water in order to provide uniform distribution of the vertical pressure on top of the soil sample. Three types of dry Leighton Buzzard sand were used. Mild steel and galvanized steel grids were employed.

They showed the influence of the top boundary in the test results. Two tests were run, one using a rigid plate to apply the vertical pressure and the other a flexible bag filled with water. A decrease in the friction coefficient

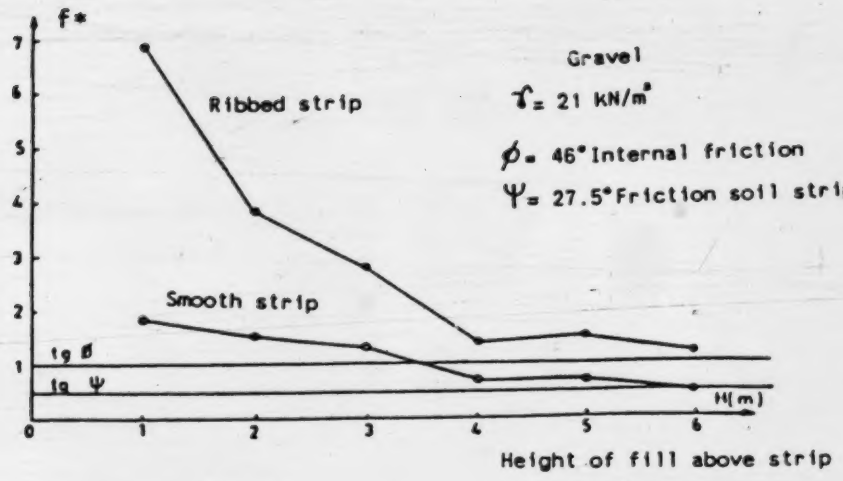

Influence of Overburden

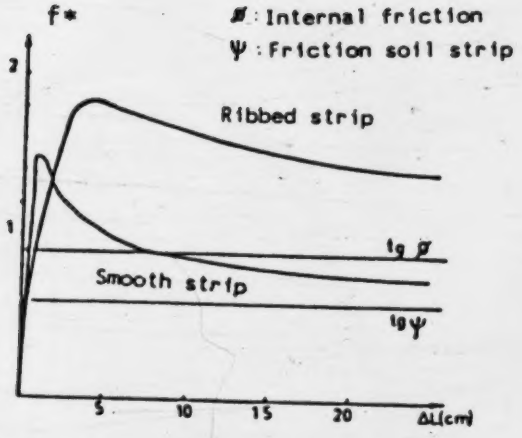

Influence of the Nature of the Surface

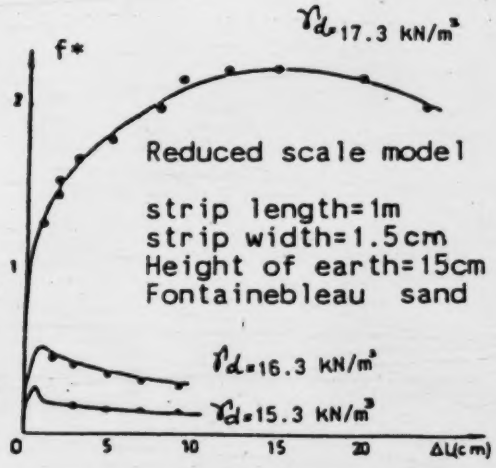

Influence of the Density

Figure 2.5 Factors Affecting the Value of the Coefficient of Bond f* (modified from Mitchell, J.K. and Schlosser, R.)

was obtained when using a flexible top boundary. Both tests led to values of apparent friction angles higher than the angle of internal friction of the sand alone.

The degree of roughness of the front wall of the box affects the pull-out test results. The friction coefficient between soil and reinforcement can be severely overestimated due to friction on the internal side of the front wall in small scale tests (box dimensions 25.3 cm long, 15 cm wide, 20 cm deep). By increasing the size of the front wall, the influence is minimized but should be taken into account for friction coefficient calculations. Figure 2.6 illustrates the effect of wall roughness on pull-out test results.

The interference between consecutive anchor members was once again investigated. Factors, such as soil particle size, surface characteristics, diameter, the spacing and the number of anchor members definitely control the interference between anchor members. Based on the concept of degree of interference in a grid, another term is added to the expression of bond coefficient, f^*, (Jewell, 1984). The resulting expression is:

$$f^* = a_s \frac{\tan\delta}{\tan\phi} + \frac{1-DI}{2\tan\phi} \cdot \frac{B}{S} \cdot \frac{\sigma'_b}{\sigma'_n} \cdot a_B \qquad [2.7]$$

where DI = degree of interference for the grid and soil

$$DI = 1 - \frac{P_p}{nP_o}$$

where,

P_p = maximum pull-out force for a grid with "n" anchor members

P_o = maximum pull-out force for an isolated anchor member of the same grid

It was observed that interference became negligible for values of S/B>50.

Large scale pull-out tests on sand reinforced with Tensar SR2 were carried out by the Department of Civil Engineering at the University of California (1984). The inside dimensions of the box were 137 cm long, 91 cm wide and 51 cm deep. Two pressure cells were installed on the front end of the box: cell #1, 63.5 cm below the slot and cell #2, 17.8 cm above the slot. For the applied pressure of 40.7 kPa, cell #1 measured 33.5 kPa, which gave a value of K_o of around 0.85. During the test, the lateral pressure increased to some value of pull-out force at failure. Values of pressure for load cell #2 were not reliable due to arching conditions. One test was carried out without the front end of the pull-out box. The maximum pull-out force was increased by 40%. The increase was thought to be due to lack of soil confinement which caused the transmission of the total normal pressure to the full length of the reinforcement. Error was also likely to be the cause of the increase in the pull-out force.

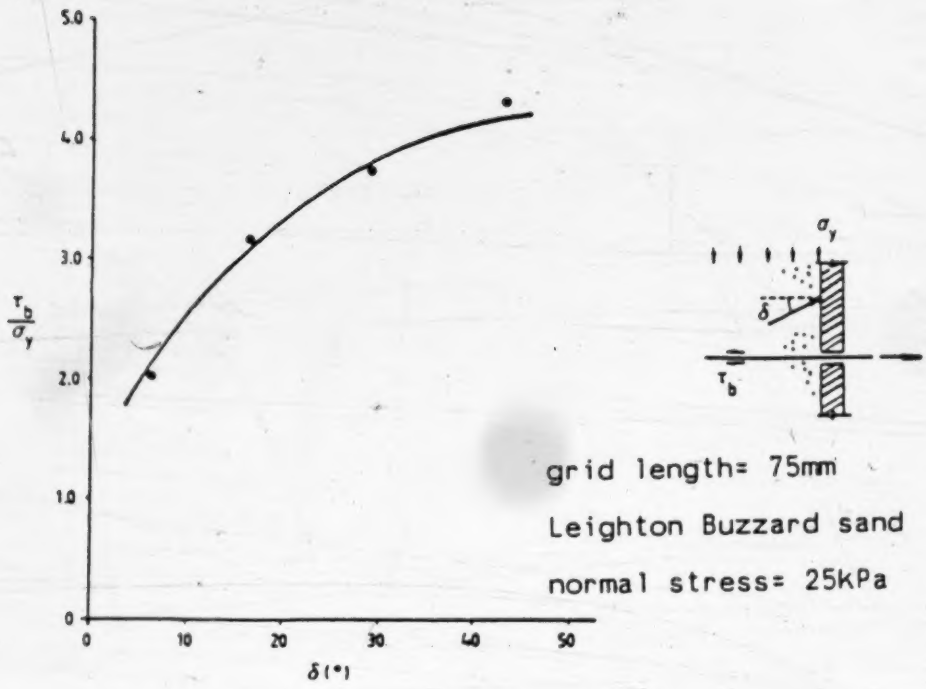

Figure 2.6 Effect of Wall Roughness on Pull-Out Test Results (modified from Palmeira, E.M. and Milligan, G.W.E., 1987)

2.5 Pull-Out Test Results

Jewell (1980) conducted a series of pull-out tests as part of his research programme. The main objectives were to investigate whether the pull-out test could model the interaction between sand and reinforcement in a shear apparatus, to investigate how the results from pull-out tests might be interpreted, and to draw conclusions about the angle of friction between sand and reinforcement, ϕ_{RS} which is needed in the analyses of reinforced earth. The pull-out box was 25.3 cm long, 15.0 cm wide, 20.0 cm deep. The soil employed was a dense Leighton Buzzard sand, and the reinforcements were of three kinds: closed coiled tension spring type 3, artificially stiffened tension spring type 3 and steel grid (bar radius = 0.82 mm).

He concluded that the pull-out displacement required to mobilize the peak pull-out force for a grid was approximately twice as large as for the bar. The loss of pull-out force with continued displacement, after peak, was much more gradual and controlled for the grid. Also, the zone of influence (zone of major strain in the sand) was confined to a band of 20 mm thickness above and below the reinforcement grid. The displacements and strains in the sand were measured using radiography.

The interference between anchor members was also investigated during the pull-out test. The maximum pull-out force increased as the number of bars was increased, but the pull-out displacement required to mobilize the peak force

remained constant and independent of the number of bars used in the tests.

The load-displacement curves of a grid or a bar immersed in sand undergoing shear is different from the curves in a pull-out mechanism. While in the first, the load does not drop with increasing displacement, the pull-out curves have a well defined peak pull-out force with displacement. Furthermore, the pattern of displacement in sand in the direction parallel with a reinforcement grid in a shear test is very different from the pattern in pull-out tests. The magnitude and orientation of the principal strains which develop in sand reinforced by a grid and loaded in shear are different from the ones in pull-out. Figure 2.7 illustrates the patterns of displacement in sand during a direct shear and a pull-out test on a steel bar. These factors led Jewell to the conclusion that a pull-out test cannot model the mechanism that occurs in sand reinforced by either a grid or a bar in a shear test. This idea supports the necessity to run pull-out tests.

Jewell (1980) also concluded that the apparent coefficient of friction between sand and reinforcement derived for a pull-out test was not a fundamental parameter as it depends on the stress level, either σ_n or σ_{RS}. σ_{RS} is defined as the normal stress on the surface of circular bar reinforcement, $\sigma_{RS} = f(\sigma_n, K_o)$.

Ingold (1980) carried out pull-out tests in both sand and clay soils. The reinforcements were polymer net

structures, polymer fabrics, mild steel sheet and steel rod mesh. The pull-out box had the following internal dimensions: 50 cm long, 29 cm wide and 30 cm deep. A reinforced rubber water bag was used to distribute the normal force.

Ingold also compared results from both direct shear and pull-out tests. While the apparent coefficient of friction measured in the direct shear test for sand reinforced with polymer nets and steel sheet and steel rod mesh ranged from 0.6 to 1, with a mean value of 0.95, the same value was about 0.86 when measured in a pull-out test.

For the undrained analyses with kaolin clay reinforced with either Netlon 1168 (polypropylene, diamond mesh) or Terran RF/12 (polyethylene and polypropylene, composite), the difference was even greater. The adhesion factors measured in the direct shear test were 0.86 and 0.89 for TERRAM RF/12 and NETLON 1168, respectively. The values obtained from pull-out tests were 0.16 and 0.18 respectively. These results are illustrated in Figure 2.8. The adhesion factor is defined as:

$$\alpha = \frac{N_c c_u \Sigma a_b + \beta c_u \Sigma a_s}{P} \qquad [2.8]$$

where P is the maximum measured pull-out force.

It was concluded that a different mechanism is involved in the two types of tests. The frictional resistance observed for the stiffer reinforcement in the shear tests

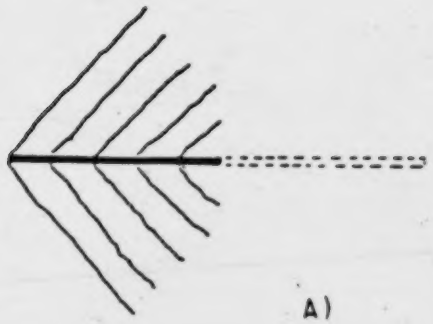

A)

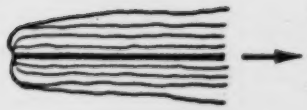

B)

Figure 2.7 Pattern of Displacement in Sand Parallel to a Grid Reinforcement (after Jewell, 1980) a) in a direct shear test and b) in a pull-out test

was lower than that in the pull-out test. For the more extensible fabrics, while the pull-out resistance presented a pronounced levelling of pull-out resistance with increasing normal stress levels, the values of angle of bond stress remained constant and independent of the normal stress level.

The limited study of undrained pull-out resistance led to the following conclusions: the adhesion factor could be evaluated from the pullout test results once the undrained shear strength of the soil and the geometry of the reinforcement are known. The measured and calculated values of factors of adhesion were in good agreement.

Another important conclusion was that factors of adhesion calculated from undrained shear box tests were much higher than those measured in a pull-out test. The reason for the difference between factors of adhesion measured in the two tests is likely to be a function of the relative stiffness of the reinforcement and the soil.

Rowe et.al. (1985) studied the soil-geotextile/geogrid interface strength in a direct shear and in a pull-out box. The soils used were a conventional granular fill and a lightweight fill (sawdust). Six kinds of geotextiles and Tensar SR2 geogrid were tested. The results from pull-out tests and direct shear tests on natural fill (ϕ=31°) are illustrated in Table 2.1. As can be seen, the values of interface shear friction angles are in good agreement with one another except for the Tensar geogrid. The lower value

Table 2.1 Interface Frictional Angle (after Rowe et.al. 1985)

Geotextile	Pullout	Direct Shear
None	-	31°-32°
Permaliner M1195	32°	32°
Mirafi P600 X	32°	32°
Mirafi P500	32°	32°
Geolon 1250	35°	35°
Terrafix 370RS	37°	36°
Terrafix 1200R	36°	36°
Tensar SR2*	18°	30°

*Tests in the longitudinal direction.

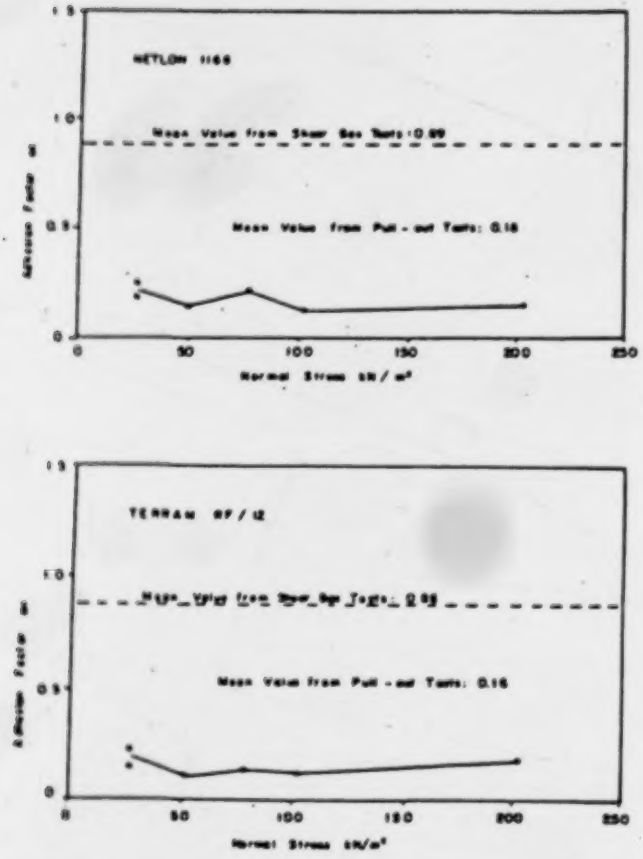

Figure 2.8 The Adhesion Factors Measured in a Pull-Out Test a) Netlon 1168 b) Terran Rf/12

of shear friction from the pull-out test compared with the direct shear test is due to the difference in interface mechanisms. Moreover, a pull-out test on a single tension member of the Tensar SR2 resulted in interface friction angle of 29°. As the Tensar SR2 geogrid consists of 45% solids, the apparent friction angle due to soil-geogrid interface friction was about 14°, ($\tan^{-1}(0.45\tan 29°)$), and the other 4° was due to the passive resistance against the anchor members.

Large scale pull-out tests on sand reinforced with Tensar SR2 geogrid, (Department of Civil Engineering, Univeristy of California, 1984) resulted in a mean value of shear friction angle of 1.4ϕ.

Mowafy (1986) studied the pull-out resistance mechanism of meshes immersed in sand. Steel meshes, plastic geogrids and glass grid were tested. The pull-out box was 102 cm long, 23.2 cm wide and 38.0 cm deep. The vertical load was applied by lead and steel shot.

He divided the mechanism of interaction between soil and reinforcement into two mechanisms: the primary mechanism is concerned with mechanical properties of the mesh, interlock between the mesh and the soil and confinement provided by the mesh. The secondary is concerned with interface friction between the mesh and the soil.

In order to evaluate the different pull-out resistance components, pull-out tests on plane sheets of reinforcement were run. Among his conclusions, for the Tensar geogrids

tested (SS1, SS2 and AR), 70% of the total maximum pull-out force was due to interlock and confinement while the other 30% was due to friction only. In the case of mesh reinforcement, 93% of the total pull-out resistance was due to the primary mechanism and only 7% was due to the secondary mechanism.

The interlock and confinement resistance components depend on the mesh opening and soil particle size. From his study, it was recommended that the soil particle size be equal to one quarter to one third of the smallest mesh dimension.

For the purpose of studying the pull-out resistance and interaction of different kinds of reinforcement and soil for projects of reinforced earth walls, field and laboratory pull-out tests were conducted on both large and small scales (Chang et.al., 1977). The field pull-out tests on steel strips (3mm thick and 60 mm wide) were carried out on additional dummy steel strips in reinforced earth walls at different elevations during construction., all located on Cal-39 Highway in the San Gabriel Mountains, California. The fill material was decomposed granite (sandy gravel, gravel sand, silty clay and gravel).

Typical load-deformation curves were obtained that led to the following conclusions:

1. The maximum tensile stress in the reinforcement is developed near the front face of the wall for any externally applied pull force.

2. The soil will not be strained significantly until the proportional limit (yield point) is reached. At this point, the load-deformation curve becomes non-linear for the composite steel strip and soil material (soil-steel interaction as a composite material).

Two strips were instrumented with strain gauges on both top and bottom at 1.5 m intervals. The strips were 7 m and 14 m long. For the 7 m long strip, externally applied pull load induced additional tensile force for almost the entire length of the strip; however, the externally applied pull load only stressed the 14 m long strip up to 3.1 m into the fill. There were no additional forces measured beyond this point other than the existing forces induced by the embankment load before testing.

Large scale pull-out tests were conducted so that the interaction between the soil and reinforcements could be understood. The test apparatus consisted of a rigid steel box, 137 cm long, 91.4 cm wide and 45.7 cm deep. The maximum normal load simulated the overburden load up to 15.2 m of earth fill. The tests were run at a constant rate of 0.05 mm/min and the front side of the box was removed so that free unrestrained face of the soil specimen was provided. The reinforcements used were: bar mesh, smooth bars, solid steel plate and steel strips. The soils used were poorly graded gravelly sand and silty clay.

The failure mode resulting from the laboratory tests indicated that all bar mesh reinforcement failed because a

coneshaped soil wedge developed at the front while longitudinal bars and steel strip reinforcement failed because of slippage. The soil-steel plate reinforcement also failed because a small cone-shaped soil wedge developed. This mode of failure is believed to represent full mobilization of soil resistance by the development of a passive pressure wedge. Other conclusions drawn were as follows:

1. For the same surface area, plain bar mesh reinforcement has nearly six times the pull-out resistance of a steel strip or plain longitudinal bar reinforcement in gravelly sandy soil.
2. Bar mesh reinforcement embedded in dense silty clean soil exhibited greater pull resistance than bar mesh embedded in less dense gravelly sandy soil.
3. An increase in mesh opening will substantially reduce the pull-out resistance of the bar mesh reinforcement.
4. The skin friction angle between a galvanized steel strip and granular soil is only slightly smaller than the internal friction angle of the soil. It can be taken as 10% smaller than the internal friction angle of the soil for practical design purposes.

Salomone (1978) carried out pull-out tests on sand reinforced with an industrial grade woven polyester (Teknisk vav No.600). The pull-out box was 190 cm long, 70cm wide and 70 cm deep and the normal stress ranged from 17 to 41 kPa. A pressure bag reacting against the pull-out box lid was used

to apply the normal load. A rheological model was developed from a partial differential equation to predict the length of fabric required for a given pull-out force. Figure 2.9 illustrates some results for σ_n=22.7 kPa, γ_d=17.7 kN/m^3.

Holtz (1978) using the same soil and equipment as Salomone (1978), tried to model the mechanism that occurs in a pull-out test with a modified wave equation for piles. The model utilized empirical soil and reinforcement data and an estimate of the overall tensile force capacity of the reinforcement to predict the distribution of tensile force along the reinforcement. Good agreement was found between results from in situ pull-out tests on metal strips (Chang et.al., 1977) and this model. Figure 2.10 illustrates the comparison between predicted and actual values of axial force along the reinforcement.

Table 2.2 summarizes typical results of pull-out tests on geosynthetics embedded in cohesionless soils. Collois (1981) reported values of the interface frictional coefficient between sand and gravel and geotextiles, for a range of normal stresses, and lengths of reinforcement. The values in the table are referred to fixed lengths of 0.30 m. The influence of the gradation of the soil, normal stresses and tensile moduli of the geotextiles, on the value of the coefficient of interface friction, was investigated. The interface frictional coefficient is defined as:

$$\frac{\tan\phi_{GS}}{\tan\phi}$$

National Library of Canada

Canadian Theses Service

Bibliothèque nationale du Canada

Service des thèses canadiennes

NOTICE

AVIS

The quality of this microfiche is heavily dependent upon the quality of the thesis submitted for microfilming.

La qualité de cette microfiche dépend grandement de la qualité de la thèse soumise au microfilmage.

Please refer to the National Library of Canada target (sheet 1, frame 2) entitled:

Veuillez consulter la cible de la Bibliothèque nationale du Canada (microfiche 1, image 2) intitulée:

NOTICE

AVIS

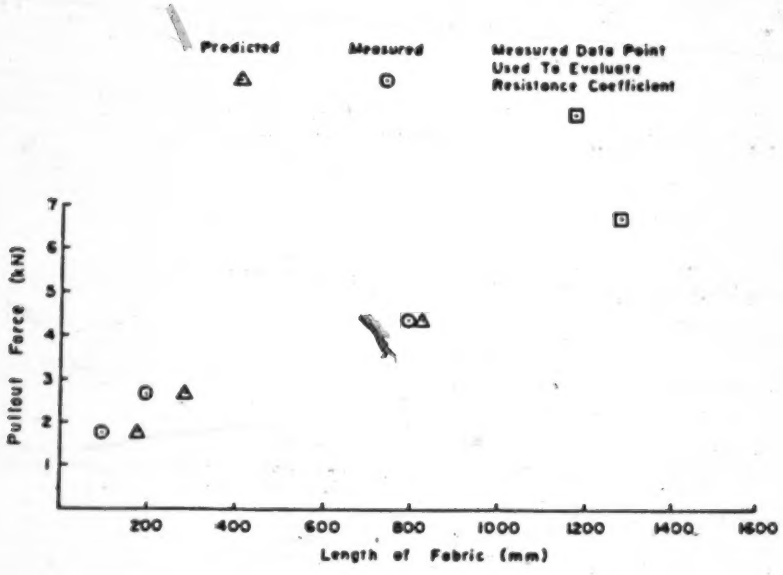

Figure 2.9 The Required Length of Reinforcement to Prevent Sliding (after Salomone, 1978)

where $\tan\phi_{GS} = \frac{\tau_{max}}{\sigma_n}$, $\tau_{max} = \frac{T_{max}}{2A}$

T_{max} = maximum pull-out force

σ_n = normal stress

Generally, the coefficient increases with the decrease of the geotextile tensile moduli. In Table 2.2, it can be seen that the values are very sensitive to the flexibility of the geotextiles, (Bidim U64 (nonwoven polyester) and Bidim Arme), despite the similar angles of friction of the two materials (35° and 32°, respectively). The variation of the interface frictional component with the soil gradations is shown in results with Bidim Arme embedded in sand and in crushed gravel.

The results on nonwoven Typar 3807 show the increase in the coefficient with the increase in normal stress. The pattern is not the same for all tests which suggests that non uniform distribution of the normal stress within the tested samples caused the variation in behaviour. A piston and rigid plate were used to apply and distribute the normal forces. Another factor that is likely to have influenced the test results was reported by Schlosser and Elias (1978): the increase in normal stress causes suppression of dilation in the sand and a consequent decrease in the value of the interface frictional angle. The increase of the interface friction angle with the increase in dry unit weight can be seen in some results of Mowafy's pull-out tests on geogrids,

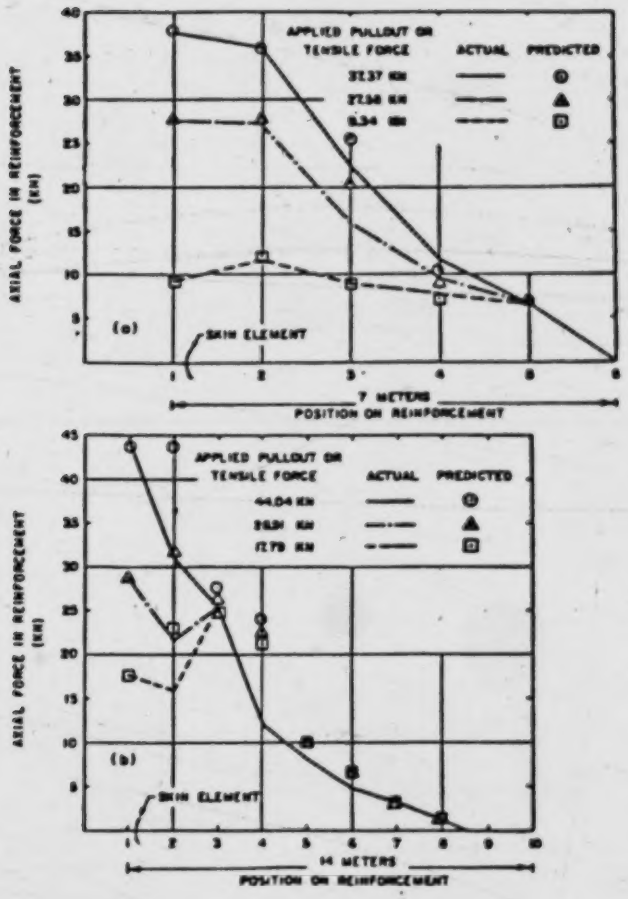

Figure 2.10 Tensile Force Along Reinforcement (after Holtz, 1978)

sheet metal and polypropylene sheets embedded in crushed stone. Also, the contribution of each mechanism in the pull-out failure can be obtained from these results.

Table 2.2 Summary of Pull-Out Test Results

AUTHOR	PULL-OUT BOX (cm^3)	SOIL DESCRIPTION				REINFORCEMENT	NORMAL STRESS (kPa)	RESULTS
		TYPE	DRY UNIT WEIGHT (kN/m^3)	ϕ (°)	C (kPa)			COEFF. OF FRICTION & INTERFACE FRICT. ANGLE
COLLIOS (1981)	40X25 0.1mm/min	SAND partical size 0.2 to 5mm	15.8	39	0	NON WOVEN TYPAR 3807 (E=105kN/m)	25	0.28
			16.5				50	0.42
						BIDIM ARME 40052 (E=327.7kN/m)	25	0.41
							50	0.47
							75	0.42
						BIDIM U64 (E=100kN/m)	25	0.80
							50	0.66
							75	0.47
						BIDIM U44 (E=44kN/m)	25	0.60
							50	0.52
						BIDIM U24 (E=22kN/m)	25	0.52
						WOVEN TRI-X 13174 (E=269kN/m)	50	0.70
							75	0.66
		CRUSHED GRAVEL Cu=1.95	14.2	53	0	BIDIM ARME 40052 (E=327.5kN/m)	25	0.77
							50	0.55
							75	0.53
MOWAFY (1986)	102X23.2X 38	CRUSHED STONE GRANULAR A partical size 10,16,19mm	16.0	38	0	AR1 (E=17.6kN/m)	4 to 22	33°, 32°
						SS2 (E=17.2kN/m)		36°, 32°
						SS1 (E=12.2kN/m)		33°, 32°
						SHEET METAL		25° to 31°
						POLYPROPYLENE SHEET		10°
			19.0	45	0	SHEET METAL	"	53°, 52°
			22.0	53	0	AR1, SS2		49°
						SS1		42°
						SHEET METAL		57°, 56°
						POLYPROPYLENE SHEET		10°
						GLASSGRID		24.5°

3. PROPERTIES OF THE SOIL AND REINFORCEMENTS

3.1 Introduction

This chapter discusses the properties of the cohesive soil used in the series of pull-out tests and the properties of the reinforcements. Properties such as Atterberg limits, grain size distribution, compaction curve, consolidation and undrained shear strength from direct shear tests are presented. Typical curves of force-deformation for each reinforcement employed in this research are shown.

3.2 Properties of the Cohesive Soil

3.2.1 Index, Particle Size and Specific Gravity Tests

The cohesive soil tested was a well graded silty clay that was taken from a borrow pit near Devon, Alberta. The soil was supplied by the Alberta Transportation Laboratory which had air dried and bagged the soil in 20 kg batches.

One specimen was prepared and tested to determine the Atterberg limits and the particle size distribution (ASTM D421, D422 and D4318). The liquid and plastic limits were 42.4% and 21.3%, respectively. The value of the Plasticity Index is 21.2%. A typical grain size distribution is shown in Figure 3.1. As can be seen, from an average of two tests, 23% of the grains are finer than 2μm; therefore, the activity is 0.92. The specific gravity of the soil was measured to be 2.66 (ASTM D854).

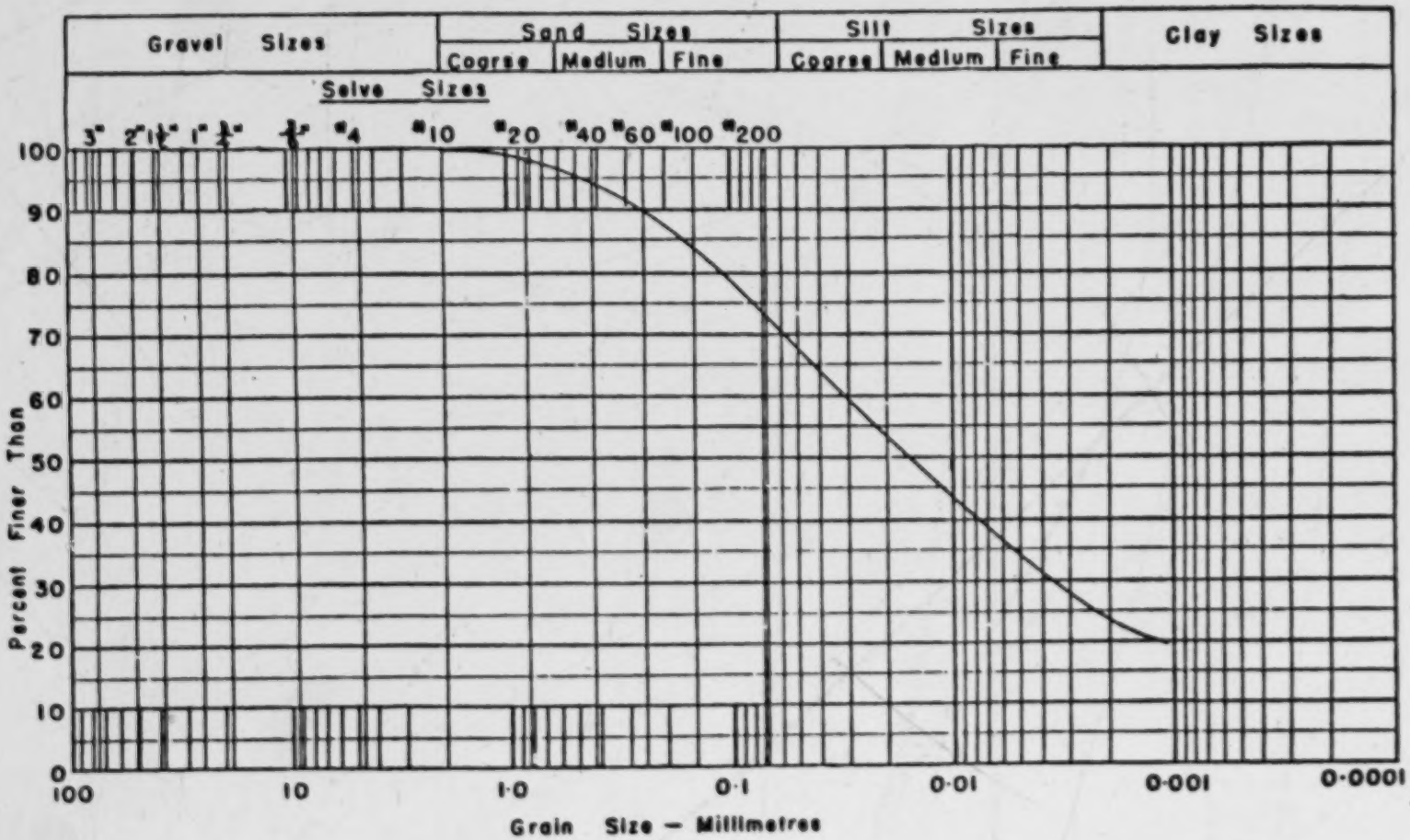

Figure 3.1 Grain Size Distribution, Devon Silty Clay

3.2.2 Compaction Curve

The relationship between dry density and water content was determined by the dynamic standard compaction method (ASTM D698). The optimum moisture content and maximum dry density are 23.2% and 1.57 g/cm³, respectively. Figure 3.2 illustrates the compaction curve.

3.2.3 Consolidation Test

A consolidation test was run in a sample that was compacted with the same specific energy applied to the pull-out test samples. The initial moisture content was 24.6%, the initial dry unit weight was 15.11 kN/m³, and the initial degree of saturation was 90%. Figure 3.3 illustrates the consolidation curve. The preconsolidation pressure from the compaction energy of the silty clay is about 165 kPa. The values of the coefficient of consolidation, c_v, were determined for each stage of loading and the mean value is 1.4×10^{-3} cm²/sec.

3.2.4 Consolidated Undrained Shear Strength

A series of 23 direct shear tests was run to evaluate the undrained shear strength of the silty clay. The water contents and densities of the specimens were varied slightly to show their effect on the undrained shear strength. The samples (6 x 6 cm²) were either cut from pull-out test samples immediately after the tests or cut from compacted mold samples. From each mold, two direct shear samples were

taken and the samples were consolidated under the same normal stresses used in the pull-out tests (20 kPa, 50 kPa and 100 kPa).

The variation in moisture contents and dry densities in the samples were less than those in the pull-out samples. The average moisture content was 24.7% with a standard deviation of 0.4%. The mean value of the initial dry unit weight was 15.0 kN/m³ with a standard deviation of 0.24 kN/m³. The degree of saturation was 88.4% average, with a standard deviation of 3.4%.

All tests were run at a displacement rate of 0.9 mm/min which ensured that the test would be run in undrained conditions. Table 3.1 summarizes the results of 21 direct shear tests. The failure envelope is illustrated in Figure 3.4. The soil parameters are c_u = 29.6 kPa and ϕ_u = 19.5°. Among the 23 consolidated undrained direct shear test results performed, only 17 were plotted in Figure 3.4 due to variations in moisture contents and dry densities.

An attempt was made to find a correlation among moisture content, dry unit weight, degree of saturation and undrained shear strength. However, no such correlation could be found and average values were used.

A series of consolidated undrained direct shear tests was run on the same soil in another testing program. The envelope is illustrated in Figure 3.5. It can be seen that these results (c_u=34.2 kPa and ϕ_u=17°) support the results obtained in this research. The mean values and standard

Table 3.1 Consolidated Undrained Direct Shear Test Results on Silty Clay

TEST (#)	Wi (%)	Wf (%)	INI.UNIT WEIGHT (kN/m^3)	INI.DRY UNIT WEIGHT (kN/m^3)	Si (%)	PEAK SHEAR STRENGTH (kPa)	NORMAL STRESS (kPa)	SAMPLE
1	24.8	25.5	18.6	14.9	88	39.2	50	BLOCK
2	23.0	23.4	19.5	15.9	95	54.4	20	MOLD
3	22.9	23.6	19.6	16.0	96	37.7	46.2	MOLD
4	24.7	25.2	18.9	15.2	91	57.0	50	BLOCK
5	25.0	25.4	18.2	14.5	84	39.0	50	BLOCK
6	25.0	25.4	18.9	15.1	92	46.0	51.7	BLOCK
7	22.5	25.4	17.9	14.6	77	36.0	50	BLOCK
8	24.8	25.6	18.6	14.9	88	42.0	20	MOLD
9	24.8	25.6	18.7	15.0	89	41.0	50	MOLD
10	24.4	25.2	18.4	14.8	85	65.0	100	MOLD
11	23.1	25.0	18.6	15.1	85	25.0	20	MOLD
12	24.7	24.9	18.6	14.9	88	45.0	50	MOLD
13	23.9	24.4	18.5	14.9	85	63.0	100	MOLD
14	24.0	25.4	18.9	15.3	90	37.0	20	MOLD
15	23.2	24.2	19.0	15.4	90	42.0	50	MOLD
16	24.0	23.7	19.2	15.5	93	75.0	100	MOLD
17	25.4	25.3	18.9	15.1	93	35.2	20	MOLD
18	24.8	25.2	19.0	15.2	93	42.0	50	MOLD
19	24.6	24.4	18.5	14.9	87	43.0	20	MOLD
20	24.8	24.4	18.6	14.9	88	53.5	50	MOLD
21	24.8	24.5	18.3	14.7	85	63.5	100	MOLD

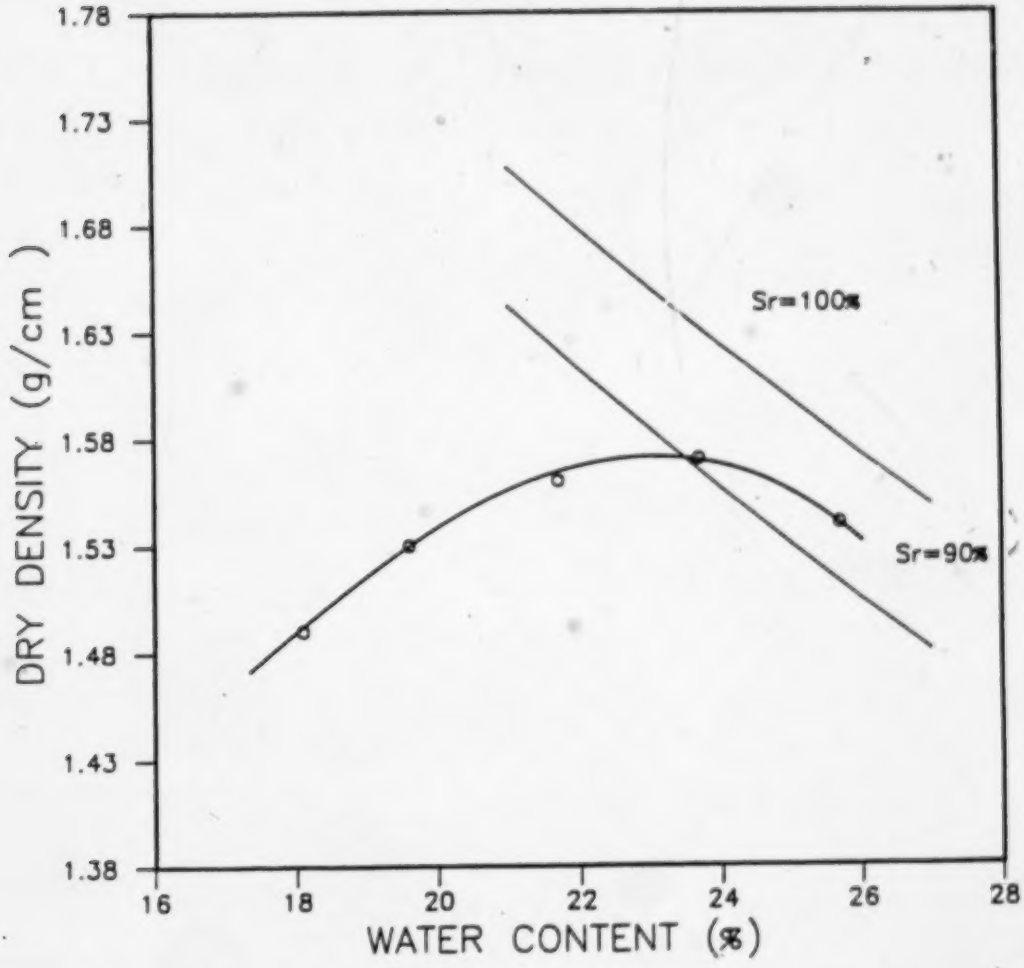

Figure 3.2 Compaction Curve

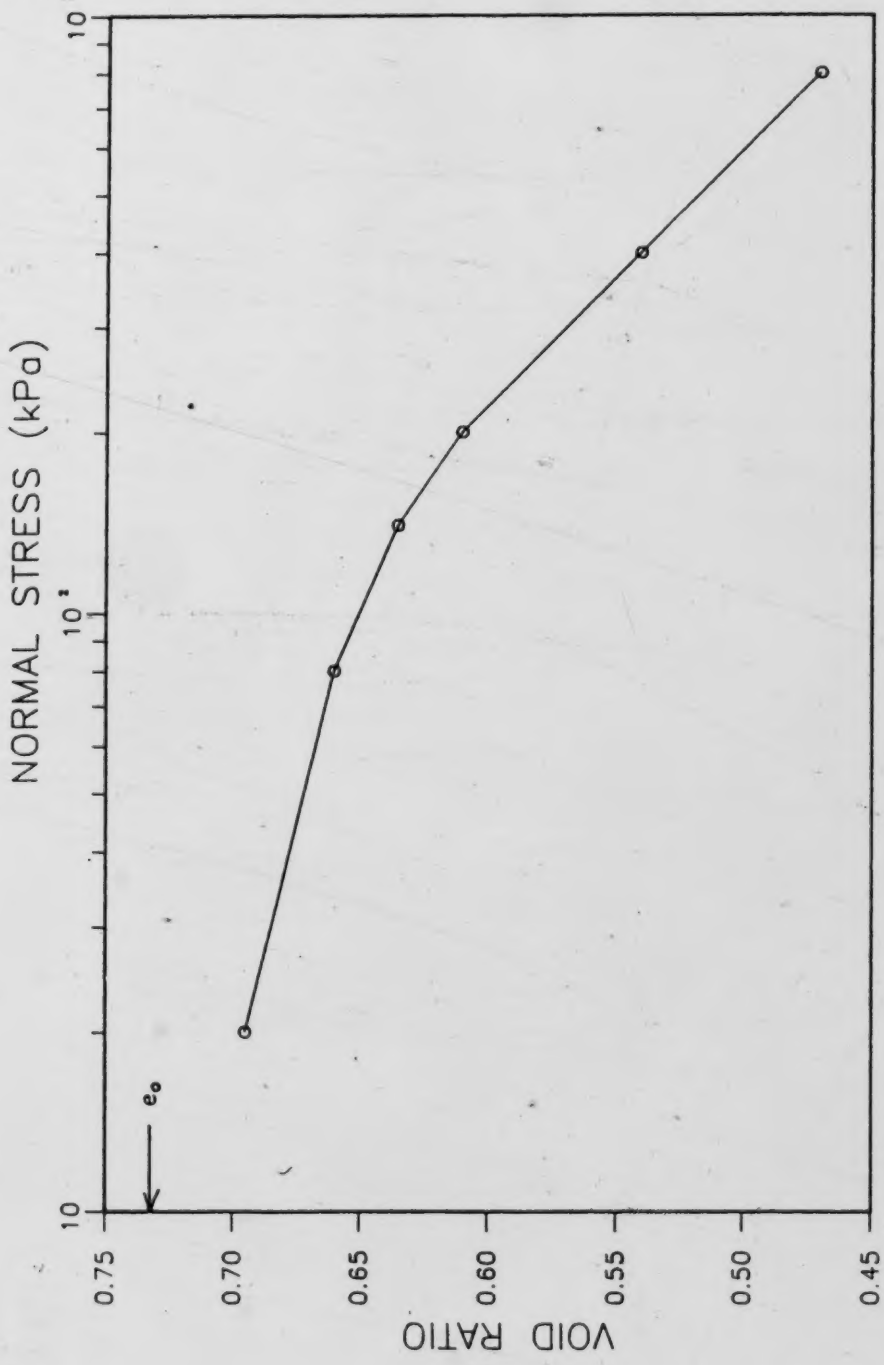

Figure 3.3 Consolidation Curve

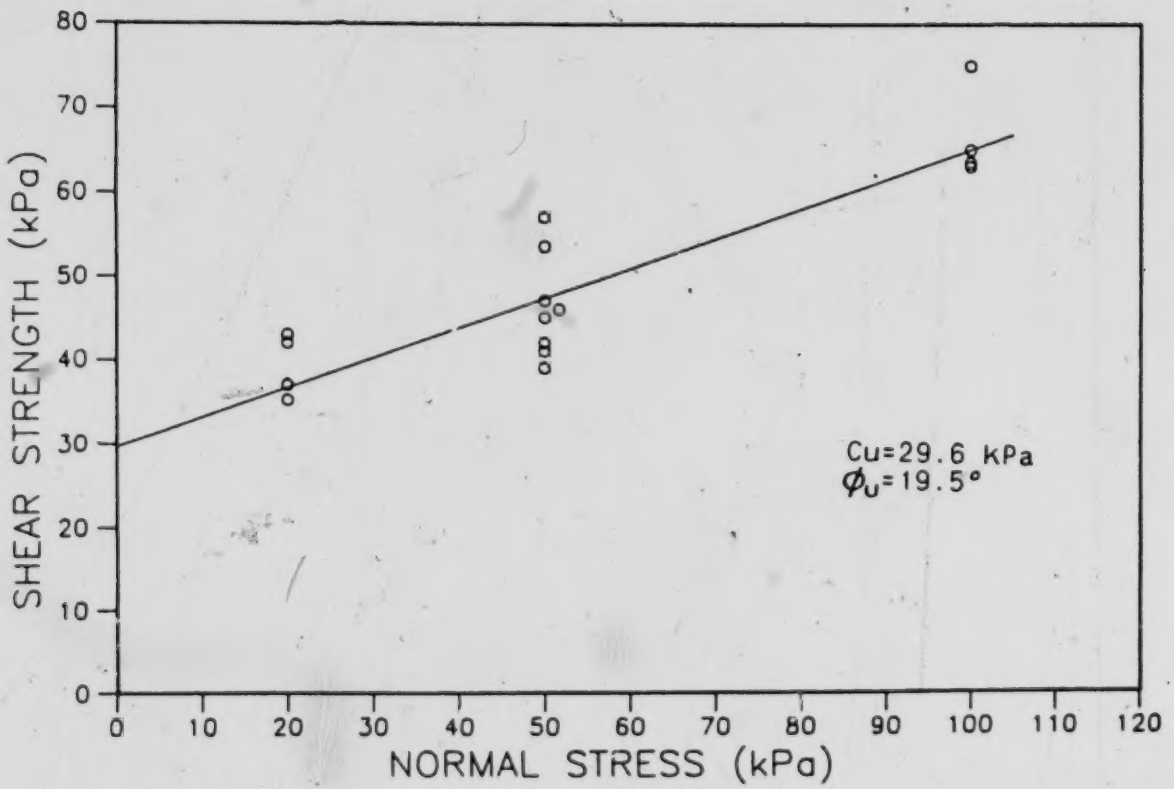

Figure 3.4 Consolidated Undrained Direct Shear Test on Silty Clay

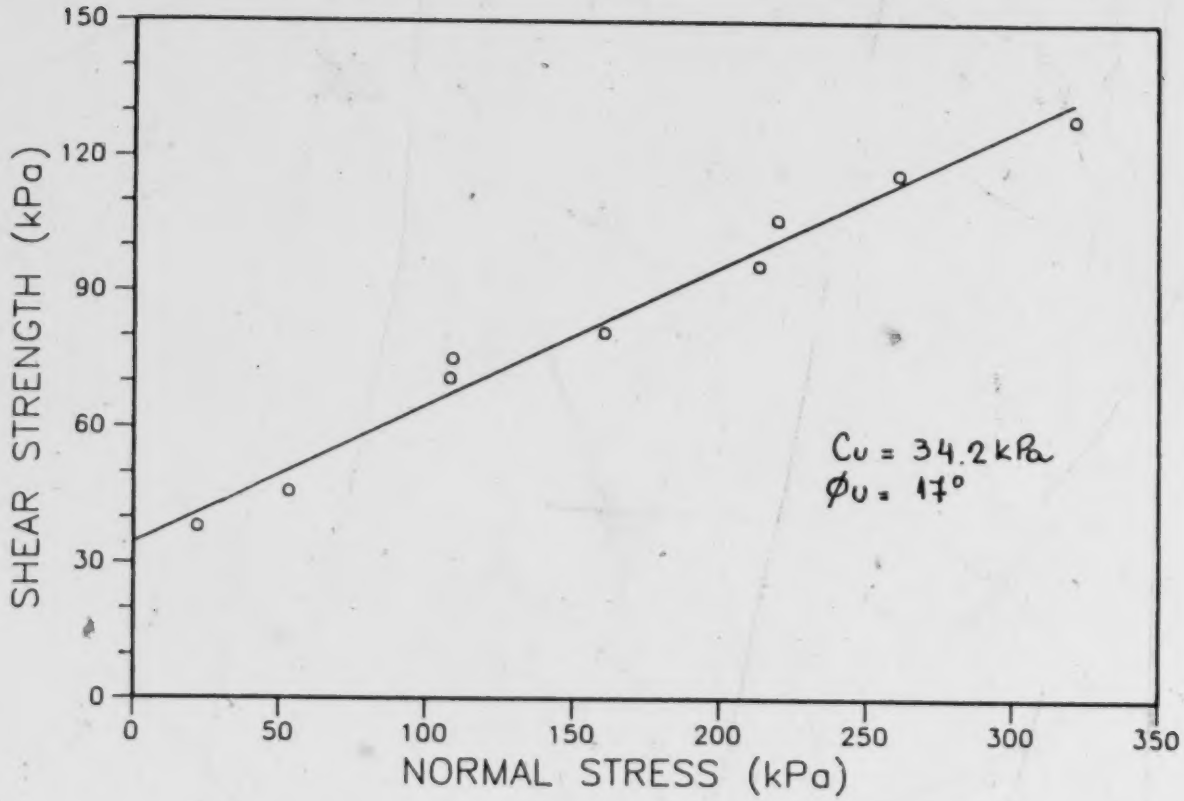

Figure 3.5 Consolidated Undrained Direct Shear on Silty Clay
(Results from Graduate Laboratory)

deviations, s, of the initial moisture content, degree of saturation and initial dry unit weight were 23.5% (s=1.1%), 91% (s=2.5%) and 15.5 kN/m³ (s=0.1 kN/m³), respectively for all samples.

3.3 Properties of the Reinforcements

Three geogrids were employed in this research: Tensar SR2, Signode/ITW TNX5001 and ParaGrid 50S. Plates 3.1 to 3.3 illustrate the reinforcements. Table 3.2 presents some characteristics of each geogrid. The values of peak tensile strengths were taken from the geogrid manufacturers trade literature.

Results from tensile tests on the geogrids are illustrated in Figures 3.6 to 3.8. It should be noted that the tensile curves for the SR2 were measured during the pull-out tests, by two LVDTs placed on anchor members 2 and 3 between the front of the box and the jaw. On the other hand, the curves for the TNX5001 and ParaGrid 50S were measured in tensile tests (ASTM D4595-96) on the Instron Machine.

The effect of specimen dimensions and strain rate upon the measured force-deformation characteristics of geosynthetics was investigated by Rowe and Ho (1986). Although the SR2 geogrid reduction in modulus measured at a strain rate of 0.2%/min is approximately 45% when compared with values of moduli at a strain rate of 10%/min, the specimen size does not affect the values of moduli. McGown

Table 3.2 Properties of the Reinforcements

GEOGRID TRADE NAME	TYPE OF POLYMER	STRUCTURE	JUNCTION METHOD	GEOMETRY					TENSILE PROPERTIES
				WEIGHT (g/m)	OPEN AREA (%)	APERTURE SIZE (mm)	THICKNESS (mm)	COLOR	PEAK TENSILE STRENGTH (kN/m)
PARAGRID 80S	POLYESTER POLYPROPYLENE	SQUARE GRID	WELDED	930	78	*MD 66.2 *CMD 66.2 S/B 26.5	*T 2.50 JUNCTION 4.5	YELLOW	80
THX 5001	POLYESTER POLYETHYLENE and TEREPHTHALATE	RECTANGULAR GRID	WELDED	544	58	MD 89.7 CMD 26.2 S/B 120	T 0.75 JUNCTION 1.50	BLACK	87.5
SR2	HIGH DENSITY POLYETHYLENE	UNIAXIAL GRID	PLANAR	930	55	MD 88.1 CMD 15.2 S/B 22	T 1.27 JUNCTION 4.75	BLACK	78.8

*MD = MACHINE DIRECTION
*CMD = CROSS MACHINE DIRECTION
*T = TENSION MEMBER

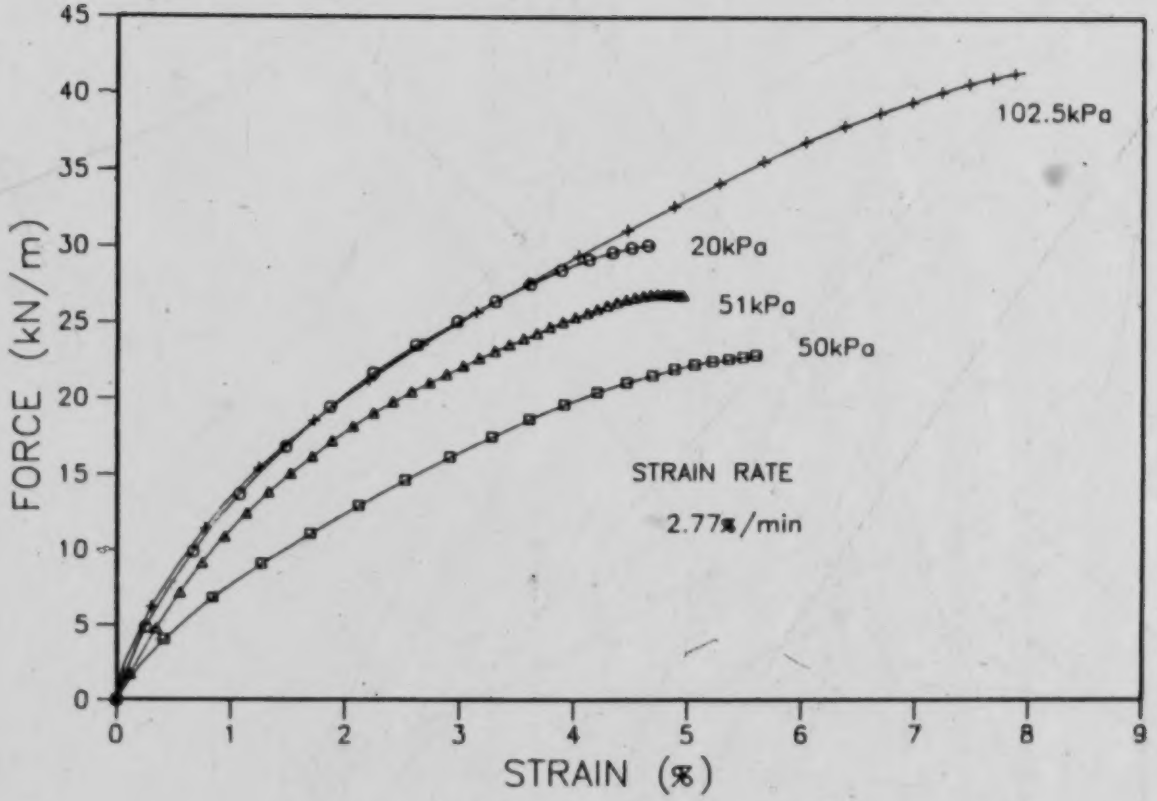

Figure 3.6 Force Strain Curves of the SR2

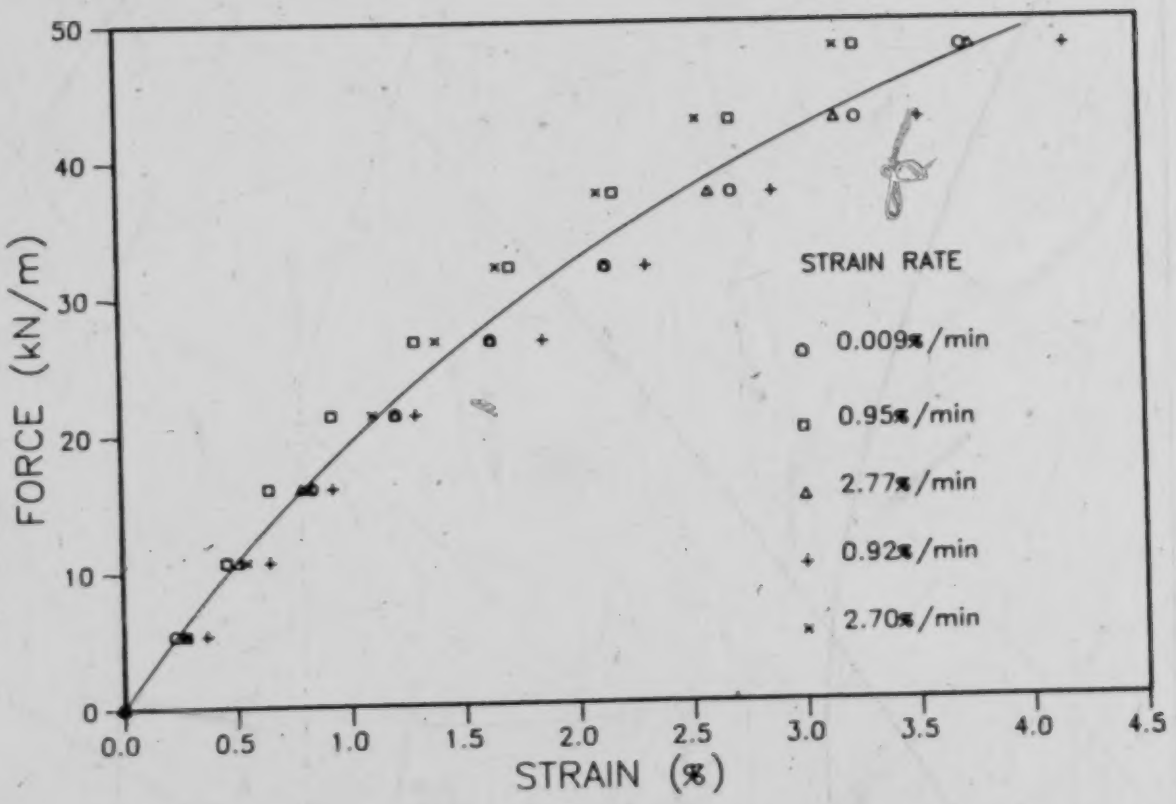

Figure 3.7 Force Strain Curves of the TNX5001

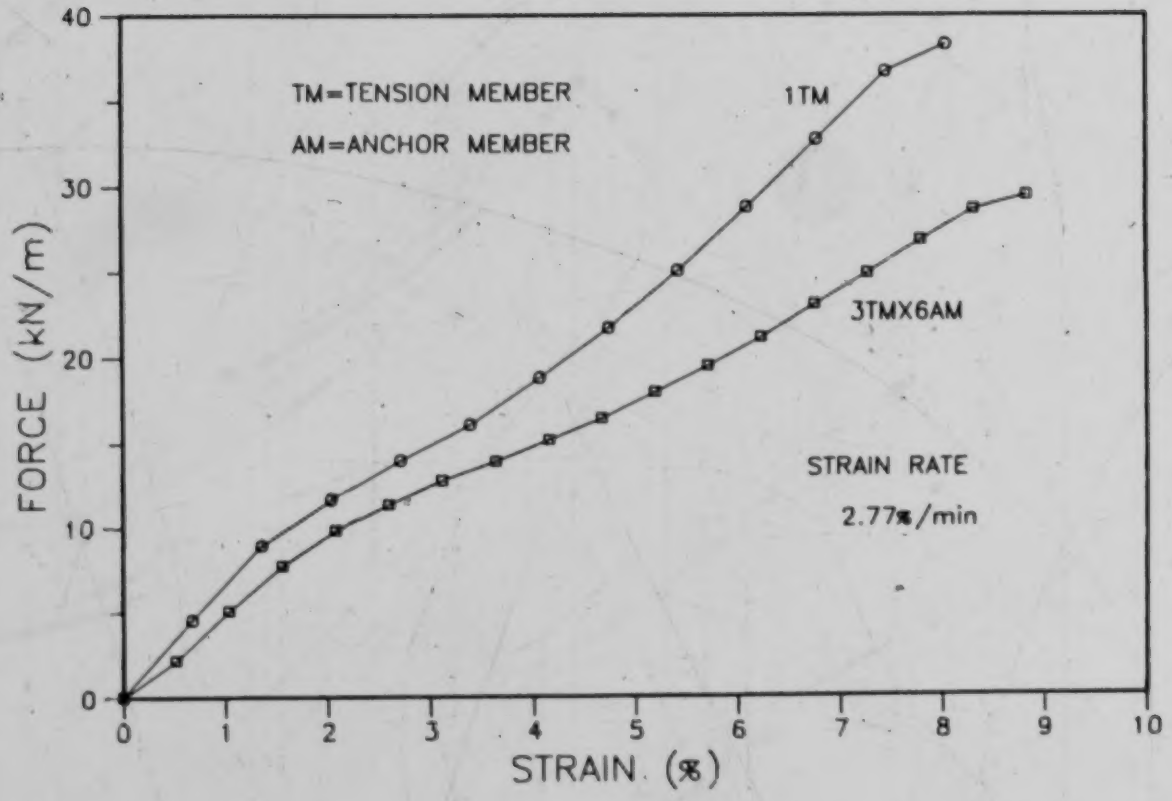

Figure 3.8 Force Strain Curves of the ParaGrid 50S

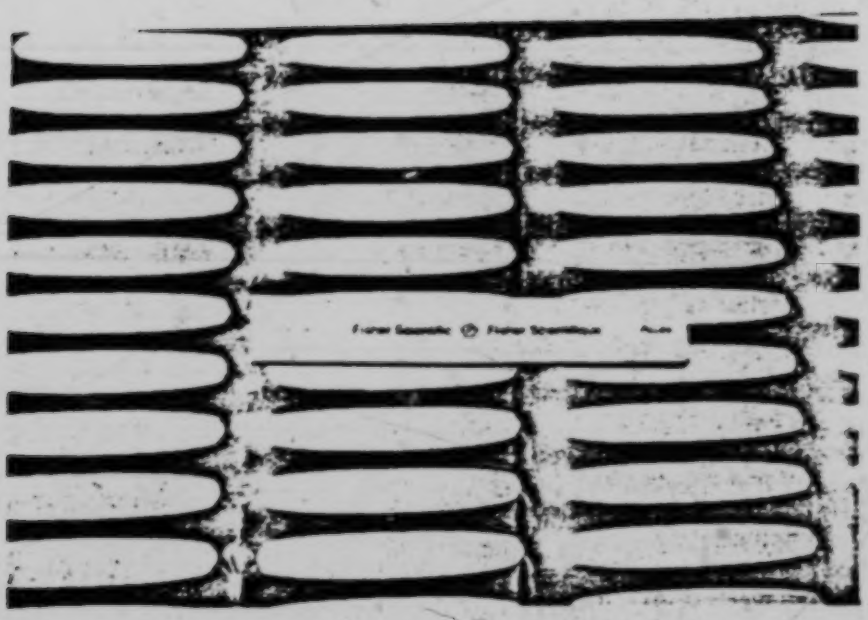

Plate 3.1 Tensar SR2

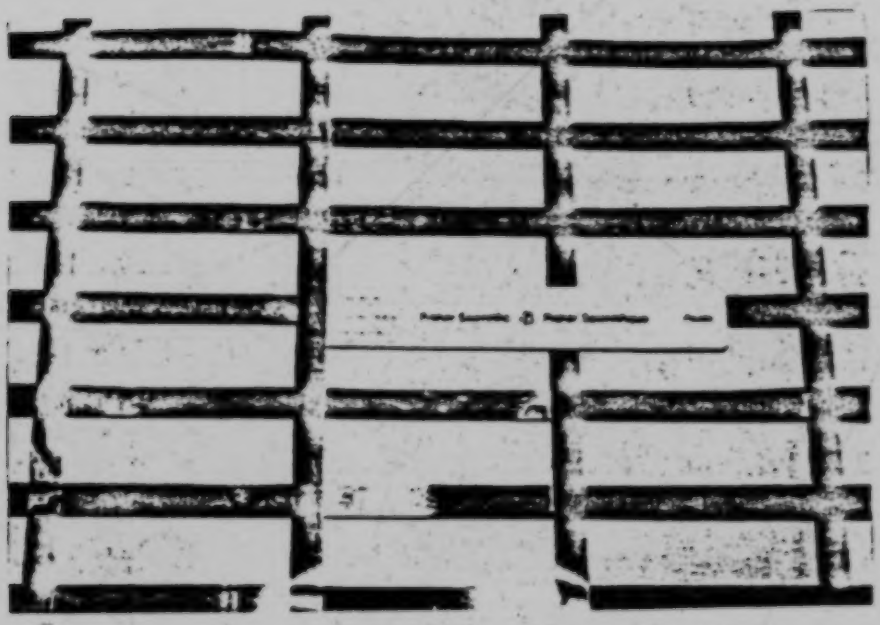

Plate 3.2 Signode /ITW TNX5001

Plate 3.3 ParaGrid 50S

et.al. (1984), who studied the load-strain-time behaviour of Tensar geogrids tested at a constant rate of strain, noted that the behaviour was influenced by temperature. Rapid loading creep tests were shown to be suitable for the measurement of the load-strain-time relationship of this geogrid. The pull-out tests carried out in this research lasted for 5 minutes each. As the period of time is very small, creep was not considered in the analysis of the pull-out test data.

The TNX5001 geogrid is polyester. Studies by Finnigan (1977), showed that high tenacity polyester and polyamide yarns present low levels of creep. Typically about a 1% change in length over 10 years when a yarn is loaded to 20% of its breaking load is expected. Tensile tests on TNX5001 geogrid, six tension member by six anchor member samples, at different strain rates (0.009%/min to 2.77%/min) were run and no significant change in modulus was observed. Figure 3.7 illustrates the average curve.

Two tensile tests were run with the ParaGrid 50S at a strain rate of 2.77%/min. One test was run on only one tension member sample taken from an undamaged roll and the other one on a sample of three tension members by six anchor members. Significant difference was observed in the tensile strength of the material. The peak strength value for the one tension member was about 34% stronger than that for a 3 x 6 member sample. Furthermore, the failure observed in the 3 x 6 member sample occurred at the junctions which

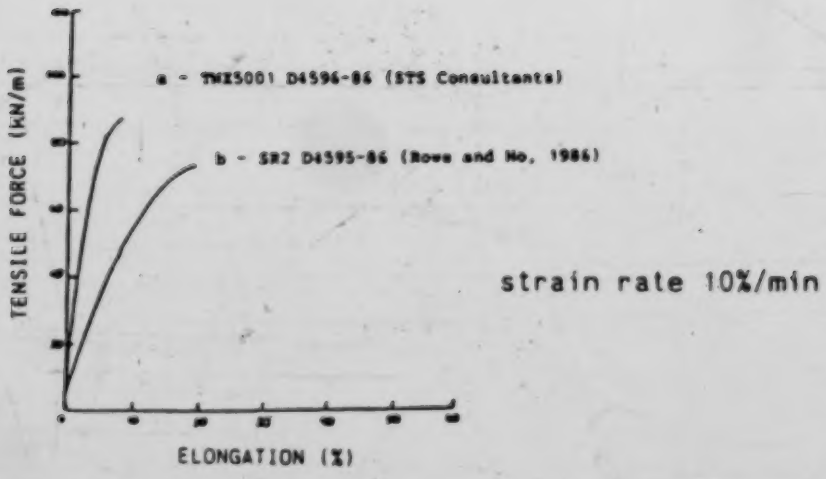

Figure 3.9 Typical Force Strain Curves - SR2 and TNX5001 (modified from Beech, 1987)

suggested that the material was damaged at the junctions where the tension and anchor members had been heat bonded.

The secant modulus at 2% strain for the Signode material is about 1624 kN/m. For the Tensar SR2, the secant modulus is about 900 kN/m, average. It is concluded that TNX5001 proved to be not only stronger, in terms of peak tensile strength, but also with a higher initial tensile modulus than the SR2 geogrid. Beech, 1987, in his paper on stress-strain relationships in reinforced soil system designs, also made some comparison in terms of tensile moduli between SR2 and TNX5001 geogrids. His results support the findings presented herein. Figure 3.9 illustrates his results.

4. PULL-OUT TEST

4.1 Introduction

Many tests can be employed to evaluate the magnitude of the bond developed between soils and geosynthetics; however, in terms of pull-out resistance, it is imperative to use the appropriate testing techniques.

This chapter describes the pull-out test. The pull-out apparatus, loading systems and instrumentation utilized during the pull-out tests are presented. A description of the sample preparation, test procedure and tests performed in this research are presented.

4.2 Large Pull-out Apparatus

A large pull-out apparatus was designed by means of modifications to a Large Direct Shear Test Apparatus developed by Brandt (1985). The modifications were introduced in all four features that comprise the apparatus: reaction frame, box, horizontal loading system and vertical loading system.

4.2.1 Pull-out Box

The inside dimensions of the box are: 106 cm long, 36 cm wide and 20 cm deep. These dimensions were based on two criteria: 1) the length of the box should be short enough to avoid rupture of the geogrids in tension during the pull-out tests, 2) the length of the box should be long enough to

allow the development of progressive displacements before reaching the ultimate strength of the interface. As well, the original dimensions of Brandt's (1985) direct shear apparatus placed some limitations on the dimensions of the pull-out box.

The sides of the box are constructed of two 20 cm high "C" steel channel sections. To avoid friction between the sides of the box and the soil, two layers of a smooth satin fabric were placed between the contact (Brandt, 1985). This fabric has an angle of friction of 2.8° which is lower than the Teflon friction angle (around 8.5°).

The front and back plates are 1.27 cm thick. Both plates have a slot 2 cm high that runs the full width of the box. The purpose of the slot in the back plate is to allow the prestressed wires attached to the geogrids (geogrid instrumentation) to come out of the box. The middle height of the slots coincides with the middle height of the soil sample, usually 5 cm.

The bottom of the box consists of a piece of expanded metal, 0.362 cm thick welded to a steel plate which has drainage holes drilled at 5 cm centres to allow consolidation of the soil sample. The purpose of the expanded metal mesh is to hold the soil in place during a test. Another piece of expanded metal is placed on top of the sample so that symmetry in boundary conditions can represent the field conditions. This top mesh was held in the horizontal direction (vertical movement free) by means

of two bolts at the back plate.

The five parts of the pull-out box are bolted together so that at the end of each test, the progressive displacements of the geogrid sample can be seen when the box is taken apart.

The pull-out box is held to the reaction frame by means of bolts and steel angles to avoid any displacement during the tests. It rests on a reinforced concrete block which dimensions are: 100 cm x 100 cm x 27 cm. Plate 4.1 illustrates the pull-out box with the bottom mesh in place.

4.2.2 Horizontal Loading System

The requirements of the horizontal loading system are accurate determination of the pull-out force and the ability to apply the pull-out force at a constant rate according to the drainage conditions (drained or undrained) and type of soil used in the test (sand or clay) (Ingold, 1980). The method of fixing the end of a geogrid prior to tensile testing has a significant effect on the maximum tensile strength (Brand and Duffy, 1987). Neither slippage of the geogrid nor concentration of stress at the jaws are allowed during the pull-out test; therefore, different jaws or different ways of placing the geogrid in the jaws are required for good pull-out test performance.

A constant strain rate of approximately 3%/min (12 mm/min) was selected in order to ensure that the test conditions would be undrained. The constant velocity was

imposed by a motor mounted on the double "I" beam frame attached to the concrete block.

In order to minimize stress concentrations at the point of "grabbing" the geogrid piece, appropriate steel jaws were designed. For the SR2 material, the first anchor member was held directly by these jaws. For the TNX 5001, epoxy was required to cast the first anchor member into the jaws, otherwise, the test would not be possible due to slippage of the geogrid sample. The epoxy, by Interstress Ltd, had a very slow rate of curing (about 24 hrs); therefore, the maximum temperature reached during the process did not damage the geogrid properties. In the case of the Paragrid 50S, the same epoxy was used, and pieces of steel rods (3.18 mm diameter) were used to tie the fibers that were taken out of the geogrid members.

In order to maintain the jaws in the same alignment of the pull-out force, a support table was mounted with adjustable height and length compatible with the travel of the loading system required to run the tests. This table was screwed in the "I" beam flanges. Two roller plates were used to eliminate friction between the jaws and support table.

The pull-out force was measured by a load cell (SN 20790) with a capacity of 4500 kg that was mounted between the jaws and the travel arm of the motor. The travel of the horizontal loading system is 15 cm which proved to be enough to run the pull-out tests. All features that comprise the horizontal loading system are shown on Plate 4.2.

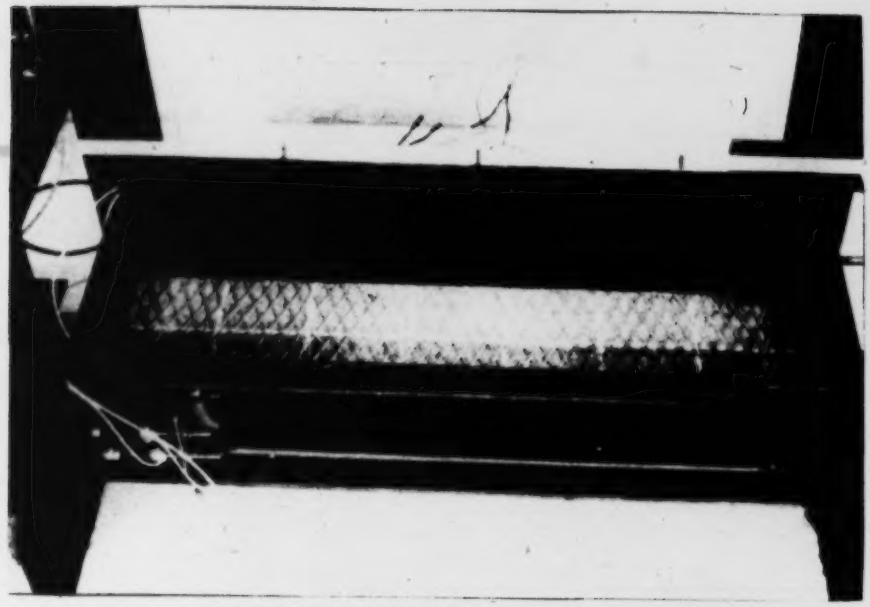

Plate 4.1 Large Pull-Out Box

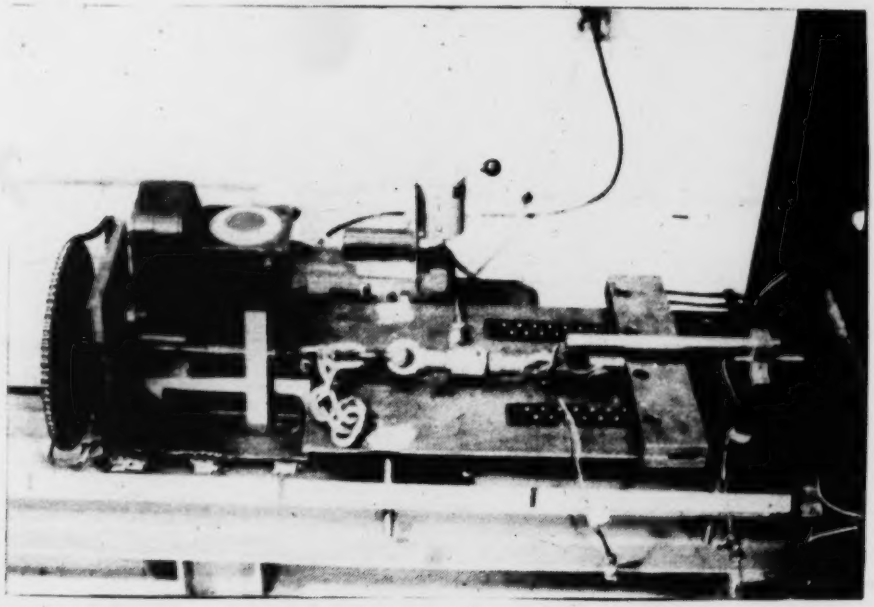

Plate 4.2 Horizontal Loading System

4.2.3 Vertical Loading System

The flexible vertical loading system consists of a series of prismatic elements forming a pyramid shaped loading head. Since this system of loading allows differential settlements, in case the soil is not homogeneous, it ensures that the distribution of normal stress is uniform.

In this research, the flexible vertical loading system was based on the one used by Brandt (1985). Some modifications were required in the assemblage of the prismatic elements in order to fit the pull-out box dimensions. The whole configuration weighs 210 kg. Figure 4.1 and Plate 4.3 illustrate the head loading.

The pyramid shape is a well known efficient method used to distribute concentrated loads. The shape is frequently used in shallow foundation designs and it is one of the most appropriate configurations to transfer load from pillars to soil mass. Another application of this system is in the laboratory, where pyramid shaped loading heads are used with some conventional shear box apparatus to transform the vertical point load into a uniform stress (Brandt, 1985).

Two rows of prismatic steel elements are used to form the pyramid. The first layer consists of 48 prismatic elements with triangular cross section. This first layer covers the whole sample. For the second layer, 24 elements are used, each one transferring its load to two others from the first layer. Another 12 prismatic elements form the

third layer and again, each of them rests on top of the two others from the second layer. The next layer consists of eight flat steel bars (5 cm x 2.5 cm) and rests at the center of the pyramid element apex. These eight bars receive the loads of four other steel bars (5 cm x 5 cm) and finally, an "I" beam (10 cm high) receives the concentrated load from the lever system.

In order to eliminate shear and torsion forces in the soil sample, ball bearings and small steel bars are placed between the contacts of the steel bars; therefore, only normal loads are transferred to the soil sample. The vertical force is applied using two symmetric lever systems and weights. The levers consist of two 10 cm high "I" beams reacting against the reaction frame. The ratio of the levers is 8:1 and they are 2.5 m long which allows the application of 58 kN of total force (29 kN per lever). The levers are levelled by means of their two reaction points which are mounted on screws.

Modifications were introduced to the reaction frame. Yokes were built at both ends to allow the placement of the pull-out box. The height was also increased by 20 cm due to the height of the head loading configuration. The reaction frame consists of extended web "H" steel sections 10 cm high and 10 cm wide which are attached to the concrete block by means of 12 threaded rods (the concrete block reinforcement).

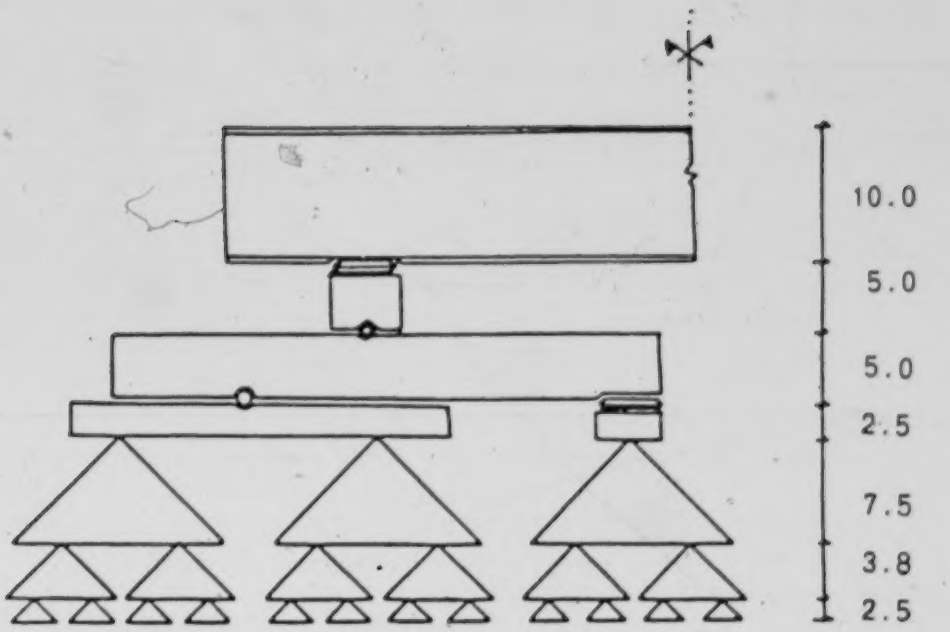

dimensions in cm

Figure 4.1 Vertical Head Loading

Plate 4.3 Vertical Head Loading

4.3 Instrumentation

The pull-out test instrumentation can be divided into two types: the pull-out box instrumentation and the geogrid sample instrumentation.

4.3.1 Pull-out Box Instrumentation

In order to evaluate the passive force that may develop in the soil at the front end of the box during a pull-out test, four load cells are mounted between the front end of the box and the box sides to measure the soil pressure on the front end. The location of the load cells is such that no bending moment can be transferred to the soil sample at the front of the box. Each load cell has a capacity of 4kN. They were manufactured at the Machine Shop of the Civil Engineering Department.

The soil sample consolidation or change in height was monitored by two LVDTs (Linear Variable Differential Transformer) in contact with the top rows of the prismatic elements. One LVDT was placed at the front of the sample 4.5 cm from the front plate and the other one, at the back of the sample, 4.5 cm away from the back plate.

4.3.2 Geogrid Instrumentation

The instrumentation of the geogrid samples can be divided into two parts: the instrumentation of the geogrid sample inside the soil mass and the instrumentation of the geogrid sample outside the pull-out box.

The outside instrumentation was used to measure the force-strain behaviour of the geogrid material and the horizontal displacements at the point of application of the pull-out force. This instrumentation consisted of two LVDTs placed at the middle width of some of the geogrid anchor members. One LVDT monitored the horizontal displacements of the second anchor member while the other LVDT monitored the differential horizontal movements between the second and the third anchor members. This procedure allowed the determination of the force-strain curve of the SR2 sample material during each pull-out test. It is important to note that the holes drilled in the geogrid cross members in order to hold the LVDT supports, did not affect the rigidity (EA) of the material. Unfortunately, the same procedure could not be followed for the other two geogrids because the method to support the LVDTs did not seem adequate due to the geometry of the geogrids. The use of strain gauges (either resistance or Bison) was out of question due to the large range of strain values expected (about 10%).

The instrumentation of the geogrid samples inside the box consisted of prestressed wires placed along the geogrid samples. The prestress was necessary to eliminate differential vertical movements along the wire during compaction of the soil sample. The horizontal displacements of seven anchor members were monitored by seven LVDTs. The wire (0.4 mm diameter), manufactured by Paxam Metals Limited, has a high elastic modulus. One end of the wire was

sewn in three holes (1.016 mm diameter) drilled at the center line of each of the seven anchor members that were monitored. The other end was attached to the LVDTs placed at the back of the pull-out box. Extensions were welded to the cores of the LVDTs and nylon threads were tied to these core extensions. From the other end of the thread, 1.5 kg weights were hung in order to prestress the wires inside the soil sample. Plate 4.4 illustrates the prestress system. The tensile stress in the wires was about 18.7 Pa which was only a small fraction of the yielding stress found in laboratory test results. Also, the holes drilled in the anchor members did not affect the geogrid properties.

Friction between the soil and the lengths of wire was avoided by simply placing them inside strong plastic tubes (ID=3.18 mm). Detail of the inside instrumentation of the geogrid samples is illustrated on Figure 4.2.

4.4 Sample Preparation

The pull-out sample preparation can be divided into two parts: the soil sample preparation and the geogrid sample preparation.

4.4.1 Soil Sample Preparation

The 970 kg of air dried, crushed soil that would be used in the pull-out test series was mixed, homogenized and separated into 30 kg bags. For each test, water was added to 65 kg until the final moisture content ranged from 24% to

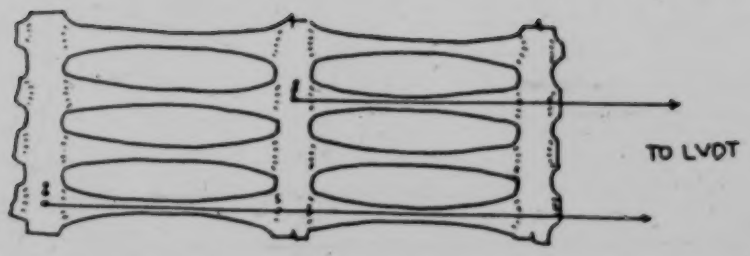

Tensar SR2

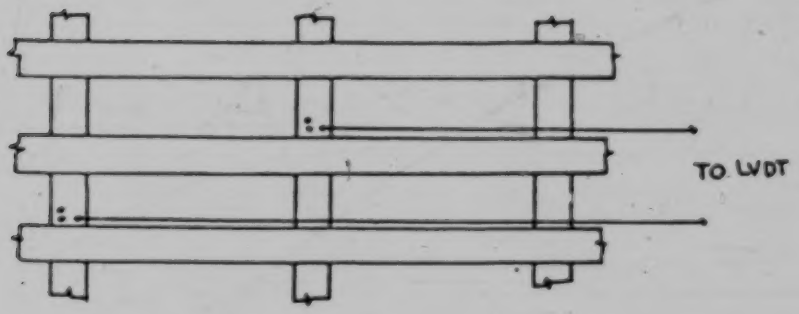

Signode /ITW TNX5001

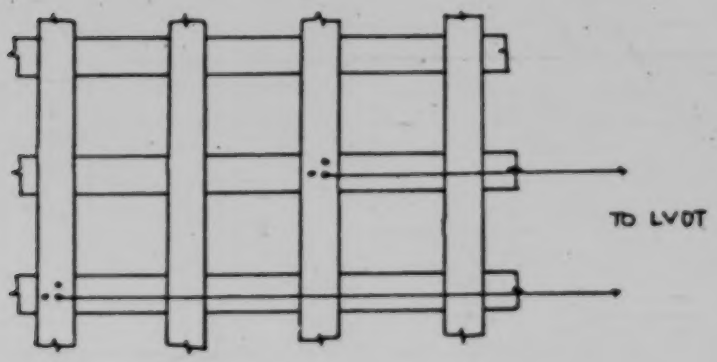

ParaGrid 50S

Figure 4.2 Instrumentation of the Geogrid Samples with Piano Wire

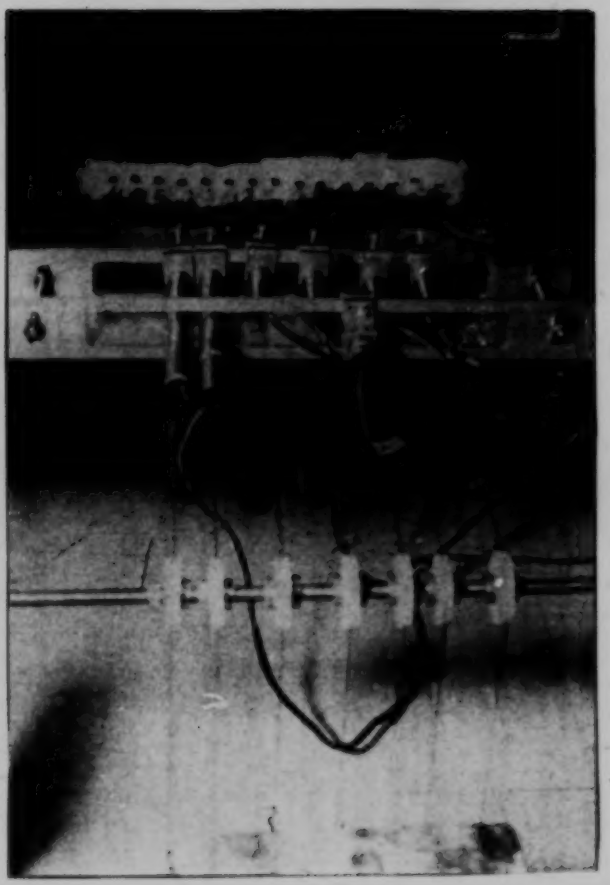

Plate 4.4 Detail of the Geogrid Instrumentation Outside the Pull-Out Box

25%. Consistency in moisture content was quite difficult to achieve due to the large quantity of soil required for each pull-out test. Loss of moisture also occurred very quickly from evaporation during preparation and compaction due to the high silt content of the soil. The process of mixing and homogenization took about 25 minutes. The soil was then divided into three batches and cured in a moisture room for 24 hours to allow moisture content equalization. Since the period of curing time influences the dry density-moisture content relationship (Casagrande and Hirschfeld, 1960), a curing time of 24 hours was selected as the standard for all tests.

4.4.1.1 Thickness of the Soil Sample

The thickness of the soil sample was chosen based on the solution of a wedge penetration in clay (Balligh and Scott, 1976). In this study, a graphic solution was proposed taking into account simplifications such as the existance of a gap behind the wedge. This simplification was necessary due to the severe requirement which implies that for the steady state motion, every soil element must have the same velocity with respect to the wedge at all times.

Analysis showed that for the geogrid SR2, whose cross member was the thickest (4.4 mm) among the geogrids tested, the soil sample height could be as thin as 3 cm. As the geometry of the box was designed for a soil sample thickness of 10 cm, this value was adopted to ensure that the top and bottom boundaries would affect the soil deformations during

pull-out.

The work by Brand and Duffy (1987) suggests that the thickness of clayey soil be at least 15.2 cm when testing the geogrid Tensar SR2. For thickness greater than 15.2 cm the normal stress loading system would not influence the pull-out force results. However, their method of applying the normal load (hydraulic jack on a metal plate), makes this conclusion not applicable for the apparatus used in this research.

4.4.2 Geogrid Sample Preparation

The geogrid specimens were cut to the appropriate lengths with tin snips. The lengths always coincided with the direction in which the geogrid batches were rolled. For the SR2, the pieces consisted of 15 anchor members and 15 tension members (34.5 cm), for the TNX 5001, 16 anchor members and 9 tension members (32.6 cm) and for the ParaGrid 50S, the samples were 19 members long and 5 members wide (34.5 cm). The next step was to measure the lengths between two consecutive anchor members and the widths of each anchor member. Mean values were evaluated for later reduction of the pull-out test data. The instrumentation of the geogrid was carried out as explained in Section 4.3.2. Table 4.1 presents the average distances from each instrumented anchor member to the front end of the pull-out box.

4.5 Test Procedure and Tests Performed

4.5.1 Tests Performed

4.5.1.1 Calibration Tests

The calibration tests were necessary since the pull-out test procedure was not yet standardized. The first four tests were used to calibrate the performance of the apparatus, the pull-out box instrumentation and the consistency of the strain rate. Density and moisture content controls were checked. The density was controlled by measurements of heights of each layer of the samples during compaction. The height values were taken all over the sample, with an average of 15 to 20 points per layer. For the calibration tests, only the Tensar SR2 material was used as reinforcement as it seemed to be the easiest to work with because no epoxy was required to place the geogrid in the jaws.

4.5.1.2 Other Tests

Another twelve pull-out tests were performed. The tests were strain controlled at a rate of about 3%/min (12 mm/min). The normal stress range was limited by the capacity of the pull-out reaction frame; therefore, 20 kPa, 50 kPa, and 100 kPa confining stresses were chosen for all tests.

For most tests, moisture content values were taken before mixing the soil (hygroscopic moisture content), just after mixing the soil, before compaction and at the end of

Table 4.1 Average Distances Related to the Front End of the Pull-Out Box (cm)

	INSTRUMENTED ANCHOR MEMBERS												
GEOGRID	AM 2 *	AM 3 *	AM 4	AM 5	AM 6	AM 7	AM 8	AM 9	AM 10	AM 11	AM 12	AM 14	AM 17
SR2	15.840	4.30	7.30	18.814	30.331	41.786	53.279	-	76.252	-	89.271	-	-
TNX5001	14.860	-	5.10	15.140	25.140	35.140	-	55.120	-	75.090	-	105.02	-
PARAGRID 50S	11.325	-	5.025	-	20.375	-	35.875	-	51.675	-	65.775	80.875	102.825

* OUTSIDE PULL-OUT BOX

the tests. The variation between before compaction and end of test moisture contents was approximately 1%.

4.5.2 Test Procedure

The procedure for eight good tests is described in this section.

The five pieces that comprised the pull-out box were bolted together. The four load cells at the front end were assembled and prestressed in order to have a reliable response during the test. The satin fabric pieces were laid on both sides of the box and the bottom plate was divided into 21 rectangles for compaction control purposes. The first layer of soil was placed and each rectangle took approximately 1.15 kg of soil. This method of placing the soil in the box was required since each layer must be level after compaction.

Immediately after placement, the soil was compacted dynamically by a hammer with a steel plate (12 x 12 cm^2) attached to one end. This hammer weighs 4.5 kg which is the same as the Modified hammer, but the height of drop is only 17.5 cm. The height of drop was limited by the distance between the reaction frame and top of each layer. Therefore, the energy applied to the soil sample was 50% of the Standard Proctor Energy: 440 blows per layer. The dry density resulting from this compaction effort ranged from 1.49 g/cm^3 to 1.58 g/cm^3.

When the compaction of the first layer was finished, the layer was levelled. Again, the top of the sample was divided into 21 rectangles and half of the weight of soil used in the first layer was placed in the pull-out box. The geogrid sample was then placed on top of the loose soil and the horizontal loading system was assembled. The back LVDT support was mounted and the lengths of wire prestressed. The other half layer of soil was then placed as before and the sample compacted. Wax was used on both the front and back slots to seal the openings avoiding moisture content loss around these areas.

The third layer followed the same procedure as the first layer. The expanded metal was placed on top of the sample and a few extra blows were applied to it in order to make it penetrate the soil sample. This extra energy effort did not affect the dry density values since the moisture content of the sample was higher than the optimum moisture content. A polyethylene sheet was placed on top of the expanded metal to prevent moisture content loss by evaporation.

The assemblage of the vertical loading system was done immediately after compaction and levelling of the third layer. The two LVDTs used to monitor consolidation of the soil sample were placed on top of the prismatic elements (one at the front and the other at the back of the box). The soil sample was loaded with the confining normal stress and left to consolidate overnight.

It is important to note that measurements of heights were done at the end of each layer after levelling so that the density could be evaluated.

The next step consisted of assembling the LVDTs at the back of the box in order to monitor the horizontal displacements of the seven anchor members of the geogrid sample. The piece of geogrid that was out of the box, at the back, was carefully cut and the wax at the front end of the box was removed. All instrumentation was hooked up to the Data Logging Acquisition System and the pull-out test was ready to start.

At the end of the test the instrumentation was taken off of the geogrid sample, and it was cut to the length of the box. The geogrid sample was then weighed and its equivalent thickness was evaluated in order to calculate the density of the soil sample.

The evidence of slippage and bearing failure between the soil and grid were clearly observed after testing when the side of the box was removed, especially for the tests run with SR2.

It will be shown that the load cells at the front end of the box changed their readings (they loosened) during compaction. Consequently it was not possible to evaluate the value of Ko during compaction. The changes in readings are likely due to the vibration of the box bottom plate during compaction. As well, the vibration of the bottom steel plate may contribute to and explain the variation of dry density

caused by the consequent variation in compaction energy.

The consolidated undrained pull-out test is a quick test to run, about 5 minutes. On the other hand, its assemblage takes about 8 hours.

5. PULL-OUT TEST RESULTS

5.1 Introduction

The following sections present the results of the pull-out test program with silty clay soil reinforced with two geogrids: SR2 and TNX5001. The results of the pull-out tests with ParaGrid 50S are shown in Appendix A. These results were not analysed due to the grids failing prematurely because of damage at the junctions of the members.

5.2 Pull-Out Test Results

A summary of the laboratory pull-out data is presented in Table 5.1. The values of initial moisture contents were used for all calculations of the dry unit weights. The difference between the initial and final moisture contents is probably due to evaporation during compaction not consolidation; therefore, the final moisture content may be more representative of the actual test conditions. An average value of 24.9% is found for the initial moisture contents. The average values of dry unit weight and degree of saturation are 15.1 kN/m^3 and 89.6%, respectively. Consolidation of the specimens under the normal stresses was small, averaging around 3.8% strain.

Table 5.1 Pull-Out Test Results

TEST (#)	GEOGRID	NORMAL STRESS (kPa)	wi (%)	wf (%)	Si (%)	TOTAL UNIT WEIGHT (kN/m^3)	DRY UNIT WEIGHT (kN/m^3)	PEAK PULL-OUT FORCE (kN/m)	DISPL. AT PEAK PULL-OUT FORCE (mm)	RESIDUAL PULL-OUT FORCE (kN/m)	DISPL. AT RES. PULL-OUT FORCE (mm)
1	SR2	51	25.3	-	95	19.1	15.3	26.8	51.6	26.7	63.9
2	SR2	102.5	24.4	-	89	18.8	15.1	41.5	58.2	39.5	80.4
3	SR2	20	23.4	-	86	18.7	15.1	30.1	43.2	25.3	86.1
4	SR2	50	25.4	25.3	93	18.9	15.1	22.9	58.6	22.3	70.5
5	TNX5001	20	25.2	23.8	86	18.6	15.0	21.4	32.1	19.6	89.4
6	TNX5001	100.7	25.5	24.1	92	19.1	15.4	38.0	34.9	34.5	98.9
7	TNX5001	51.7	25.6	23.8	93	19.1	15.5	30.8	39.6	30.2	87.7
8	TNX5001	50	24.7	24.6	83	18.2	14.6	30.2	49.3	29.2	91.8

5.2.1 Pull-Out Force

Figures 5.1 and 5.2 show the pull-out curves for reinforced soil with SR2 and TNX5001, respectively. The displacements are measured relative to anchor member 2. These curves show that in all tests, the failure occurred by pull-out rather than rupture of the geosynthetics. Also, the pull-out resistance develops at a faster rate, in terms of displacement, for the geogrid that presents the highest modulus (TNX5001). This is an important point since in design procedure, the controlling factor is the pull-out resistance at a specific displacement, not at failure of the reinforcement. While the maximum pull-out force is mobilized during the first 20 mm to 50 mm of displacement for the TNX5001 geogrid, for the SR2, it is mobilized between 40 mm and 60 mm of displacement.

Test number 3, Tensar SR2, 20 kPa, had a lower value of moisture content compared with the other three tests in the same category. Therefore, the shear strength of the soil in this test is higher than those of the other three tests despite the dry densities being alike. Consequently, the maximum value of the pull-out force for test number 3 is higher (about 31%) than that for test number 4 (50 kPa) which is about 9% more humid.

5.2.2 Progressive Horizontal Displacement

In Chapter 4, the geogrid instrumentation was presented. The progressive displacements of each

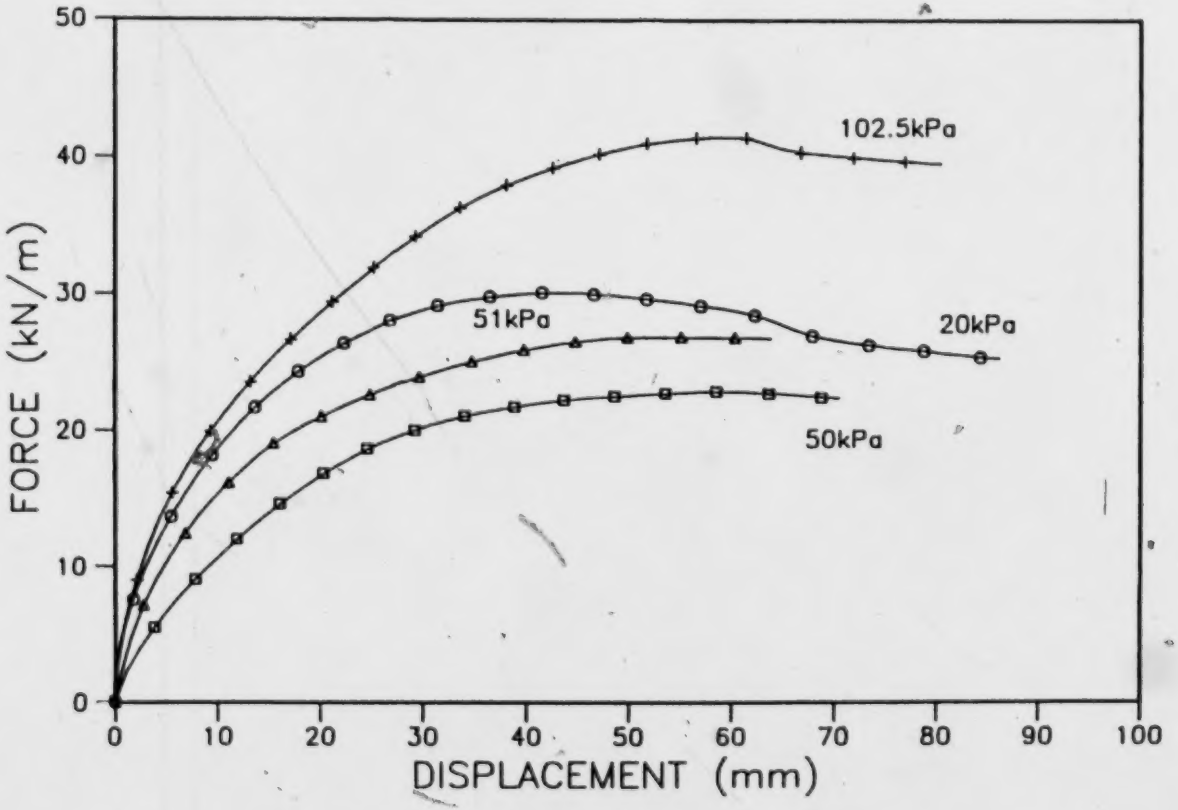

Figure 5.1 Pull-Out Force and Displacement Curves for Silty Clay Reinforced with SR2

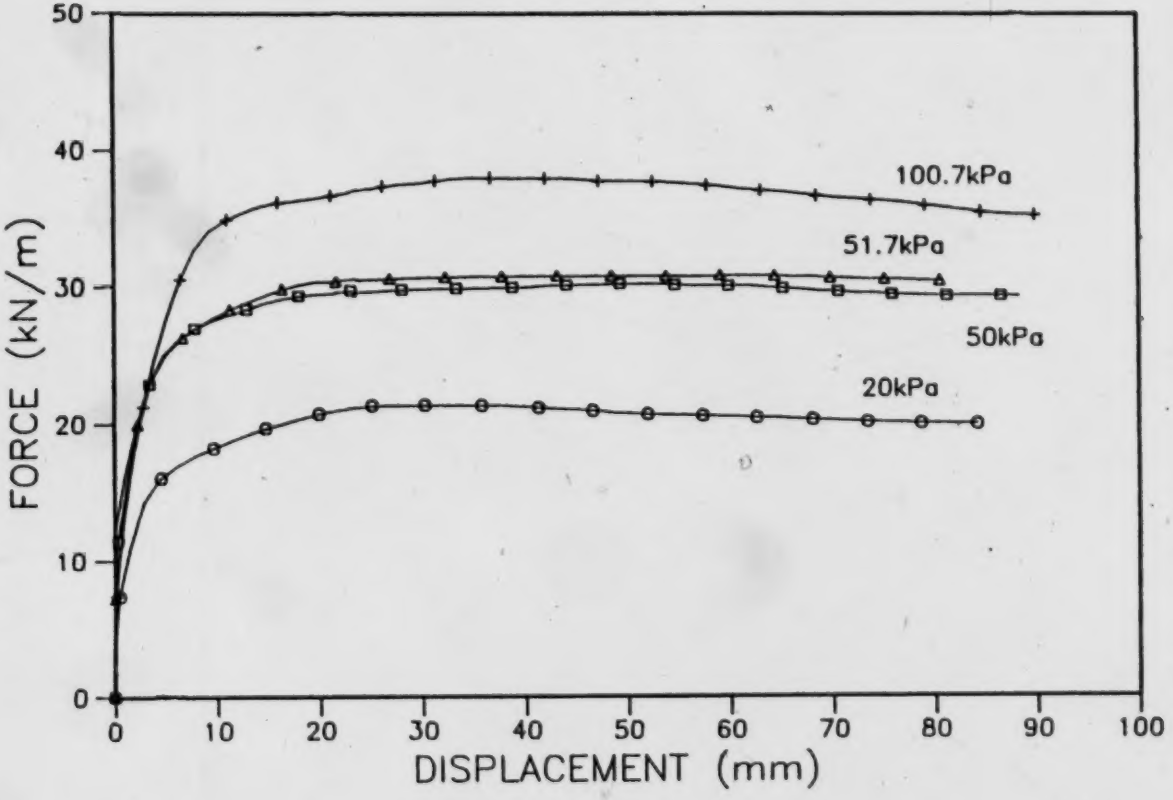

Figure 5.2 Pull-Out Force and Displacement Curves for Silty Clay Reinforced with TNX5001

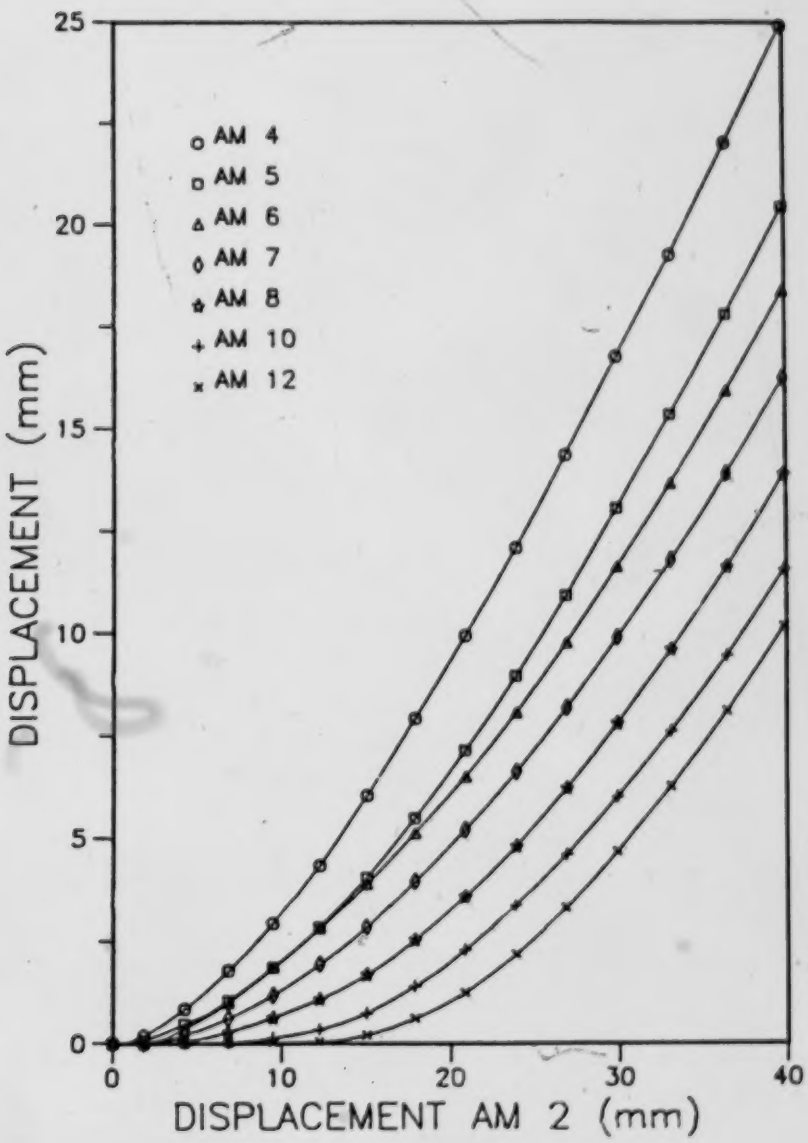

Figure 5.3 Progressive Displacements, SR2, 20 kPa

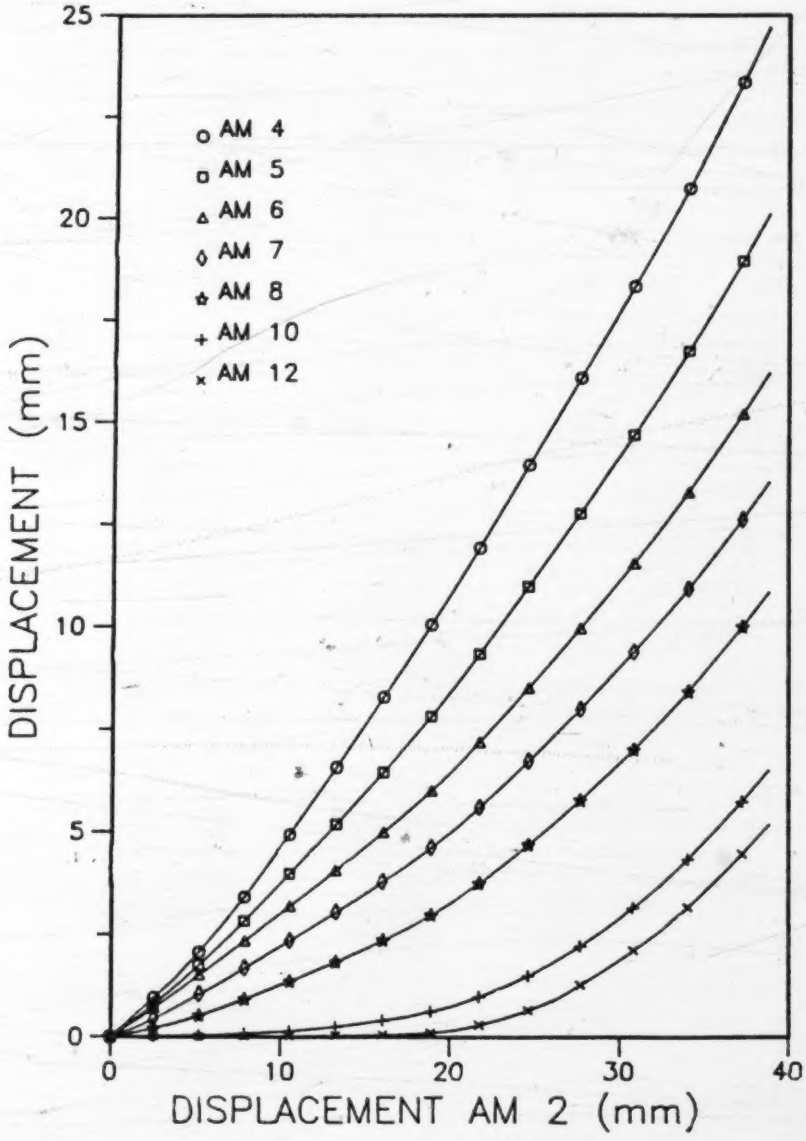

Figure 5.4 Progressive Displacements, SR2, 50 kPa

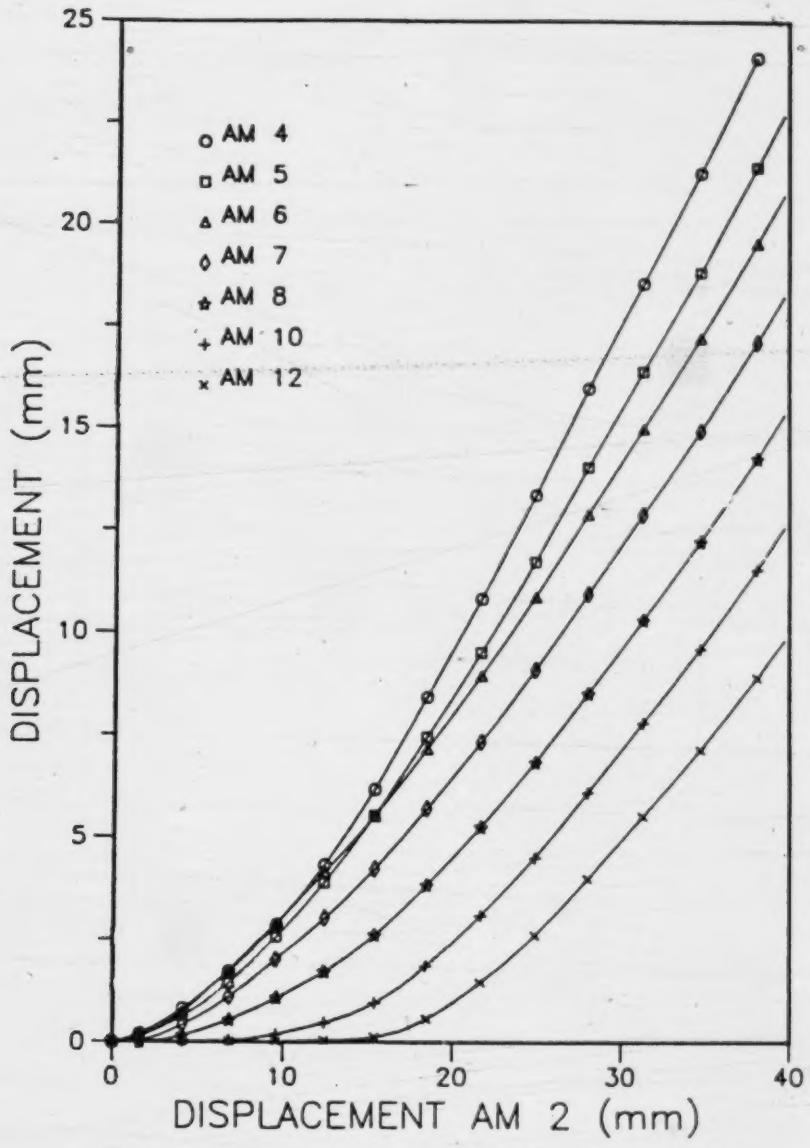

Figure 5.5 Progressive Displacements, SR2, 51 kPa

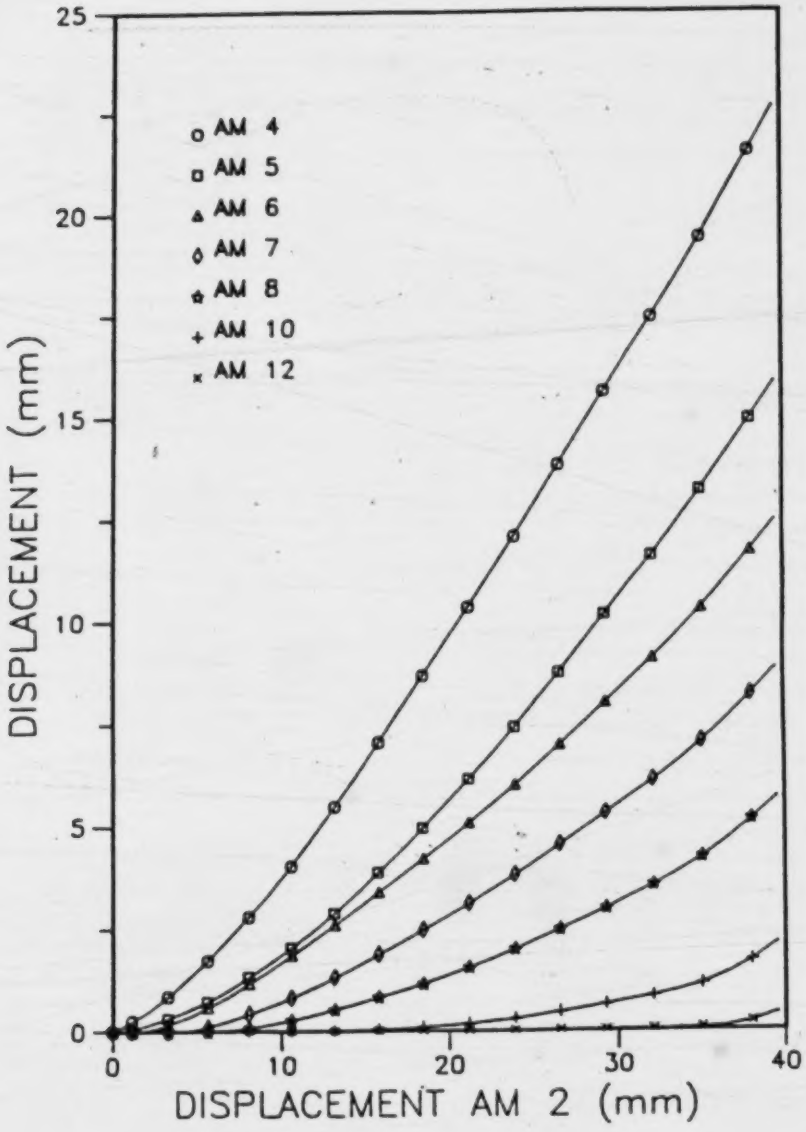

Figure 5.6 Progressive Displacements, SR2, 102.5 kPa

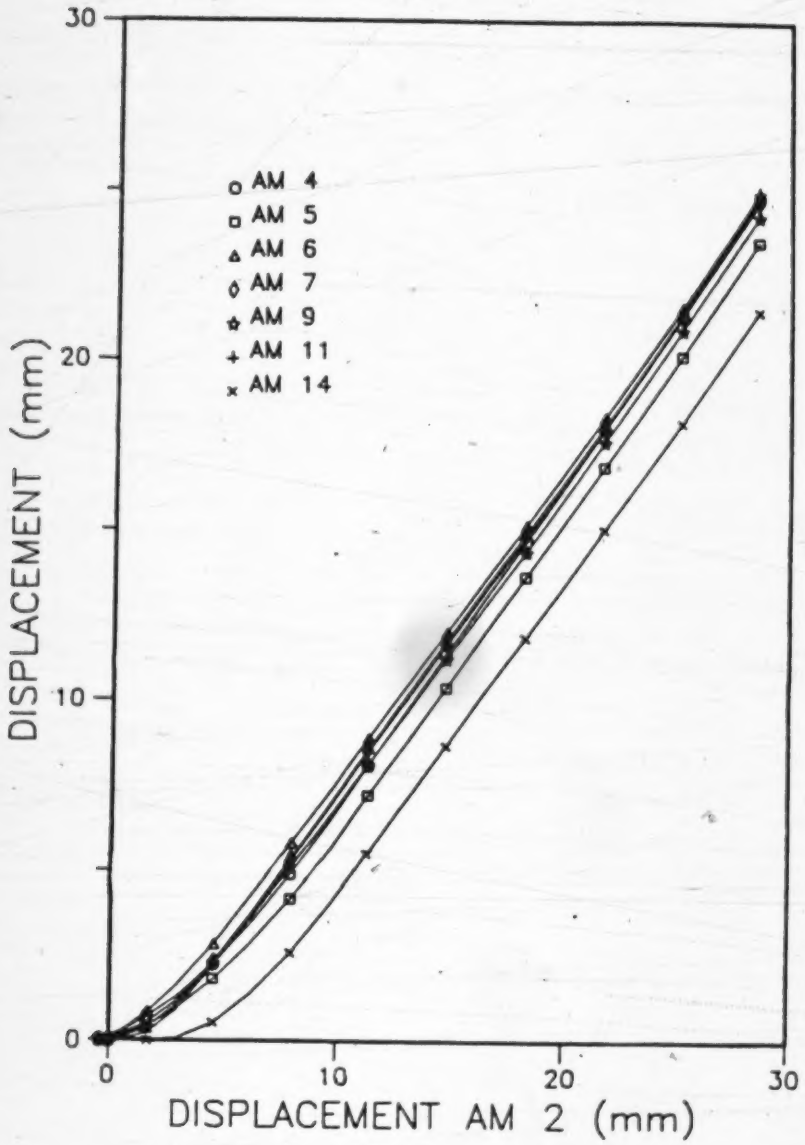

Figure 5.7 Progressive Displacements, TNX5001, 20 kPa

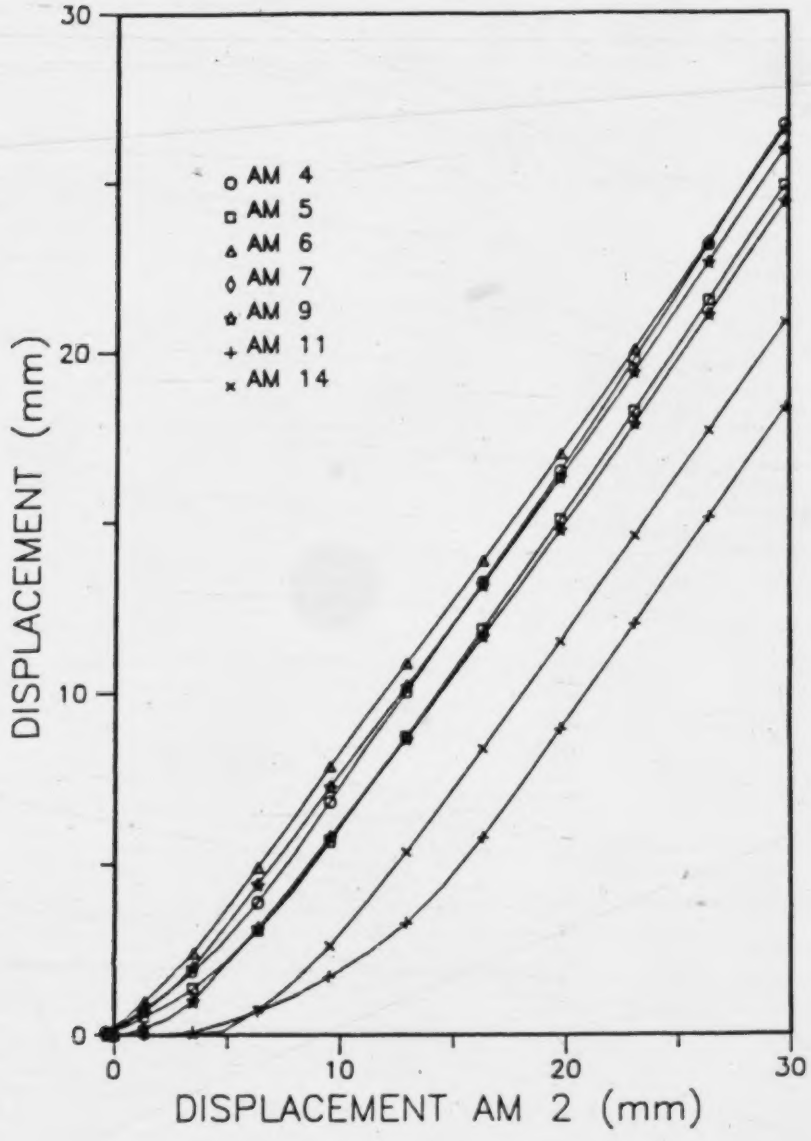

Figure 5.8 Progressive Displacements, TNX5001, 50 kPa

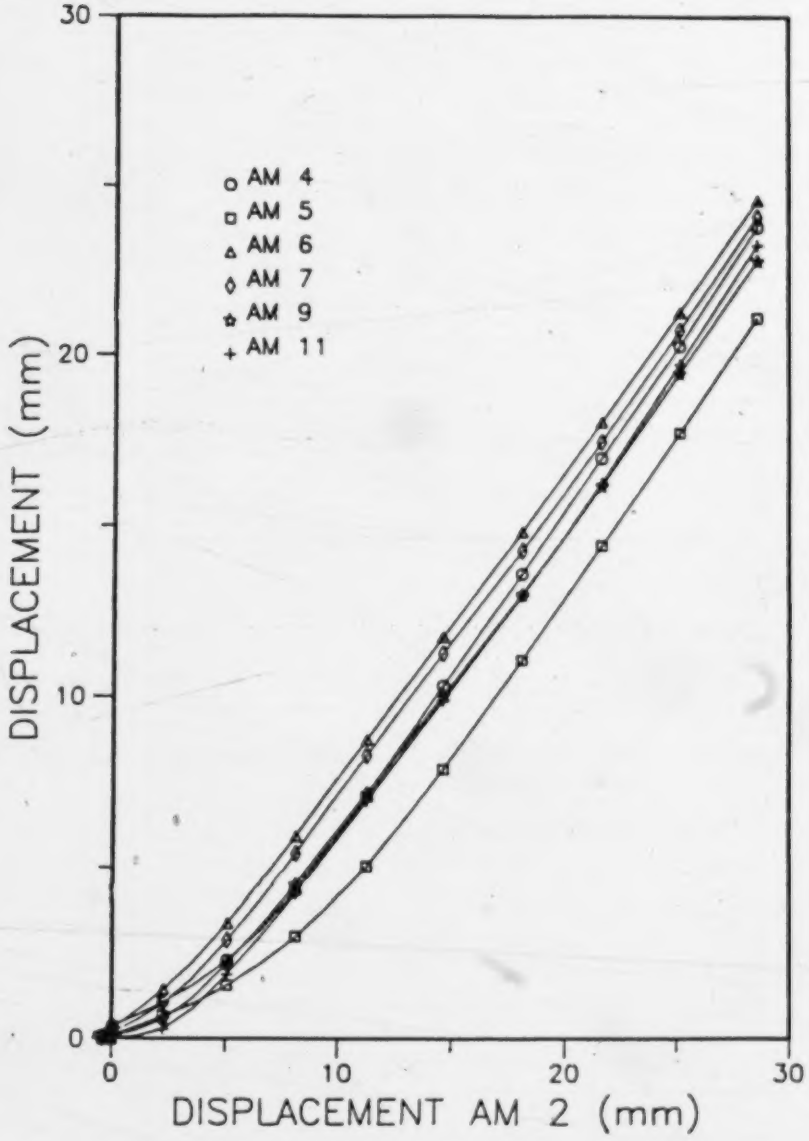

Figure 5.9 Progressive Displacements, TNX5001, 51.7 kPa

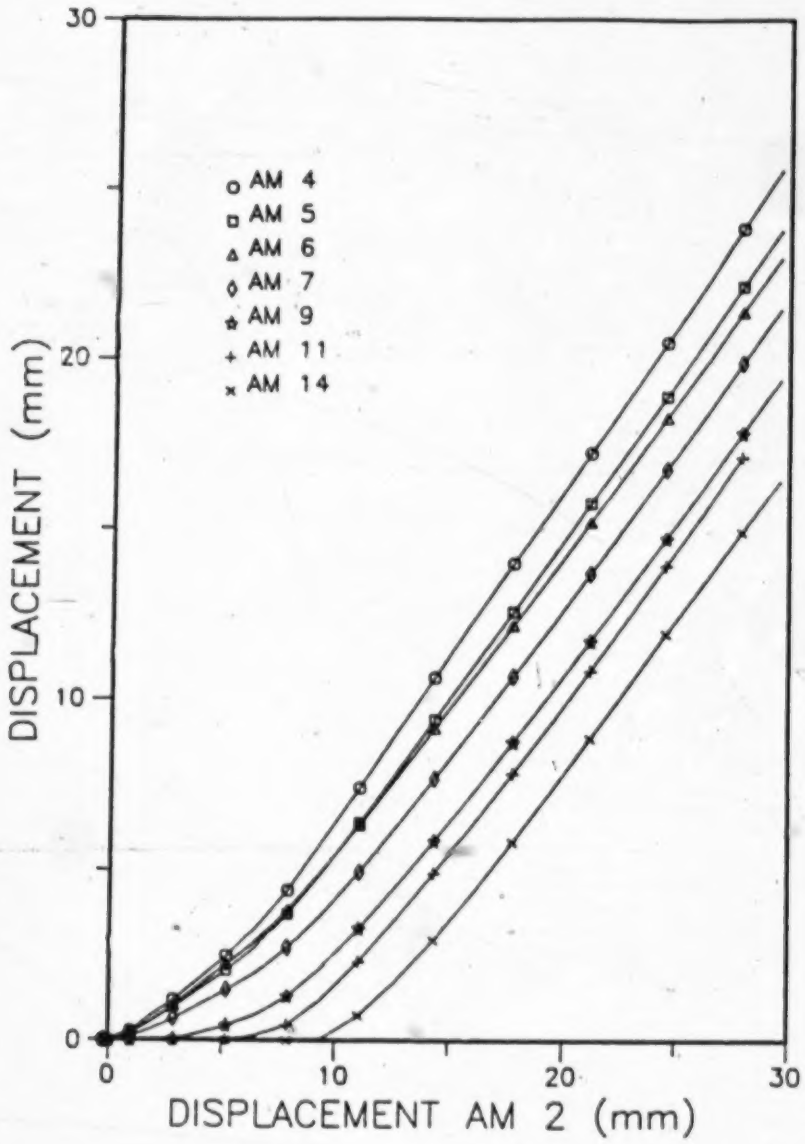

Figure 5.10 Progressive Displacements, TNX5001, 100.7 kPa

instrumented anchor member (AM) were recorded every five seconds during the pull-out tests. Figures 5.3 to 5.6 and Figures 5.7 to 5.10 show the progressive displacements of these anchor members for tests that were run with SR2 and TNX5001, respectively. The relative distance of AM2 to the front end of the pull-out box is shown in Table 4.1. Therefore, the displacements of AM2 shown in these Figures are not at the front end of the box, 0 to 4 mm of strain (depending on the value of the pull-out force took place between AM2 and the front end of the pull-out box. The curvature in the initial part of the progressive horizontal displacement curves shows the stretching of the geogrid. The progressive displacement can be better visualized in the SR2 geogrid due to its lower tensile modulus compared to TNX5001 geogrid. When the curves become linear and parallel, shear sliding is fully mobilized along the entire length of the reinforcements.

Anchor member 2 (AM#2) is located outside the pull-out box. Table 4.1 should be referred to for further details.

5.2.3 Passive Force at the Front Face of the Soil Sample

The horizontal forces against the front face of the pull-out sample were recorded for each test. Figures 5.11 to 5.14 and Figures 5.15 to 5.18 present the results for tests with SR2 and TNX5001, respectively. Load cells 1 (lc1) and load cell 3 (lc3) are located 2.5 cm below the center line of the slot and load cells 2 and 4 (lc2, lc4) are located

2.5 cm above the center line of the slot. Table 5.2 presents the results. An average of 11% of the maximum pull-out force is transmitted to the soil in a passive way. The maximum and minimum values are 18% and 6%, respectively.

It was observed that load cells 2 and 4 (above the center line of the slot) recorded very low or even compression (-) values. The geogrid level after compaction is likely to be the reason, i.e., the geogrid level was below the center line of the slot which during the tests, caused a rotation of the pull-out box front face and compressive forces were recorded in load cells 2 and 4.

If the soil were fully saturated and the pull-out test run in completely undrained condition, the increase in normal stress at the geogrid level caused by the increase in horizontal pressure would not affect the results of the pull-out test because the shear strength of the soil would not change in this condition. On the other hand, passive failure of the soil at the front of the box could take place. At the end of each test, the soil sample was examined carefully and no sign of rupture could be detected. Table 5.2 summarizes results of the maximum values of passive force against the soil sample.

5.2.4 Vertical Displacement During Tests

One LVDT (C#1) placed on top of a prismatic element, 14.5 cm from the front end and another one (C#3) placed at the back, 14.5 cm from the back end, monitored the vertical

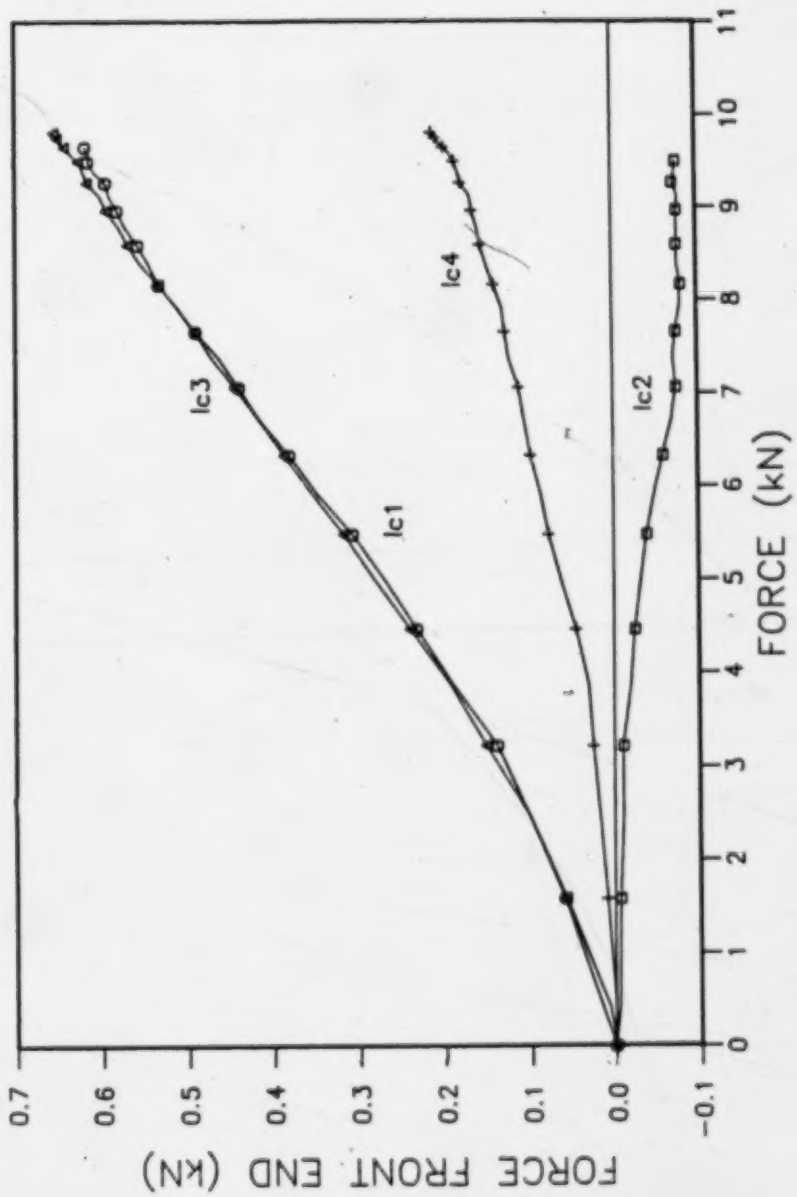

Figure 5.11 Pull-Out Force - Horizontal Force at Front End of the Box, SR2, 20 kPa

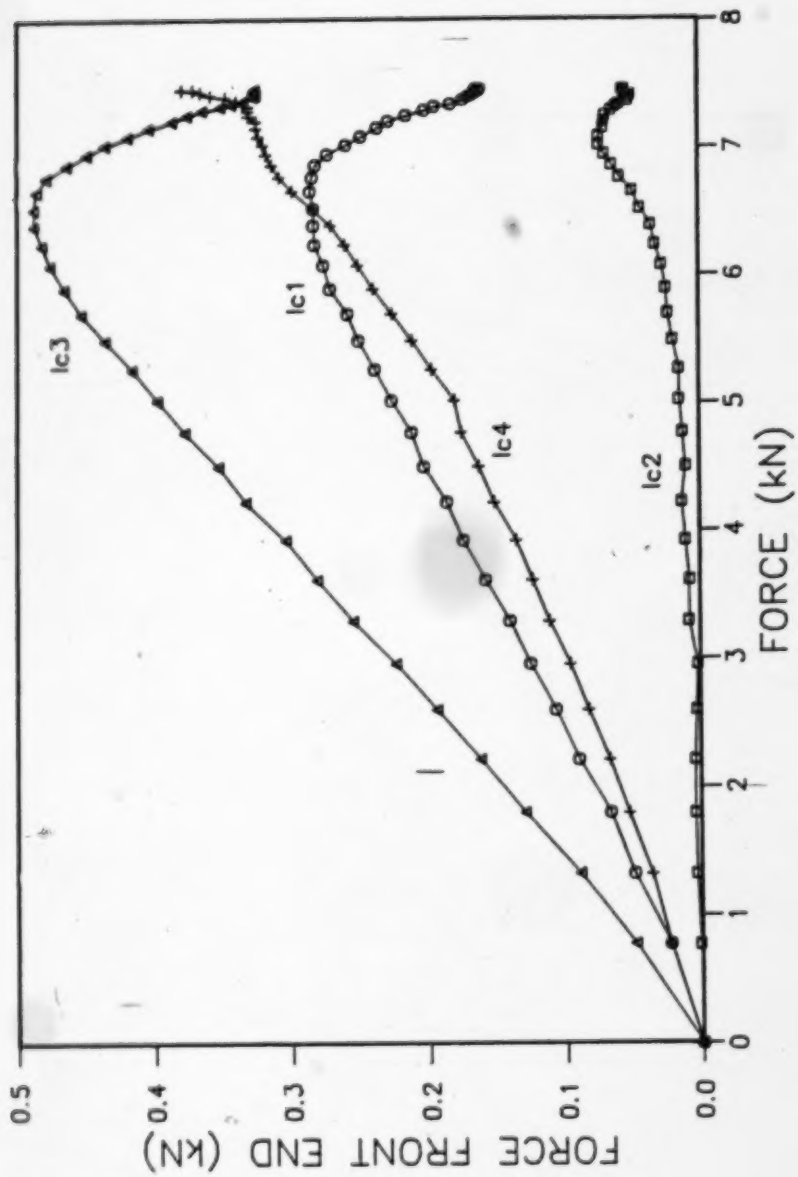

Figure 5.12 Pull-Out Force - Horizontal Force at Front End of the Box, SR2, 50 kPa

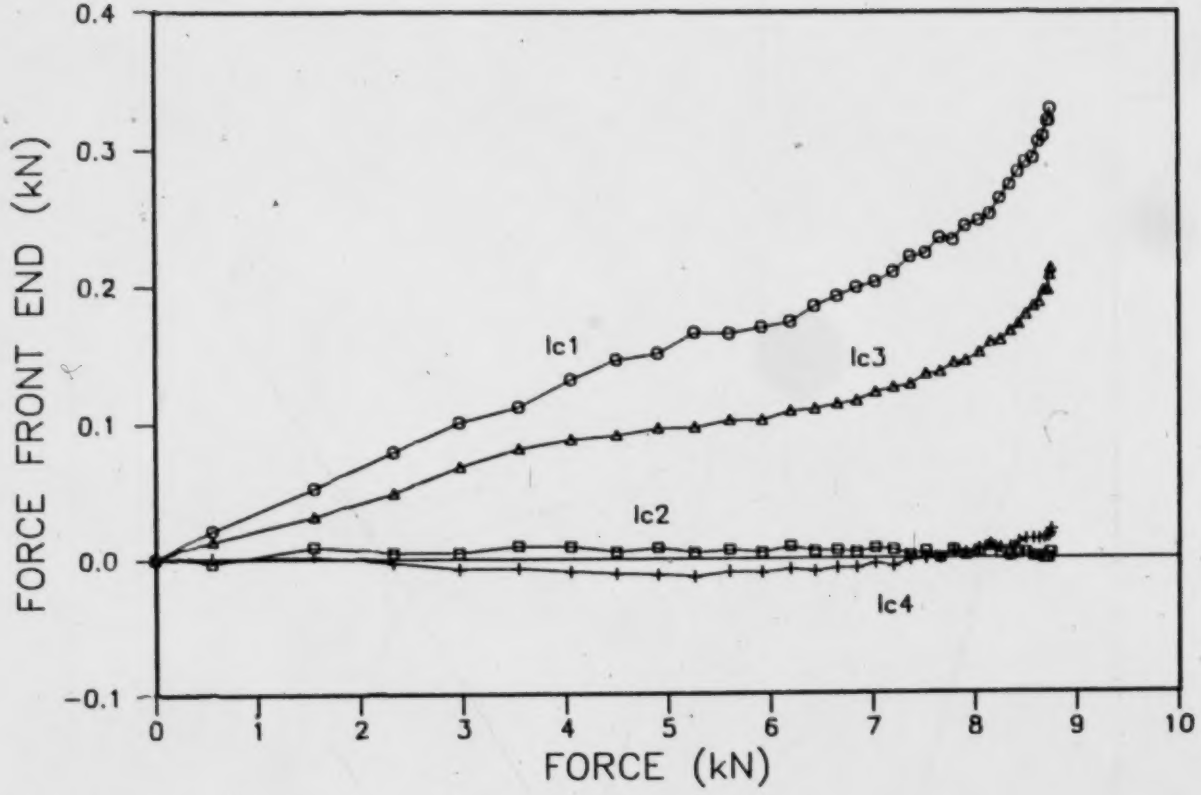

Figure 5.13 Pull-Out Force - Horizontal Force at Front End of the Box, SR2, 51 kPa

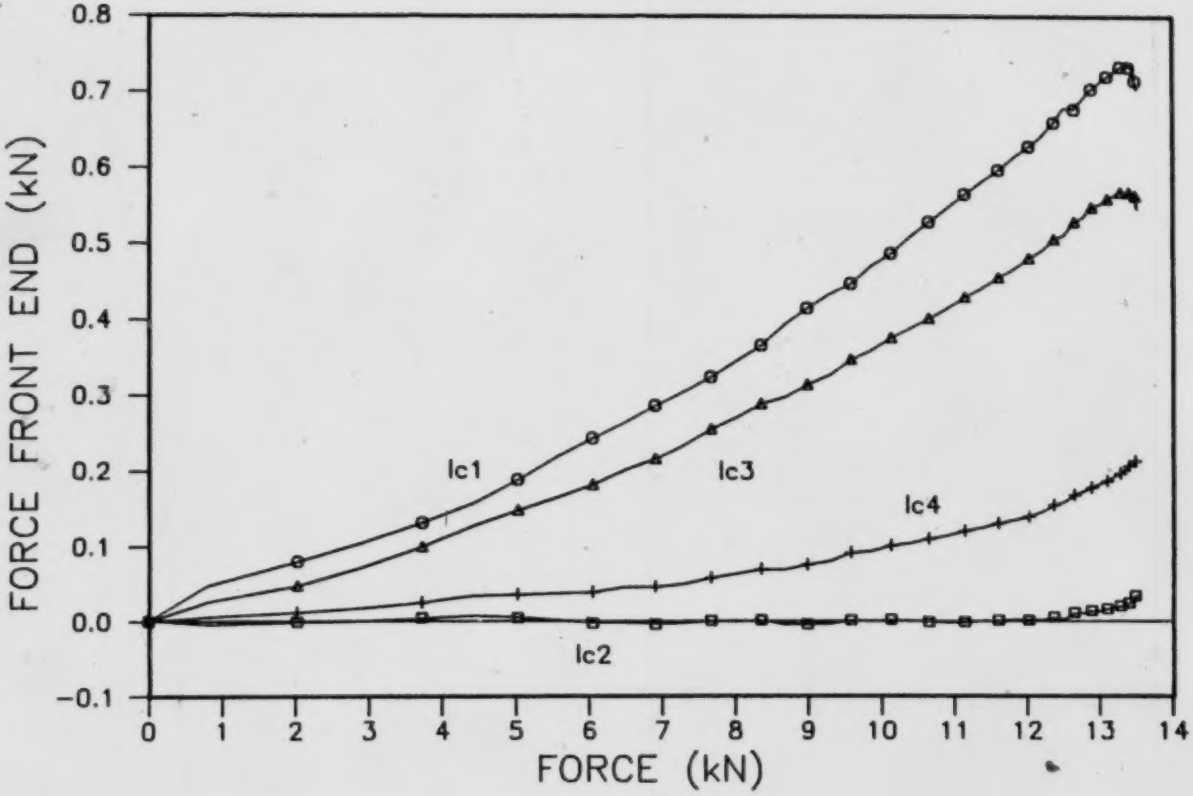

Figure 5.14 Pull-Out Force - Horizontal Force at Front End of the Box, SR2, 102.5 kPa

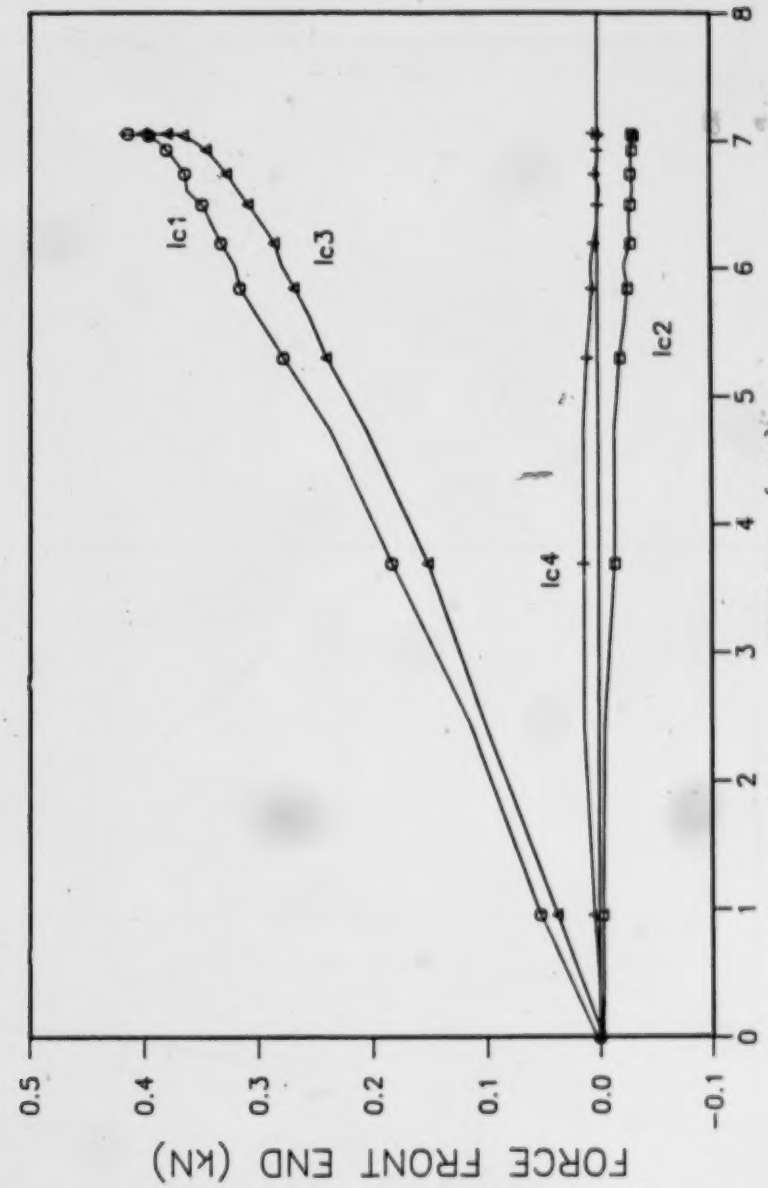

Figure 5.15 Pull-Out Force - Horizontal Force at Front End of the Box, TNX5001, 20 kPa

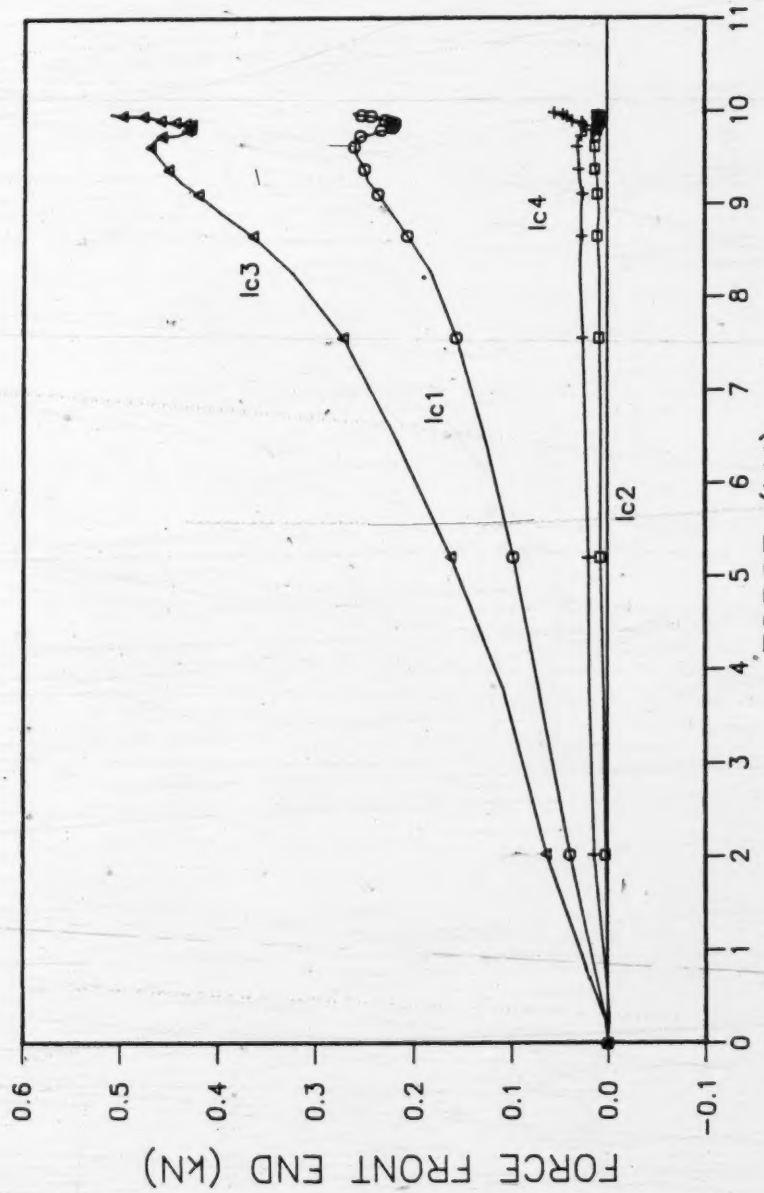

Figure 5.16 Pull-Out Force - Horizontal Force at Front End of the Box, TNX5001, 50 kPa

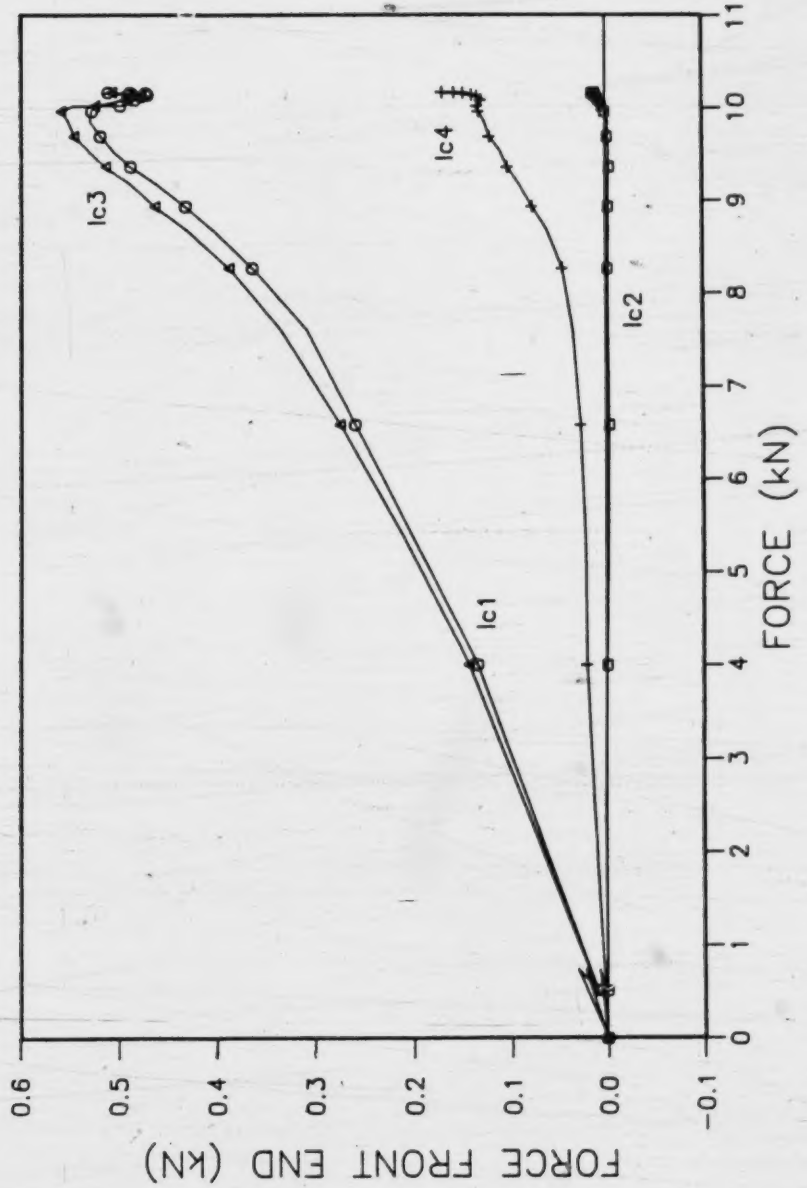

Figure 5.17 Pull-Out Force - Horizontal Force at Front End of the Box, TNX5001, 51.7 kPa

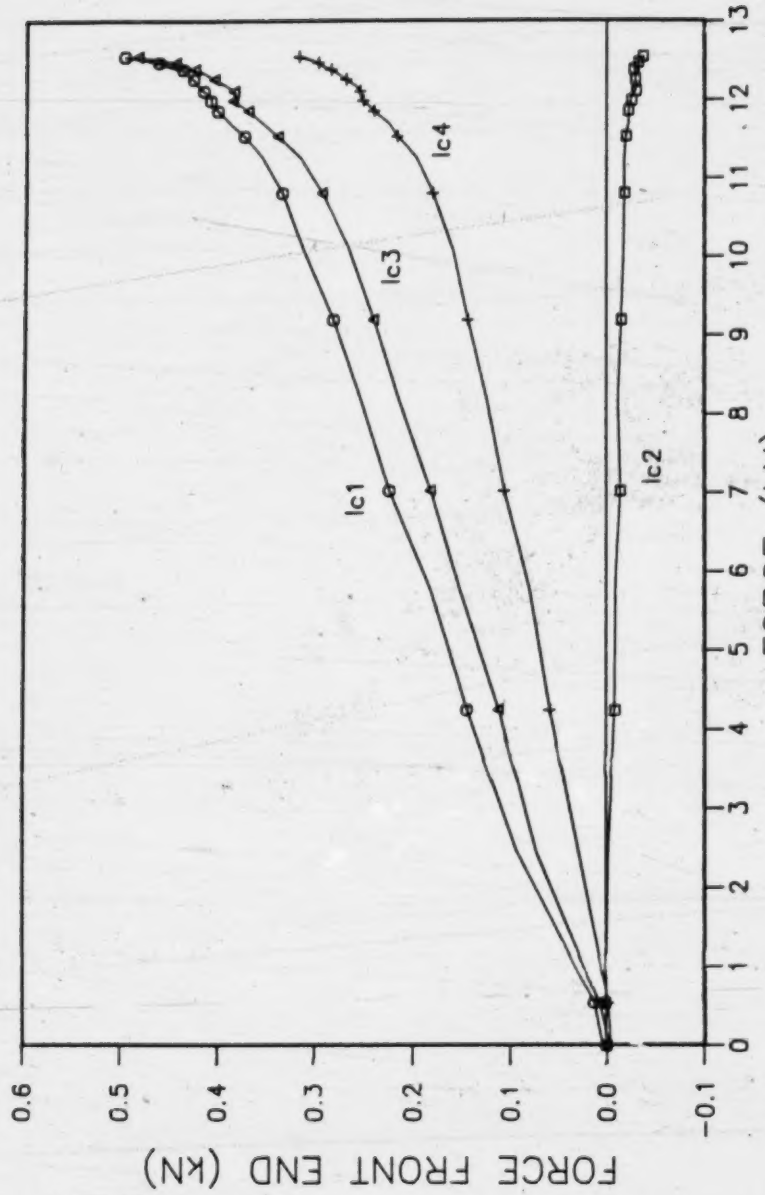

Figure 5.18 Pull-Out Force - Horizontal Force at Front End of the Box, TNX5001, 100.7 kPa

displacement during the pull-out test. Figures 5.19 to 5.22 and Figures 5.23 to 5.26 present the results for tests reinforced with SR2 and TNX5001, respectively. In these plots, the negative values represent dilation and the positive ones represent compression of the soil sample.

It can be seen that the magnitude of the vertical displacements is very small, around 2% of the soil sample height. Furthermore, dilation occurred in the samples reinforced with TNX5001, on the other hand, compression occurred in those reinforced with SR2. However, there is no significant reason for the different behaviors. The junction thickness of the TNX5001 is approximately three times smaller than that of the SR2. Taking this into account, one would expect the soil sample reinforced with SR2 to dilate rather than the one with TNX5001.

Table 5.2 Force on Front End of the Soil Sample

TEST (#)	MAX. PULL-OUT FORCE (kN)	FRONT END LOAD CELLS					SUM/ MAX PULL-OUT FORCE (%)
		lc1 (kN)	lc2 (kN)	lc3 (kN)	lc4 (kN)	SUM (kN)	
1	8.74	0.33	0	0.21	0.02	0.56	6
2	13.36	0.74	0.02	0.56	0.20	1.52	11
3	9.82	0.62	-0.08	0.66	0.22	1.42	14
4	6.66	0.28	0.07	0.49	0.33	1.17	18
5	7.08	0.42	-0.03	0.39	0	0.78	11
6	12.56	0.50	-0.04	0.48	0.32	1.26	10
7	10.00	0.51	0.01	0.52	0.17	1.21	12
8	10.20	0.26	0.01	0.51	0.05	0.83	8

(+) Compression
(-) Tension

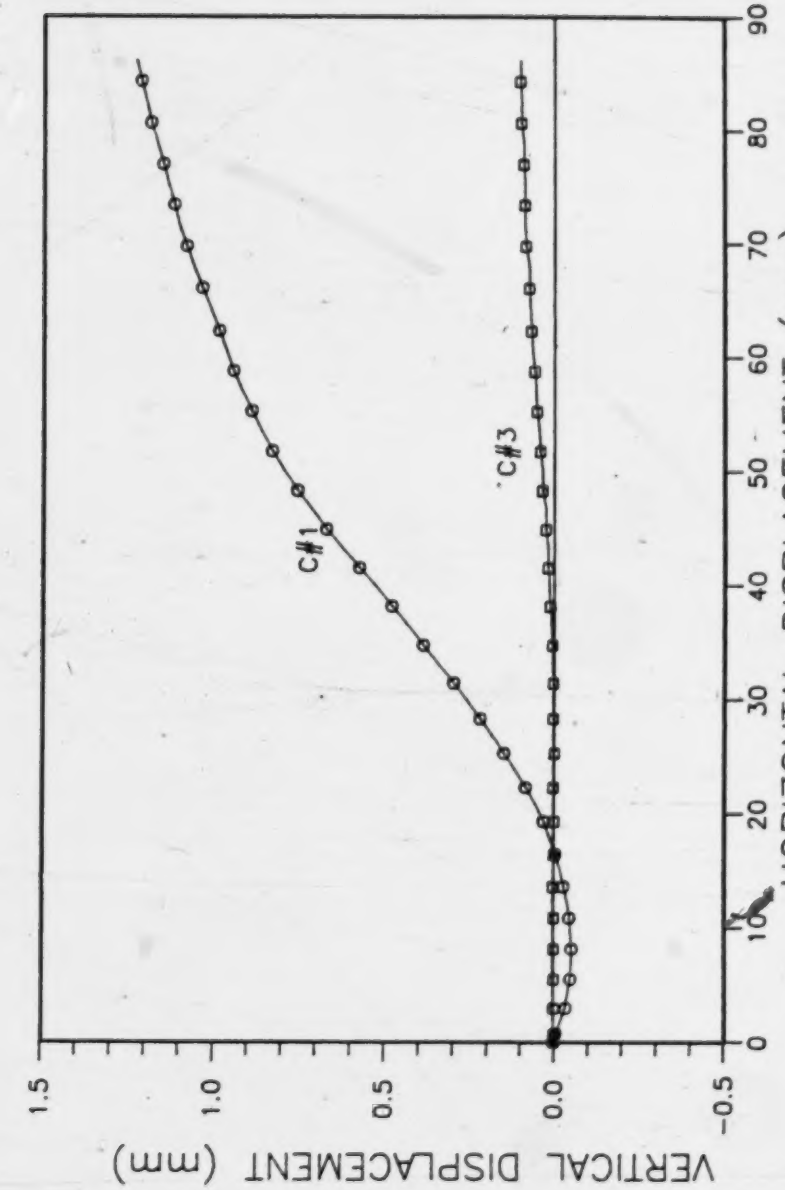

Figure 5.19 Soil Sample Behaviour During Pull-Out Test, SR2, 20 kPa

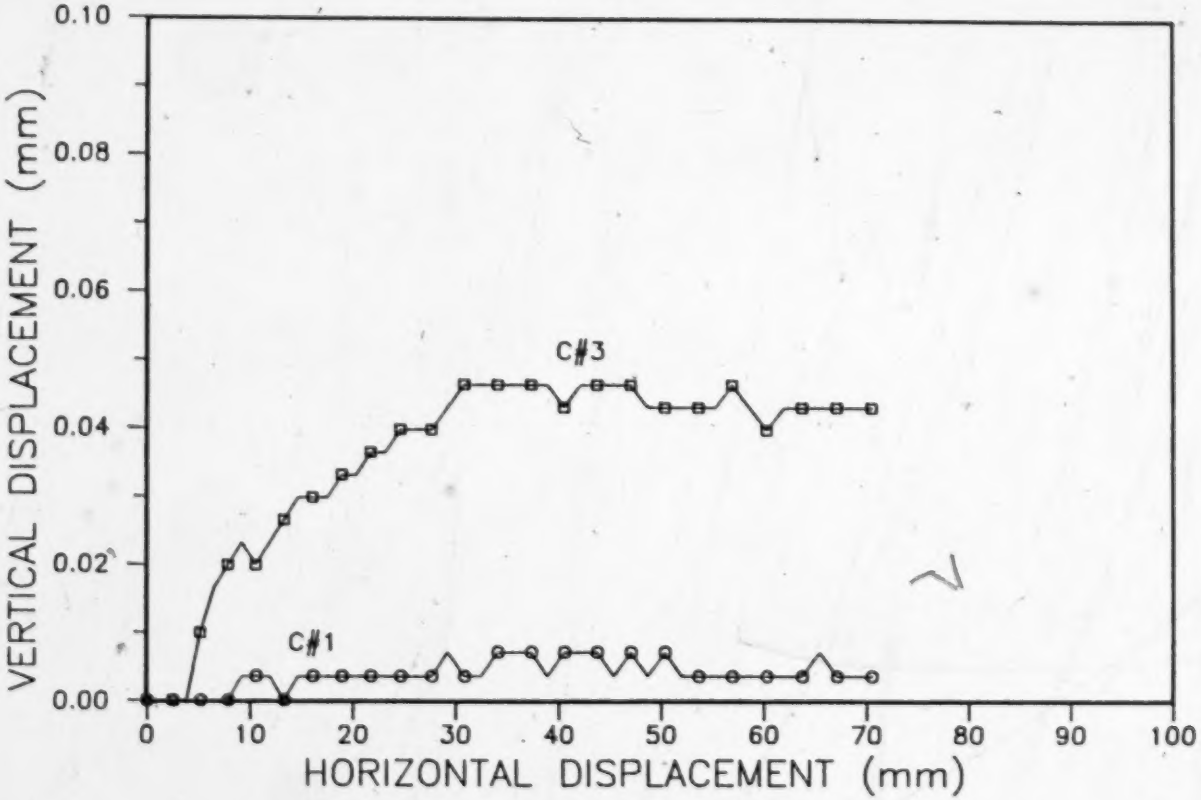

Figure 5.20 Soil Sample Behaviour During Pull-Out Test, SR2, 50 kPa

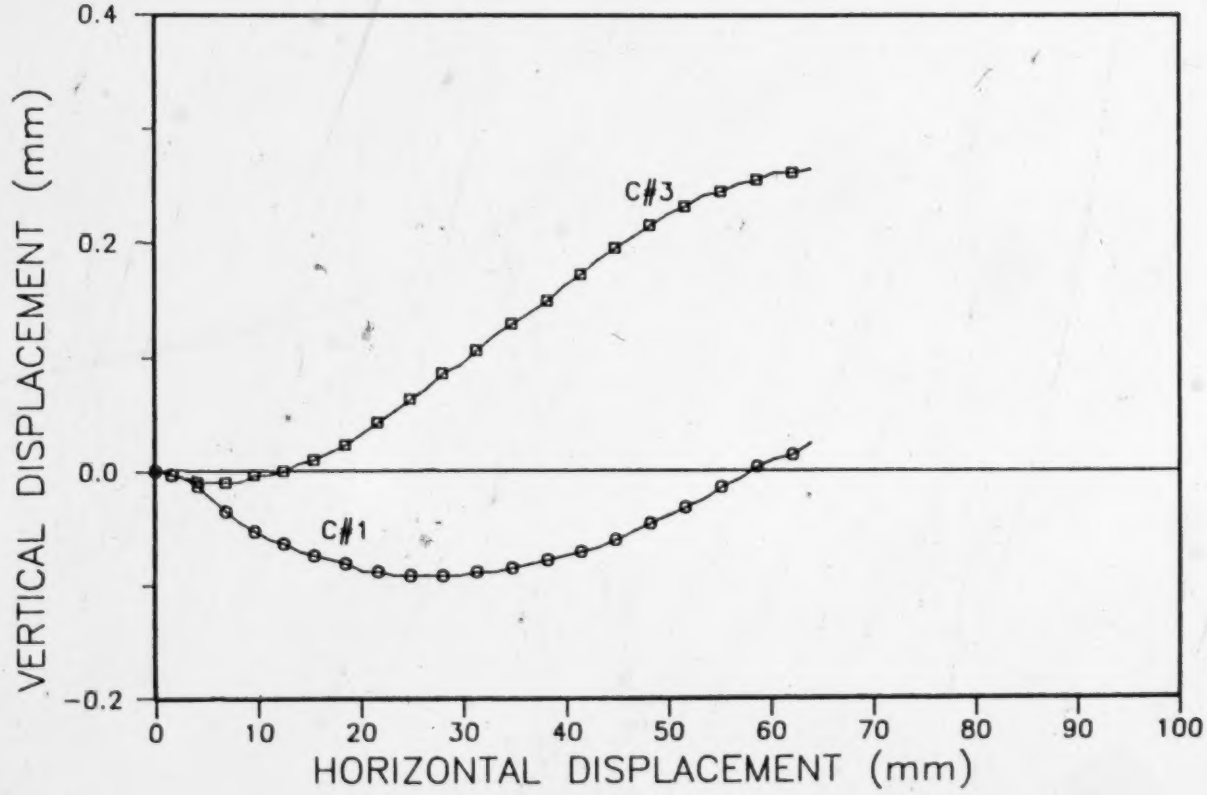

Figure 5.21 Soil Sample Behaviour During Pull-Out Test, SR2, 51 kPa

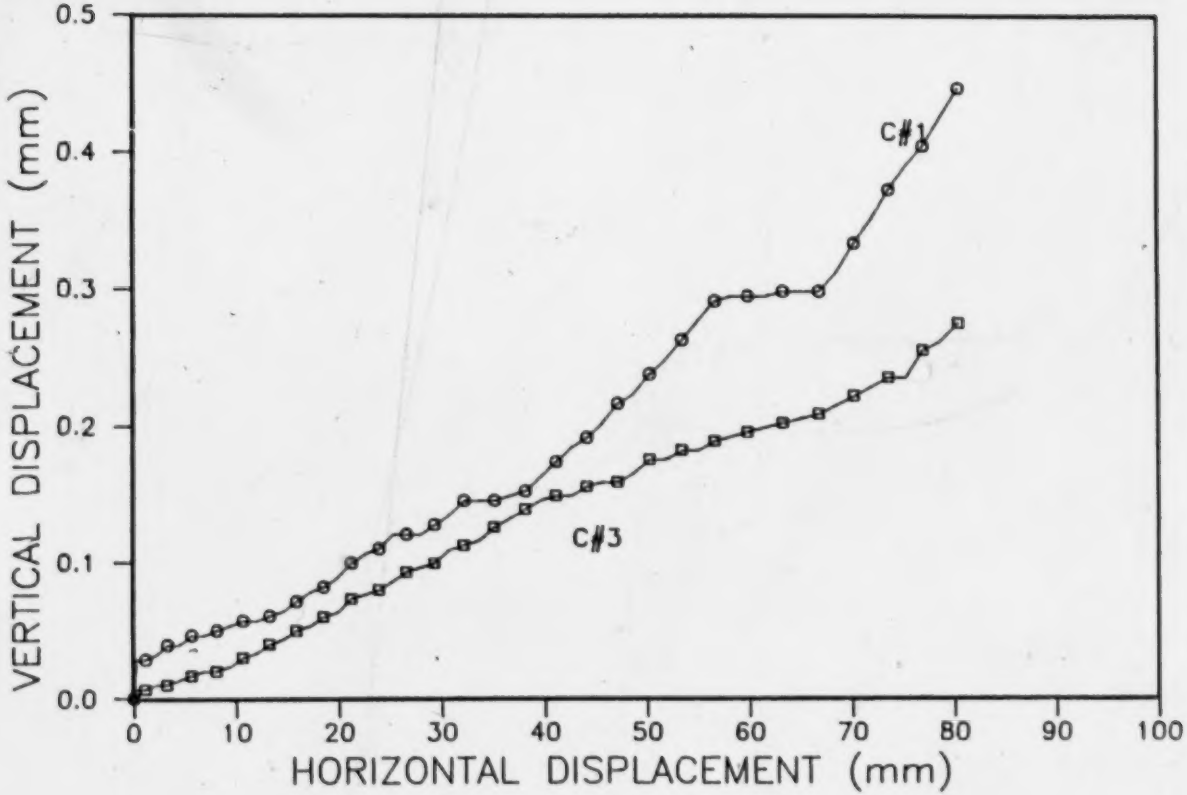

Figure 5.22 Soil Sample Behaviour During Pull-Out Test, SR2, 102.5 kPa

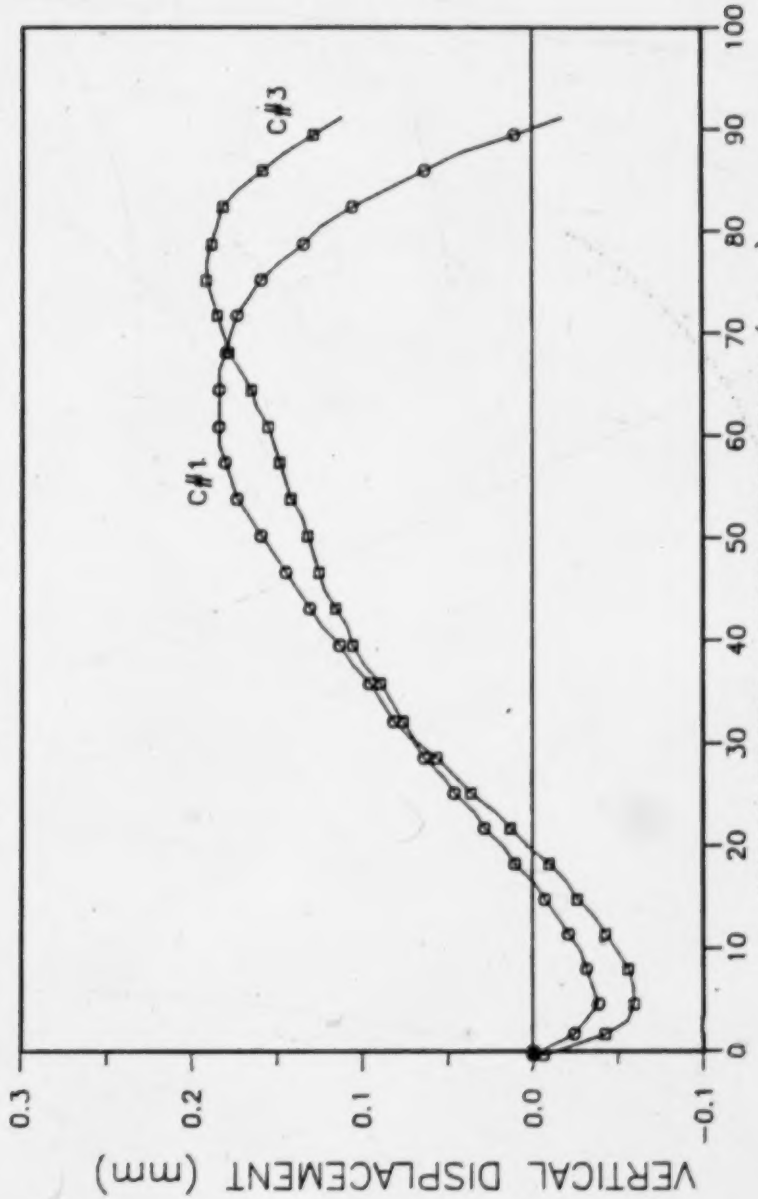

Figure 5.23 Soil Sample Behaviour During Pull-Out Test,

TNX5001, 20 kPa

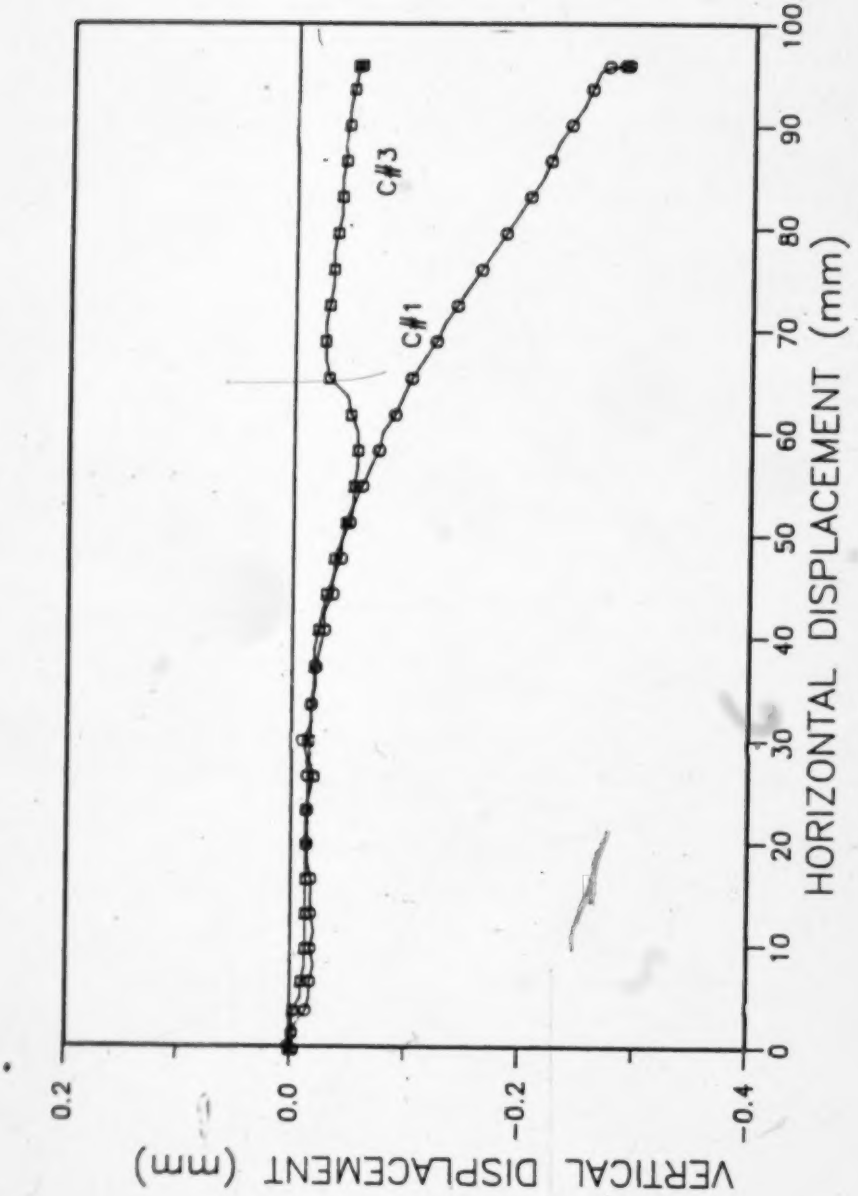

Figure 5.24 Soil Sample Behaviour During Pull-Out Test,

TNX5001, 50 kPa

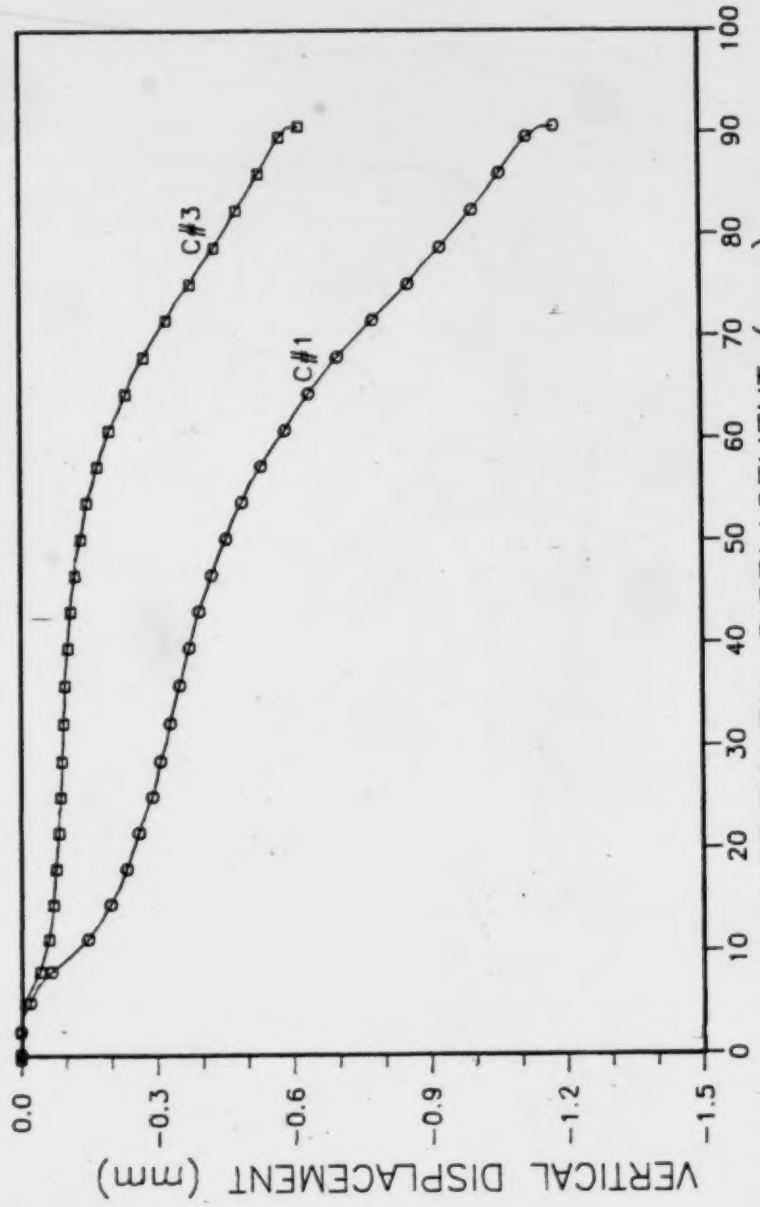

Figure 5.25 Soil Sample Behaviour During Pull-Out Test,

TNX5001, 51.7 kPa

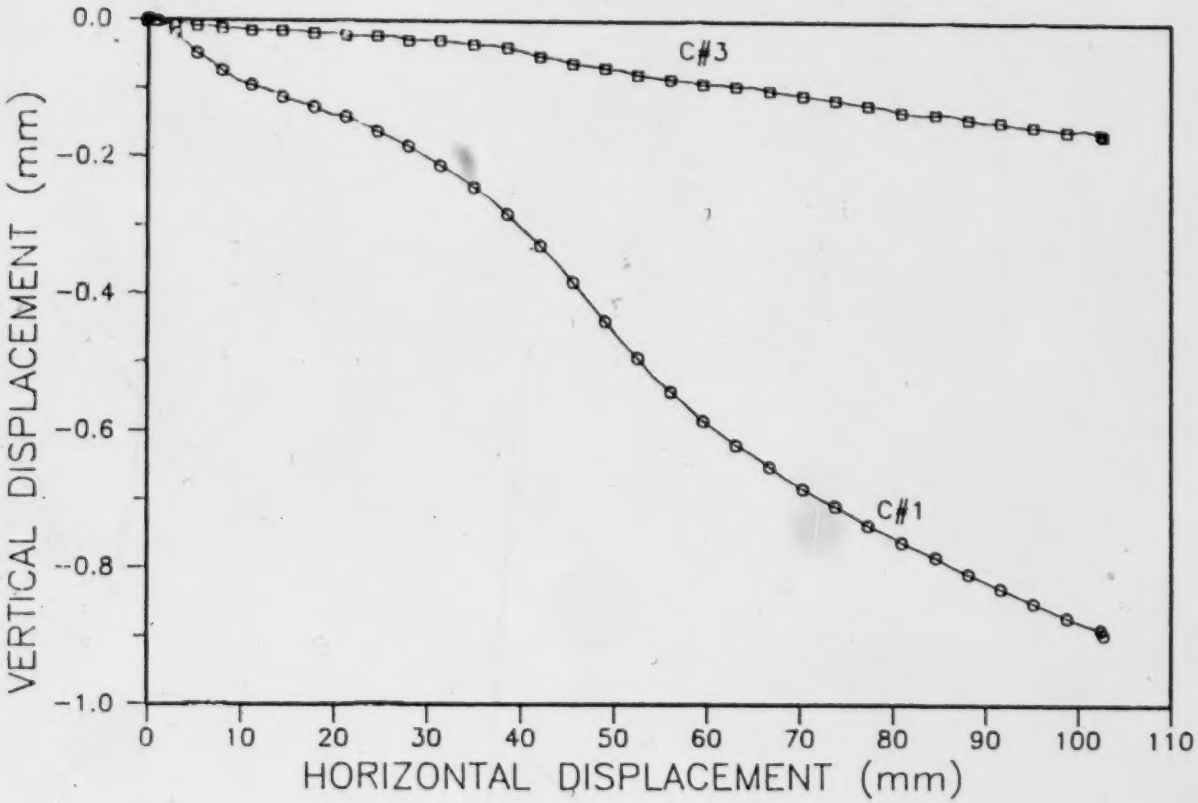

Figure 5.26 Soil Sample Behaviour During Pull-Out Test, TNX5001, 100.7 kPa

6. LOAD TRANSFER APPROACH TO PREDICT THE TENSILE FORCES ALONG THE GEOGRIDS

6.1 Introduction

"The load transfer and stress distribution between reinforcements and soil needs more careful definition for most earth reinforcement systems. Much of the data available pertain to reinforced earth and granular backfill...", (Highway Research Report 290, 1987).

The study of how the load is transferred to the soil surrounding an axially loaded pile is presented by Coyle and Reese (1966). Beech (1987), made an approach based on Coyle and Reese's load transfer method to predict the pull-out tension as a function of the displacements of reinforcement material.

The approach that is shown in this chapter is based on the same method by Coyle and Reese (1966). It is important to notice that in all figures in this chapter, the symbols stand for experimental results while the lines represent either fitting curves or results from theoretical analyses.

6.2 An Analytical Approach Based on the Load Transfer Method

An analytical approach is presented which predicts the tensile forces along the reinforcement from shear strength properties of the soil, tensile and geometric properties of the geosynthetics and pull-out test results. It is important that the distribution of the elongation (strain) of the

geogrid be taken into account because the same shear strength will not be mobilized at all points along the reinforcement.

In the load transfer approach, the analysis is one dimensional; therefore, a geogrid tension member is divided into a series of elements. The shear stress is assumed to be constant along each element, on the other hand, the tension within each element decreases from one end to the other. Consequently, the strain along each element also decreases as do the displacements at the beginning of each element. The smaller displacement at the beginning of element i+1 results in a smaller shear stress being generated along element i+1 than that along element i. The result is a decrease in mobilized shear resistance along the geogrids. Figure 6.1 illustrates the model of interaction between soil and geogrid used in this analysis. A similar model was used by Brandt (1985) to represent the behavior of a soil-concrete interface.

6.3 Soil and Reinforcement Parameters

Knowledge of the reinforcement force-strain properties and shear resistance of the soil as a function of displacement are required for the load transfer approach. The geogrid force-strain properties and soil shear strength are discussed in Chapter 3. In the case of the SR2 geogrid, due to the non-constant rigidity of the tension members, coupling tensile curves were used in which parameters (a and

b) obtained in constant cross section tensile tests were used to fit the force-strain curves (actually an average deformation between two consecutive anchor members) obtained during the pull-out tests. The σ vs ϵ curves (tensile tests on constant cross section of SR2 anchor member) were fitted using the expression $\sigma = \frac{a.\epsilon}{b+\epsilon}$. The resulting values of a and b were used to fit the curves F x ϵ obtained during the pull-out tests as follows:

$$F_i = \sigma_i A_i$$

$$F_i = \left(\frac{a\epsilon_i}{b+\epsilon_i}\right) A_i$$

where,

σ_i = axial stress

F_i = pull-out forces

A_i = cross sectional area of element i

ϵ_i = elongation or strain of element i

Rearranging the latter equation,

$$\epsilon_i = \frac{(F_i/A_i).b}{(a-(F_i/A_i))}$$

The sum of ϵ_i should coincide with the value of ϵ measured during the pull-out test. The SR2 tension member has a constant thickness but the width varies. A constant cross section was obtained by cutting the ends of the tension member, resulting in a constant width. Figures 6.2 to 6.9

illustrate these tensile curves for the SR2 geogrid.

6.4 Interaction Between the Soil and Reinforcements in a Pull-Out Test

The mechanisms of interaction in a pull-out test in undrained conditions are discussed in Chapter 2. The two mechanisms are: shear along the plane surface of the geosynthetic and bearing or passive resistance against the anchor members.

The effect of interference between geogrid anchor members was not taken into account since S/B>5, (Milligan and Palmeira, 1987). The values of S/B are 120 and 22 for the TNX5001 and SR2, respectively.

The equation to determine the maximum pull-out force is as follows:

$$P_{max} = 2\ \tau_u . A_p . \alpha_s . \beta + \tau_u . A_b . N_c \qquad [6.1]$$

where

τ_u = peak undrained shear strength of the soil

A_p = total plane area of the geogrid (WxL)

α_s = % of solid area in the geogrid

β = interfacial stress factor

A_b = cross section area where bearing forces act

N_c = coefficient of bearing capacity

6.4.1 The Interfacial Stress Factor, β

The interfacial stress factor is defined as the adhesion of the reinforcement plan area to the soil. It is a

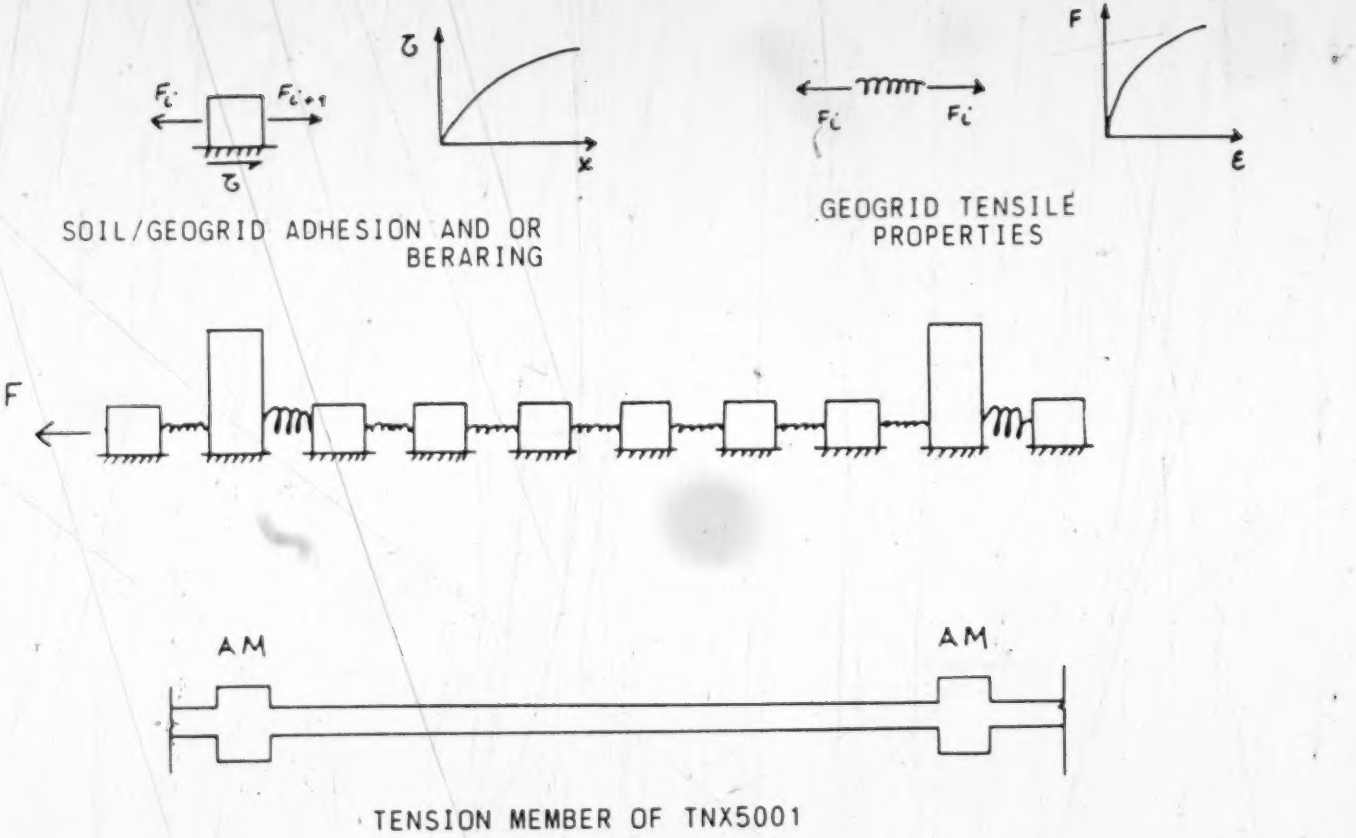

Figure 6.1 Model of Interaction Between Cohesive Soil and Geogrid in a Pull-Out Test

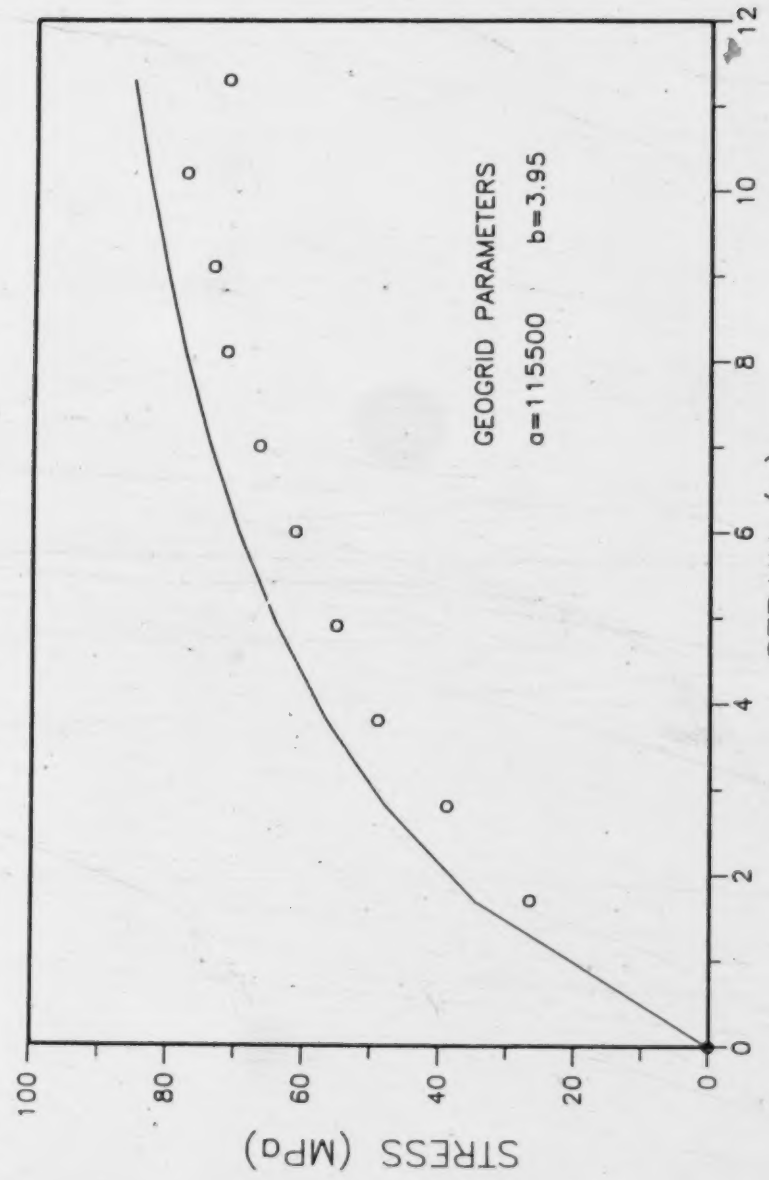

Figure 6.2 Stress-Strain Fitting and Measured Curves of Tensile Test on a Constant Cross Section of SR2, 20 kPa

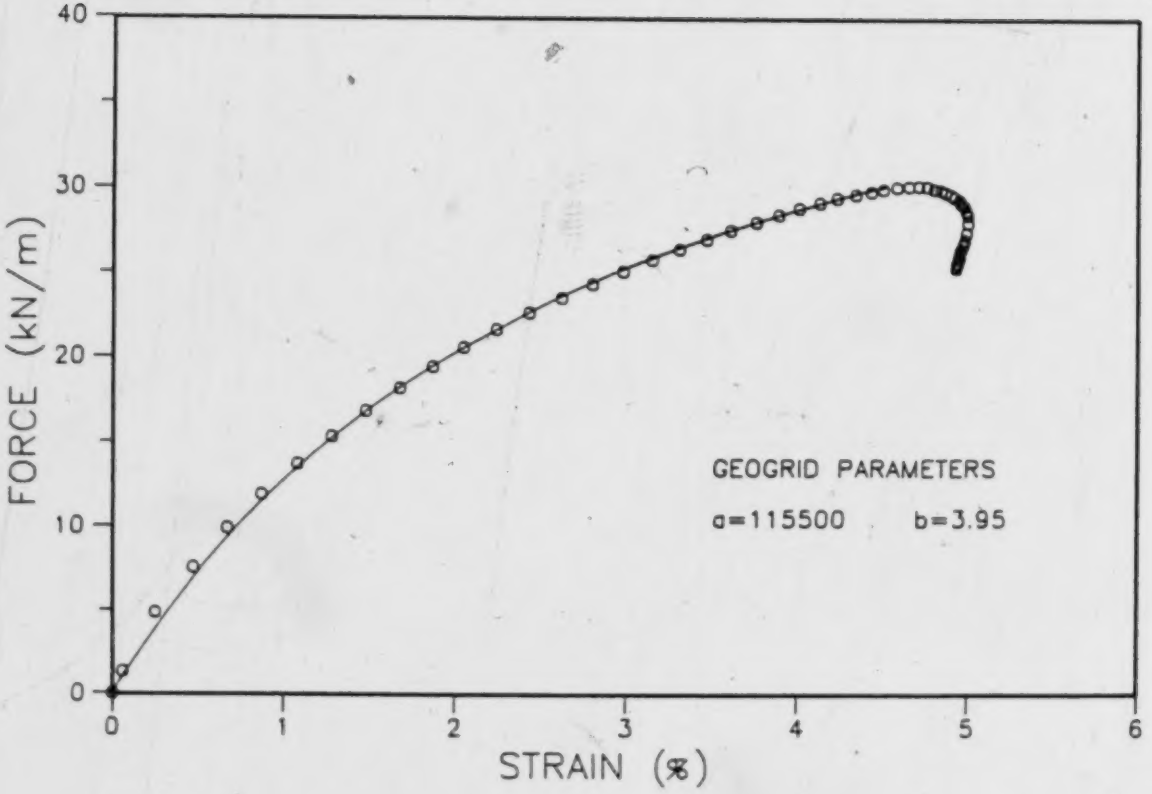

Figure 6.3 Force-Strain Fitting and Measured Curves during Pull-Out Test, SR2, 20 kPa

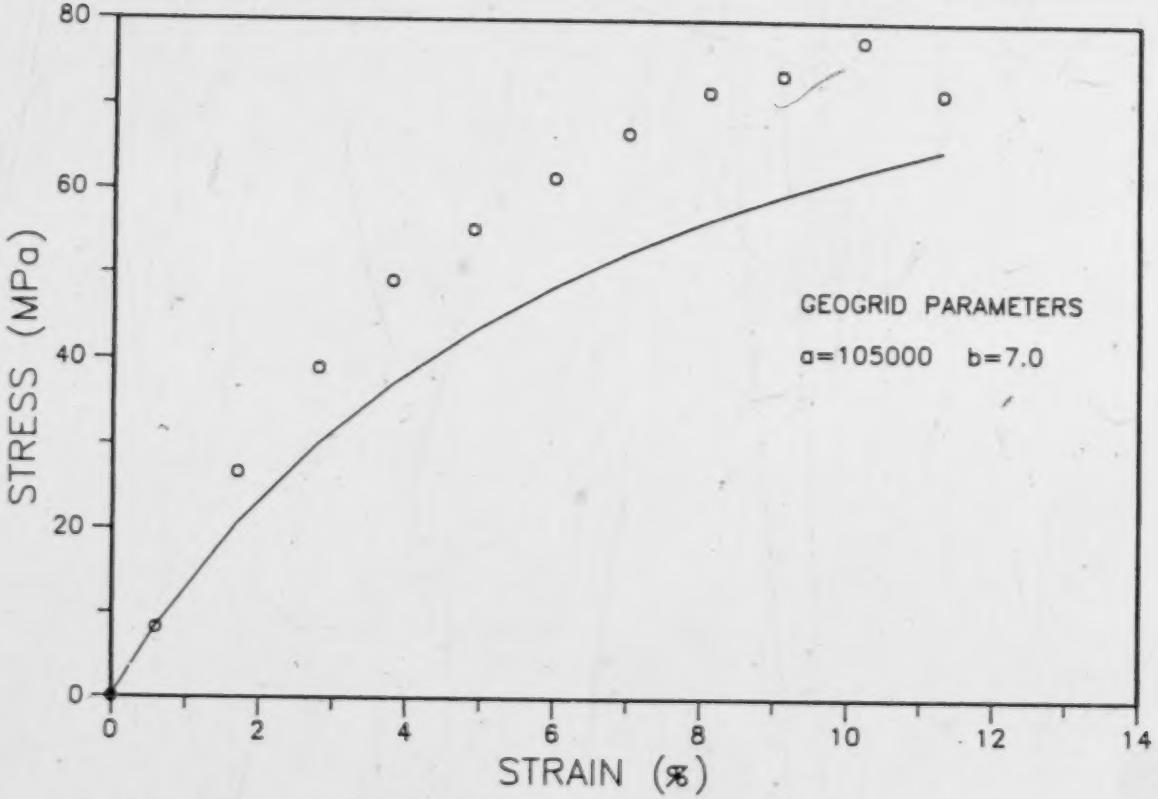

Figure 6.4 Stress-Strain Fitting and Measured Curves of Tensile Test on a Constant Cross Section of SR2, 50 kPa

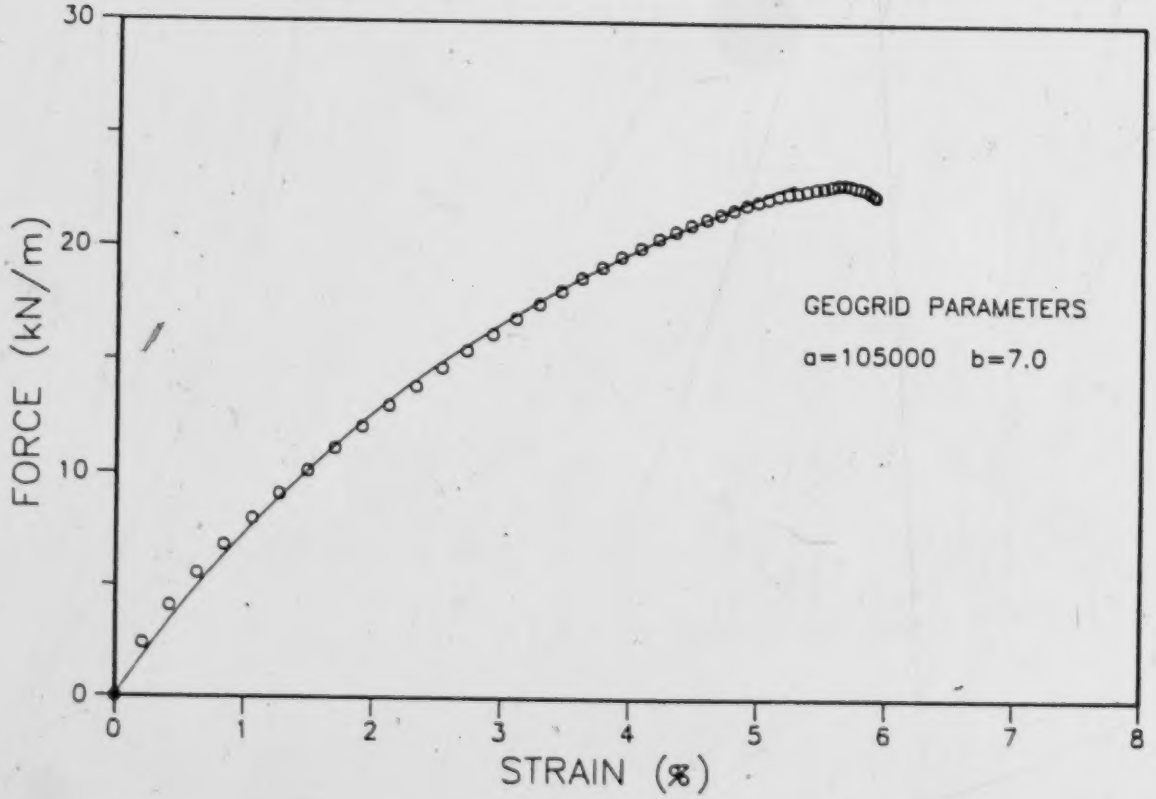

Figure 6.5 Force-Strain Fitting and Measured Curves during Pull-Out Test, SR2, 50 kPa

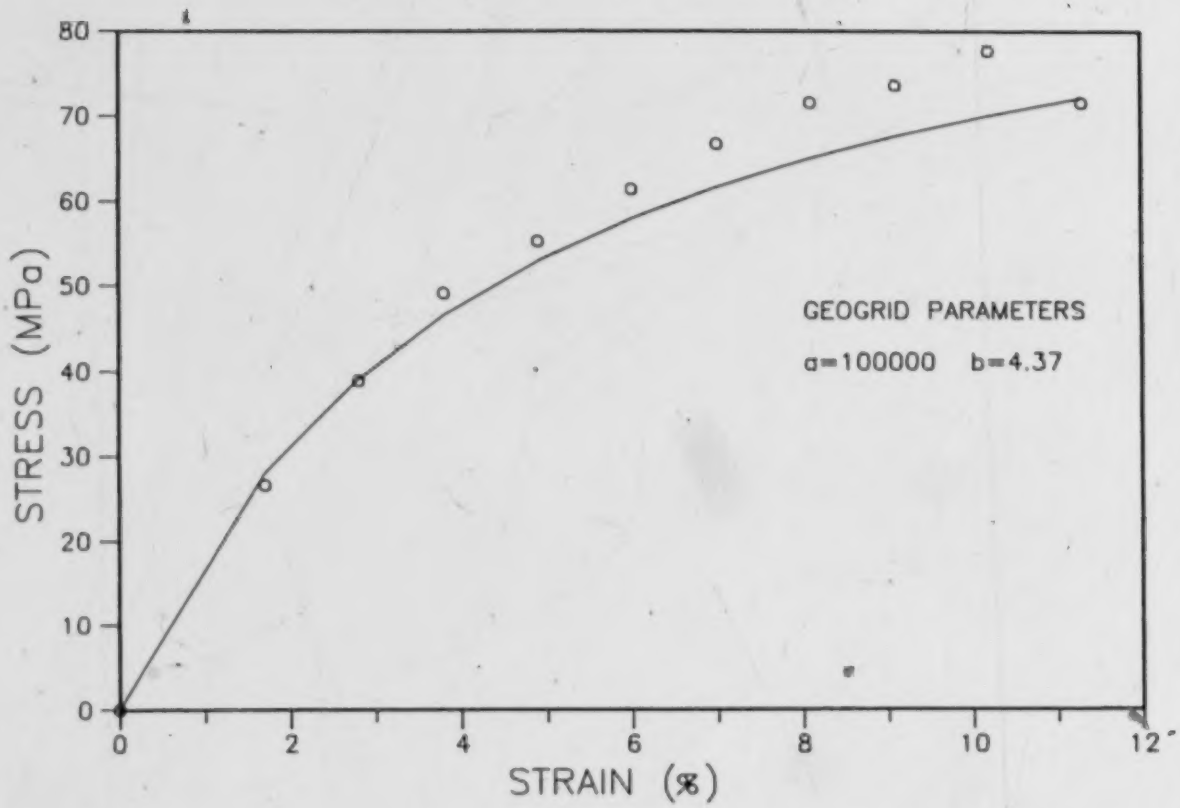

Figure 6.6 Stress-Strain Fitting and Measured Curves of Tensile Test on a Constant Cross Section of SR2, 51 kPa

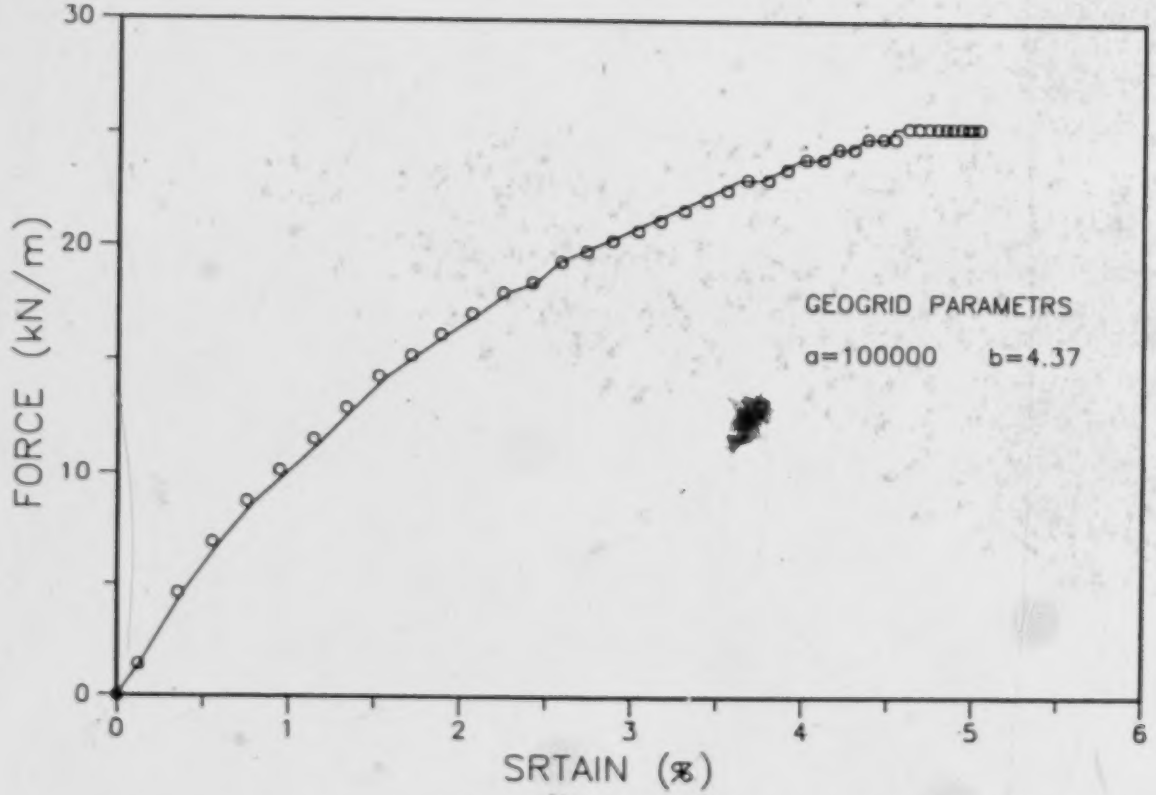

Figure 6.7 Force-Strain Fitting and Measured Curves during Pull-Out Test, SR2, 51 kPa

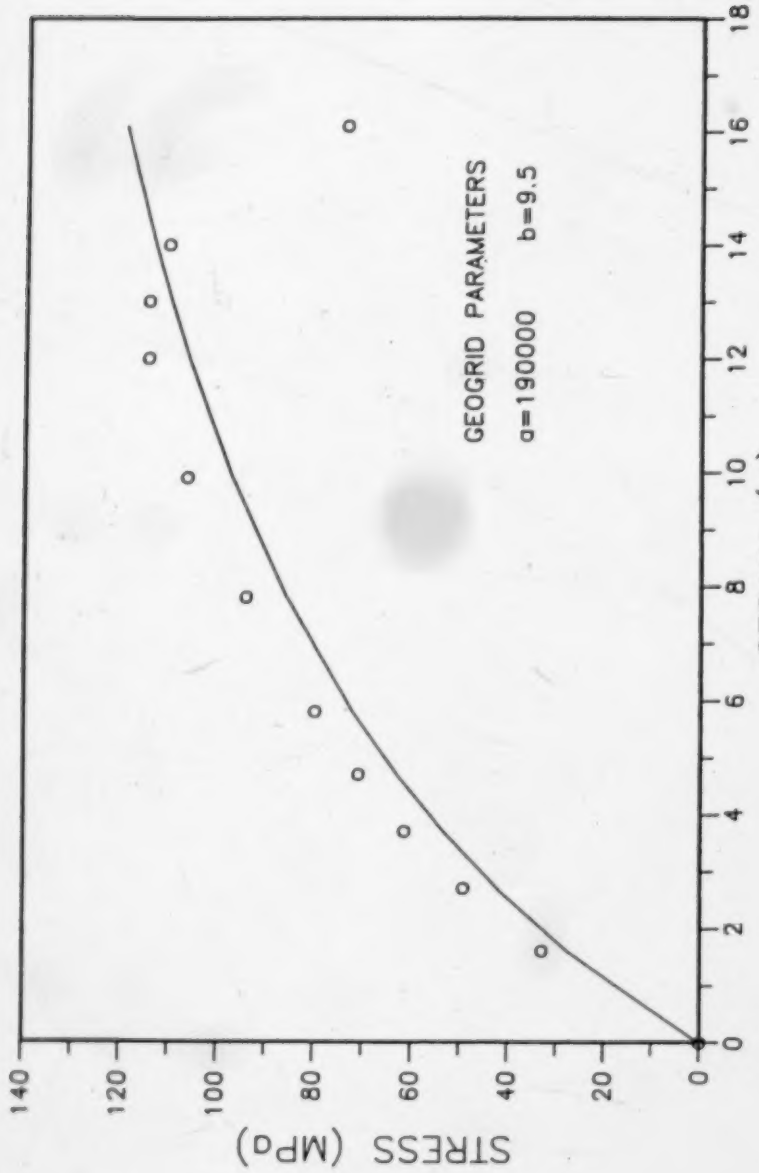

Figure 6.8 Stress-Strain Fitting and Measured Curves of Tensile Test on a Constant Cross Section of SR2, 102.5 kPa

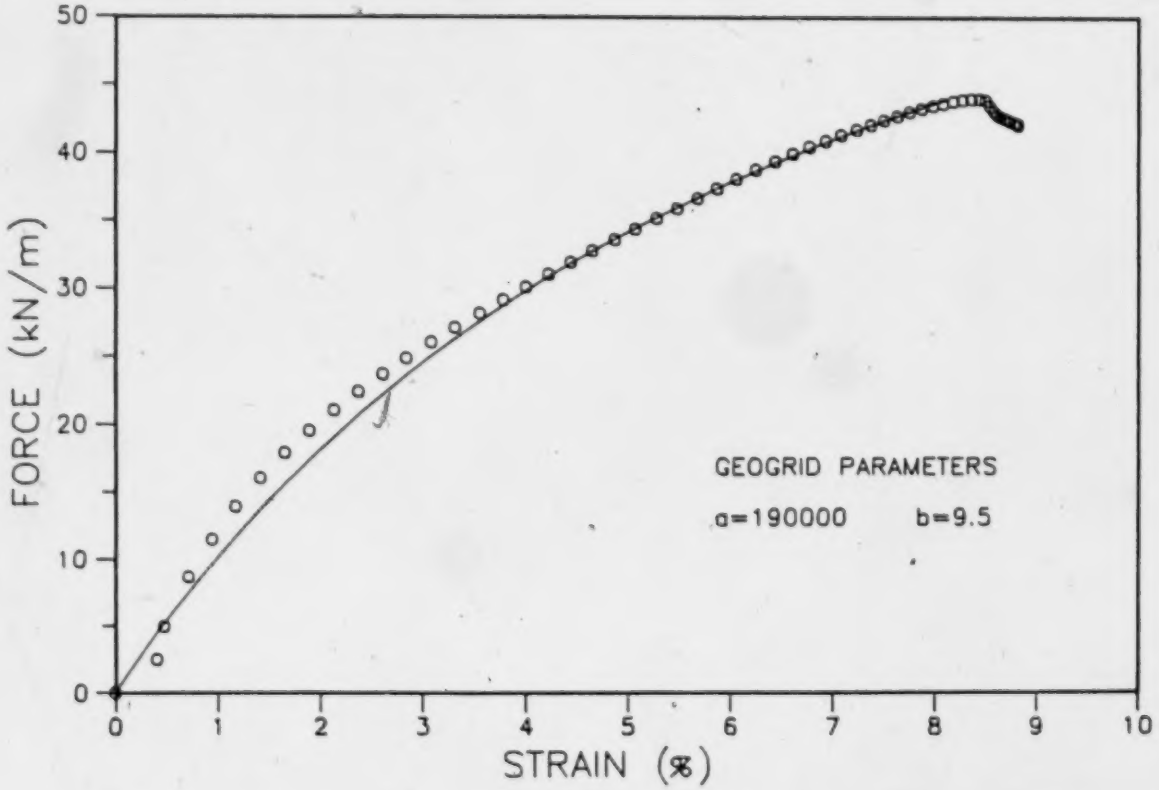

Figure 6.9 Force-Strain Fitting and Measured Curves during Pull-Out Test, SR2, 102.5 kPa

function of the surface area of the reinforcement embedded in soil, the surface roughness of the reinforcement and the overburden pressure at the level of the reinforcement (Jones, 1985; Peterson and Anderson, 1980).

Ingold (1980), carried out undrained pull-out tests on kaolin clay reinforced with Netlon 1168 and Terram RF/12. The undrained shear strength of the kaolin clay was 34 kPa for w = 35%, S = 95% and γ_t = 1.80 g/cm³. Netlon 1168 is a diamond mesh manufactured from polypropylene, while Terram RF/12 is a composite, 67% polypropylene and 33% polyethylene. Ingold used β = 0.5 to formulate the undrained pull-out resistance equation. A very good agreement was found between calculated and measured results.

Values of the interfacial stress factor (β) can be estimated from reinforced direct shear tests. In these tests, the efficiency in terms of total interfacial shear strength is defined as follows:

$$E = \frac{\tau t_p}{\tau_p}$$

where

τt_p = total interfacial shear strength

τ_p = peak shear strength of the soil

= undrained shear strength

$$E \cdot \tau_p = \tau t_p$$

$$E \cdot \tau_p = \tau_p(1-a_s) + \tau_p . a_s . \beta$$

$$\beta = \frac{E + (a_s - 1)}{a_s}$$

where a_s = % of solid area of the reinforcement. Table 6.1 summarizes the values of the interfacial stress factor for SR2 and TNX5001 immersed in Devon silty clay. The values of efficiency and undrained shear strength (from consolidated undrained direct shear tests) are from the research done by Bobey (1988). It is seen that not only the values of β for the TNX5001 are higher than those for the SR2, but also, they behave in an opposite pattern: while for the SR2, β increases with the increase in normal stress, for the TNX5001, β decreases with the increase in normal stress. No evidence was found for the decrease in the efficiency of the TNX5001 which led to the decrease of β with normal stress.

Koerner, Martin and Koerner, 1986, presented an extended work on the shear strength of various geomembranes and a number of different cohesive soils. Adapted direct shear tests were performed allowing for a determination of adhesion and friction angle values. They reported an efficiency of mobilization which is defined as follows:

$$E_c = c_a/c$$

$$E_\phi = \delta/\phi$$

where

E_c = cohesion efficiency

E_ϕ = friction angle efficiency

c_a = adhesion of geomembrane to soil

c = cohesion of soil

δ = friction angle of geomembrane to soil

ϕ = friction angle of soil

Drained direct shear tests were carried out to evaluate both the soil and the interfacial shear strengths. Table 6.2 illustrates values of β for HDPE geomembrane immersed in two types of cohesive soils which appear to be close to the Devon silty clay. It is worth noting that SR2 is manufactured from high density polyethylene (HDPE). The high values of β for the HDPE immersed in Delaware River clayey silt resulted from very high cohesion efficiency (88%) which was an exception among the other results. Moreover, as reported by the authors, for smooth liner materials, a very high adhesion would indicate strong interaction or bonding between the liner and the soil which is not likely to happen with inert liners and these kinds of soils.

Based on these results, a constant value of β=0.5 was used to analyse the results of pull-out tests reinforced with SR2. A higher value of β for the TNX5001 did not receive enough literature support, therefore, β=0.5 was also assumed in the analysis.

6.4.2 The Bearing Capacity Factor, N_c

The bearing capacity factors for a deeply buried cylindrical member vary with adhesion, a, from about 9 to 12, with about 10.5 for typical values of a/c_u. An alternative calculation based on cavity expansion suggests that in stiff compacted clay fills, a value of N_c=7.5 may be

Table 6.1 Values of the Interfacial Stress Factor from Consolidated Undrained Direct Shear Tests

NORMAL STRESS (KPA)	UNDRAINED SHEAR STRENGTH (kPa)	EFFICIENCY		INTERFACIAL STRESS FACTOR	
		SR2	TNX5001	SR2	TNX5001
20	40	0.75	0.97	0.44	0.93
50	60	0.76	0.92	0.47	0.81
100	90	0.77	0.87	0.49	0.69

Note: % solid area (SR2)=0.45
(TNX5001)=0.42

Table 6.2 Values of the Interfacial Stress Factor from Consolidated Drained Direct Shear Tests

SOIL TYPE	NORMAL STRESS (kPa)	DRAINED SHEAR STRENGTH (kPa)	DRAINED INTERFACIAL SHEAR STRESS (kPa)	INTERFACIAL STRESS FACTOR (HIGH DENSITY POLYETHYLENE)
Delaware River Clayey Silt c' = 9kPa ø' = 38°	20	24.63	17.61	0.71
	50	48.06	32.13	0.67
	100	87.13	56.35	0.65
Sandy Silty Clay c' = 12kPa ø' = 34°	20	25.49	10.44	0.41
	50	45.73	23.04	0.50
	100	79.45	44.04	0.55

(after Koerner, Martin and Koerner, 1986)

appropriate (Milligan and Palmeira, 1987).

For a strip footing embedded in clayey soil, N_c=7.5 has been used (Skempton, 1951; Bergado, Bukkanasuta and Balasubramaniam, 1987) to compare predicted with experimental results of pull-out resistance of Tensar SS2 and bamboo grids immersed in clayey soil and weathered clay soils. Ingold (1980 and 1983), also used N_c=7.5 for the undrained analysis of the pull-out tests. Because of good agreement between data were reported, it is concluded that N_c=7.5 is a reasonable assumption.

6.5 Analytical Determination of the Tensile Forces Along the Reinforcements

Firstly, the geogrid tension members are divided into 111 and 94 elements for TNX5001 and SR2 materials, respectively. Figures 6.10 and 6.11 illustrate both cases.

Some assumptions were made in order to solve the problem:

1. The interfacial stress factor, β, between soil and geogrid was assumed to be 0.5 for both geogrids (Figure 2.3).
2. The bearing capacity coefficient (N_c) was assumed to be 7.5 (Figure 2.3).
3. The bearing forces against the anchor members are concentrated at the element at the junction between anchor and tension members.
4. In order to have the tensile force equal to zero at the

end of the reinforcement length, the value of the peak shear strength was calculated assuming that the ratio between measured and calculated maximum pull-out forces be equal to one. This assumption allowed the undrained shear strength of the soil at failure to be calculated. Figures 6.12 to 6.19 illustrate the fitting curves of the soil undrained shear strength, based on this assumption.

The fourth assumption was made after many attempts to achieve convergence. The computation of the forces along the geogrid length proved to be very sensitive to some variables in the problem such as the soil shear strength and the areas of the elements. The latter however, could be determined more accurately. The values of peak shear strength resulting from this assumption are in good agreement with the pull-out soil sample characteristics such as moisture content, dry density and degree of saturation, as well as normal stress under which the samples were consolidated.

For the computation of the tensile force along the length of the geogrids, an equation such as $y = ax/(b+x)$ was used to fit the experimental data for both the soil shear strength and tensile force x strain of the geogrid behaviour. The parameters a and b for the geogrid tensile behaviour and A and B for the soil shear strength are shown in Table 6.3. The equations involved in the iteration are:

Geogrid

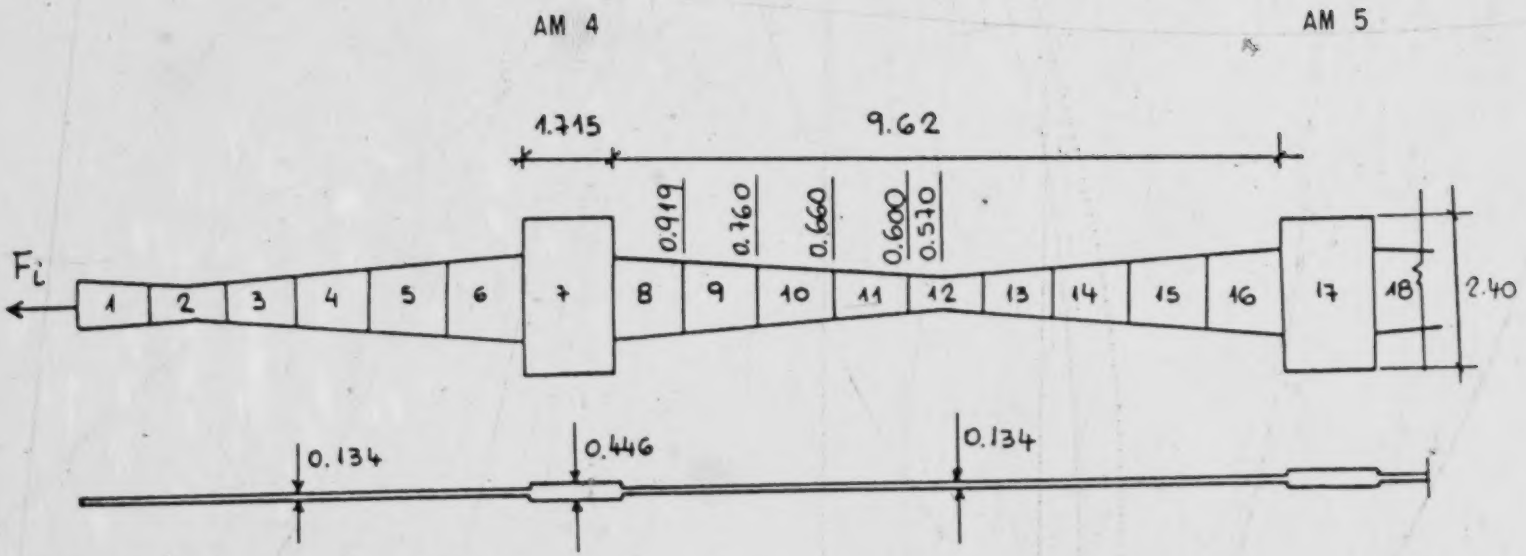

Figure 6.10 Plan and Cross Section Views of a SR2 Tension Member

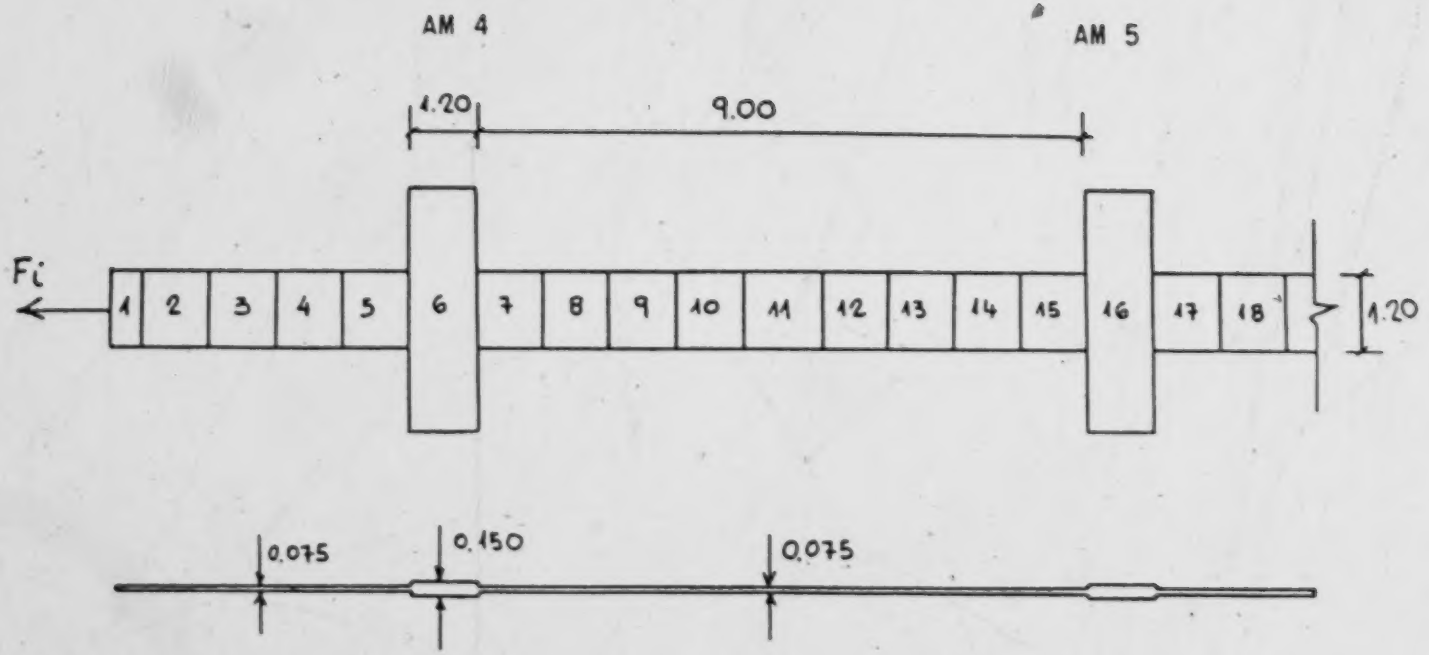

Figure 6.11 Plan and Cross Section Views of a TNX5001 Tension Member

$$F_i = \frac{a\epsilon}{b+\epsilon} = \frac{a((x_i - x_{i+1})/l)}{b+((x_i - x_{i+1})/l)} \cdot A_i \qquad [6.2]$$

where

F_i = pull-out force at the beginning of element i (from the pull-out test results).

a,b = geogrid force x strain fitting curve parameters

x_i = displacement of element i (from the pull-out test results)

l = length of element

A_i = cross section area of element i

x_{i+1} = displacement of element i+1, unknown.

From equation 6.2 the value of x_{i+1} is computed.

Soil:

$F_i - F_{i+1} = 2 \cdot \tau \cdot A_{pi}$ = mobilized shear force along element i.

$$F_i - F_{i+1} = \frac{A.x_{i+1}}{B+x_{i+1}} \times Ap_i \times \beta \times 2 \qquad [6.3]$$

where

F_{i+1} = tensile force at the beginning of element i+1

A, B = soil shear strength fitting curve parameters

Ap_i = plan area of element i

β = interfacial stress factor = 0.5.

At the junctions, besides the shear forces, bearing forces are included in the calculations and equation 6.3 turns out to be:

$$F_i - F_{i+1} = \frac{A.x_i}{B+x_i} \times (2Ap_i.\beta + Ab_i.N_c) \qquad [6.4]$$

where

N_c = bearing capacity factor = 7.5

Ab_i = bearing area of element i

From either equation 6.3 or 6.4, the value of F_{i+1} is evaluated. Substituting the value of the axial force transfered, F_{i+1} in equation 6.2, the displacement x_{i+2} is computed. The process is repeated and if at the end of the geogrid length the value of force is not equal to zero, the whole calculation is repeated assuming different values of F_i and x_i originally from the pull-out test results. When convergence is achieved, the displacements and tensile forces along the length of geogrids are plotted. Figures 6.20 to 6.27 and 6.28 to 6.35 illustrate the displacements and tensile forces along the geogrids. For this study, nine stages of pull-out forces or displacements were analysed for each of the eight tests presented. The tensile force distributions correspond to the displacement curves along the geogrids for each pull-out test.

It is noticed that the theoretical curves of displacement, for the tests with SR2 geogrid, and the curves of distribution of tensile forces, for tests with both geogrids, are not smooth. The reasons for the lack of smoothness are the non-constant rigidity of the SR2 tension member and the assumption made of concentrating the bearing forces at the junctions.

The maximum value of pull-out force is mobilized when the whole geogrid sample starts to move; therefore, the distribution of axial force along the geogrid keeps

Table 6.3 Soil Undrained Shear Strength Parameters and Geogrid Tensile Parameters

GEOGRID	NORMAL STRESS (KPA)	GEOGRID TENSILE PARAMETERS	SOIL SHEAR STRENGTH PARAMETERS
SR2	20	a=115500 b=3.95	A=47.25 B=0.20
SR2	50	a=105000 b=7.0	A=35.94 B=0.25
SR2	51	a=100000 b=4.37	A=42.1 B=0.20
SR2	102.5	a=190000 b=9.5	A=65.0 B=0.15
TNX5001	20	a=102.1 b=4.29	A=43.0 B=0.15
TNX5001	50	a=102.1 b=4.29	A=60.5 B=0.10
TNX5001	51.7	a=102.1 b=4.29	A=61.6 B=0.075
TNX5001	100.7	a=102.1 b=4.29	A=75.0 B=0.085

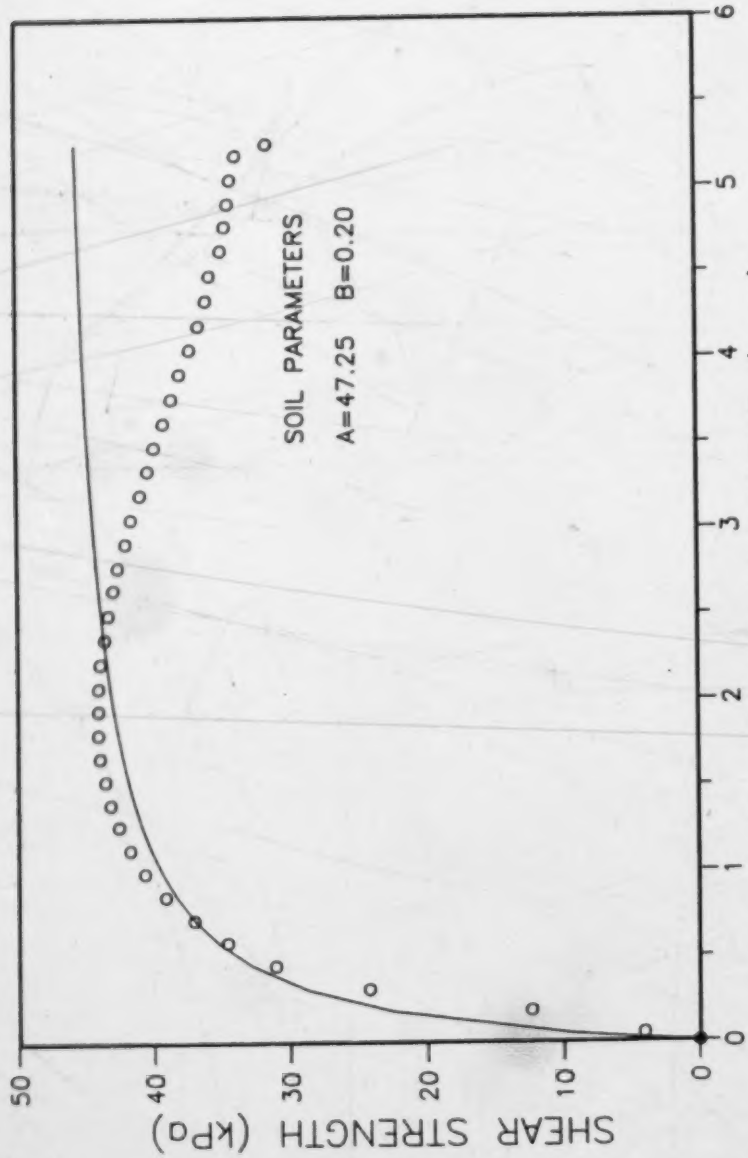

Figure 6.12 Fitting Curve of the Soil Undrained Shear Strength. Parameters Used in the SR2 20 kPa Analysis

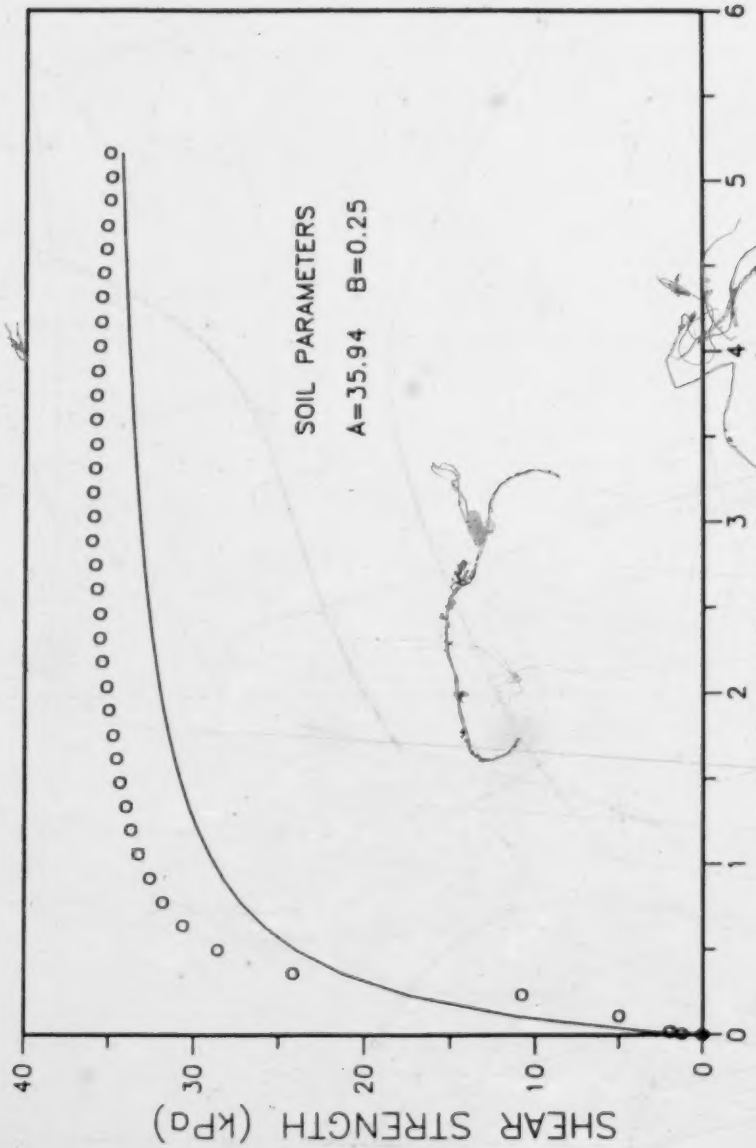

Figure 6.13 Fitting Curve of the Soil Undrained Shear Strength. Parameters Used in the SR2 50 kPa Analysis

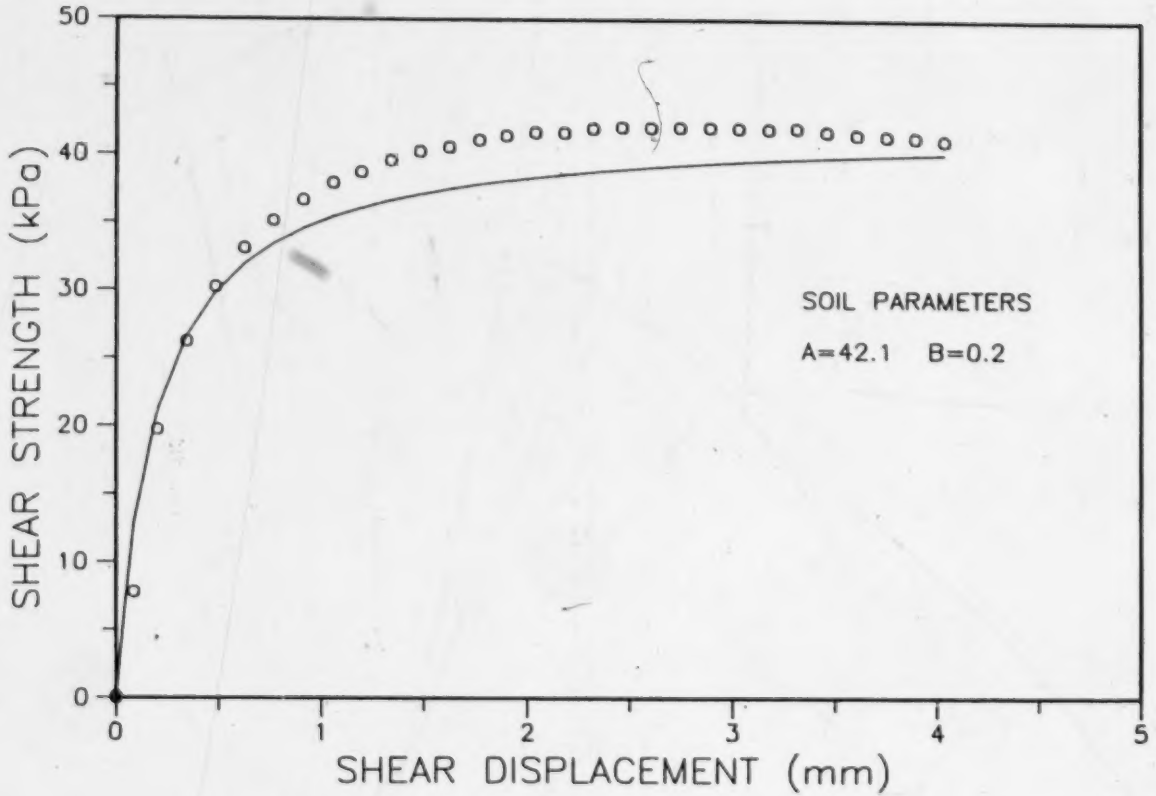

Figure 6.14 Fitting Curve of the Soil Undrained Shear Strength. Parameters Used in the SR2 51 kPa Analysis

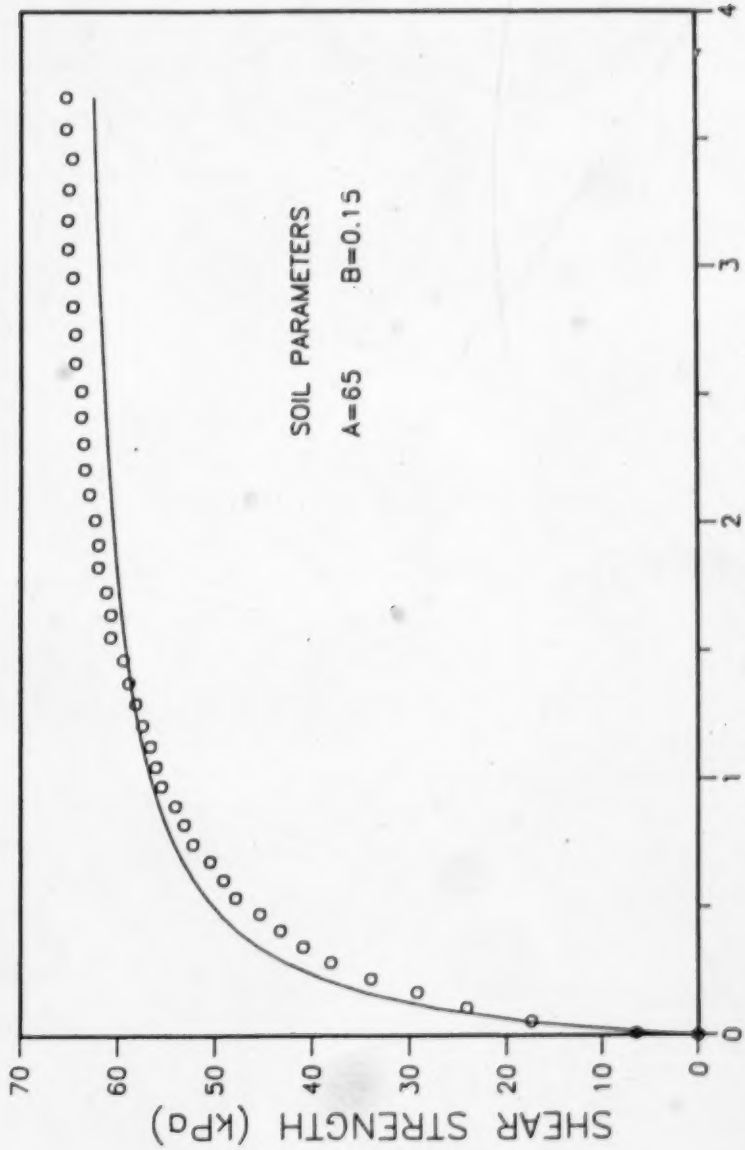

Figure 6.15 Fitting Curve of the Soil Undrained Shear Strength. Parameters Used in the SR2 102.5 kPa Analysis

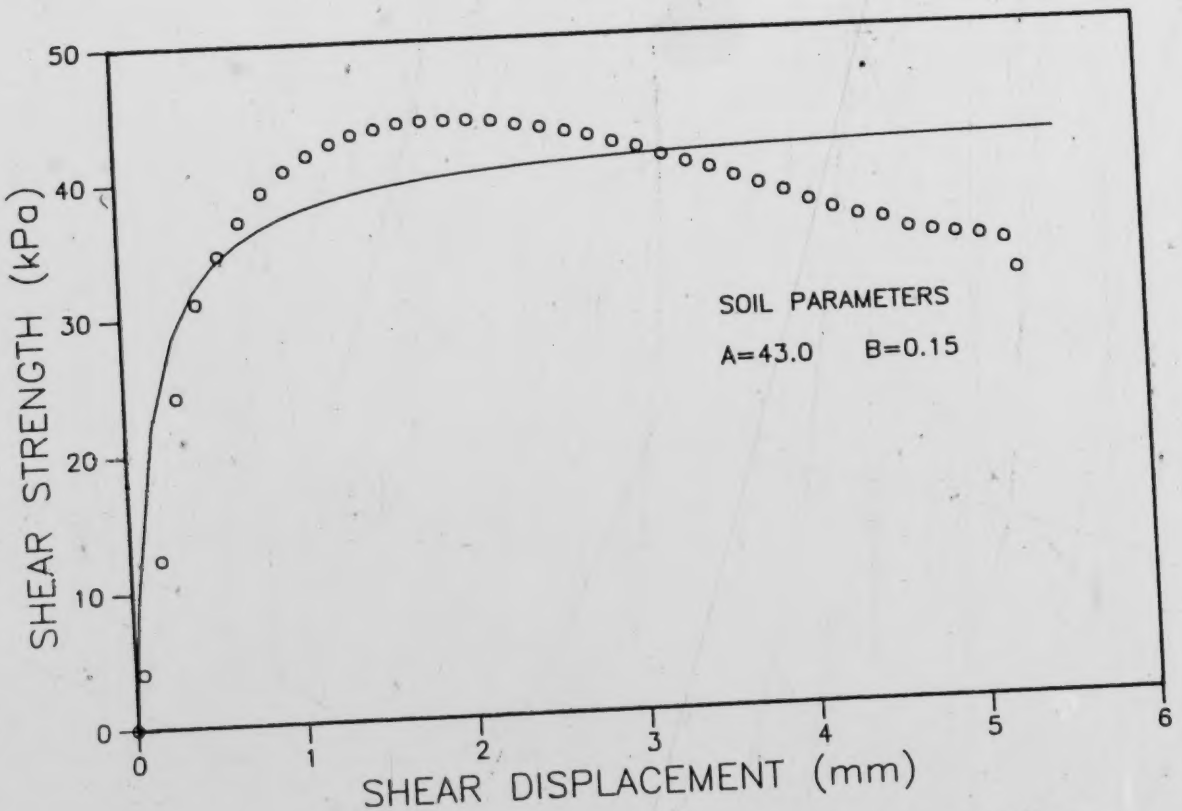

Figure 6.16 Fitting Curve of the Soil Undrained Shear Strength. Parameters Used in the TNX5001 20 kPa Analysis

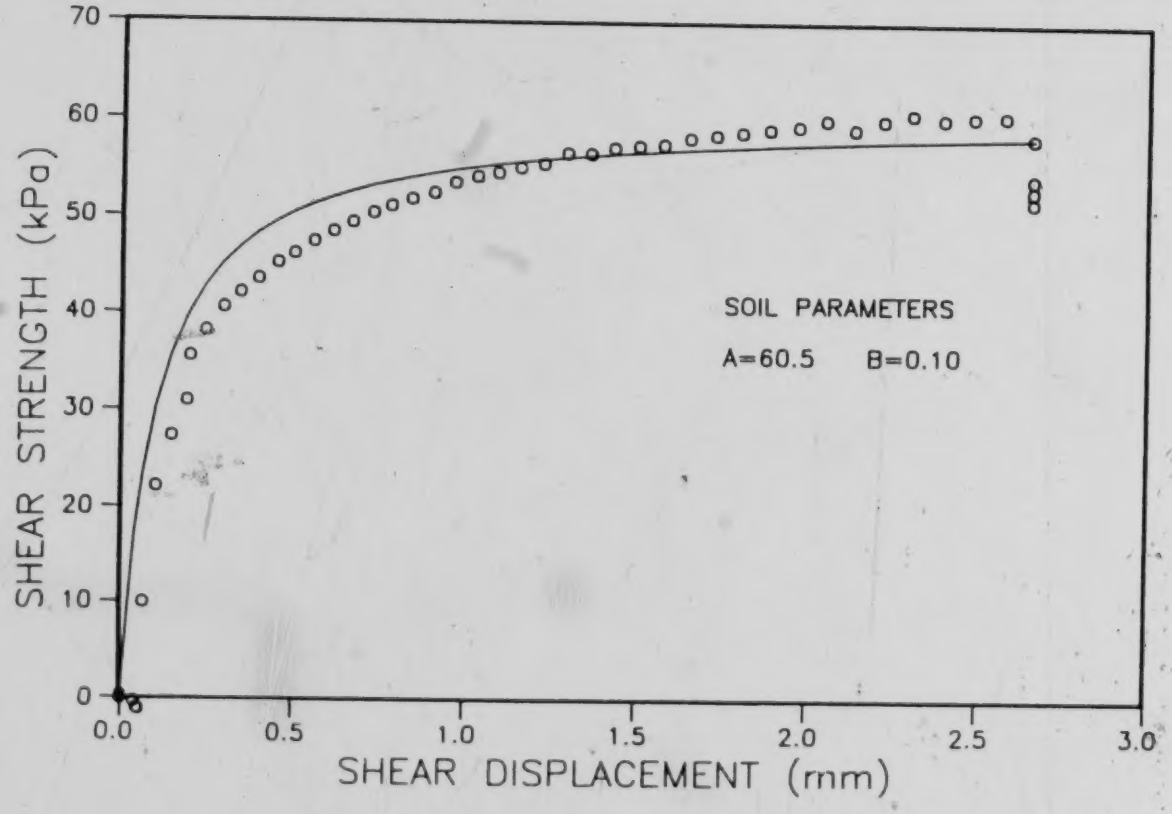

Figure 6.17 Fitting Curve of the Soil Undrained Shear Strength. Parameters Used in the TNX5001 50 kPa Analysis

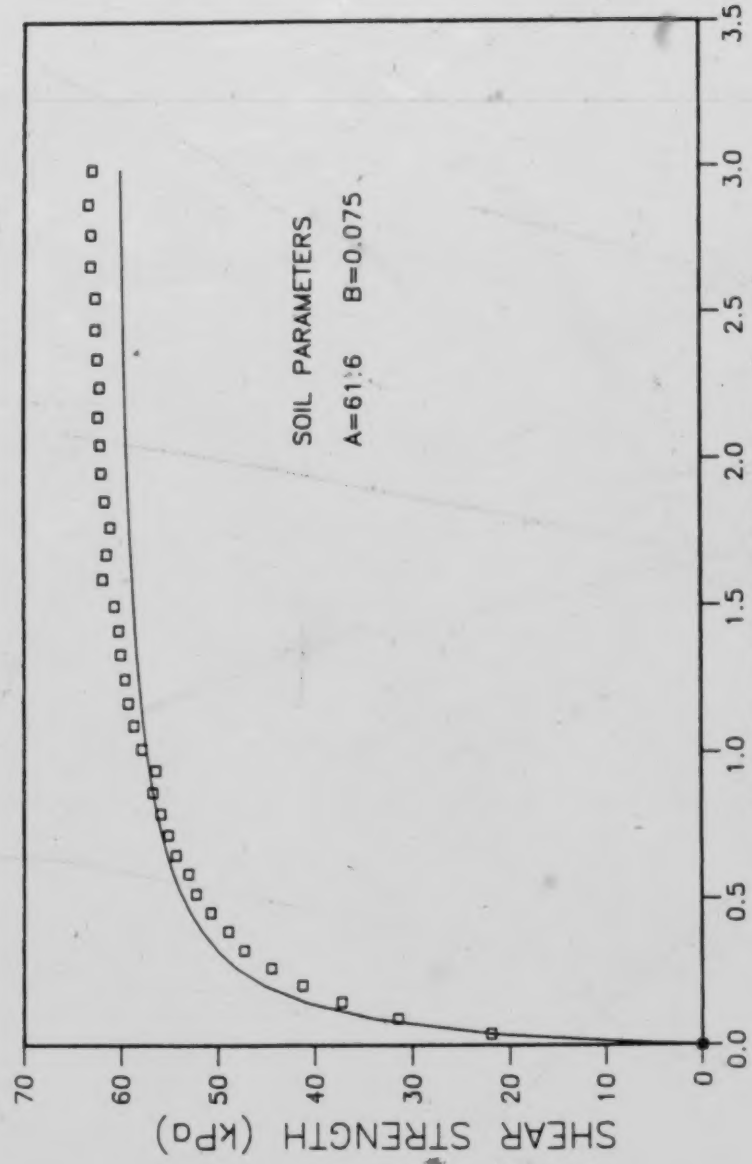

Figure 6.18 Fitting Curve of the Soil Undrained Shear Strength. Parameters Used in the TNX5001 51.7 kPa Analysis

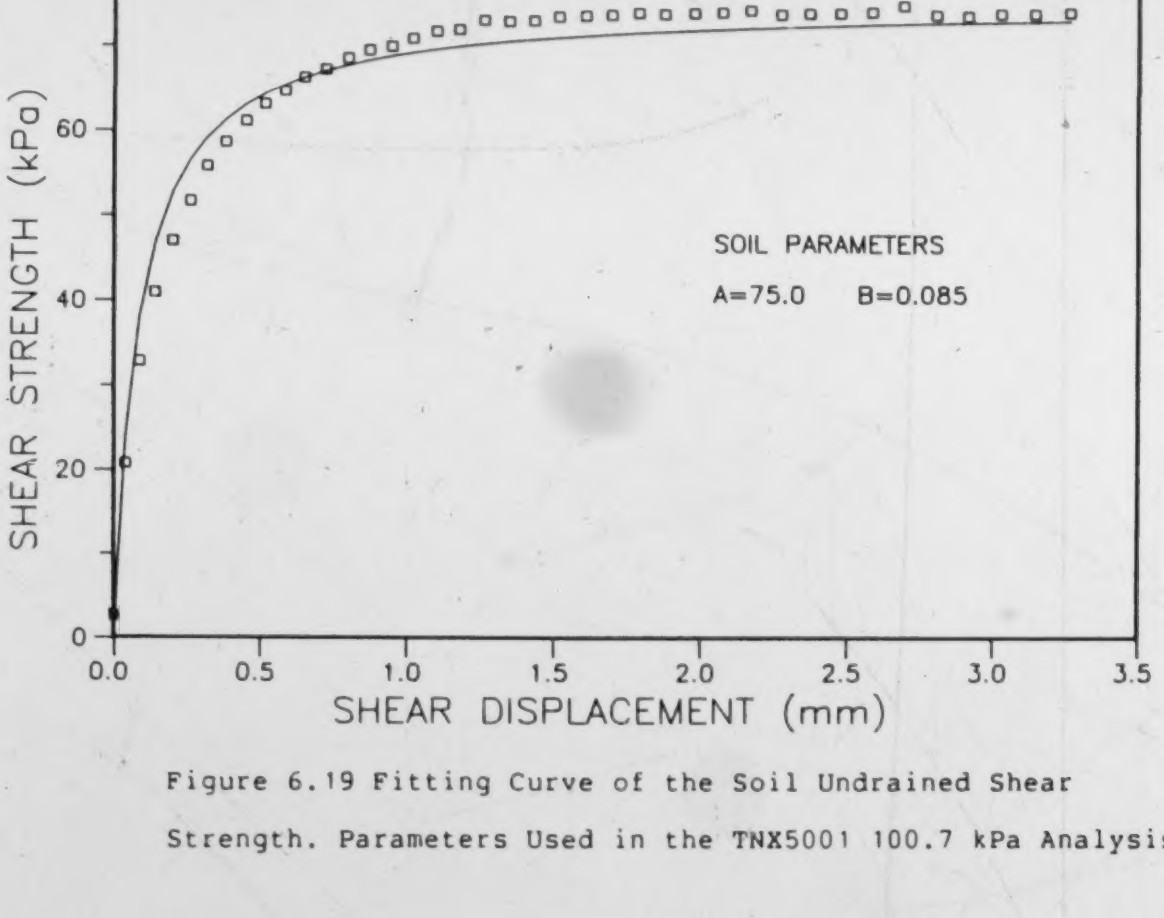

Figure 6.19 Fitting Curve of the Soil Undrained Shear Strength. Parameters Used in the TNX5001 100.7 kPa Analysis

increasing until the maximum pull-out force is reached. Beyond this point, the pull-out force reaches a plateau and the tensile force curves along the geogrids should be coincident. This can be noticed in the plots of axial force along the geogrid.

It is noted that in the figures of progressive displacements along the geogrids, the theoretical curves do not fit the experimental data perfectly, especially for the first three or four stages of the pull-out force, of the TNX5001, when failure is not reached yet. Two points, corresponding to AM4 and AM5 are delayed systematically when compared with the data from other anchor members. The reason is likely to be due to twisting of the jaws in the horizontal plane. Since the wires were fastened to the anchor members diagonally, the twist of the jaws caused one side to the geogrid to move prior to the other.

The attempt to make the interfacial stress factor greater than 0.5 for the TNX5001, i.e. 0.7 to 0.93, proved to be useless since the pull-out force at the front end of the box had to be increased by 50% and almost 100%, respectively, to obtain reasonable distribution of tensile force along the geogrid, i.e., tensile force equal to zero at the back end of the reinforcement. Figure 6.44 and 6.45 illustrate displacements and forces along TNX5001, 20 kPa for β=0.70.

The values of pull-out forces measured and predicted in the analysis are shown in Figures 6.36 to 6.43. The

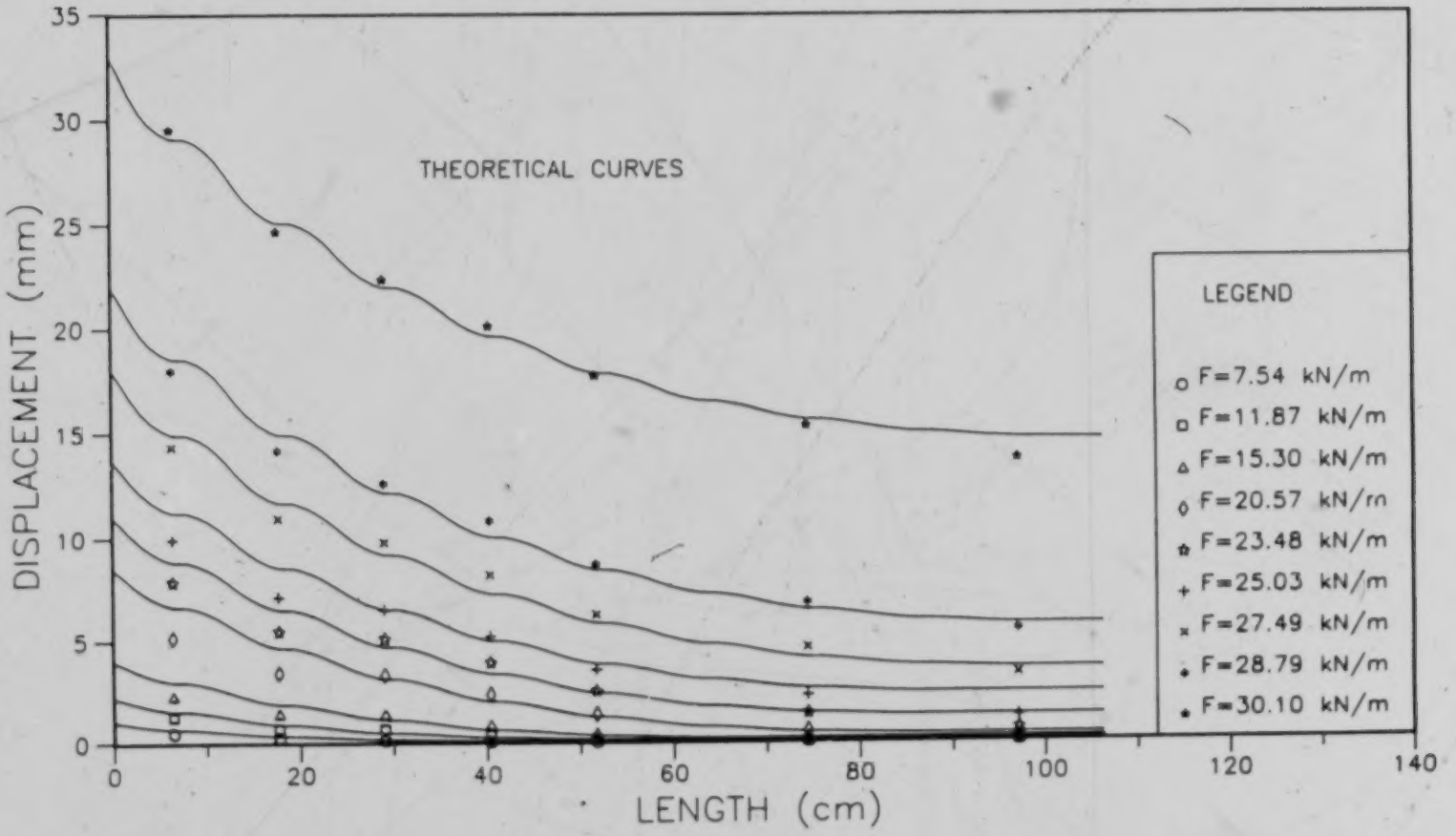

Figure 6.20 Progressive Displacements along the Geogrid SR2, 20 kPa

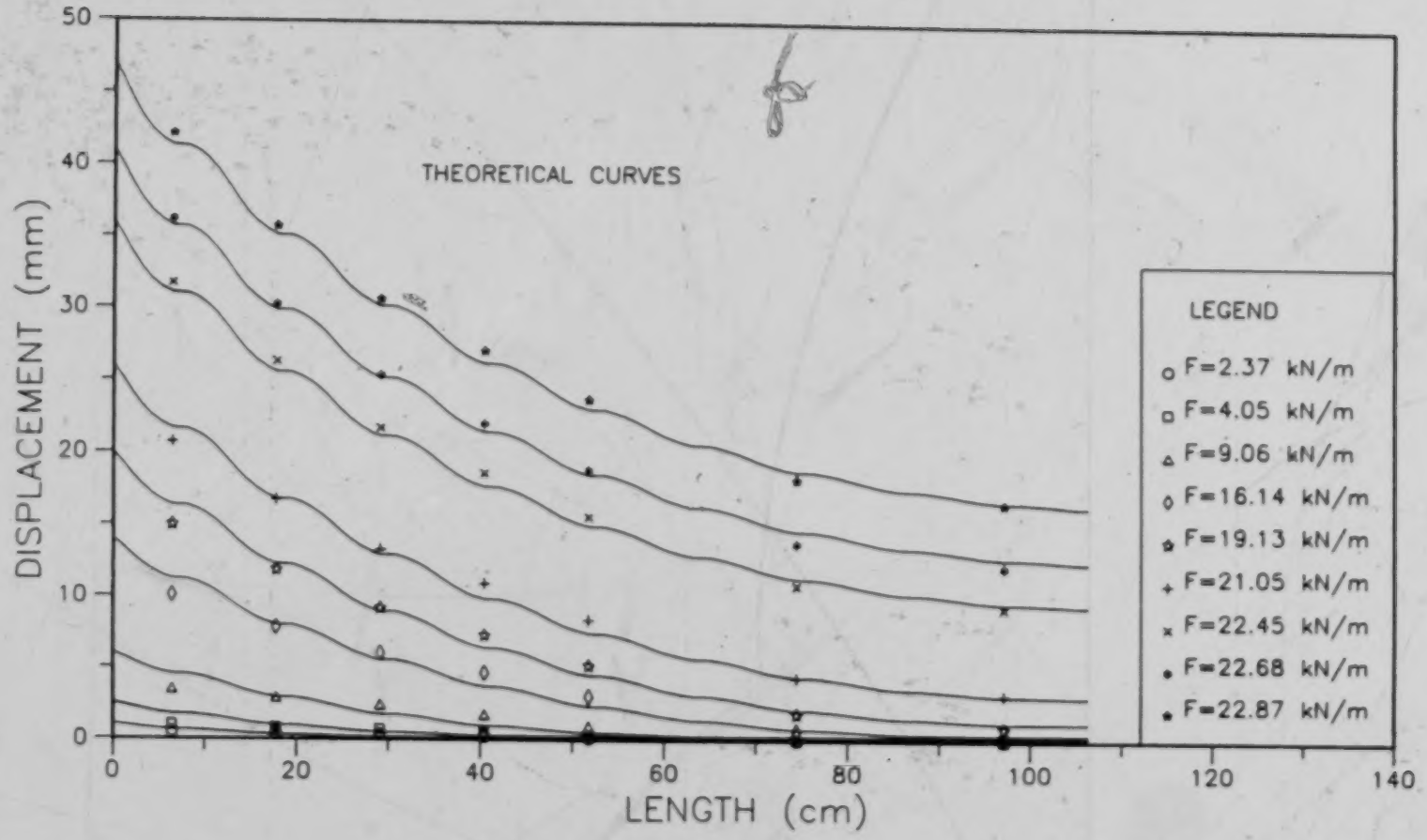

Figure 6.21 Progressive Displacements along the Geogrid SR2, 50 kPa

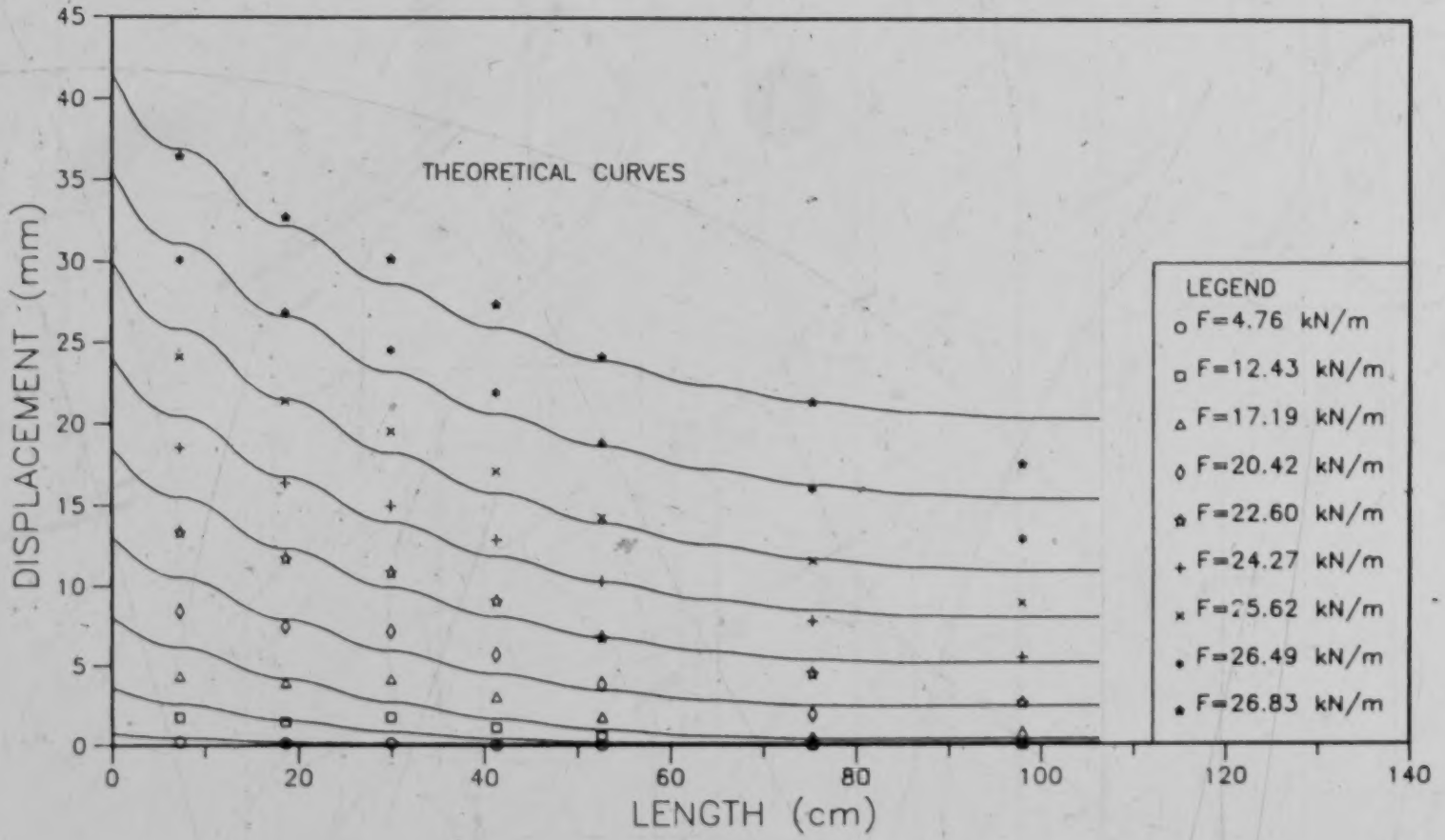

Figure 6.22 Progressive Displacements along the Geogrid SR2, 51 kPa

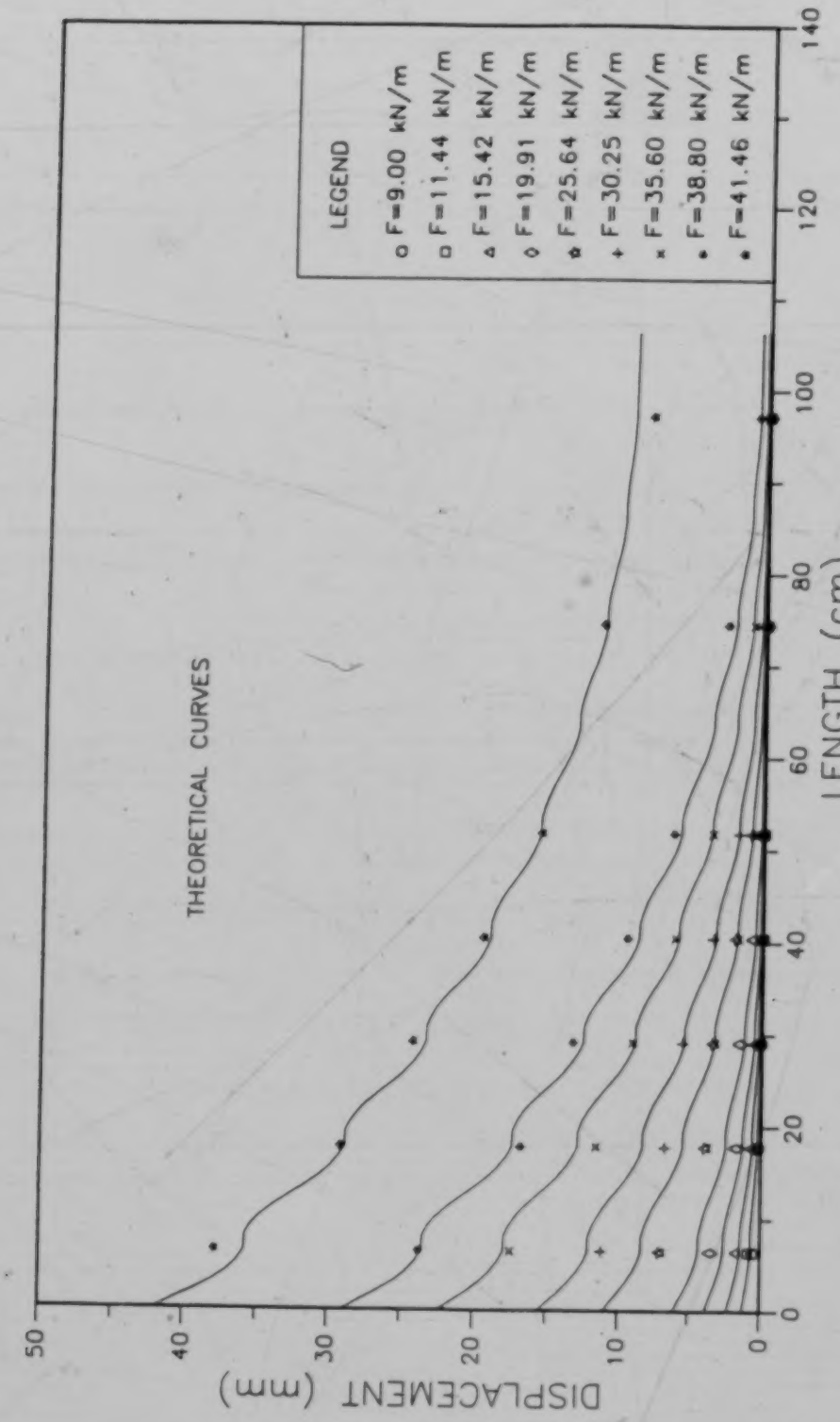

Figure 6.23 Progressive Displacements along the Geogrid SR2, 102.5 kPa

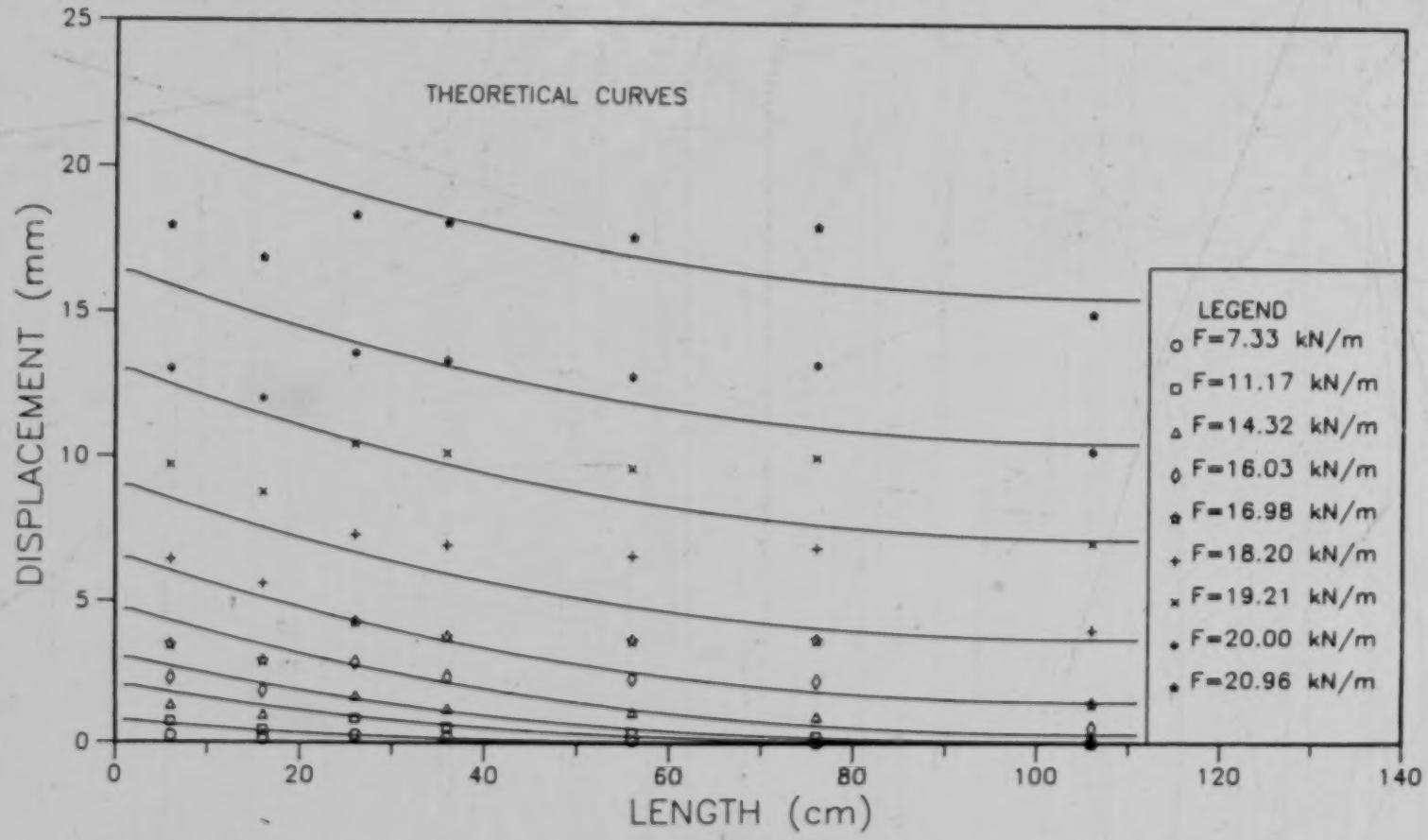

Figure 6.24 Progressive Displacements along the Geogrid TNX5001, 20 kPa

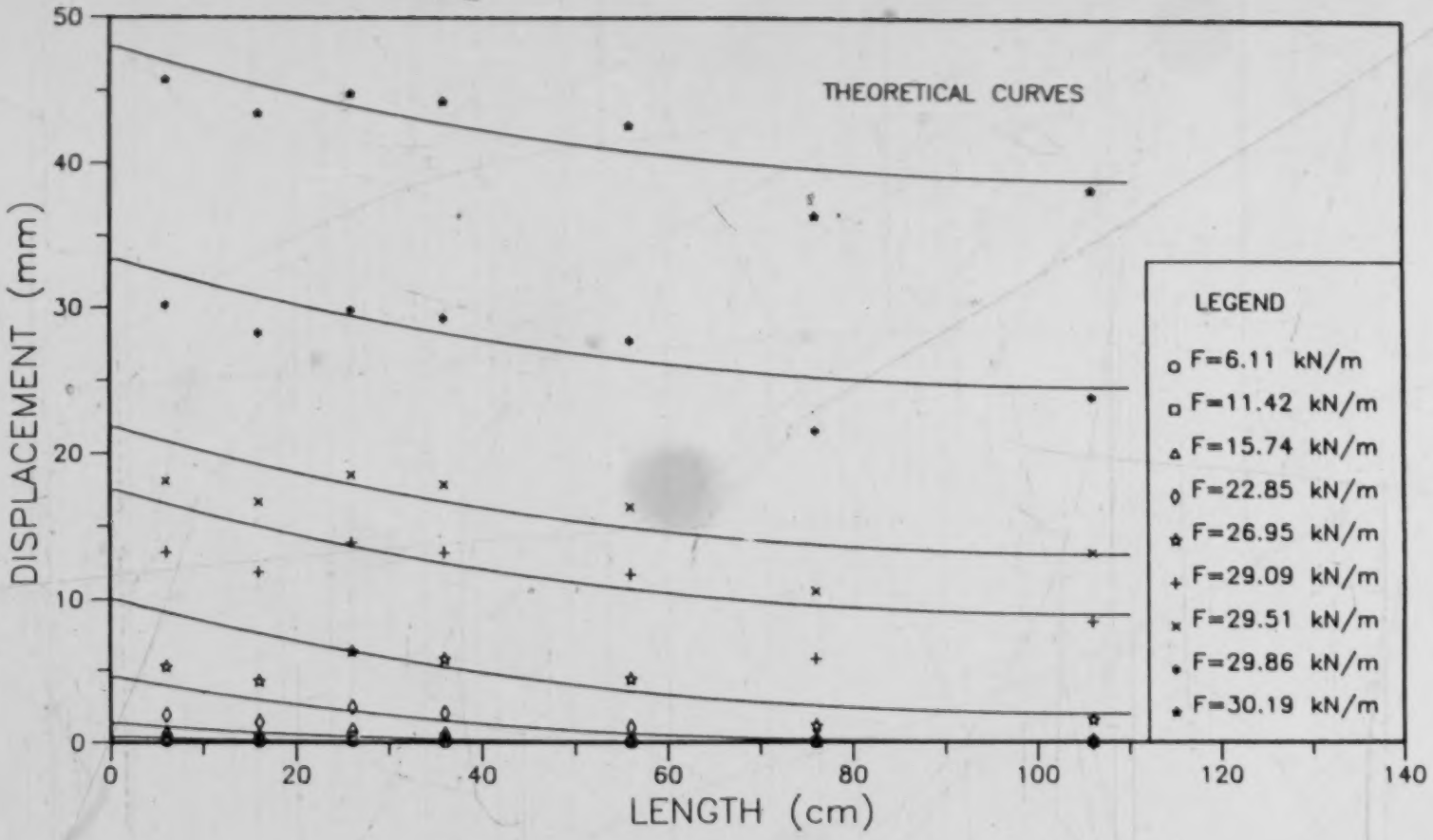

Figure 6.25 Progressive Displacements along the Geogrid TNX5001, 50 kPa

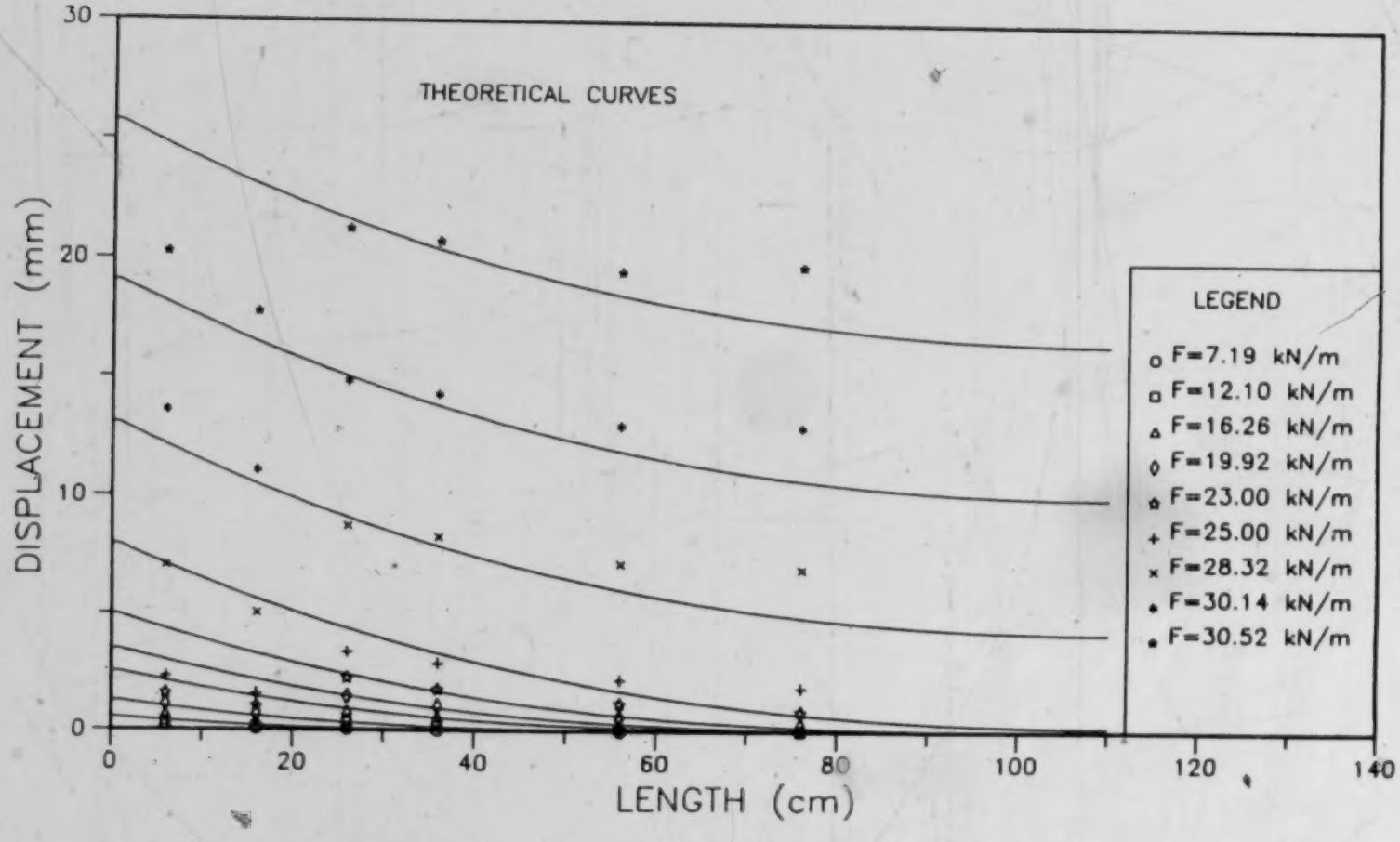

Figure 6.26 Progressive Displacements along the Geogrid TNX5001, 51.7 kPa

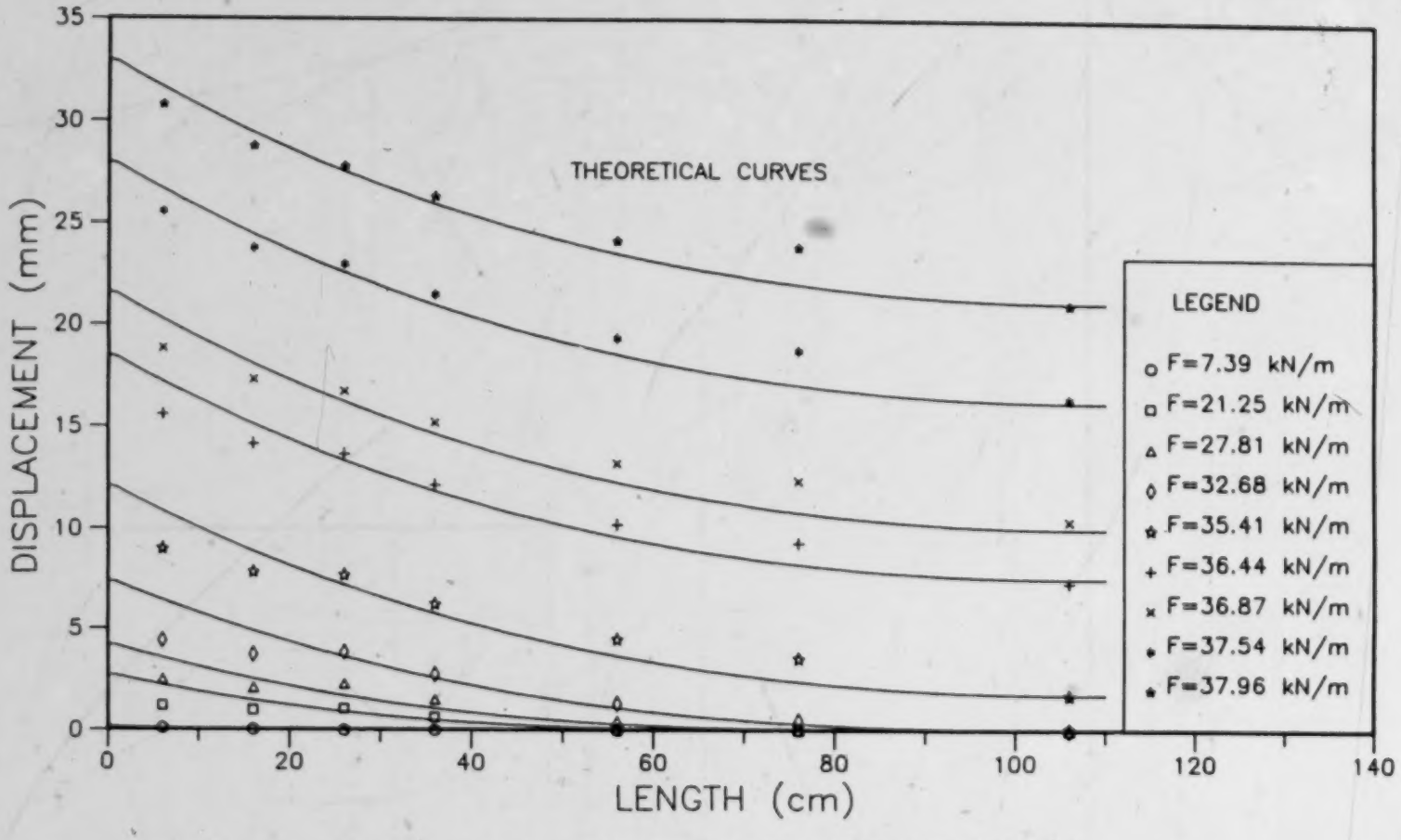

Figure 6.27 Progressive Displacements along the Geogrid TNX5001, 100.7 kPa

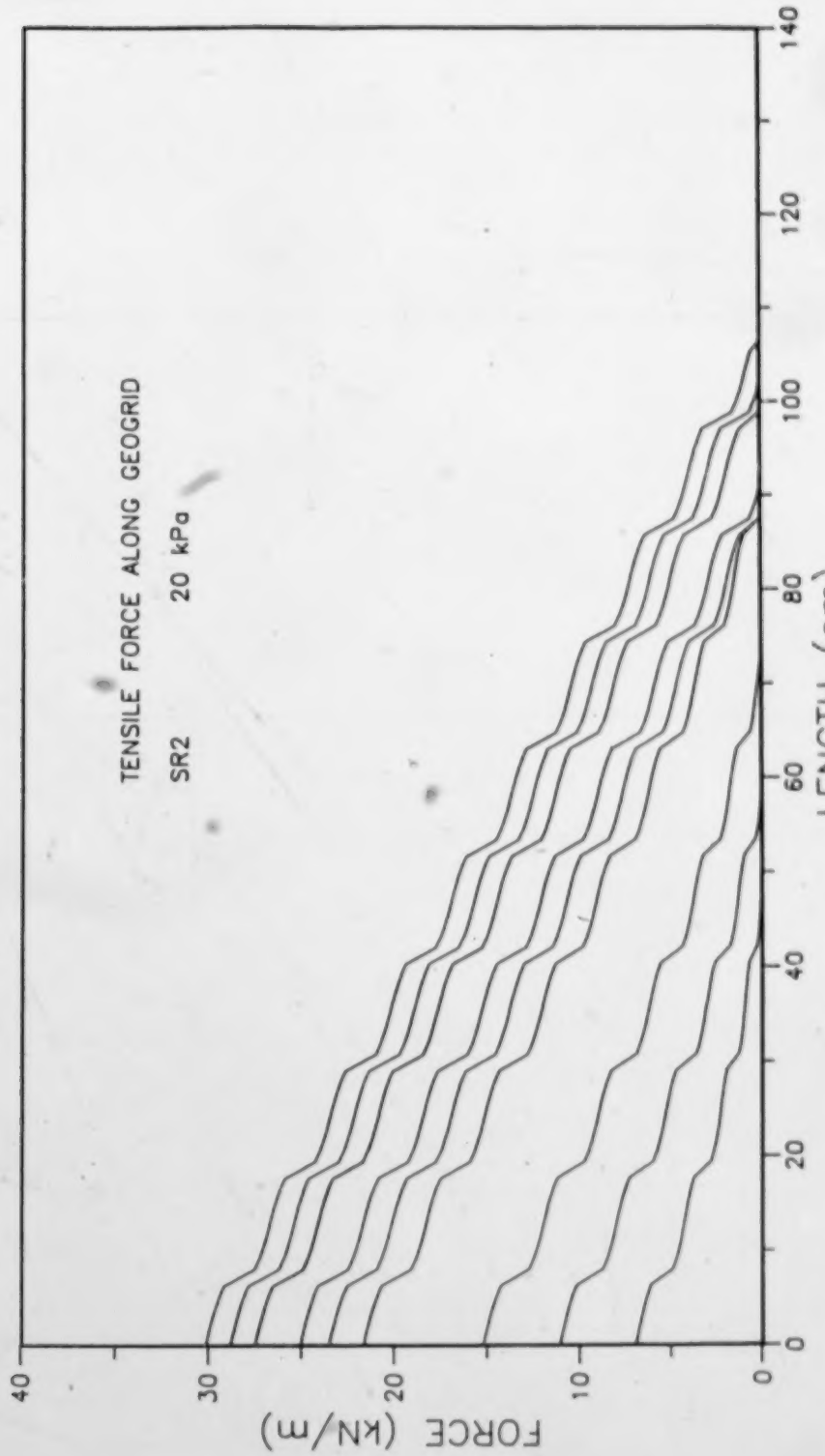

Figure 6.28 Tensile Force along Geogrid SR2, 20 kPa

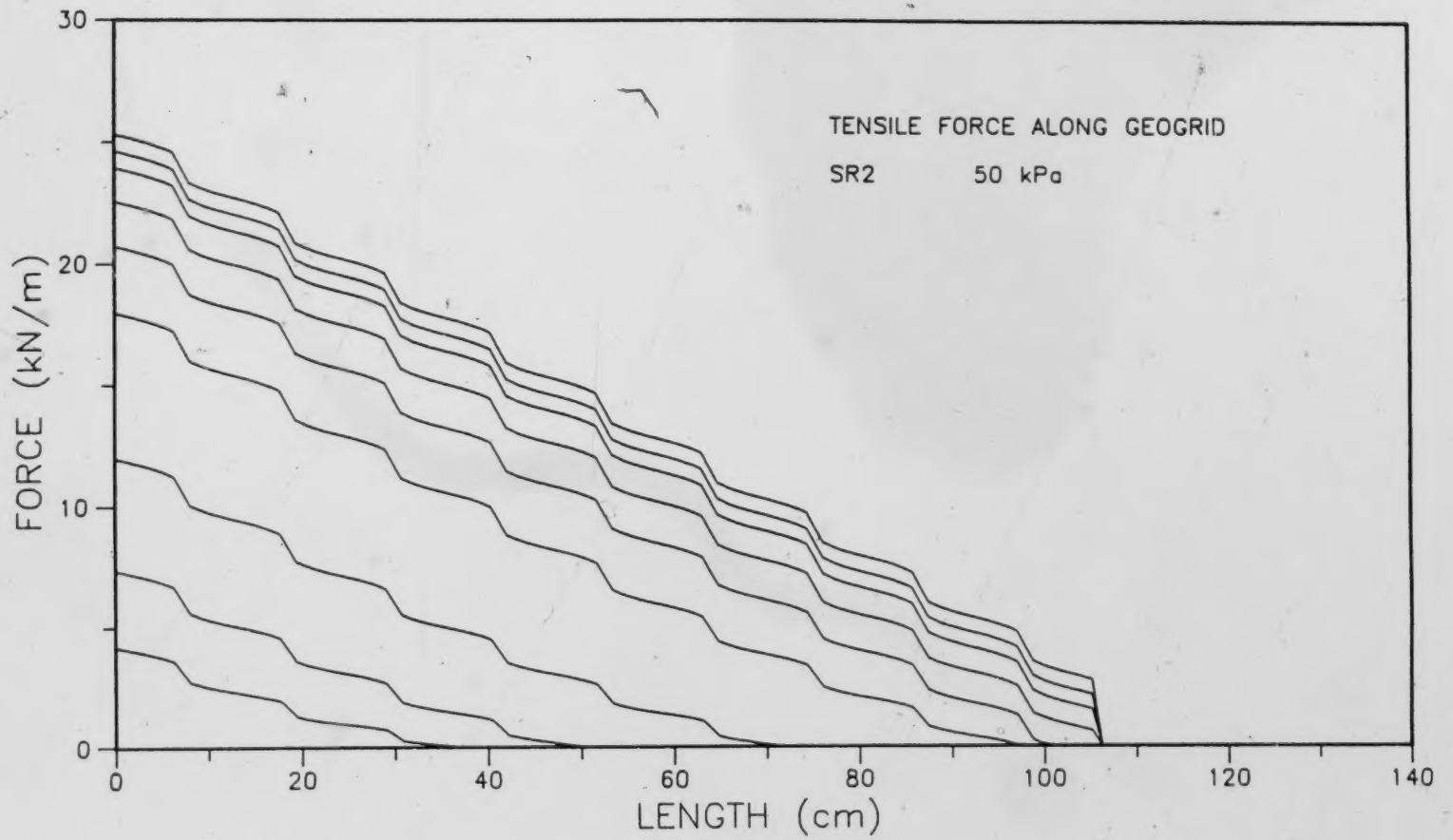

Figure 6.29 Tensile Force along Geogrid SR2, 50 kPa

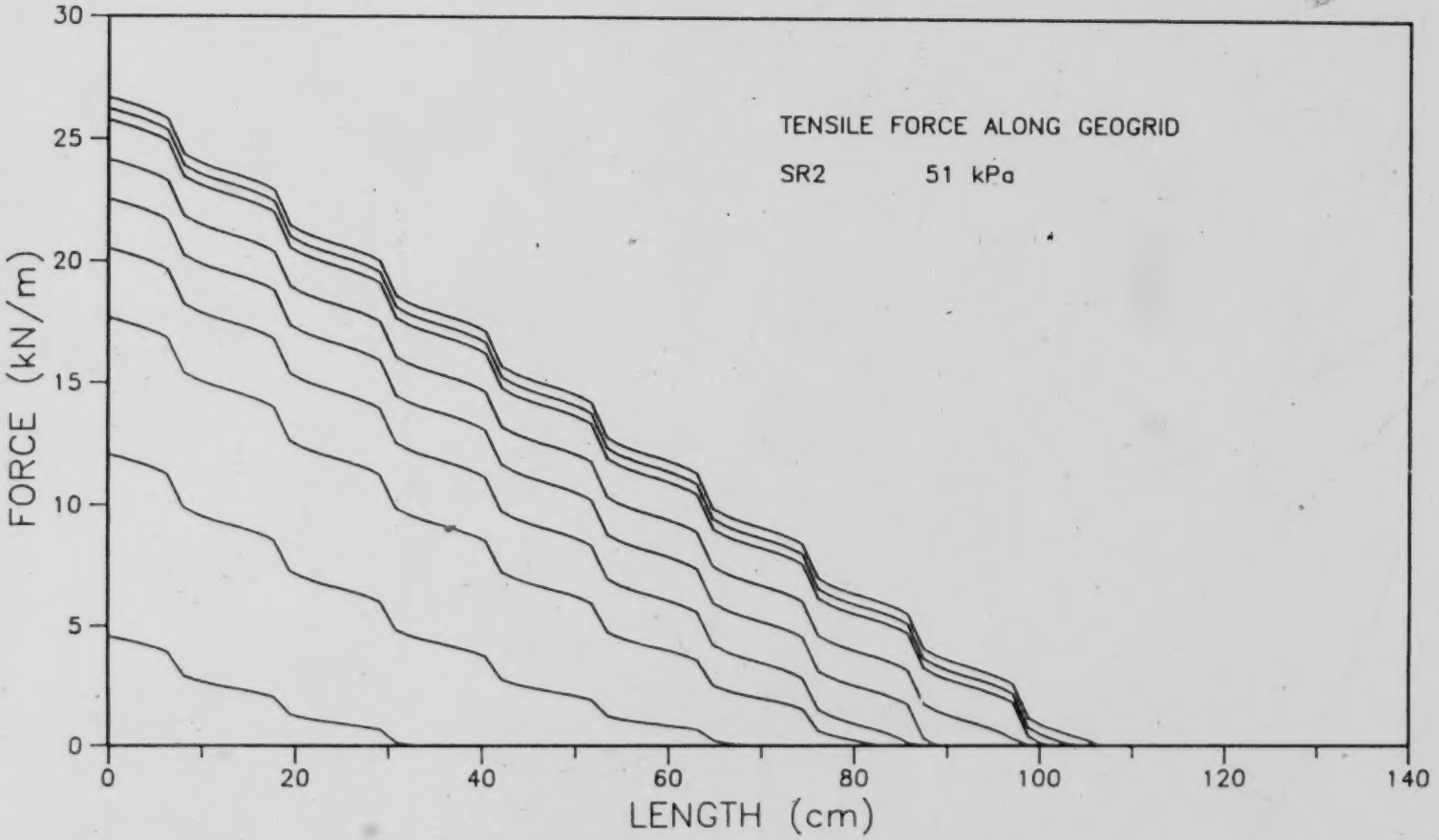

Figure 6.30 Tensile Force along Geogrid SR2, 51 kPa

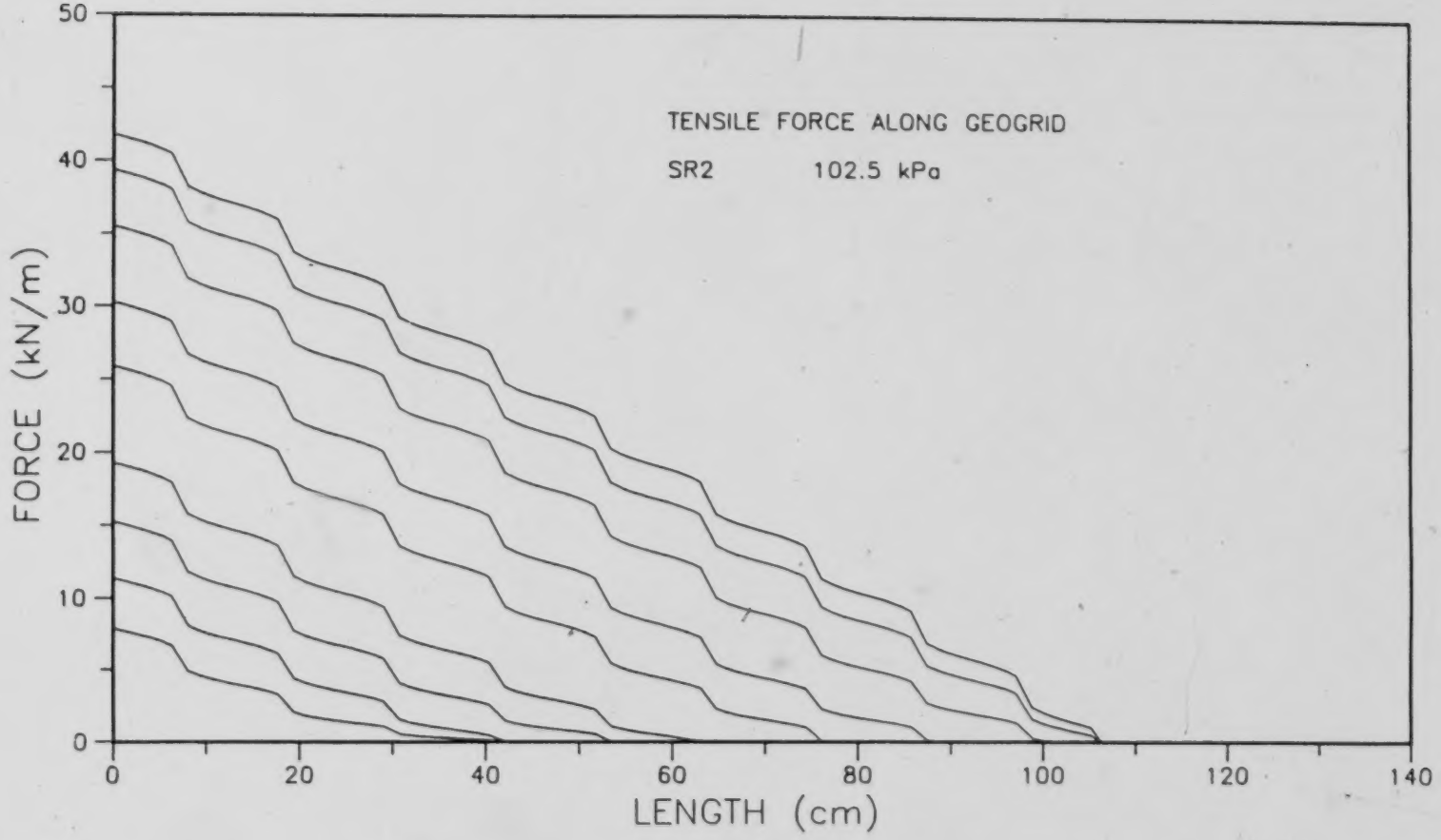

Figure 6.31 Tensile Force along Geogrid SR2, 102.5 kPa

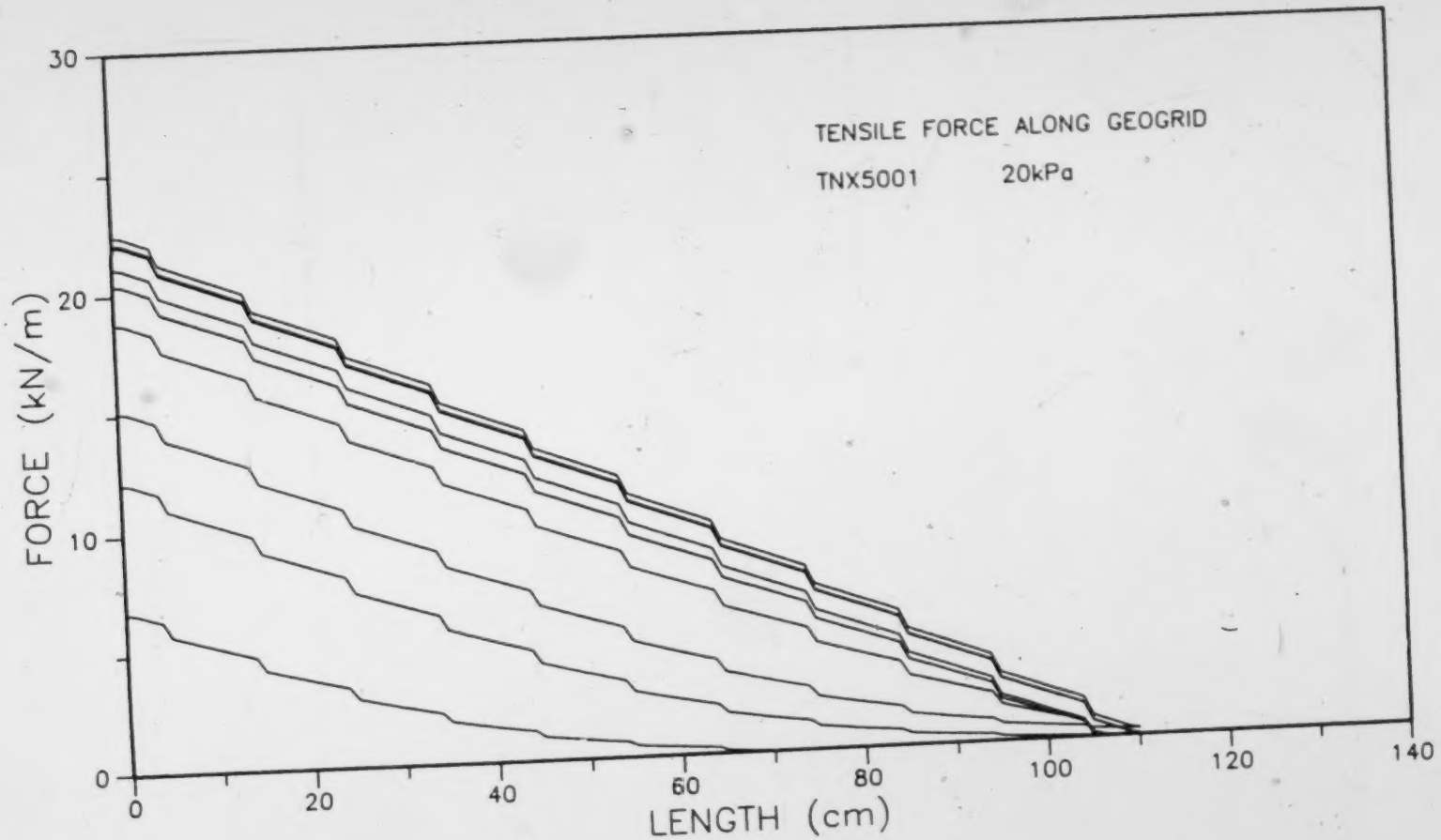

Figure 6.32 Tensile Force along Geogrid TNX5001, 20 kPa

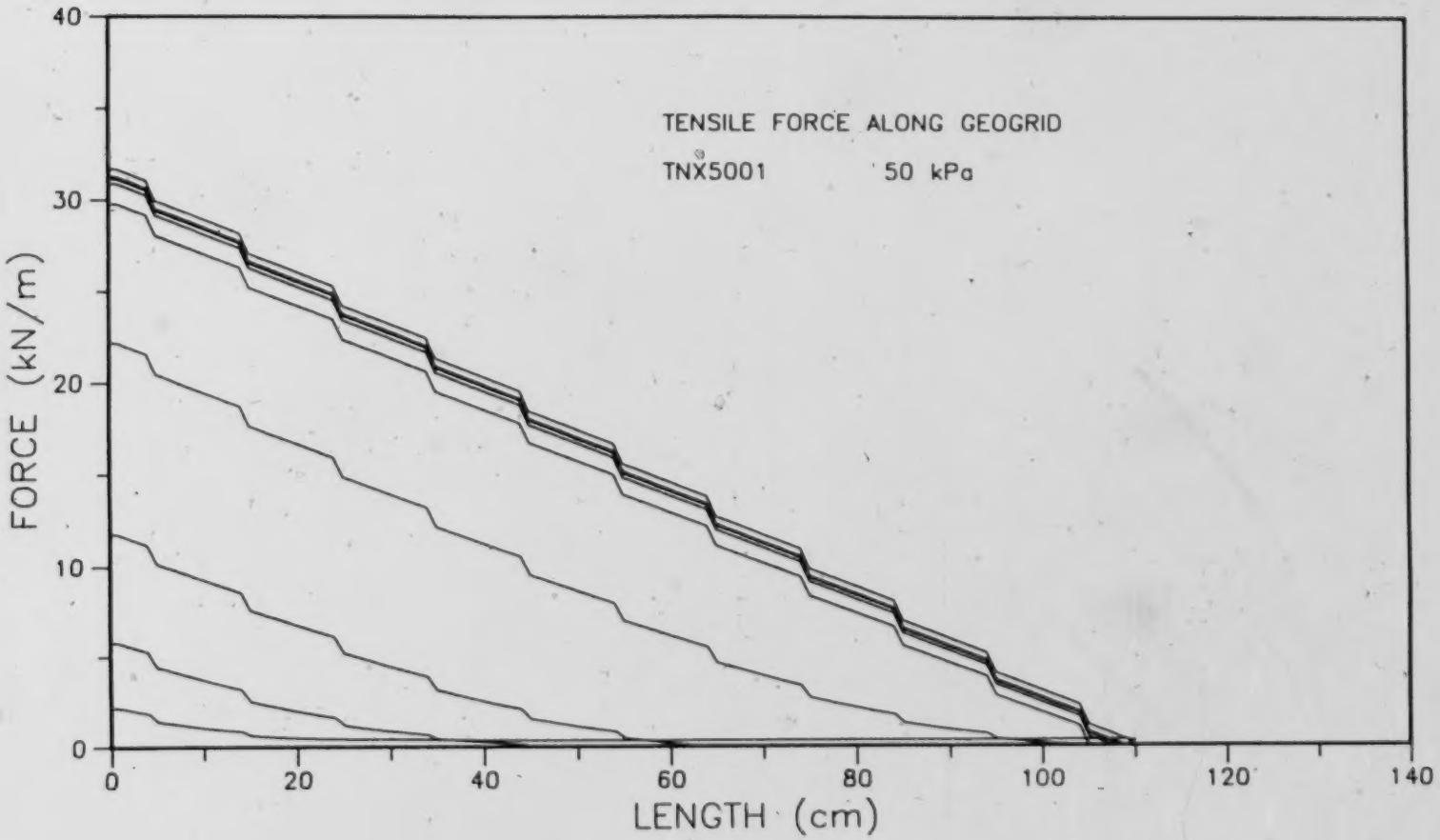

Figure 6.33 Tensile Force along Geogrid TNX5001, 50 kPa

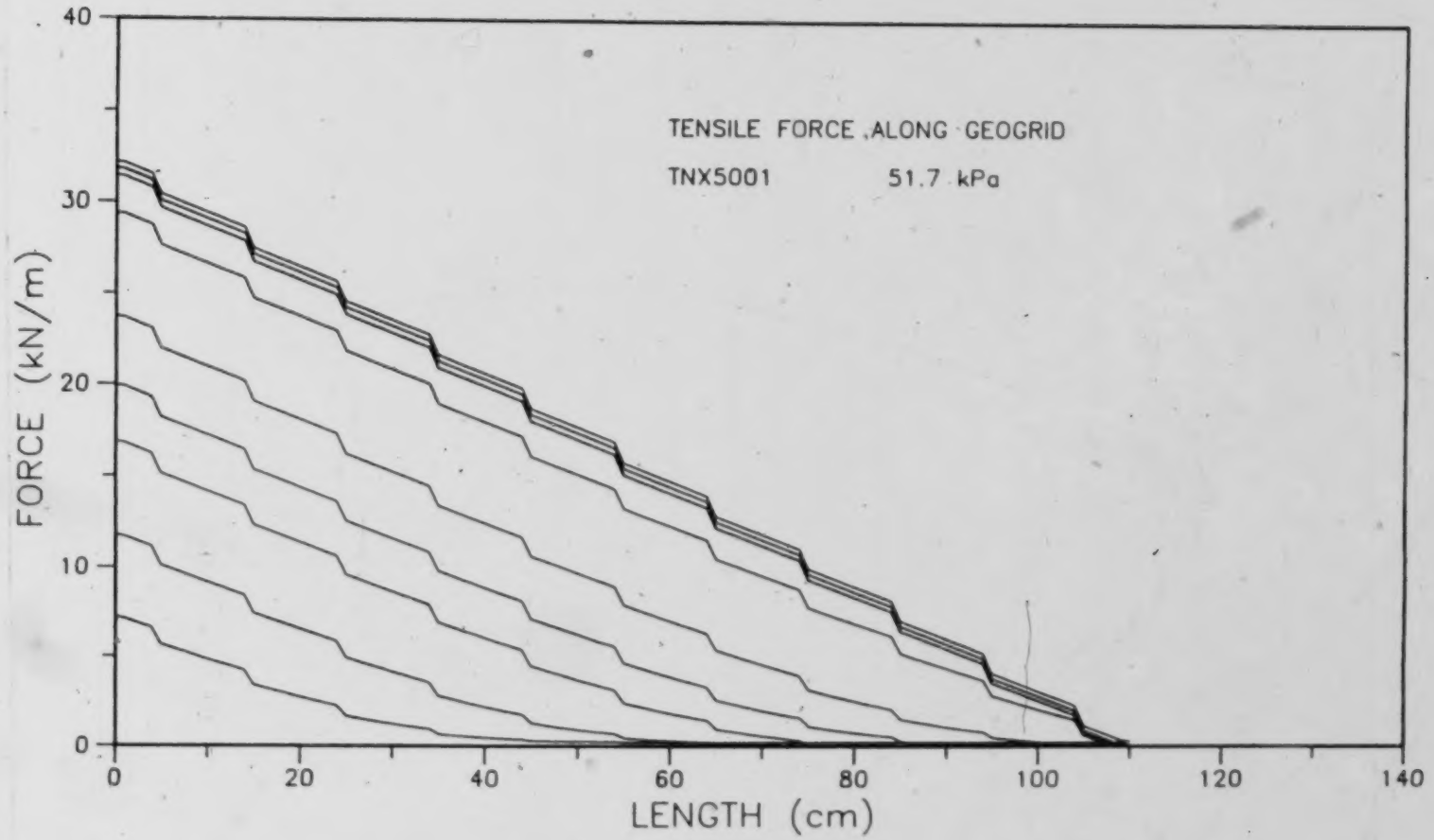

Figure 6.34 Tensile Force along Geogrid TNX5001, 51.7 kPa

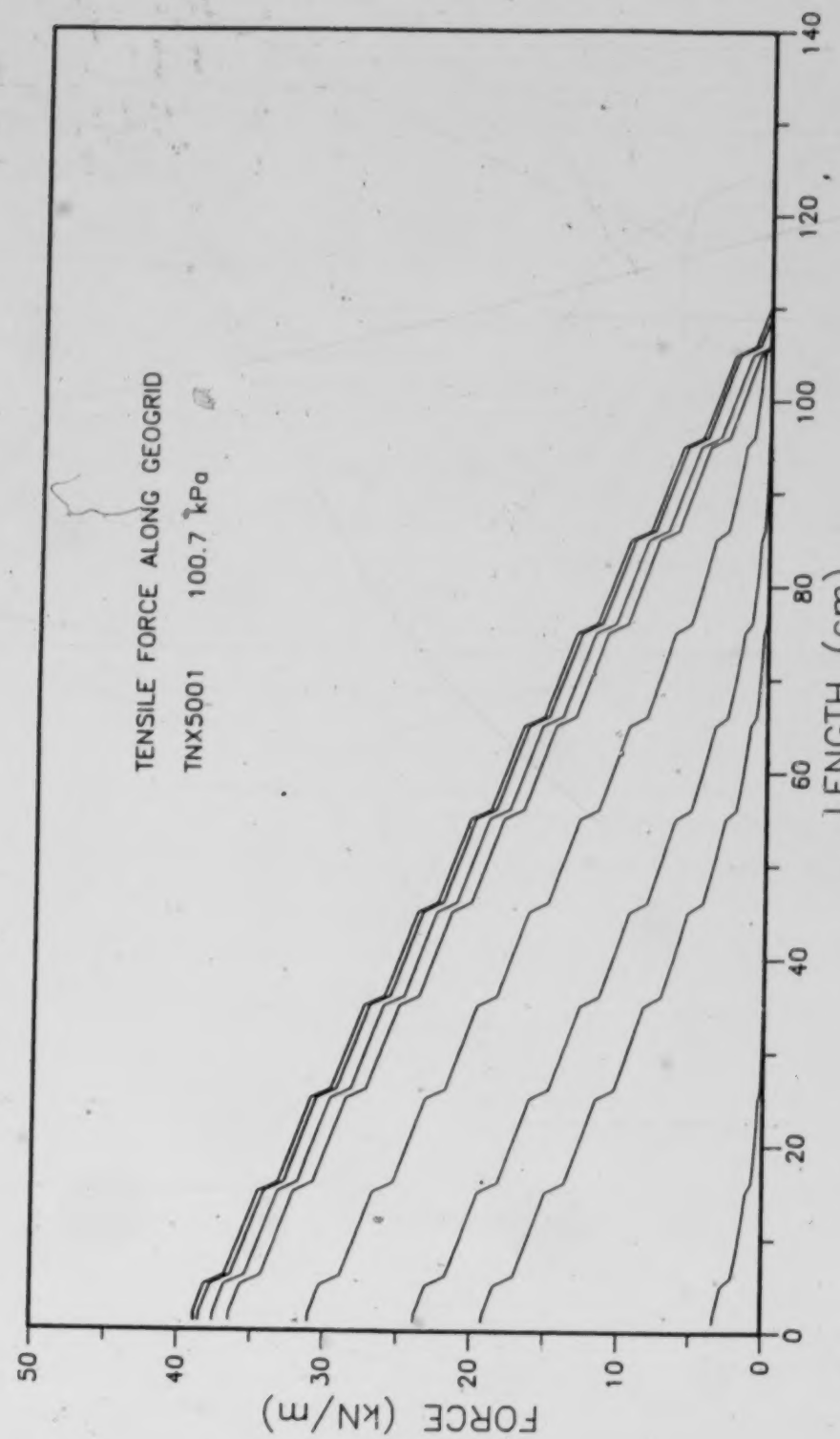

Figure 6.35 Tensile Force along Geogrid TNX5001, 100.7 kPa

agreement between the values is very encouraging in terms of the approach presented in this analysis.

When comparing the existing results from the pull-out tests with the theoretical results from this calculation, the load transfer approach seems to be promising. This is shown in the figures of displacements along the geogrids as well as in the figures of pull-out forces measured and predicted in this analysis.

6.6 Effect of the Reinforcement Tensile Moduli on the Pull-Out Resistance

The force-elongation modulus (or tensile modulus) is a measure of the slope of the force-elongation curve. The units of modulus are kN/m (force per unit width). In this section, the effect of the geogrid tensile moduli on the pull-out resistance is studied.

Assuming that the force x strain curves presented in Chapter 3 are satisfactory, comparison in terms of tensile forces along the geogrids will be made. Figures 6.46, 6.47, 6.48 and 6.49 illustrate the comparison of predicted tensile forces along the geogrids SR2 and TNX5001 for 4 mm, 8 mm and 22 mm of pull-out displacements. The results for SR2 51 kPa are compared with TNX5001 51.7 kPa, as well as, SR2 102.5 kPa with TNX5001 100.7 kPa. These were the only possible comparisons since the variations in moisture contents, dry densities and degrees of saturation did not allow further analysis. It can be observed from these figures that for

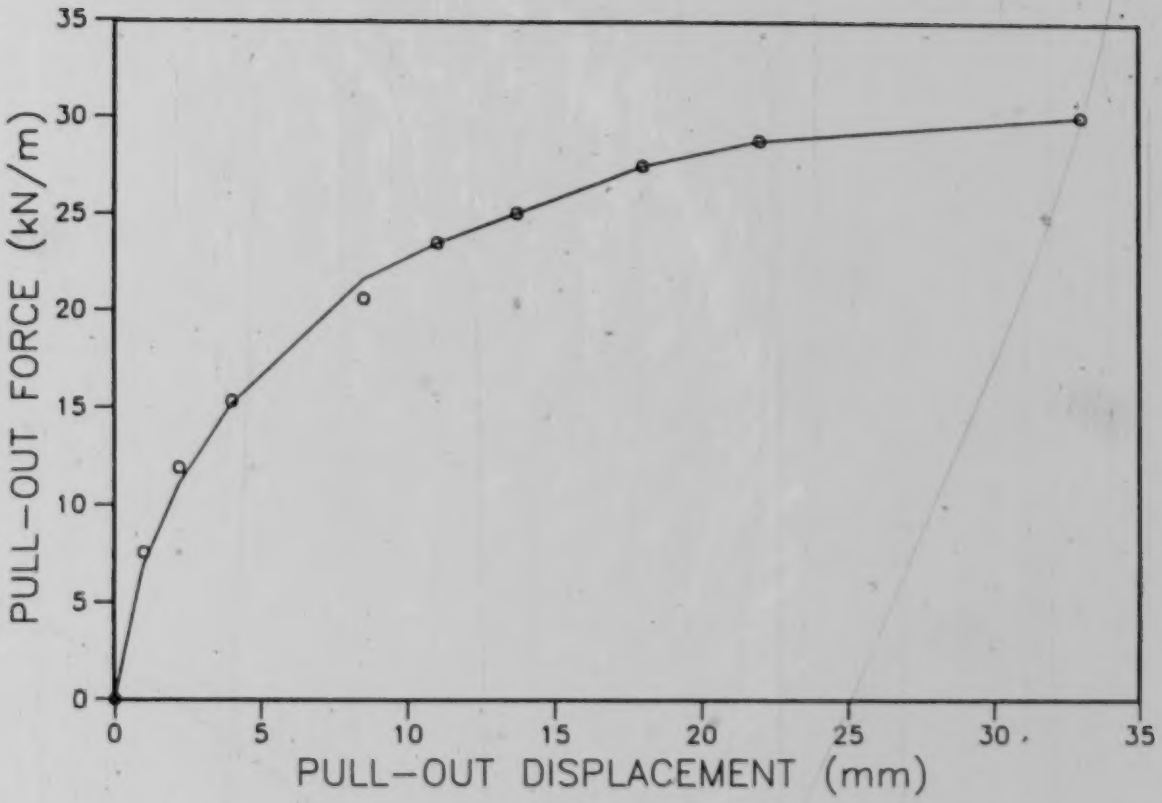

Figure 6.36 Measured and Calculated Values of Pull-Out Force, SR2, 20 kPa

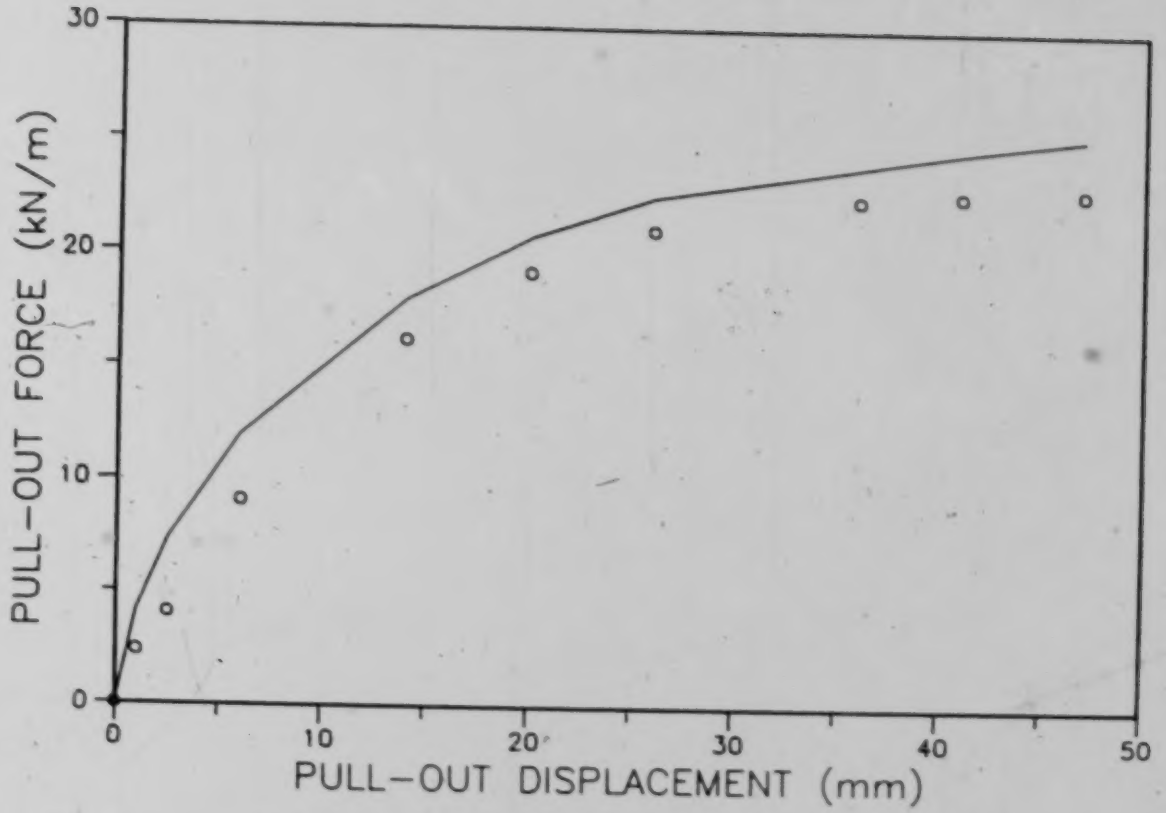

Figure 6.37 Measured and Calculated Values of Pull-Out Force, SR2, 50 kPa

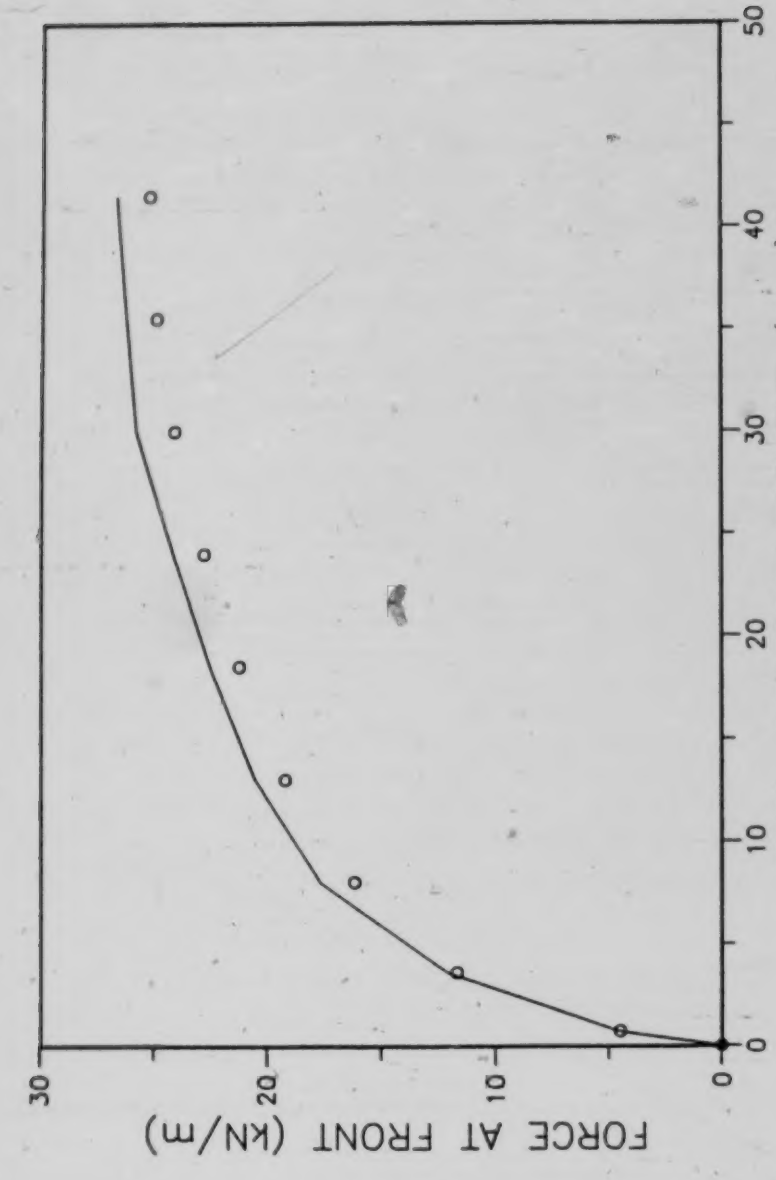

Figure 6.38 Measured and Calculated Values of Pull-Out Force, SR2, 51 kPa

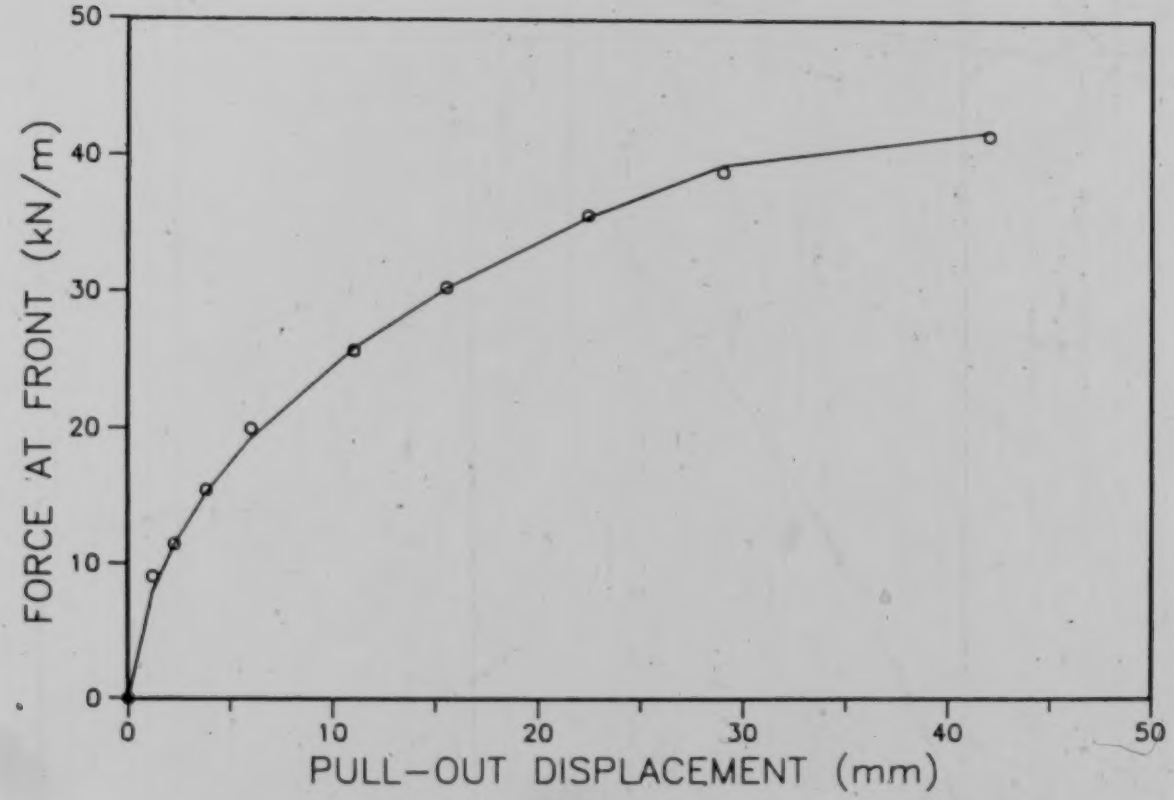

Figure 6.39 Measured and Calculated Values of Pull-Out Force, SR2, 102.5 kPa

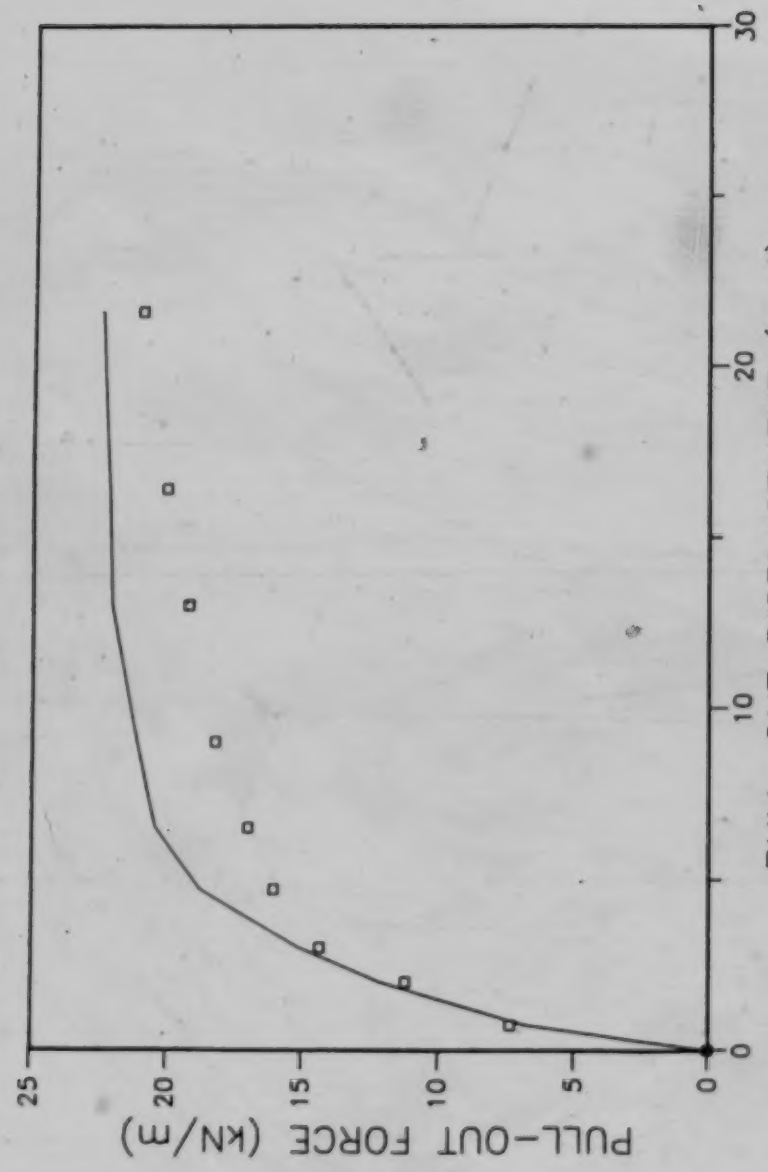

Figure 6.40 Measured and Calculated Values of Pull-Out Force, TNX5001, 20 kPa

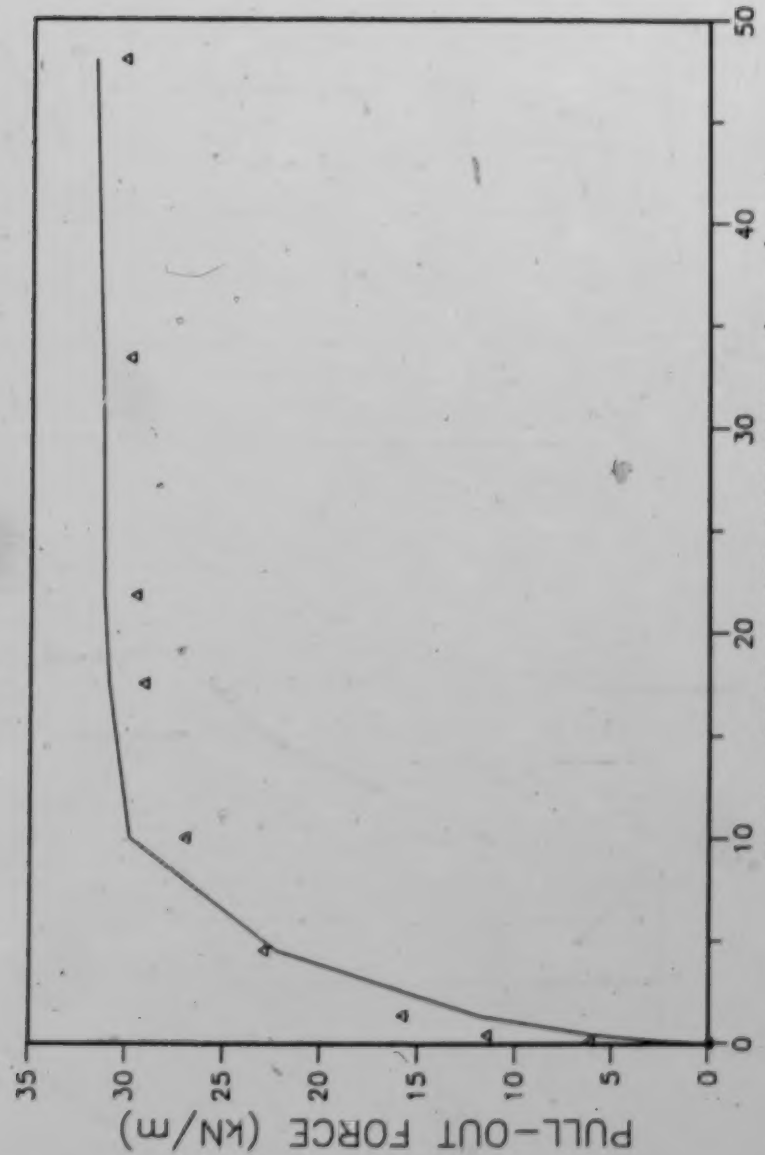

Figure 6.41 Measured and Calculated Values of Pull-Out Force, TNX5001, 50 kPa

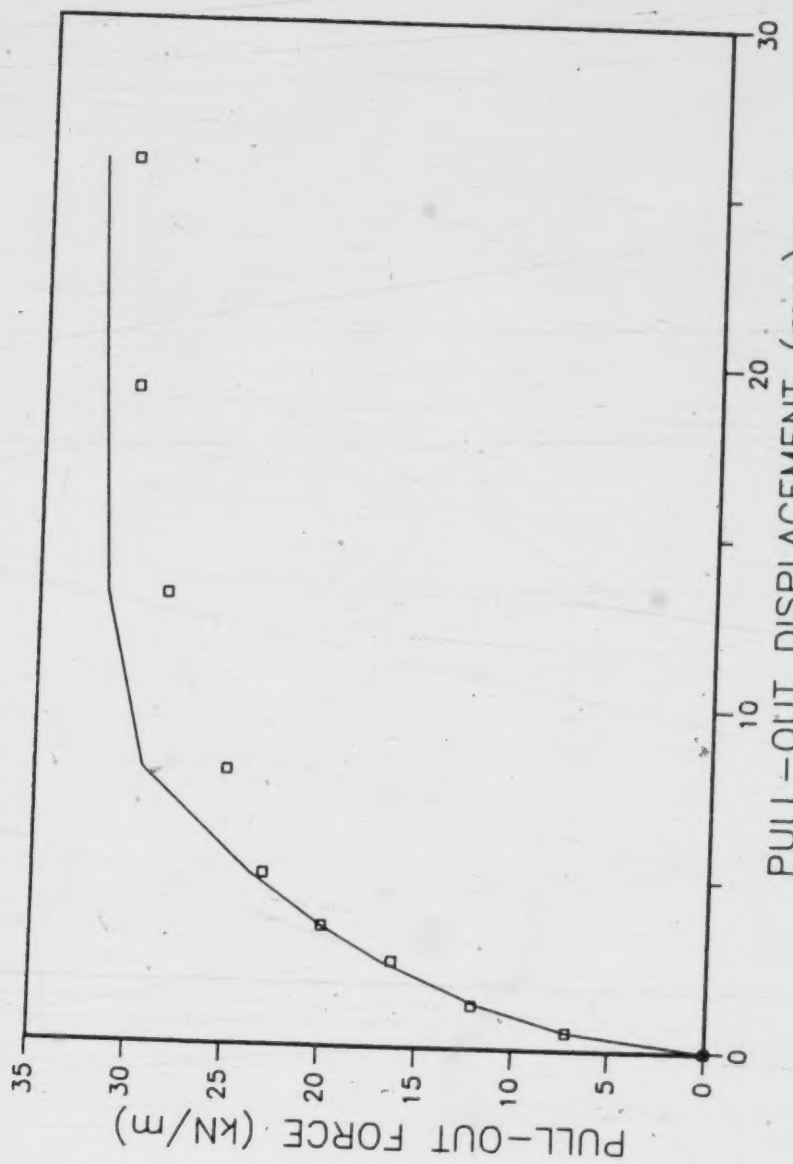

Figure 6.42 Measured and Calculated Values of Pull-Out Force, TNX5001, 51.7 kPa

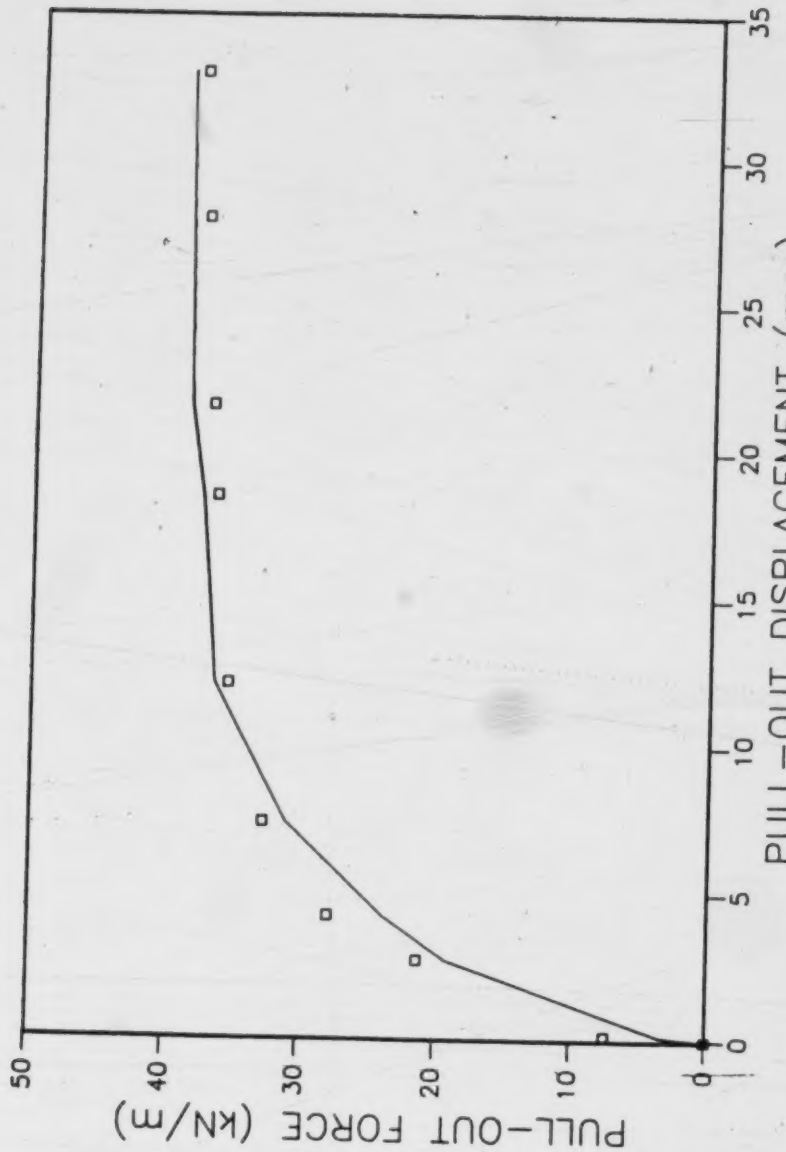

Figure 6.43 Measured and Calculated Values of Pull-Out Force, TNX5001, 100.7 kPa

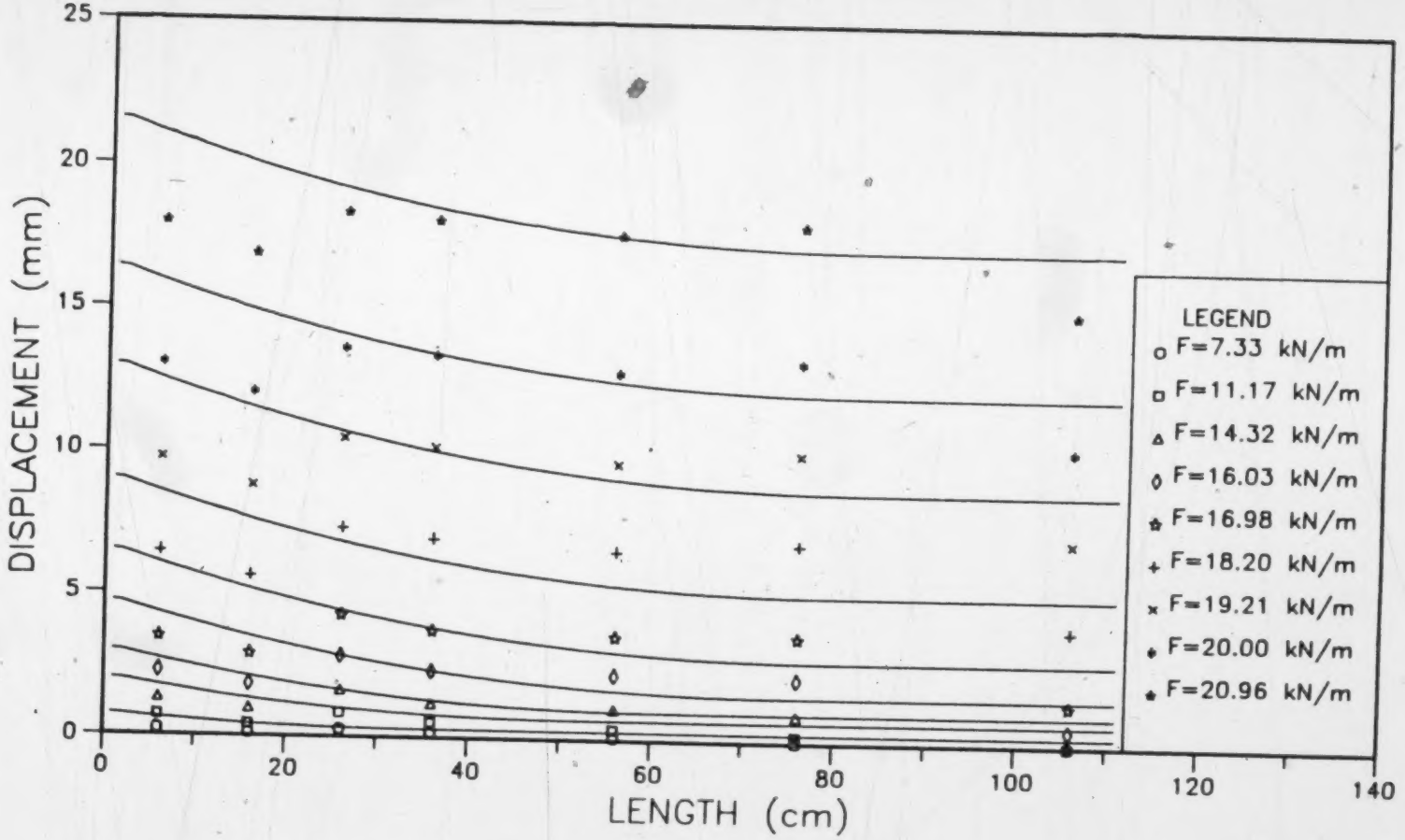

Figure 6.44 Progressive Displacement Along the Geogrid TNX5001, 20 kPa, β=0.7

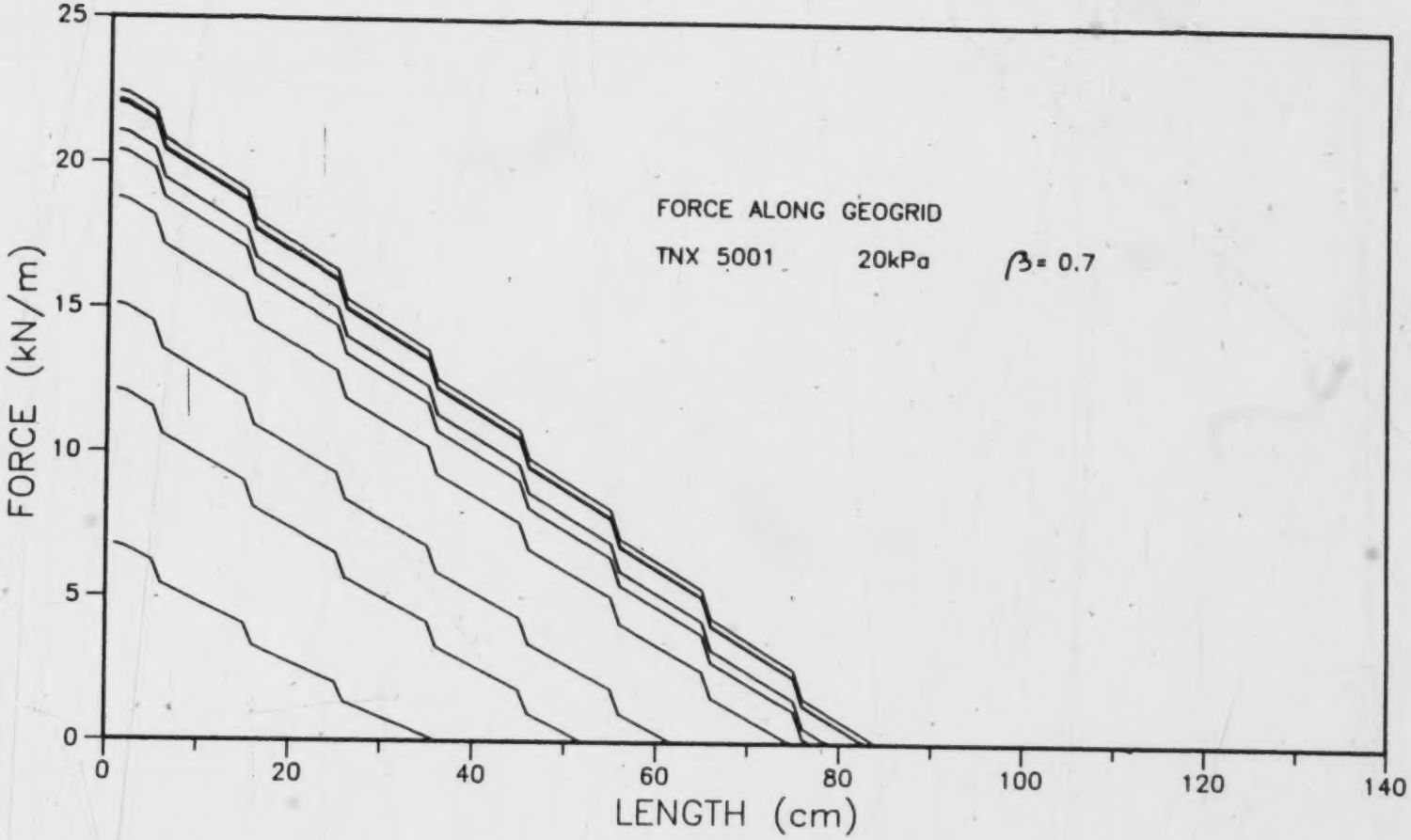

Figure 6.45 Tensile Force Along Geogrid TNX5001, 20 kPa, β=0.7

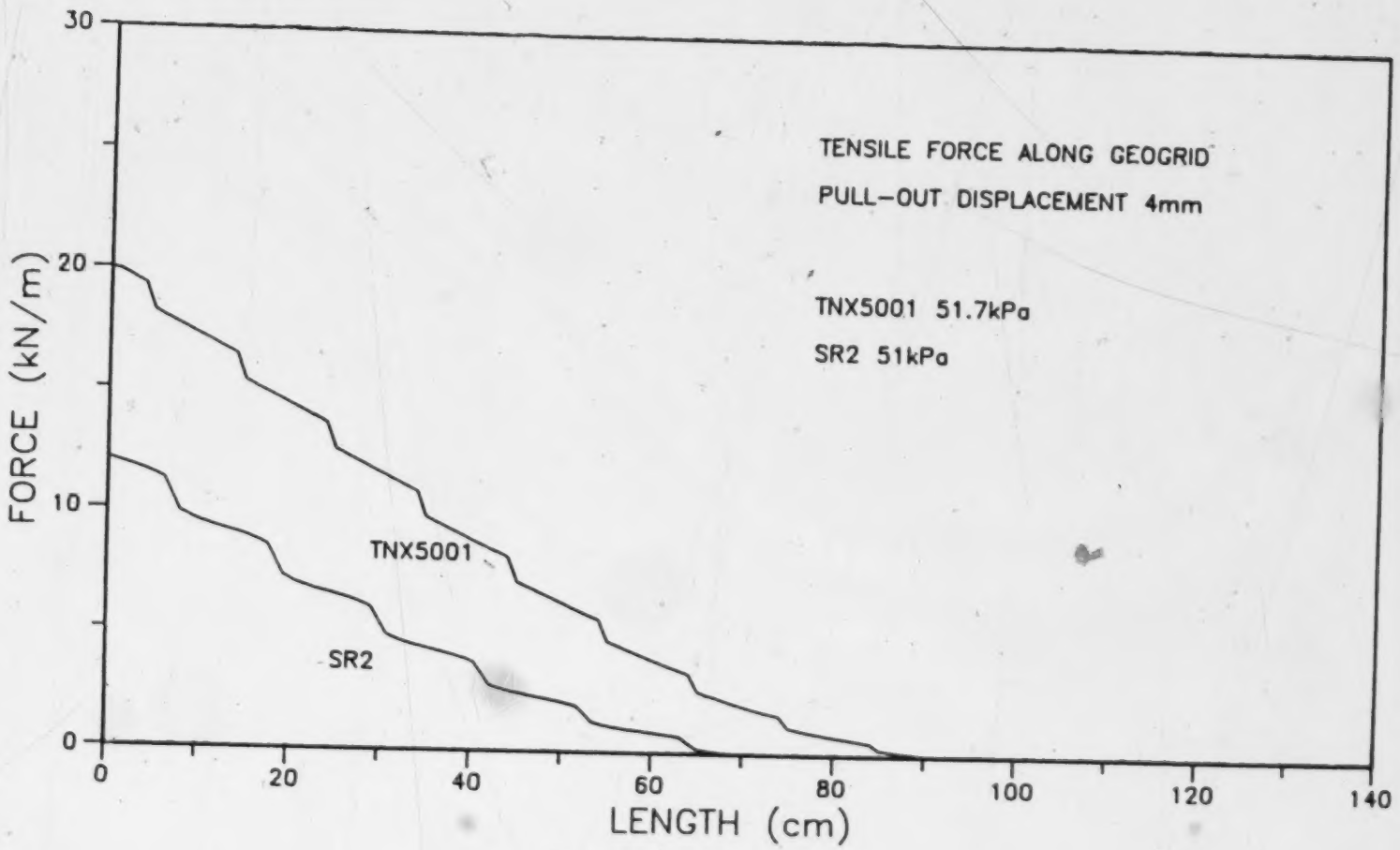

Figure 6.46 Predicted Tensile Forces along Geogrids SR2 (51 kPa) and TNX5001 (51.7 kPa) at Pull-Out Displacement of 4 mm

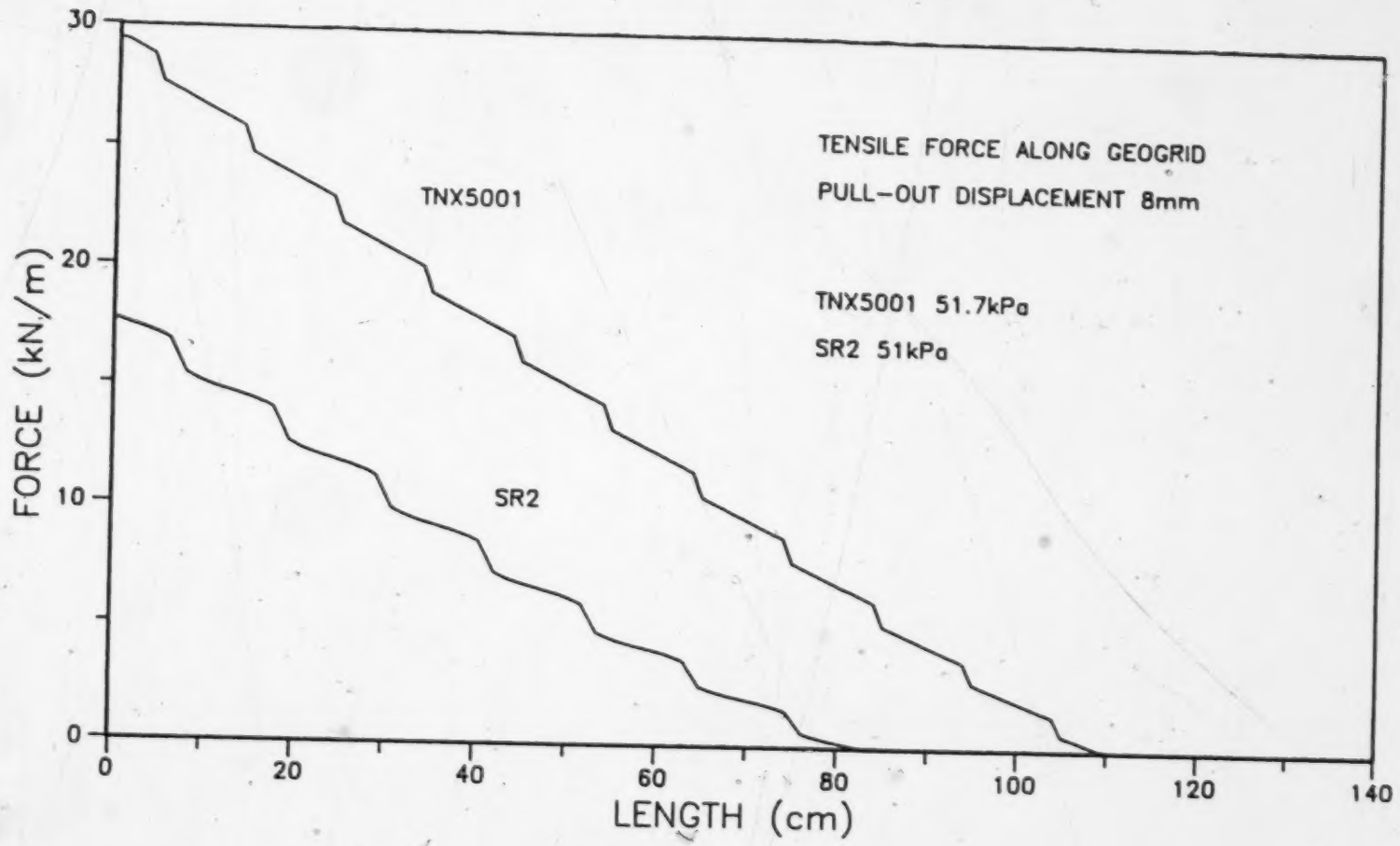

Figure 6.47 Predicted Tensile Forces along Geogrids SR2 (51 kPa) and TNX5001 (51.7 kPa) at Pull-Out Displacement of 8 mm

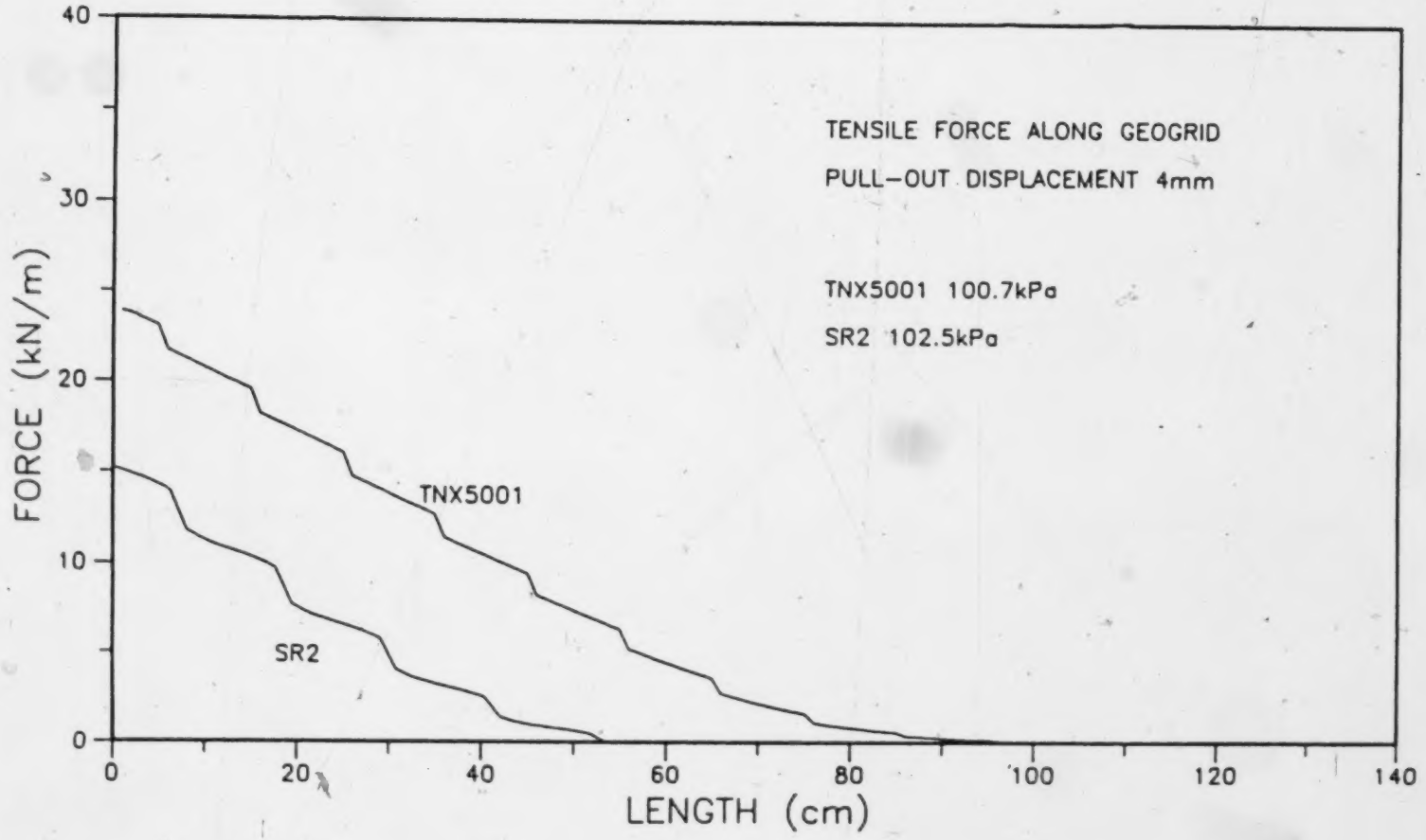

Figure 6.48 Predicted Tensile Forces along Geogrids SR2 (102.5 kPa) and TNX5001 (100.7 kPa) at Pull-Out Displacement of 4 mm

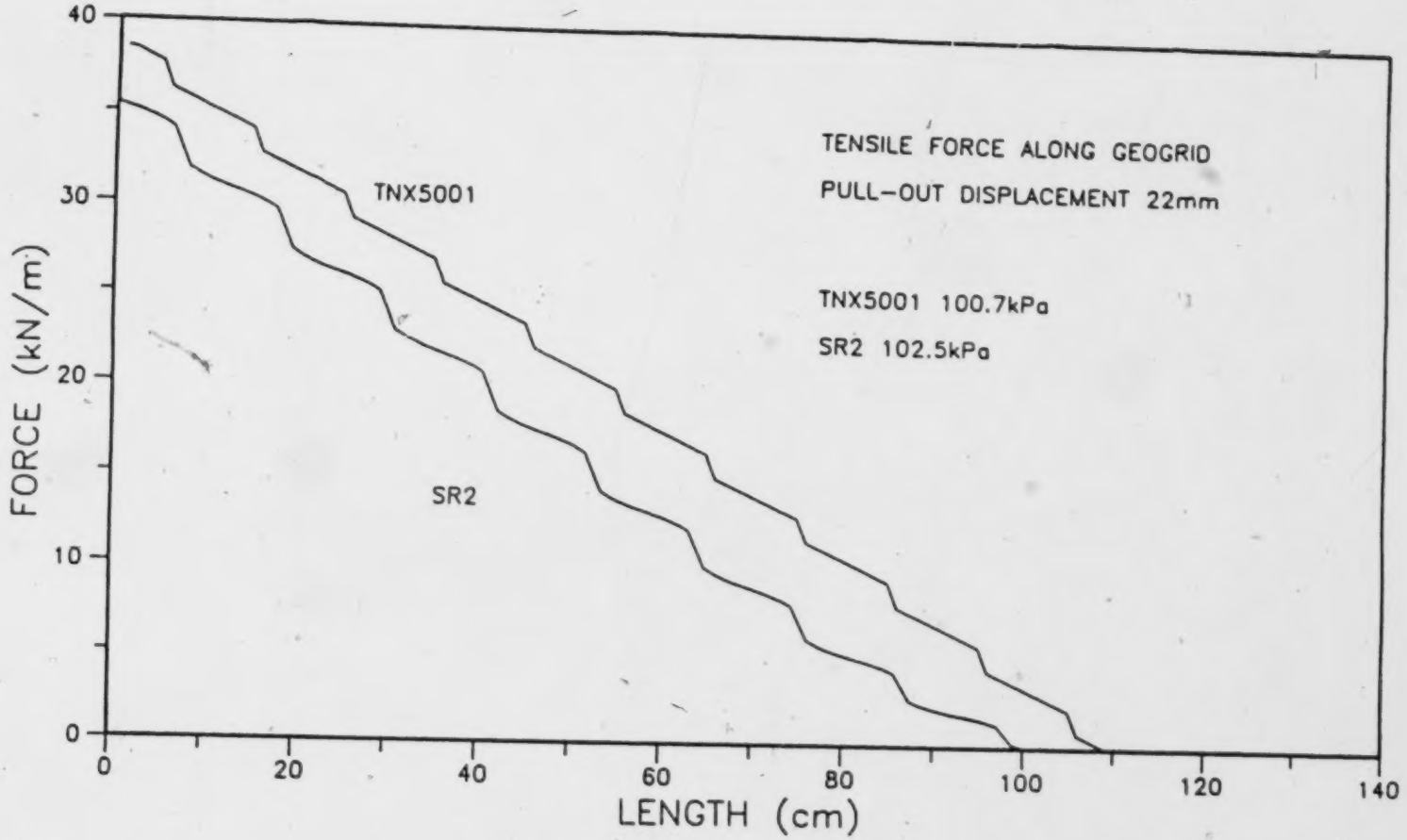

Figure 6.49 Predicted Tensile Forces along Geogrids SR2 (102.5 kPa) and TNX5001 (100.7 kPa) at Pull-Out Displacement of 22 mm

this soil, the TNX5001 geogrid mobilizes higher tensile force than the SR2 for the same displacements. This occurs because the TNX5001 has higher tensile modulus than the SR2 geogrid. The difference is about 80% for the secant modulus at 2% strain, with a strain rate of 2.77%/min. The difference in the distribution of tensile force is larger for smaller pull-out displacements because the difference in initial tensile moduli is also larger. For a large displacement (22 mm), Figure 6.49, the difference in the distribution of tensile force along the two geogrids is smaller than that for a small pull-out displacement (4 mm).

6.7 Contribution of each Mechanism of Interaction between Soil and Geogrid in the Total Pull-Out Force

Assuming that the values of the interfacial stress factor β=0.5 and the coefficient of bearing capacity N_c=7.5 are reasonable, the contribution of each mechanism that takes part in the pull-out mechanism can be assessed (Ingold, 1980).

$P_{bond} = P_a + P_b$

P_{bond} = maximum pull-out force

P_a = force due to adhesion

P_b = force due to bearing

$P_{bond} = \tau_u . \Sigma A_p . \beta + \tau_u \Sigma_b N_c$

Table 6.4 summarizes each contribution.

It is shown that the shear forces on the plan surfaces of the geogrid prevail over the bearing forces against the

Table 6.4 Contribution of Each Mechanism in the Maximum Pull-Out Force

TEST (#)	GEOGRID	NORMAL STRESS (kPa)	PULL-OUT FORCE (kN)	Pa (kN)	Pb (kN)
1	SR2	51	8.75	6.93	1.82
2	SR2	102.5	13.53	10.70	2.81
3	SR2	20	9.82	7.78	2.04
4	SR2	50	7.46	5.91	1.55
5	TNX5001	20	7.08	6.24	0.77
6	TNX5001	100.7	12.56	10.89	1.34
7	TNX5001	51.7	10.2	8.94	1.10
8	TNX5001	50	10.0	8.78	1.08

anchor members. For the Tensar SR2 geogrid, 79% of the maximum pull-out force is due to shear forces along the surface of the geogrid while the same mechanism represents 88% for the Signode TNX5001. The remaining 21% and 12% are due to bearing forces against the anchor members of the geogrids. It should be noticed that these contributions depend on the geometric properties of the reinforcement, grain size of the soil and soil density and shear strength. From Figure 6.50, it is seen that for the mechanism of shear on the plan area of the geogrids the soil shear strength prevails over the geometric properties.

6.8 Design Procedure to Predict the Required Anchoring Length of a Geogrid

The load transfer approach presented in this research can be used in a design procedure to predict the required anchoring length of a geogrid in a reinforced retaining wall or a reinforced slope.

The required parameters for the design procedure are:

P_i: maximum allowable tensile force in the reinforcement (at the potential failure surface)

x_i: allowable displacement of the reinforcement (at the potential failure surface)

Force-strain properties of the geogrid for varying strain rate and temperature.

Stress strain curve of the soil for a range of normal stresses.

Geometric properties of the geogrid.

Interfacial stress factor (β) between soil and polymer surfaces.

Bearing capacity factor (N_c) for the reinforcement geometry.

The interfacial stress factor can be obtained from a pull-out test on a single tension member. An initial length of the reinforcement is required to start the calculation. The criterium for the anchoring length would be to have no force (F=0) at the end of the reinforcement. The calculation should follow the steps explained in Section 6.5.

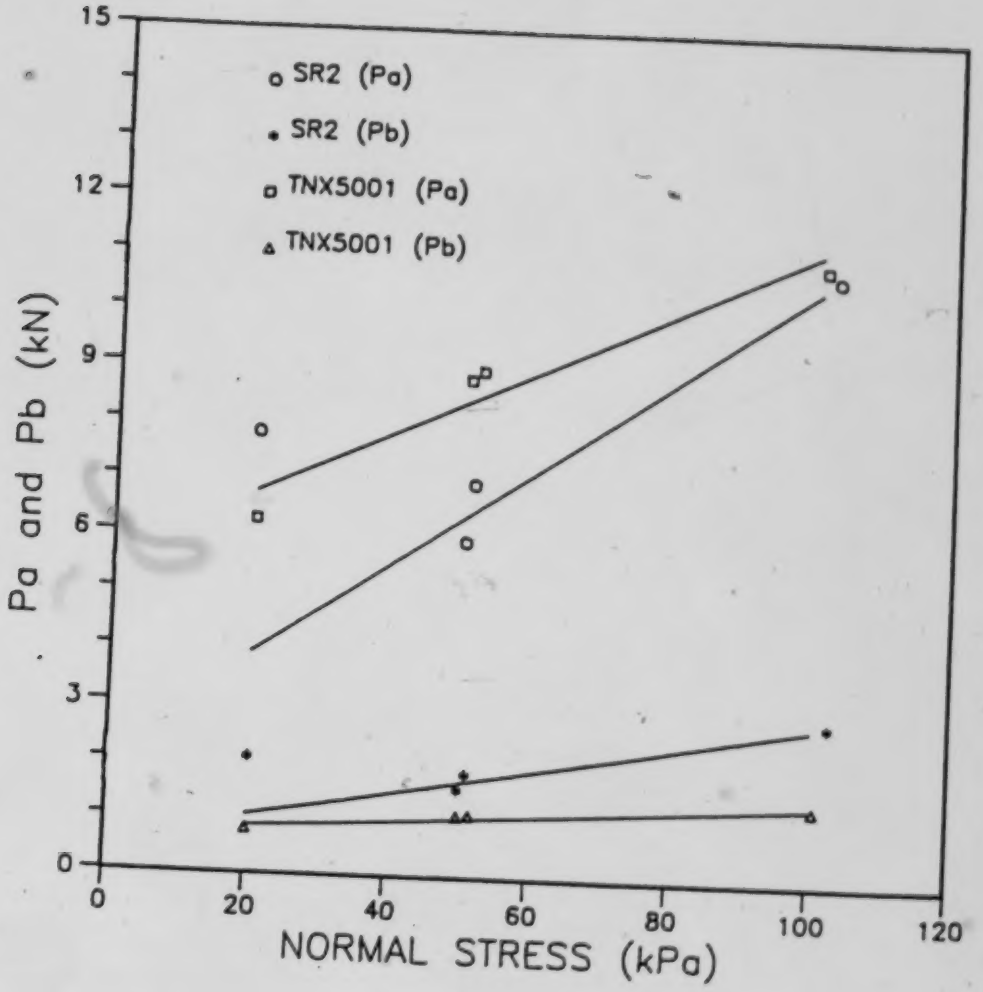

Figure 6.50 Contribution of Each Mechanism of Interaction between Soil and Geogrid in the Maximum Pull-Out Force

7. CONCLUSIONS AND RECOMMENDATIONS FOR FUTURE RESEARCH

7.1 Summary

The purpose of this research program was to determine the mechanism of load transfer between a cohesive soil and three kinds of geogrids. Due to material damage, one geogrid could not be fully tested. In addition, a large pull-out apparatus was designed and constructed and a testing procedure was developed for this research. A total of 12 consolidated undrained pull-out tests on silty clay soil and two types of geogrids were performed. The experimental results of eight tests have been reported in Chapter 5. The results from two tests performed with the third type of geogrid are presented in Appendix A.

An approach, based on the load transfer method applied to piles loaded axially, was formulated to predict the tensile force distribution along the geogrids. The influence of the tensile properties of the geogrids was used to evaluate the results from this approach.

7.2 Conclusions

7.2.1 Analyses and Results

The load transfer method can be applied to predict the pull-out mechanism of soil-geosynthetic reinforcement systems. The tensile moduli of a geosynthetic will influence its pull-out characteristics and the higher the tensile

modulus, the more efficiently the geosynthetic develops pull-out resistance in reinforced soil structures.

The bond strength of the geogrid junctions did not affect the results of the distribution of tensile force in the geogrids with the clayey soil used in this research. The TNX5001 junctions (welded) are not as strong as those of the SR2. Despite this fact, the former presented a higher pull-out modulus than the latter.

For the type of soil used in this study and geometric characteristics of the geogrids, the mechanisms of shear on the planar surface of the geosynthetics prevail over the mechanisms of bearing against the geosynthetic anchor members. The surface shear force was 88% and 79% of the total maximum pull-out force for the TNX5001 and SR2 geogrids, respectively. The remaining 12% and 21% of the pull-out force being accounted for by the mechanism of bearing.

7.2.2 Test Apparatus and Procedure

This study showed that the large pull-out apparatus was appropriate for the study of load transfer between soil and geosynthetic reinforcements. The testing procedure developed for this research was suitable for assessing the distribution of axial force along the geogrids. The instrumentation used to measure the displacements of different points along the geogrids proved to be accurate for this scale of testing. Finally, the load cells located

at the front of the pull-out box proved to be a very reasonable way to measure the passive force against the front of the soil sample. Values of passive force ranging from 6 to 18% of the total pull-out force were measured.

7.3 Recommendations for Future Research

1. The magnitudes and mechanisms of drained pull-out tests on reinforced silty clay needs further study.
2. Interaction experimental results for other reinforcements and soil types are needed, especially for those which develop the majority of their resistance by bearing against the anchor members and by combined friction or adhesion and bearing.
3. The flexible vertical loading system should be replaced by an air or water pressure bag. This would save time and energy during the assembly of the pull-out test apparatus.
4. More data on the interfacial stress factor and its influence on the distribution of force on the geogrids are needed.

REFERENCES

Balligh, M.M., and Scott, R.F., 1976. Analysis of wedge penetration in clay. Geotechnique, 26(1), pp.185-208.

Beech, J.F., 1987. Importance of stress-strain relationships in reinforced soil system designs. Proceedings, Geosynthetic '87 Conference, New Orleans, Feb., Vol.1, pp.133-144.

Bergado, D.T., Bukkanasuta, A., and Balasubramaniam, A.S., 1987. Laboratory pull-out tests using bamboo and polymer geogrids including a case study. Geotextiles and Geomembranes, Vol. 5, No. 3, pp.153-189.

Bobey, L.W.M., 1987. Soil-geogrid interfacial shear strength. M.Sc. Thesis, University of Alberta, December, 176 p.

Brand, S.R. and Duffy, D.M., 1987. Strength and pullout testing of geogrids. Proceedings, Geosynthetic '87 Conference, New Orleans, Feb., Vol. 2, pp.226-236.

Brandt, J.R.T. 1985. Behaviour of soil concrete interfaces. Ph.D. Thesis, Univeristy of Alberta, April, 376 p.

Casagrande, A. and Hirchfeld, R.C., 1960. First progress report on investigation of stress-deformation and strength characteristics of compacted clays. Harvard Soil Mechanics Series, No. 61, May, 52 p.

Chang, J.C., Hannon, J.B. and Forsyth, R.A., 1977. Pull resistance and interaction of earthwork reinforcement and soil. Transportation Research Record 640, Washington, D.C.

Collios, A., 1981. Loi d'interaction mecanique sol-geotextile. Ph.D. Thesis, L'Universite Scientifique et Medicale de Grenoble, June, 299 p.

Coyle, H.M. and Reese, L.C., 1966. Load transfer for axially loaded piles in clay. Journal of the Soil Mechanics and Foundation Division, A.S.C.E., Vol. 92, SM2, March, pp.1-26.

Department of Civil Engineering, 1984. Large-scale pull-out tests on Tensar geogrids. Report for the Tensar Corporation, University of California, July, 53 p.

Finnigan, J.A., 1977. The creep behaviour of high tenacity yarns and fabrics used in civil engineering applications. Proceedings, International Conference on the Use of Fabrics in Geotechnics, Vol. II, Paris, April, pp.305-309.

Giroud, J.P., 1986. From geotextiles to geosynthetics: A revolution in geotechnical engineering. Proceedings, Third International Conference on Geotextiles, Vienna, pp. 1-17.

Highway Research Report 1987. Reinforcement of earth slopes and embankments. Transportation Research Board, Report 290, Washington, D.C.

Holtz, R.D., 1977. Laboratory studies of reinforced earth using a woven polyester fabric. Proceedings, International Conference on the Use of Fabrics in Geotechniques, Vol. I, Paris, April, pp. 149-154.

Holtz, R.D., 1978. Reinforced earth works mechanics. Final Technical Report, Purdue University, Aug., 60 p.

Ingold, T.W., 1980. Reinforced clay. Ph.D. Thesis, University of Surrey, 252 p.

Ingold, T.S., 1983. Laboratory investigation of grid reinforcement in clay. Geotechnical Testing Journal, Vol. 6, No. 3, pp. 112-119.

Ingold, T.W., 1984. Introduction to polymer grids: written discussion contributions. Proceedings, Symposium on Polymer Grid Reinforcement in Civil Engineering, London, pp. 40-45.

Jewell, R.A., Milligan, G.W.E., Sarsby, R.W. and Du Bois, D., 1984. Interaction between soil and geogrids. Proceedings, Symposium on Polymer Grid Reinforcement in Civil Engineering, London, England, pp. 1.3.1-1.3.13.

Jones, C.J.F.P., 1985. Earth reinforcement and soil structures. Butterworths Books Co., London. 183 p.

Lee, K.L., 1978. Mechanisms, analysis and design of reinforced earth: state-of-the-art report. Proceedings, ASCE Symposium on Earth Reinforcement, Pittsburgh, April, pp. 62-76.

McGown, A., Andrawes, K.L. and Yeo, K.C., 1984. The load-strain-time behaviour of Tensar geogrids. Proceedings, Polymer Grid Reinforcement. Thomas Telford Ltd., London, March, pp. 11-17.

McKittrick, D.P., 1979. Reinforced earth: application of theory and research to practice. Ground Engineering, Jan., pp 19-31.

Milligan, G.W.E. and Palmeira, E.P., 1987. Prediction of bond between soil and reinforcement. Proceedings, Symposium on Prediction and Performance in Geotechnical Engineering, Calgary, June, pp. 147-153.

Mitchell, J.K., 1987. Reinforcement for earthwork construction and ground stabilization. Proceedings, 8th Pan American Congress of Soil Mechanics and Foundation Engineering, Cartagena, Aug., pp. 349-380.

Mowafy, M.M.Y., 1986. Analysis of grid reinforced earth structures. Ph.D. Thesis, Carleton University, Ottawa, Jan., pp. 189-247.

Murray, R.T., Carder, D.R. and Krawczyk, J.V., 1980. Pull-out tests on reinforcement embedded in uniformly graded sand subject to vibration. Proceedings 7th European Conference on Soil Mechanics and Foundation Engineering, Brighton, Vol. 3, pp. 115-120.

Palmeira, E.M. and Milligan, G.W.E., 1987. Scale and other factors affecting the results of pull-out tests of grids buried in sands. University of Oxford, Department of Engineering Science, Report Q.U.E.L. 1678/87, 43 p.

Peterson, L.M. and Anderson, L.R., 1980. Pull-out resistance of welded wire mesh embedded in soil. Research Report Submitted to Hilfiker Pipe Company, Department of Civil

and Environmental Engineering, Utah State University, Logan, Utah, U.S.A.

Prandtl, L., 1921. Uber die eindringungsfestigkeit plastisher baustoffe und die festigkeit von schneiden. zeitschrift fur Angewandte Mathematik und Mechanik, 1:1, pp. 15-20.

Reissner, H., 1924. Zum erddruchkproblem. Proceedings, First International Conference on Applied Mechanics, Delft., pp. 295-311.

Rowe, R.K., Ho, S.K. and Fisher, D.G., 1985. Determination of soil-geotextile interface strength properties. Proceedings Canadian Symposium on Geotextiles and geomembranes, Edmonton, Sept., pp. 25-34.

Rowe, R.K. and Ho, S.K., 1986. Determination of geotextile stress-strain characteristics using a wide strip test. Proceedings, Third International Conference on Geotextiles, Vienna, pp. 885-890.

Salomone, W.G., 1978. Soil reinforcement interaction. Ph.D. Thesis, Purdue University, West Lafayette, Indiana, 70 p.

Skempton, A.W., 1951. The bearing capacity of clay. Building Research Congress, England.

Schlosser, F. and Elias, V., 1978. Friction in reinforced earth. ASCE Convention, Pittsburgh, U.S.A., pp. 757-761.

Schlosser, F., 1978. History, current and future developments of reinforced earth. Proceedings, Symposium on Soil Reinforcing and Stabilising Techniques. N.S.W. Institute of Technology, pp. 5-28.

A. PULL-OUT TEST RESULTS ON SILTY CLAY SOIL REINFORCED WITH PARAGRID 50S

Table A.1 Pull-Out Test Results on Silty Clay Reinforced with ParaGrid 50S

TEST (#)	NORMAL STRESS (kPa)	Wi (%)	NAT.INI. DENSITY (kN/m^3)	DRY DENSITY (kN/m^3)	MAX. FORCE (*) (kN/m)
A1	50	24.5	18.8	15.1	26.2
A2	20	26.0	19.1	15.2	19.4

(*) Geogrid failure at junctions

Table A.2 Force on Front End of the Soil Sample

TEST (#)	MAX. PULL-OUT FORCE (kN)	FRONT END LOAD CELLS					SUM/ MAX PULL-OUT FORCE (%)
		lc1 (kN)	lc2 (kN)	lc3 (kN)	lc4 (kN)	SUM (kN)	
1	9.24	-0.04	0.29	0.10	3.10	3.45	37.4
2	4.25	0.16	0.25	0.56	0.02	0.99	23.3

(+) Compression
(-) Tension

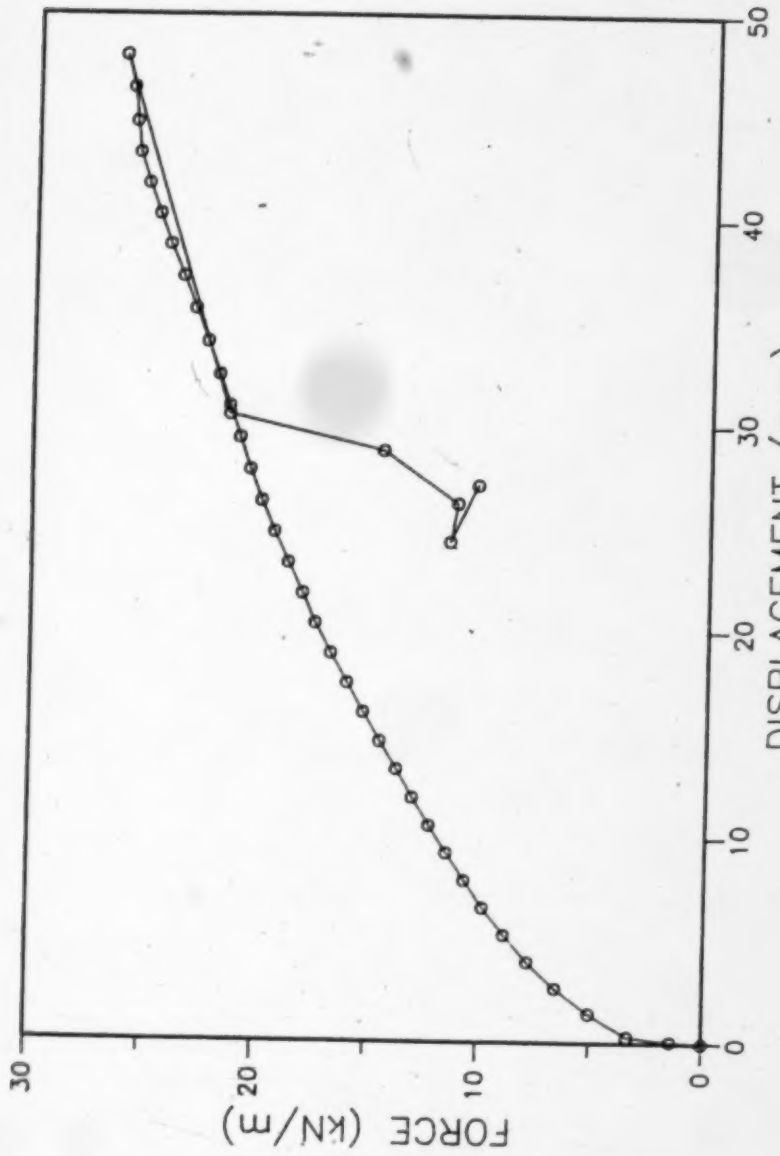

Figure A.1 Pull-Out Force and Displacement Curve, ParaGrid, 50 kPa

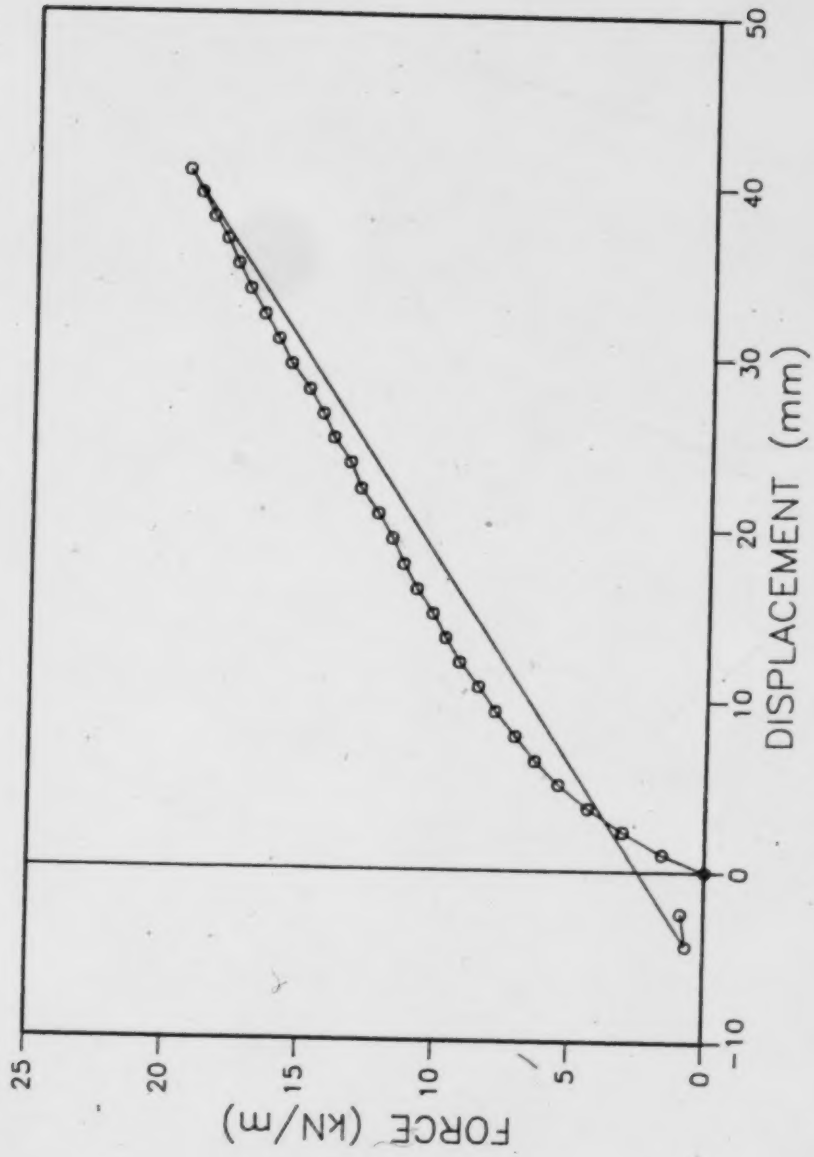

Figure A.2 Pull-Out Force and Displacement Curve, ParaGrid, 20 kPa

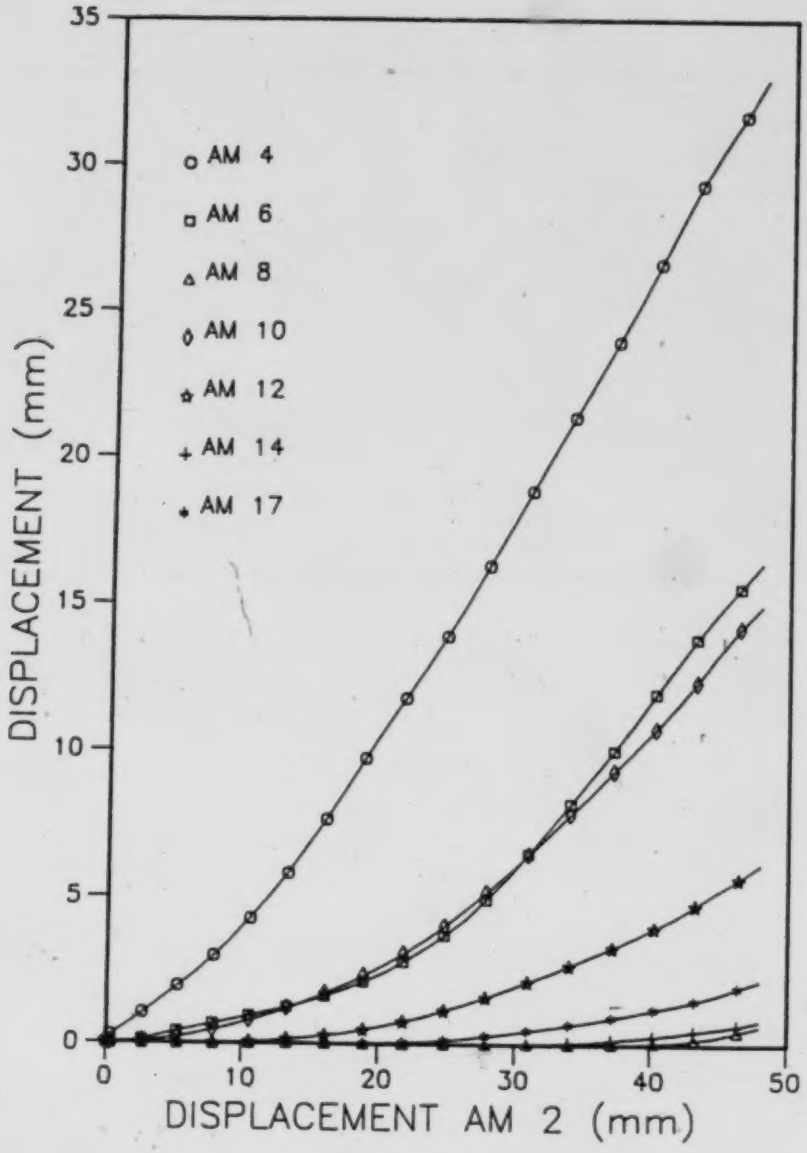

Figure A.3 Progressive Horizontal Displacement, ParaGrid 50 kPa

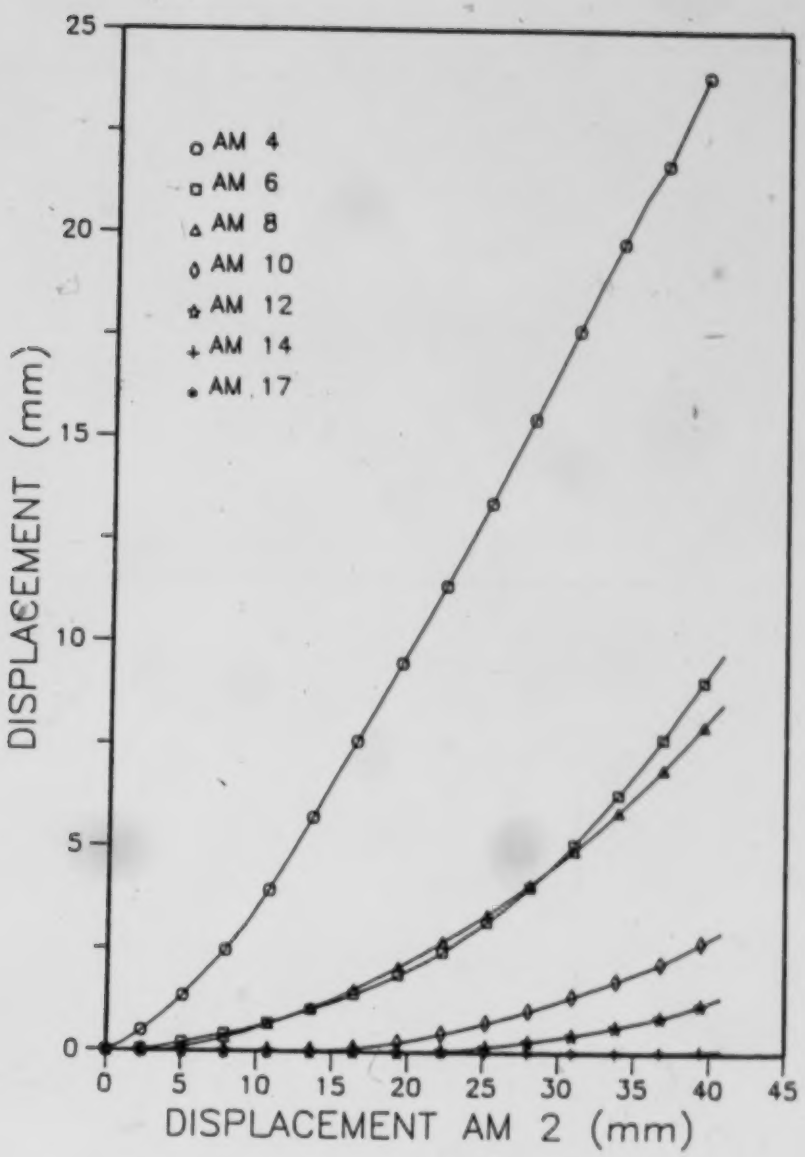

Figure A.4 Progressive Horizontal Displacement, ParaGrid 20 kPa

B. CALIBRATION AND COMPLIANCE OF PULL-OUT APPARATUS

Table B.1 Calibration Factors and Correlation Coefficients for Linear Variable Differential Transformers

LVDT (#)	COEFFICIENT (V/mm)	r
1	1.5664	0.99998
2	1.5256	0.99998
3	1.2230	0.99980
4	5.6398	0.99994
5	5.8086	0.99992
6	1.1866	0.99998
7	1.5509	0.99996
8	4.6937	1.00000
A	16.2450	0.99997
B	-3.8358	0.99995
C#1	3.5445	0.99905
C#3	3.3100	0.99990

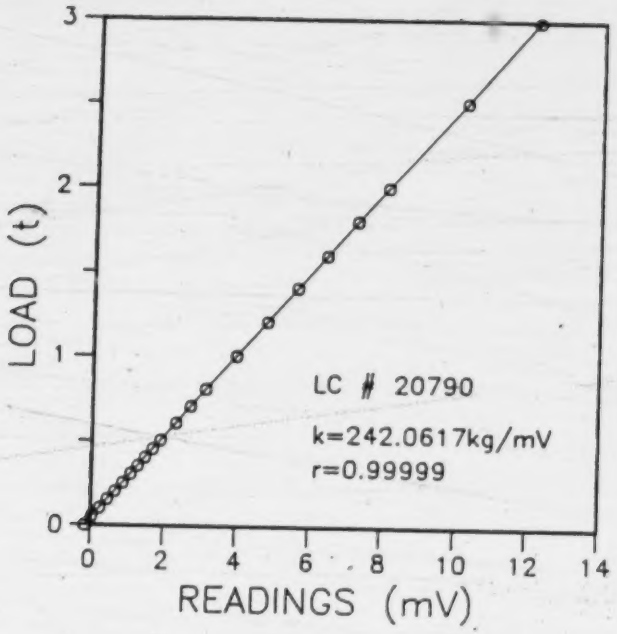

Figure B.1 Calibration Curve for Load Cell 20790

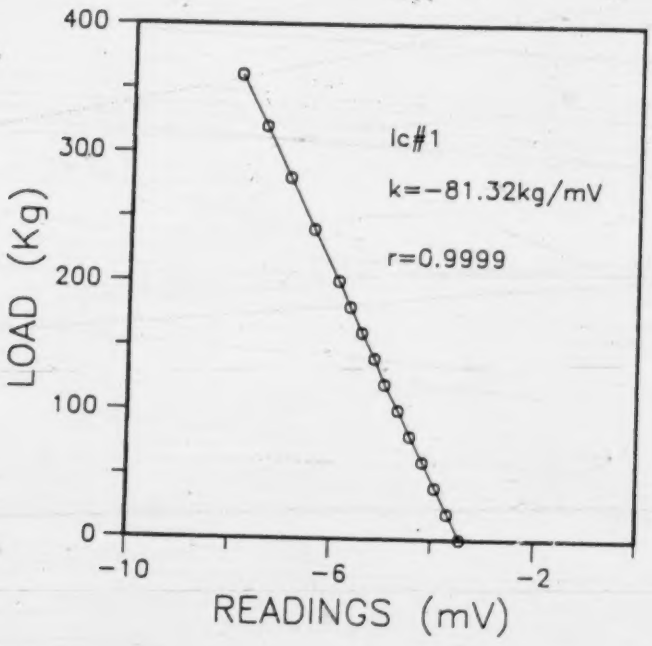

Figure B.2 Calibration Curve for Load Cell 1

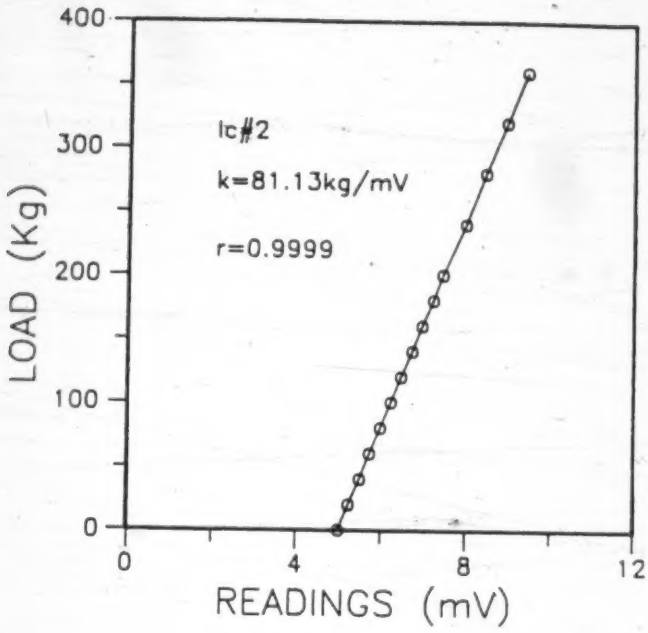

Figure B.3 Calibration Curve for Load Cell 2

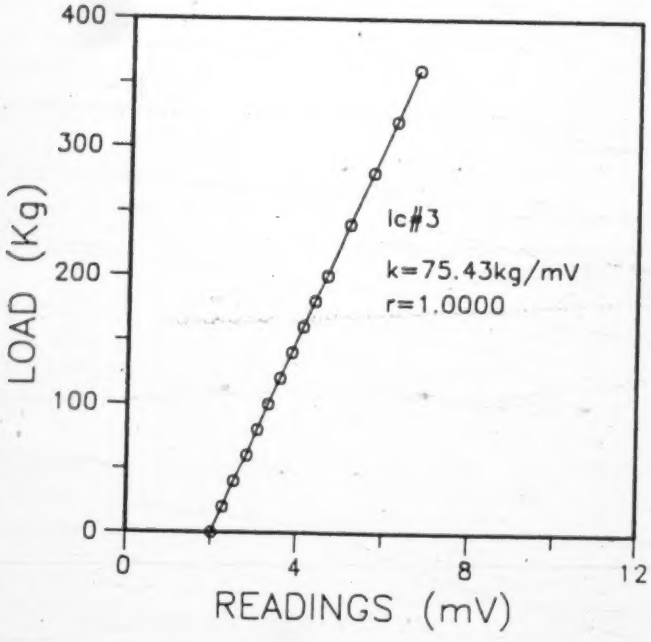

Figure B.4 Calibration Curve for Load Cell 3

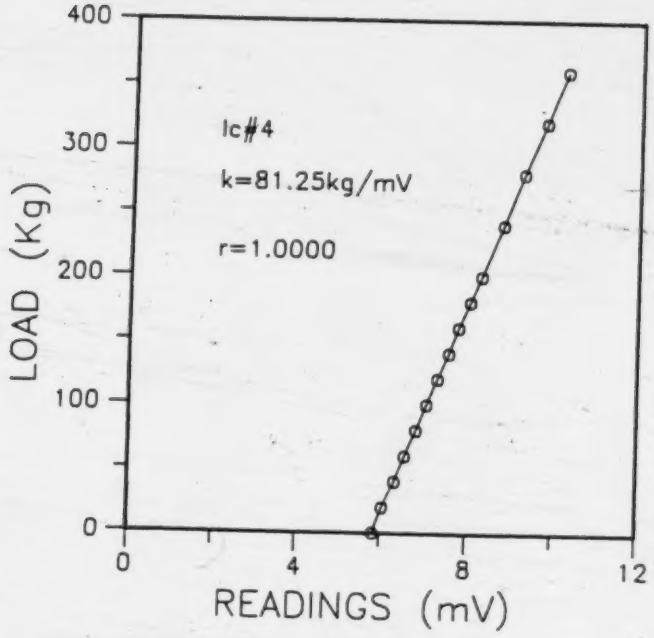

Figure B.5 Calibration Curve for Load Cell 4

C. Listing of the Basic Program which Calculates the Axial Force and Displacements along the Geogrids SR2 and TNX5001

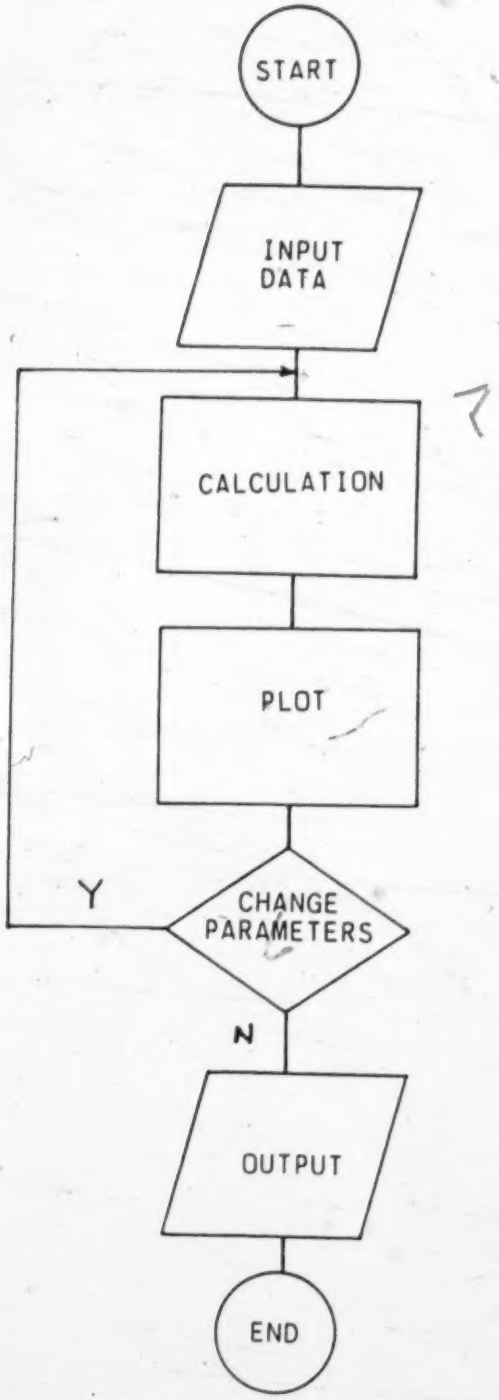

Figure C.1 Flow Chart

```
5 CLS
20 REM $STATIC
50 DIM A(120),TS(35,5),TS$(35),F(95)
60 REM $DYNAMIC
70 DIM XS(1,1),XS$(1),YS(1,1),YS$(1),PV(1,1,1),NP(1),XY(1,1
),LNHX(1,1),LNHY(1,1),LIG$(1),GRID$(1),SMB$(1),LLG(1),AAG(1
),AAS(1),MEAN(1) : REM "GRAPHIC SCALE"
   DEF FNX(X,F,AG,LG)=(F*X/AG+F*MEAN(NOFC/2+4)/100/AG*LG-ME
AN(NOFC/2+3)*X)/(F/AG-MEAN(NOFC/2+3))
   DEF FNF(X,F,A,B,SR)=F-(A*X/(B+X))*SR
   INPUT "ENTER 'TST' FILE NAME ";BB$
   OPEN "I",#1,BB$
   INPUT #1,NOFC
   REDIM NP(NOFC*2),ARQNOME$(NOFC),LGNM$(NOFC*2)
   INPUT #1,TITX$,XSCL$,XL,XU,XS
   INPUT #1,TITY$,YSCL$,YL,YU,YS
   INPUT #1,TIT1$,TIT2$
   FOR I=1 TO NOFC : INPUT #1,ARQNOME$(I) : NEXT I : CLOSE
#1
   XSCL$="("+XSCL$+")"
   YSCL$="("+YSCL$+")"
        NPMAX=0
        FOR J%=1 TO NOFC
        OPEN "I",#1,ARQNOME$(J%)
        INPUT #1,NPT
        IF NPT)NPMAX THEN NPMAX=NPT
        CLOSE #1
        NEXT J%
          NOFC=NOFC*2 :NPMAX=95
          XYDM=((NPMAX+2)*NOFC)+150
          REDIM PV(NPMAX,2,NOFC),XY(XYDM,4),LNHX(NPMAX+2,NO
FC),LNHY(NPMAX+2,NOFC)
          REDIM MEAN(NOFC/2+4),FR(NOFC/2),LIG$(NOFC),GRID$(
2),SMB$(NOFC),AAG(NPMAX),AAS(NPMAX),LLG(NPMAX)
          OPEN "I",#1,"GEOM.DAT"
          FOR I%=1 TO 95
          INPUT #1,A,PV(I%,1,NOFC/2+1),LLG(I%),AAG(I%),AAS(
I%)
          AAG(I%)=AAG(I%)*1E-4 : LLG(I%)=LLG(I%)*10
            FOR J%=NOFC/2+2 TO NOFC
              PV(I%,1,J%)=PV(I%,1,NOFC/2+1)
            NEXT J%
          NEXT I%
          CLOSE #1
  FOR J%=1 TO NOFC/2
100 OPEN "I",#1,ARQNOME$(J%)
110 INPUT #1,NP(J%),LGNM$(J%)
120 FOR I% =1 TO NP(J%)
130 INPUT #1,PV(I%,1,J%),PV(I% ,2,J%)
    PV(I%,1,J%)=PV(PV(I%,1,J%),1,NOFC/2+1)
140 NEXT I% : CLOSE #1
    NEXT J%
    GOSUB 9000
    FF$="OUT"
```

```
     GOSUB 10000
     END
 9000 INPUT "ENTER 'CHT' FILE ";AA$
      OPEN "I",#2,AA$
      FOR J%=1 TO NOFC/2+4
      INPUT #2,MEAN(J%)
      NEXT J%
      FOR J%=1 TO NOFC/2
      INPUT #2,FR(J%)
      NEXT J%
      CLOSE #2
      RETURN

10000      FOR W1%=1 TO NOFC/2
             W0%=NOFC/2
             NP(W1%+W0%)=95
             LGNM$(W1%+W0%)=LGNM$(W1%)+"CORR."
             PV(1,2,W1%+W0%)=MEAN(W1%)
             F(1)=FR(W1%)
             AREA=AAS(1)*1E-4
               F(2)=FNF(PV(1,2,W1%+W0%),F(1),MEAN(NOFC/2+1),
MEAN(NOFC/2+2),AREA)
               PV(2,2,W1%+W0%)=FNX(PV(1,2,W1%+W0%),F(2),AAG(
1),LLG(1))
                  FOR W2%=3 TO 94
                    AREA=AAS(W2%-1)*1E-4
                    A=MEAN(NOFC/2+1) : B=MEAN(NOFC/2+2)
                    F(W2%)=FNF(PV(W2%-1,2,W1%+W0%),F(W2%-1),
A,B,AREA)
                    PV(W2%,2,W1%+W0%)=FNX(PV(W2%-1,2,W1%+W0%
),F(W2%),AAG(W2%-1),LLG(W2%-1))
                      IF PV(W2%,2,W1%+W0%)<0 OR PV(W2%,2,W1%
+W0%))=PV(W2%-1,2,W1%+W0%) THEN PV(W2%,2,W1%+W0%)=PV(W2%-1,
2,W1%+W0%)
                     IF F(W2%))=F(W2%-1) OR F(W2%)<0 THEN F(
W2%)=0 : PV(W2%,2,W1%+W0%)=PV(W2%-1,2,W1%+W0%)
                  NEXT W2%
            AREA=AAS(94)
              F(95)=FNF(PV(94,2,W1%+W0%),F(94),MEAN(NOFC/2+1
),MEAN(NOFC/2+2),AREA)
              PV(95,2,W1%+W0%)=FNX(PV(94,2,W1%+W0%),F(95),AA
G(94),LLG(94))
                    IF PV(95,2,W1%+W0%)<0 OR PV(95,2,W1%+W0%
))=PV(94,2,W1%+W0%) THEN PV(95,2,W1%+W0%)=PV(94,2,W1%+W0%)
                    IF F(95))=F(94) OR PV(95,2,W1%+W0%)=PV(9
4,2,W1%+W0%) OR F(95)<0 THEN F(95)=0 : PV(95,2,W1%+W0%)=PV(
94,2,W1%+W0%)
             A$=FF$+RIGHT$(STR$(W1%),1)
             OPEN "O",#5,A$
             PRINT #5,95;", FORCA ";W1%
             FOR II%=1 TO 95 : PRINT #5,PV(II%,1,NOFC/2+1);"
,";F(II%) : NEXT II%
             CLOSE #5
10002     NEXT W1%
```

```
              AAA$=FF$+".DSL"
              OPEN "O",#5,AAA$
              FOR IJK%=1 TO 95
             PRINT #5,PV(IJK%,1,NOFC/2+1);",";PV(IJK%,2,1+NOF
C/2);",";PV(IJK%,2,2+NOFC/2);",";PV(IJK%,2,3+NOFC/2);",";PV
(IJK%,2,4+NOFC/2);",";PV(IJK%,2,5+NOFC/2);",";PV(IJK%,2,6+N
OFC/2);",";PV(IJK%,2,7+NOFC/2);",";PV(IJK%,2,8+NOFC/2);",";
PV(IJK%,2,9+NOFC/2)
              NEXT IJK%
              CLOSE #5
10004       CLS
           RETURN
```

The input data required to run the program consists of the following files:

NAME.CHT — These extension file names are required by the program.

NAME.TST

NAME.PSS

GEOM.DAT — This file name should not be changed.

All these files should be generated as ASCII codes and as sequential files. Most of the commom text editors available up to now, substitute a sequence of ASCII spaces by a "TAB" code for a sequence of typed blank space. When it is read by a Basic program, it is interpreted as a zero or space depending on the case; therefore, it is suggested that no blanked spaces be typed when creating the files. The used separated character is equivalent to ASCII code comma, although any other character accepted by BASIC can be used. The following files are examples of how to input data. If too many elements are used in the discretization of the tension member, it is suggestd that the files be converted to Random Access type because in this mode, straight access of data can be done and array dimensioning can be avoided (either "static" or "dynamic"). It is important to note that all units should be compatible according to definitions in the thesis text.

NAME$_1$.PSS

In these files, the experimental data from the pull-out tests are listed. It should be according to definitions in Section 6.8 and Figure 6.20

N, K_{unit}	(number of coordinates, stage of force)
x_i, y_i	x_i = length from front end of box
	y_i = pull-out displacement measured during pull-out test

GEOM.DAT

This corresponds to what is shown in Figure 6.10 for SR2 and 6.11 for TNX5001. The units should be compatible with each other.

No. of elements	position of element	length of element	cross section area
i - 1	x_{i-1}	l_{i-1}	a_{i-1}
i	x_i	l_i	a_i
i + 1	x_{i+1}	l_{i+1}	a_{i+1}
n	x_n	l_n	a_n

NAME.CHT

$x_{1,1}$	measured displacement at front end of two
$x_{1,2}$	stages of pull-out force
.	
.	
.	
A	soil shear strength parameters

B

a geogrid tensile parameters

b

$F_{1,1}$ measured forces at the front end of the box

$F_{1,2}$ for 2 stages of pull-out forces

$NAME_i$.TST

This is the manager file of the program. It calls all the N stages of the test

N

Length, cm, 0, 120, 10

Force, kN/member, 0, 10, 1

Bottom title, Top title

NAME1.PSS

.

.

.

NAMEN.PSS

OUTPUT Files

OUT_i

OUT.DSL

In OUT_i, the forces x length are listed for each stage analysed.

In OUT.DSL, the displacements x length are listed for each stage analysed.

These output files are all ASCII sequencial files, using

"commas" as the separater character. Since most spreadsheet programs available for plotting can import these kinds of files (for ex. Lotus 123, AS-EASY-AS, among others), it is a trivial task to put the results in a graphical form.